Examining *Bdellovibrio bacteriovorus* cell division processes and their metabolic cues during predation

Thesis submitted to the University of Nottingham for the degree of Doctor of Philosophy

BBSRC Doctoral Training Programme

Luke Jonathan Ray B.Sc. (Hons)

November 2021

Abstract

Bdellovibrio bacteriovorus is a predatory bacterium that invades and digests other Gram-negative bacteria in its host dependent (HD) lifestyle. This predator traverses the outer membrane and digests a pore in the cell wall of the prey cell; it then enters the inner periplasm, sealing the pore and outer membrane, and establishing itself. Through modification of the host cell wall, the prey is rounded forming a bdelloplast. From the inner periplasm, *B. bacteriovorus* digest the host biomass sequentially and uses it to fuel their own growth, undergoing filamentous growth in the bdelloplast. Once prey nutrients have been consumed, the filament undergoes septation to create a variable number of progeny. This number is dependent on the available resources from the bdelloplast and can be odd or even. Following on from former PhD student David Milner's work, my study focussed on the interaction partners of DivIVA, using pairwise Bacterial Two Hybrid (BTH) assays and then constructing a BTH library. Additionally, I investigated the *divIVA* operon with bioinformatics and fluorescent microscopy. Finally, while shielding from COVID-19, I bioinformatically analysed the *division and cell wall* (dcw) cluster of *B. bacteriovorus* and produced a phylogenetic tree for a study on its deacetylases, which includes lysozymes specific to prey entry and exit.

DivIVA is a protein initially studied in Firmicutes, such as *Bacillus subtilis*. Its homologues have been implicated in regulating sporulation, cell morphology, apical growth, and several other processes in multiple, mainly Gram-positive, bacteria. Milner previously showed that DivIVA in *B. bacteriovorus* had roles in cell morphology and, potentially, septal site selection. I continued work on this protein by testing for interacting partners of DivIVA using pairwise BTH. This revealed a potential network of interactions that connect the roles of DivIVA with amino acid and cofactor Pyridoxal 5'-Phosphate (PLP) homeostasis, as well as chromosome partitioning. This involved proteins transcribed from neighbouring genes *bd0466* and *bd0465*; YggS, for PLP homeostasis, and pyrroline 5-carboxylate reductase, for proline synthesis. Further interactions were found between Bd0465 and the canonical chromosome partitioning protein ParA3.

This led to me investigating unknown interaction partners through the construction and use of a BTH library. This found several potential interacting proteins. A TrmJ homologue suggests crosstalk between DivIVA and the oxidative stress response, a link that has previously been found in *Mycobacterium tuberculosis* and *Streptococcus suis*. A MenE homologue was also identified as a potential interactor; this functions in menaquinone biosynthesis, a compound used in the electron transport chain. In Gram-negative bacteria, it is used for respiration in low oxygen environments, which could be emulated by the bdelloplast.

During the pandemic and shielding from COVID-19, I analysed the *dcw* cluster of *B. bacteriovorus*. In rod shaped bacteria, the *dcw* cluster is a highly conserved region of the genome containing an operon encoding division, septation and cell wall synthesis proteins, including FtsZ. Both the genes and the order in which they are transcribed is conserved among bacteria, however, *B. bacteriovorus* have fifteen genes inserted into the cluster, fragmenting the ancestral operon. Investigating these genes shows varying roles for the encoded proteins. These include amino acid and nucleotide synthesis and homeostasis, stress response and DNA repair, and outer membrane lipid synthesis proteins.

Finally, I produced a phylogenetic tree for a publication on the family of deacetylases that target deacetylated GlcNac. *B. bacteriovorus* modify the prey cell wall upon invasion, deacetylating GlcNAc. This serves to soften the wall and prevent other *B. bacteriovorus* from invading. Three deacetylases, which target the cell wall, were identified and one, DslA, was shown to lyse the bdelloplast at the end of the HD cycle. My phylogenetic analysis shows that DslA is related to lysozymes in several α-proteobacteria, including some plant root symbiotes, as well as some β- and γ-proteobacteria.

Altogether, these results show complex regulation of division and septation in this predatory bacterium. This study primes further investigation into the crosstalk between division and other systems during the growth phase of *B. bacteriovorus* in the bdelloplast, while also identifying several novel metabolic interactions of DivIVA that can be further studied.

Acknowledgements

Firstly, I must say thank you to my PhD supervisor, Liz Sockett, who has supported me through this process on both an academic and personal level. You have helped to keep me going through the tough times, even when our coffee chats could not be face-to-face. You always had time, thank you.

I must also thank everyone in C15, whether they have moved on or are still furthering the *Bdellovibrio* agenda. Rob Till has helped me with all aspects of cloning and was instrumental in both my initial experiments and in constructing the library (no spoilers, you will have to read the rest of the thesis). Carey Lambert has always fielded my questions, stupid or otherwise, and explained to me numerous times how to use the microscope and follow protocols. He has also pioneered our use of FIJI and MicrobeJ, used extensively in this thesis. Thanks to Simona Huwiler for use of her unpublished RNA-seq data and an endless supply of Swiss chocolate. Also, to Jess Tyson and Paul Radford for support in my lab work when I needed an extra few sets of hands, and the supply of useful strains. Thanks to everyone I have worked alongside with for jumping to help when I have been too ill to make it to the lab or have had to leave early. An additional thanks goes to the A team, whose diligent work and positivity prevents the entire collapse of the department.

All your help, and seemingly infinite patience, was always appreciated, especially when I decided to go part time and impose myself on you for longer. Without you, I may have sat in a corner and panicked for at least twice as long as I have done. The help you have all given me, inside and outside of the lab (having a burger on the porch with Jess and Callum), will always be appreciated.

Also, a big thank you to the BBSRC DTP programme for funding my PhD and to both them and the School of Life Sciences in their support when I chose to switch to part time research.

I thank my family for their patience and support during my studies. Without them, this would not have been possible. My father has always pushed me to go further (literally, in a wheelchair) and allowing my mother to brag that her son is a doctor is truly the most noble motivation for research. I would also like to thank my daughter, who came about near the end of this process, and my fiancée for keeping me sane these past, and sometimes difficult, years.

Table of contents

Table of figures

List of tables

List of abbreviations

%	percentage
=	equals
<	less than
>	greater than
~	approximately
±	plus-minus 95% confidence interval (unless stated otherwise)
°C	degrees centigrade
3’	3 prime (hydroxyl) end of DNA/RNA molecule
5’	5 prime (phosphate) end of DNA/RNA molecule
4HTP	4-phosphohydroxy-L-threonine
ABC	ATP-Binding Cassette
ADP	adenosine diphosphate
AGP	arabinogalactan-proteins
Amp	ampicillin
AP	attack phase
ATP	adenosine triphosphate
asRNA	antisense-RNA
bp	base pair
BALO	*Bdellovibrio*-and-like organism
BTH	bacterial two-hybrid
cAMP	cyclic adenosine monophosphate
CAP	catabolite activator protein
CCR	carbon catabolite repression
cfu	colony forming unit
CoA	coenzyme A
CRP	cyclic AMP receptor protein
CTP	cytosine triphosphate
Dap	diaminopimelic acid
dcw	*division and cell wall*
DNase	deoxyribonuclease
dNTPs	deoxynucleotide triphosphates
DXP	deoxyxylulose-5-phosphate
E4P	erythrose 4-phosphate
EDTA	Ethylenediaminetetraacetic acid
Epd	erythrose 4-phosphate dehydrogenase
FIS	factor for inversion stimulation
g	gravitational acceleration force (9.8 N/kg)
GlcNAc	N-acetyl-glucosamine
GNAT	Gcn5-related N-acetyltransferase
GNPNAT1	glucosamine 6-phosphate N-acetyltransferase
GRHPR	glyoxylate hydroxypyruvate reductase
HD	host-dependent
HEPES	4-(2-hydroxyethyl)-1-piperazineethanesulfonic acid
HI	host independent
HRDC	helicase and RNaseD C-terminal
HTH	helix-turn-helix
IHF	integration host factor
IM	inner membrane

IPTG	Isopropyl β-D-1-thiogalactopyranoside
LDF	linear discriminant function
kb	kilobases
Kn	kanamycin
LGT	lateral gene transfer
LPS	lipopolysaccharide
M	molar
mCerulean	monomeric cerulean fluorescent protein
mCherry	monomeric cherry fluorescent protein
MCP	methyl-accepting chemotaxis protein
mM	millimolar
mTFP	monomeric teal fluorescent protein
MOPS	3-(N-morpholino)propanesulfonic acid
MurNAc	N-acetyl-muramic acid
NA	nutrient agar
OAT	aminotransferase
OD	optical density
OD_{600}	optical density at 600 nm
OM	outer membrane
ONP	ortho-nitrophenol
ONPG	ortho-nitrophenol β-D-galactopyranoside
ORF	open reading frame
oriC	origin of replication
OSB	o-Succinylbenzoyl
P5CR	pyrroline-5-carboxylate reductase
PBP	penicillin binding protein
PCR	polymerase chain reaction
pfu	plaque forming units
PG	peptidoglycan
PL	pyridoxal
PLP	pyridoxal 5'-phosphate
PM	pyridoxamine
PN	pyridoxine
PNP	pyridoxine 5'-phosphate
ROS	reactive oxygen species
rRNA	ribosomal ribonucleic acid; component of the ribosome
RPM	revolutions per minute
RT-PCR	reverse-transcriptase polymerase chain reaction
SAM	S-adenosyl-L-methionine
SDS	sodium dodecyl sulphate
SDW	sterile distilled water
SE	standard error
STK	serine threonine kinase
T18	domain of CyaA from *Bordetella pertussis*, complements T25
T25	domain of CyaA from *Bordetella pertussis*, complements T18
Tat	twin-arginine transport
TE	tris and EDTA buffer
TEM	transmission electron microscopy
UAS	upstream activating sequence
UDP	uridine diphosphate

UMA	UDP-N-acetylmuramoyl-L-alanine
USP	universal stress protein
UTR	untranslated region
VKOR	vitamin K epoxide reductase
WT	wild type
YPSC	yeast extract, peptone, sodium acetate, calcium chloride
v/v	volume to volume concentration
vs	versus
w/v	mass to volume concentration
X-gal	5-bromo-4-chloro-3-indolyl-β-D-galactopyranoside
α	alpha
β	beta
β-gal	β-galactosidase
δ	delta
Δ	Delta, denotes gene deletion
γ	gamma

1 Chapter 1: General introduction

1.1 *Bdellovibrio bacteriovorus*: intracellular predators

Bdellovibrio are predatory Oligoflexia, a class of Proteobacteria, that prey upon other Gram-negative bacteria. *Bdellovibrio bacteriovorus* attach to the cell surface of prey and invade by digesting a hole in the outer membrane to access the outer periplasm, between the cell wall and the outer membrane (Sockett, 2009, Hahn et al., 2017, Waite et al., 2020). A further pore is digested in the prey cell wall and the predator enters the inner periplasm, between the inner membrane and the cell wall, where it remains for the duration of the cycle. It reseals the pores to maintain host membrane and wall integrity, and digests host biomass to fuel its own growth (Kuru et al., 2017). Once the *B. bacteriovorus* cell has penetrated the cell wall and become established in the prey, it loses motility by shedding the flagellum. The prey cell then becomes rounded and is termed a bdelloplast. From the position in the periplasm, *B. bacteriovorus* digest, import and process the biomass of their prey for the nutrients required for growth. Rather than binary fission, *B. bacteriovorus* grow filamentously (Fenton et al., 2010). This filament extends from both poles and then septates into a variable number of progeny, determined by the available biomass; a larger prey cell, with more biomass, will allow the predator to produce more progeny than smaller prey. The progeny mature, developing motility, and the bdelloplast is lysed, releasing new *B. bacteriovorus* cells to continue the cycle.

Two *B. bacteriovorus* subspecies which have been genomically sequenced are HD100 and Tiberius (Genome size is 3.78mbp for HD100 and 3.98mbp for Tiberius) (Hobley et al., 2012b, Rendulic et al., 2004). HD100 is ubiquitous in soil and aquatic environments; Tiberius was isolated from the river Tiber. The genomes of these two are very similar but there are some significant differences, such as additional genes in Tiberius that the authors suggested were attained via lateral gene transfer, likely to be involved with the varied environments of plants and animals in the river. Tiberius are also more prone to host independent (HI) growth. The HI lifecycle allows *B. bacteriovorus* to grow on media in the absence of prey. HD and HI growth phases are typically

exclusive in HD100, with very few cells in the HD population being capable of growth as an HI, typically one in 10^7. Tiberius, however, were observed to have both phases present in the population, even when prey were available. Of these, HD100 is the focus of this thesis, with some comparisons made to Tiberius.

Another species of *Bdellovibrio, B. exovorus* (genome size 3.65mbp) consumes its prey externally by attaching to the cell surface and extracting the prey contents from there (Koval et al., 2013). They are also thought to divide via binary fission, rather than producing a filament, and are also used for comparison in this thesis.

Until recently, the order Bdellovibrionales (which includes genera *Bdellovibrio, bacteriovorax* and *Halobacteriovorax*) were δ-proteobacteria but have recently been reclassified as Oligoflexia, another Class of Proteobacteria most closely related to δ-proteobacteria (Hahn et al., 2017, Euzéby, 2006). The phylum Proteobacteria consists of Gram-negative bacteria. Initially, this group consisted of Classes α-proteobacteria, β-proteobacteria, γ-proteobacteria, δ-proteobacteria and ε-proteobacteria (Euzéby, 2006). Many more classes have since been added to this group, as seen in the NCBI taxonomy browser (NCBI Taxonomy Browser. Bethesda (MD): National Library of Medicine (US), National Center for Biotechnology Information – [cited 17.01.2022.]. Available from: https://www.ncbi.nlm.nih.gov/Taxonomy/Browser) (Sayers et al., 2021, Schoch et al., 2020). For the purposes of this study, these classes are defined as seen in the NCBI taxonomy browser; taxonomy ID 28221 for δ-proteobacteria and 1553900 for Oligoflexia (Schoch et al., 2020).

A more general term has been previously used to define all known predatory Gram-negative bacteria: *Bdellovibrio*-and-like organisms (BALOs). This term was originally based on observations of the environments and predatory lifestyles of several Gram-negative bacteria (Snyder et al., 2002). These include two groups of bacteria; the Oligoflexia Order Bdellovibrionales (as above), as well as α-proteobacteria genus *Micavibrio* (Hahn et al., 2017, Davidov et al., 2006).

1.2 Major events in the HD cycle

Imaging the growth and division processes of *B. bacteriovorus* presents some unique challenges. While free swimming, the predator is easily imaged but once it is established in the host cell it becomes a lot harder to distinguish the growing filament. This has largely been tackled using fluorescent tags for the predator's proteins and/or general prey fluorescence as a backdrop. Many studies since have focussed on the expression of potentially predatory or non-predatory genes and their regulation. This includes points in the cycle where a switch will occur, such as the change from attack phase and invasion to digestion and growth. Here, I will consider the current evidence for when these events occur in the HD cycle to have a definitive reference point for future comparison. This will give a defined period, with specific activity, with which to relate the expression of the genes relevant to this thesis from RTPCR and RNA-seq evidence. This should provide greater insight into when and how such genes are functioning and the processes they may be interacting with, or that are simultaneously being performed. This is summarised in **figure 1.1**.

1.2.1 Early events and metabolic cues in the HD cycle

When imaging synchronous predatory culture samples are taken at specific intervals. At time 0, when predator and prey have just been introduced, the HD100 attack phase cells are free-swimming using their single flagellum; the prey are unaffected. One study has found that two thirds of genes upregulated for attack phase are controlled by Bd3318, a FliA homologue (Karunker et al., 2013).

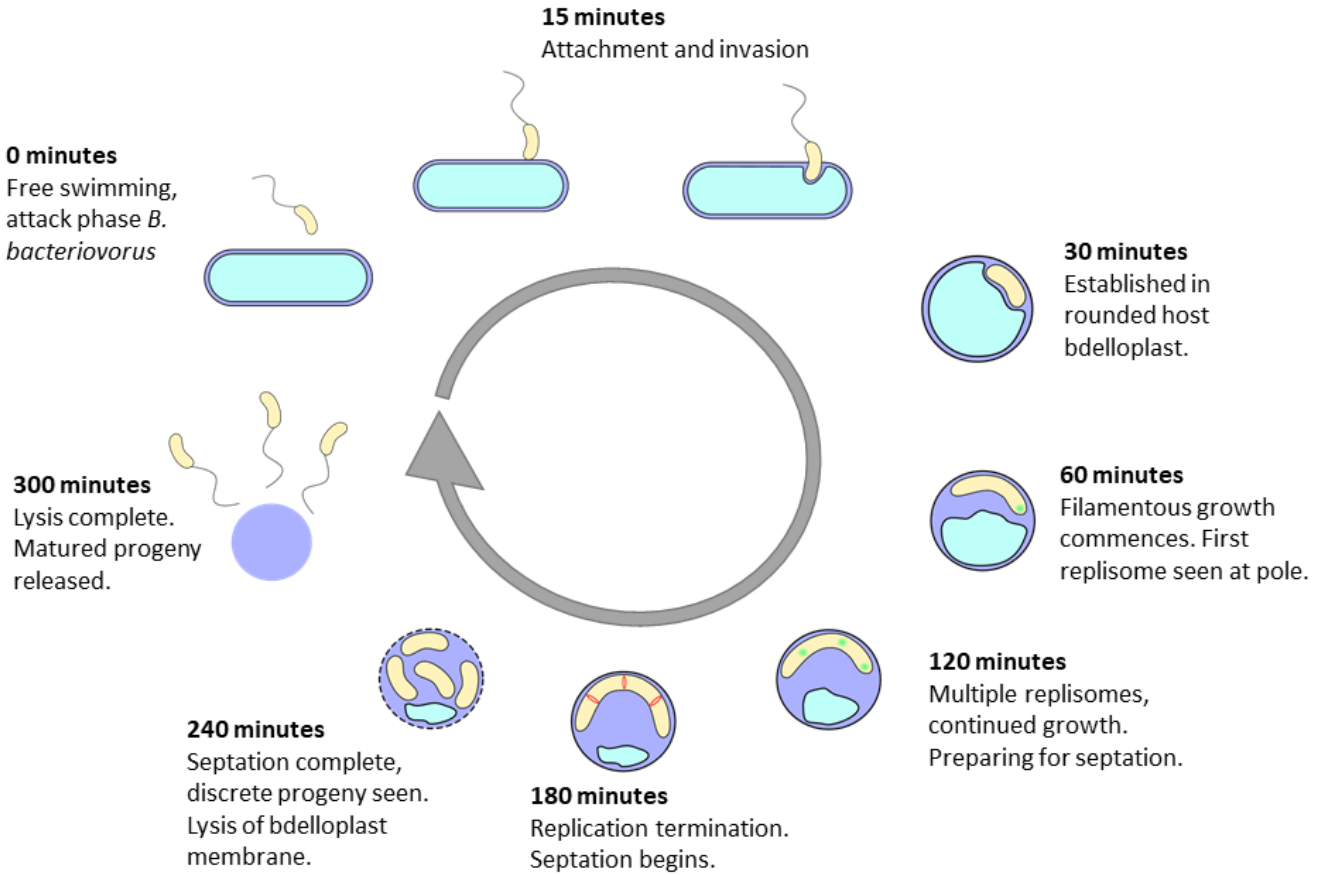
15 minutes
Attachment and invasion
0 minutes
Free swimming, attack phase *B. bacteriovorus*
30 minutes
Established in rounded host bdelloplast.
60 minutes
Filamentous growth commences. First replisome seen at pole.
120 minutes
Multiple replisomes, continued growth. Preparing for septation.
180 minutes
Replication termination. Septation begins.
240 minutes
Septation complete, discrete progeny seen. Lysis of bdelloplast membrane.
300 minutes
Lysis complete. Matured progeny released.

Figure 1.1. A cartoon representation of the HD lifecycle of *B. bacteriovorus* annotated with major events at specific time points. This summarises the major events that occur during the HD lifecycle at the time points commonly used in synchronous predatory cultures to image the *B. bacteriovorus* cell as it invades and grows in the bdelloplast. At 0 mins, the *B. bacteriovorus* cells are free swimming attack phase cells (the yellow cell), searching for a Gram-negative host (large blue cell). By 15 mins, the *B. bacteriovorus* cells are seen to have attached to prey and begun invasion. At 30 mins, the predator has established in the host and rounded the cell, killing it, and forming the bdelloplast. At 60 minutes the *B. bacteriovorus* cell has begun filamentous growth and the first replisome is seen at the invading pole. By 120 minutes, multiples replisomes can be seen as growth continues. Replication is terminated, and the replisomes dissipated, at 180 minutes, as the filament prepares to septate into a number of progeny determined by the digested biomass of the host cell. Septation is complete by 240 minutes, the new progeny have matured, and the membrane of the host bdelloplast is being lysed. At 300 minutes, the progeny have been released as attack phase cells, although morphological changes can be seen immediately after lysis compared to older attack phase cells.

The authors also suggest the possibility that FliA regulates the other regulators for attack phase specific genes, which could account for the remaining third. Their data showed that it is highly expressed at attack phase but is much lower in the growth phase, the distinction between the phases being the time sampled; a newly mixed sample for attack phase, and samples from 60 and 180 minutes for growth phase.

At 15-20 minutes, the HD100 cells are attached to the prey and beginning invasion (Evans et al., 2007). This process requires type four pili at the pole opposite to the flagellum for prey attachment. There are several events in the early stages of the HD cycle, from attachment, invasion and establishment, 15 to 60 minutes post-infection, that could serve to provide metabolic cues to the predator to signal transition from invasion to growth. At these time points, the predator must gain access through the outer membrane and cell wall of the prey, with modifications to the wall that causes the rounding seen with an established bdelloplast. Cell wall composition and structure can vary greatly between different prey, but *B. bacteriovorus* effectively rounds them all. This

process has not been completely elucidated, but one study identified two DacB homologues, with both DD-carboxypeptidase and DD-endopeptidase activity, used for these purposes.

Of the three *dacB* homologues identified in *B. bacteriovorus*, Lerner *et al.* found two that were expressed during invasion; *bd0816* and *bd3459* were upregulated at 15 minutes post-infection, when *B. bacteriovorus* attaches to the prey, followed by downregulation at 30 minutes, once the predator is established in the bdelloplast, with no discernible expression at 45 minutes (Lerner et al., 2012). The third *dacB* homologue, *bd3244*, was found to have constitutive expression throughout the cycle, leading the authors to conclude it had a role in peptidoglycan housekeeping and regular turnover. The authors found that null mutants of *bd3459* had non-rounded bdelloplasts in the samples; this increased with the *Δbd0816 Δbd3459* strain where fewer than 10% of bdelloplasts were rounded. Further *in vitro* assays showed that Bd3459 was a PBP with DD-carboxypeptidase and DD-endopeptidase activity. A pentapeptide-rich *E. coli* prey strain, when exposed to Bd3459, had a huge increase in tetrapeptide levels and a marked drop in pentapeptides, as well as a decrease in crosslinks, both tetra-tetra and tetra-penta. The authors concluded that Bd3459 is secreted into the prey periplasm where it acts on prey peptidoglycan, cutting cross links and converting pentapeptides to tetrapeptides. This modification rounds the prey cell, producing the shape of the bdelloplast. A by-product of this digestion would be an increase in free D-Ala in the periplasm, removed from the pentapeptides. This could act as a clear signal to the predator, moving from establishment in the bdelloplast onto active digestion of the prey.

Another source of the D-Ala signal could be from the action of L,D-transpeptidases. These enzymes create 3-3 crosslinks in peptidoglycan, and a study by Kuru *et al.* found two genes, *bd0886* and *bd1176*, whose products act upon the prey cell wall from 15 to 60 minutes (Kuru et al., 2017). These are active from invasion; however, unlike Bd3459, they continue their activity through to the beginning of the growth phase at 60 minutes. The authors suggest this activity creates a robust cell wall capable of withstanding turgor and osmotic forces acting on the bdelloplast. Again, this activity would

produce D-Ala, which could signal to the predator that it is established in a bdelloplast and can begin to digest the prey and grow. Taken together, this suggests that a D-Ala signal, from the initial invasion and modification of the prey could be a cue early in the cycle to transition from the establishment phase, 15 to 60 minutes, to the growth phase, 60 minutes onwards.

Two deacetylases, Bd0468 and Bd3279, have also been found to act early in the HD cycle (Lambert et al., 2016). Peak expression for their encoding genes was seen at 15 minutes, and the authors concluded these were GlcNAc deacetylases acting upon the prey cell wall. Deleting both genes resulted in the predator occupying the outer periplasmic space of the host, between the wall and outer membrane, rather than the inner periplasmic space. Following progeny exit, the authors observed the presence of ovoid structures that they determined to be the intact cell wall and inner membrane material of the prey, dubbed “prey ghosts”. Additional deletions of the above L,D-transpeptidases, *bd0886 and bd1176*, also abolished the rounding of the host, leaving rod shaped ghosts. The action of the GlcNAc deacetylases produces acetate which, like D-Ala, could be an early signal for the progression of the cycle from establishment to active digestion and growth.

By 30 minutes, HD100 have established themselves in the prey periplasm, rounding the host and forming the bdelloplast (Makowski et al., 2019). It is at this point that upregulation of predatory genes occurs; around 240 genes specific to the host dependent life cycle and the digestion and utilisation of prey biomass (Lambert et al., 2010). While this does not represent the full arsenal of digestive enzymes encoded in the HD100 genome, it does include a set of proteases, nucleases, and hydrolases, thus marking this point as the beginning of digestion. Additionally, there are downregulated genes that mark the transition from attack phase to established in the bdelloplast; genes for motility and chemotaxis, as well as a large group of outer membrane proteins that may have a role in prey sensing, attachment, and invasion.

1.2.2 Chromosome replication and filamentous growth

One study showed that the first replisome can be seen 80 minutes post-infection, typically at the pili pole of the HD100 (Makowski et al., 2019). Later

in the cycle, around 120 minutes, multiple replisomes can be seen. Another recent study characterised two secreted nucleases, Bd0934 and Bd3507, that they concluded to be part of the predatosome, digesting the DNA in the prey (Bukowska-Faniband et al., 2020). In their work, they describe the expression pattern of these nucleases and determined that they are upregulated from 30 mins, when the predator is established in the host, to 120 minutes, when there are still multiple replisomes. These nucleases were then downregulated at 180 minutes, when replication is reported to stop, and the filaments begin septation. These studies define a period of digestion, growth and replication before the cell is ready to septate. Unpublished RNA-seq data **(from Simona Huwiler, collaborator [Research Group Leader, SNSF Ambizione, University of Zurich])** also shows that *dnaA*, which encodes for the master DNA replication initiator protein, is upregulated at 60 and 120 minutes, when the replisome(s) is active, but is downregulated at 180 minutes, when Makowski *et al*. show that replisome fluorescence becomes diffuse. This marks the end of genome replication.

It is currently unknown what signals are required to progress through these phases of the cycle; specifically, between 120 and 180 minutes, the filament switches from digestion, chromosome replication and filamentous growth, to septation and maturation. It is reasonable to assume that there may be many contributors to this switch. To produce a variable number of progeny, *B. bacteriovorus* must have a means of determining when resources are abundant enough to make another copy of the chromosome and further extend the filament, and when resources have become too limited, and the cell must stop growth and divide. This could be a measure of digestion products available to the filament, and/or a measure of digestive by-products such as oxidative agents. These sensory pathways would have to interact with division-related proteins, as well as cause the dissipation of the replisome and other growth processes.

There have been recent studies in other systems to determine the relationship between nutrients and DNA replication that may bear relevance to *B. bacteriovorus*. Several insights were recently made by Murray and Koh in *B. subtilis* (Murray and Koh, 2014). They determined that nutrient-mediated

growth rate regulation of DNA replication initiation required both DnaA and the origin of replication, *oriC*; however, changes in the level of DnaA present did not account for this regulation. Additionally, the ParA homologue in *B. subtilis*, Soj, was not required. Using genetically altered strains, the authors found that disrupting certain metabolic pathways inhibited the initiation of DNA replication. These pathways included respiration, central carbon metabolism, protein synthesis, fatty acid synthesis, and phospholipid synthesis. In *B. bacteriovorus*, these could be collectively used as a signal to determine when to stop replication and begin septation. When depleting prey resources, lower activity from these pathways could prevent further replication initiation in the predator, subsequently initiating septation. Further links have also been found in *E. coli* between metabolites from central carbon metabolism and DNA replication (Krause et al., 2020). In this study, altering the concentration of metabolites pyruvate, acetate, succinate, fumarate, a-ketoglutarate, malate and lactate could suppress the phenotypes of mutant DNA replication genes, specifically mutations in *DnaA, DnaB, DnaC, DnaE, DnaG* and *DnaN*. This was seen when these mutants were grown at restrictive termperatures. Without intervention, incorrect division led to the formation of filaments and changes in nucleoid localisation. The addition of certain metabolites suppressed, and in some cases abolished, these aberrant phenotypes. Again, this could relate to HD cycle regulation in *B. bacteriovorus*. By sensing the concentrations of these metabolites, DNA replication could be slowed or stopped in preparation for septation.

1.2.3 Septation, maturation and lysis

The RNA-seq data shows that *ftsZ* is expressed from 120 minutes post infection. This shows that the filament is preparing to determine the sites of septation, although this is a process with many other proteins regulating Z-ring formation to control its spatial and temporal assembly. Fenton *et al*. observed that at 180 minutes post-infection, septation had occurred and the progeny number could be counted in the bdelloplast. Makowski *et al.* placed this event at 240 minutes post infection, after replication termination at 180 minutes. Many of the proteins involved in septation are encoded from the *dcw* cluster, mentioned above, as are many peptidoglycan synthesis proteins. The septated

progeny mature roughly 26 minutes following the division event. Maturation is the development of polar structures, such as the flagellum, and these were observed before lysis of the host occurred.

Finally, from 240-300 minutes, the bdelloplast lyses and the mature progeny are released as attack phase cells. Exiting the exhausted prey requires gliding motility, and deletion of a diguanylate cyclase gene *dgcA bd0367*, has previously been shown to abolish this (Hobley et al., 2012a). RNA-seq data shows that this gene is expressed highest at attack phase and 300 minutes, when the cells should be motile and searching for prey, but it is also expressed at a lower level throughout the cycle, with minimal transcription at 120-180 minutes, the period in which growth is concluding and the filament prepares for septation. Expression of *dgcA* increased at 240 minutes, when the filament has septated and the progeny are maturing. This expression pattern shows the transition to mature attack phase cells capable of leaving the exhausted bdelloplast via gliding.

Flagellum development of the progeny appears to occur after gliding is established. The RNA-seq data shows that several flagellum-related genes are expressed highest during attack phase, but with continued expression as the HD100 cell invades and establishes itself in the bdelloplast at 15 to 30 minutes. It is then downregulated from 60 mins, through to and including 240 minutes, and again upregulated at 300 minutes. The specific genes are *flgE*, *fliF* and the three pairs of *motAB* genes present in the HD100 genome; all these genes share a similar expression pattern that suggests flagellum-based motility develops after gliding motility, possibly only fully assembled and active following lysis of the bdelloplast and gliding exit.

Additionally, a study has shown that lysozyme encoding gene *bd0314* begins low level expression at fifteen minutes, building up to a peak at 240 minutes; the 300 minute time point was not used in this study but unpublished RNA-seq data suggests that expression at 300 minutes is the same as at 240 minutes (Harding et al., 2020). This lysozyme, DslA, was determined to lyse the bdelloplast to release the mature progeny, with deletion mutants taking longer

to do so. Peak expression at 240- and 300-minute time points accounts for the lysis and escape period.

1.2.4 Defining the time points in a synchronous predatory culture

Given this evidence, I will define, and refer to, the processes occurring at the time points as follows:

0 minutes – Attack phase, free swimming.

15 minutes – Prey attachment and penetration.

30 minutes – Bdelloplast establishment, preparing to digest.

60 minutes – Filamentous growth, chromosome replication begins.

120 minutes – Growth, multiple replisomes, and septa preparation.

180 minutes – Growth and chromosome replication stop. Septation begins.

240 minutes – Septation, maturation and lysis.

300 minutes – Lysis ends, mature attack phase cells released

1.3 Cellular components for septation

Imaging the life cycle of *B. bacteriovorus* was initially addressed by Fenton *et al.* with the use of fluorescence, whereby the host expressed a GFP tagged protein ubiquitously in the cytoplasm. This allowed them to image the filament, which appears black against the fluorescent host, and document the process of growth and the production of multiple progeny. It is this phase in the life cycle that this study focuses on; specifically, the switch from growing to dividing, and the division homologues present in *B. bacteriovorus* that facilitate this.

Despite the major differences between the life styles of *B. bacteriovorus* and non-predatory bacteria, there are many known division proteins that are conserved throughout bacteria that are also found in *Bdellovibrio* (Tsang and Bernhardt, 2015, Lutkenhaus, 2007). As a core process, there is typically a high degree of homology, and *Bdellovibrio* retain recognisable systems for division. This section assesses several of the major processes of division in studied bacteria and compares them to the genes and proteins that exist in *B.*

bacteriovorus. Interestingly, although the Oligoflexia are Gram-negative bacteria, some traditionally Gram-positive associated components are found in *B. bacteriovorus*. Therefore, the models of *Escherichia coli, Bacillus subtilis, Streptomyces coelicolor* and *Mycobacterium smegmatis* are discussed here; *E. coli* as the most studied system, and the others for their relationship to the genes in this thesis.

Superficially, division in bacteria can vary greatly but there are fundamental processes and requirements shared within the kingdom (Monahan et al., 2014, Harry et al., 2006, Vicente et al., 2006). Firstly, the bacteria require enough nutrients to carry out the process. The chromosome must be replicated, such that each daughter cell has a full copy of the genome, and each chromosome is segregated away from the site of division. Septa, the specific point at which contraction of the membranes and PG wall occurs, must be able to form at the correct site away from segregated chromosomes. Additionally, peptidoglycan must be incorporated at the septa so that the progeny have a PG wall completely surrounding them once the chromosomes are partitioned and the cell has divided.

E. coli is a Gram-negative γ-proteobacterium, the closest relation to *B. bacteriovorus* among these paradigms. It has both inner and outer phospholipid membranes surrounding the peptidoglycan wall. *B. subtilis* is a Gram-positive Firmicute. It has an inner membrane and PG wall, but no outer membrane. *S. coelicolor* and *M. smegmatis* are both Gram-positive Actinobacteria. Neither have a typical outer membrane, but Mycobacteria are characterised by the presence of an outer wall constructed from mycolic acids. This has been studied, particularly in human and bovine pathogen species, and shown to function in antibiotic resistance and the pathogenesis of tuberculosis in animal hosts.

B. subtilis sporulates in unfavourable conditions, as can *S. coelicolor* for replication (Hammond et al., 2019). Sporulation is a mechanism of cell differentiation in which the bacteria leave the vegetative growth cycle, due to unfavourable environmental conditions such as lack of nutrients, and instead package their genetic content into a spore. The spore is highly resistant to

external conditions and allows the cell to revive itself once the environment it inhabits has become more favourable. *S. coelicolor* grows filamentously as hyphae, similar to filamentous fungi, and releases its spores into the air to disperse them. To do so the growing, vegetative hyphae become aerial hyphae, which extend vertically to release the spores. Filamentous growth is a shared trait with *B. bacteriovorus*, although this is only for division in the latter. This mode of growth gives it an outwardly different appearance to the other models, but the processes for division are of a common lineage, and much of the process can be compared directly. It should be noted that *E. coli* and *B. bacteriovorus* do not undergo sporulation. Here I will introduce several division processes in these systems before addressing the known homologues in *B. bacteriovorus.*

1.3.1 The Z-ring and septal site recruitment

Whilst the process and interactions between division related proteins is complex, the basic septum protein assembly model forming the divisome in *E. coli* can be shown in a linear fashion, seen in **figure 1.2**. Several of these proteins are encoded from the *dcw* cluster and are highly conserved among most bacteria, including *Bdellovibrio*. It should be noted that many of the proteins involved have multiple interactions among each other, which are not necessarily highlighted in this linear description (Lutkenhaus, 2007, Vicente et al., 2006). The stepwise assembly of septal proteins is known but recruitment and interactions remain to be properly characterised. Many of the early-stage proteins are thought to interact with late-stage proteins, forming a complex system of interactions. Additionally, the division ring described is a dynamic structure that grows from the cytoplasm out to the peptidoglycan wall.

Initially, FtsZ localises in the cytoplasm near the site where septation will occur guided by the MinCDE system, discussed below, although it does not yet form a ring at the inner membrane. FtsZ then recruits ZipA and FtsA to the vicinity. These assemble at the inner membrane in a non FtsZ dependent manner. FtsZ then assembles as a ring (the Z-ring) at the septa, attaching to the ZipA and FtsA already assembled on the inner membrane. ZipA and FtsA function to stabilise the FtsZ ring, although they both have other roles in cell division, recruiting further proteins.

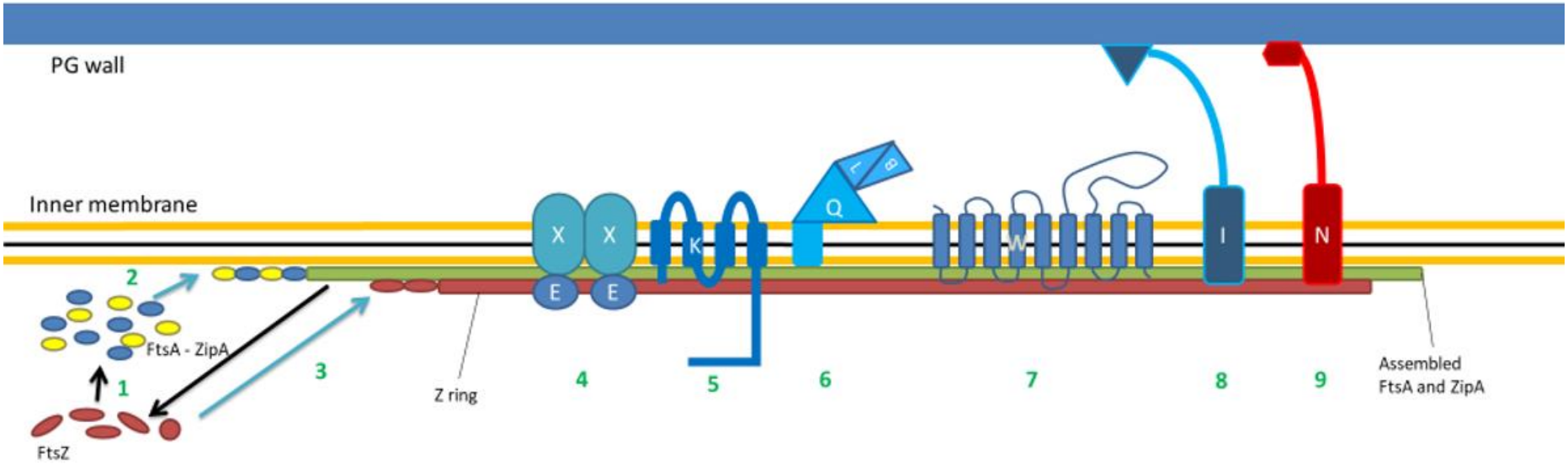

Figure 1.2. The stepwise assembly of septal proteins as studied in *E. coli*. (1) Initially, FtsZ is guided to the septum by the MinCDE system (not shown). (2) FtsZ then recruits FtsA and ZipA, which form a ring at the septum in a non FtsZ dependent manner. (3) FtsZ attaches to the FtsA/ZipA ring, forming the Z-ring. (4) The FtsEX complex associates to the Z-ring, likely via FtsE, and recruits further proteins. (5) FtsK, a DNA translocase, associates to the septum followed by (6) FtsQ which, after its own recruitment, forms a complex with FtsL and FtsB. FtsQ is essential to division and interacts with many of the proteins in this assembly. (7) FtsW, which acts in the peptidoglycan synthesis pathway as a flippase, is recruited and in turn recruits (8) FtsI, a penicillin binding protein that integrates newly synthesised peptidoglycan into the cell wall. (9) FtsN is the final protein. It is also essential to division and interacts with many of these proteins. Once assembled, septation can occur with the contraction of the Z-ring and incorporation of peptidoglycan at the new cell poles (Buddelmeijer and Beckwith, 2004, Karimova et al., 2005, Whitley et al., 2021).

Late-stage assembly follows, extending across the inner membrane to the PG wall. An FtsEX complex is recruited to the septa by FtsZ. This is composed of two FtsX proteins, which span the membrane, and two FtsE proteins, which are joined to the FtsX proteins on the cytoplasmic side of the membrane. It is likely that the FtsE portion of the complex interacts with FtsZ when being recruited. FtsK is recruited, followed by FtsQ. Before recruitment, FtsQ forms a complex with FtsL and FtsB. FtsQ has been shown to interact with many of the discussed proteins in this pathway and is essential for division.

FtsW localises next and is thought to recruit the penicillin binding protein FtsI, which integrates new peptidoglycan into the cell wall for septal growth. The final protein is FtsN, which is essential for division. Its exact function is not known, but it interacts with early and late-stage proteins at the septum and likely stabilises the ring. When septation is triggered, the Z-ring contracts and pulls the membranes and cell walls together, eventually dividing the mother cell into two daughter cells.

Recently, the dynamics of the Z-ring have been detailed in *B. subtilis.* Imaging of the Z-ring by Whitley *et al*., showed that there are three distinct stages to its assembly; nascent, mature and constricting (Whitley et al., 2021). In the nascent stage, the filaments assemble transiently over a large area of the midcell. In the mature stage, these filaments condense but do not yet constrict. In the final stage, around 10 minutes after the filaments condense, the Z-ring constricts until division is complete.

1.3.2 Peptidoglycan synthesis and cell division

Septal assembly spans from the cytoplasm out to the periplasm, allowing the dividing cell to coordinate the compartmental processes. As the Z-ring constricts, peptidoglycan must be modified and incorporated at the septa to facilitate the formation of the new poles. The process, as studied in *E. coli*, is summarised in **figure 1.3** (Teo and Roper, 2015, Egan et al., 2020). In this pathway, uridine diphosphate (UDP)- N-acetylmuramic acid (MurNAc) is formed from UDP-glucosamine (GlcNAc). A pentapeptide stem is attached to the UDP-MurNAc; the MurNAc is then

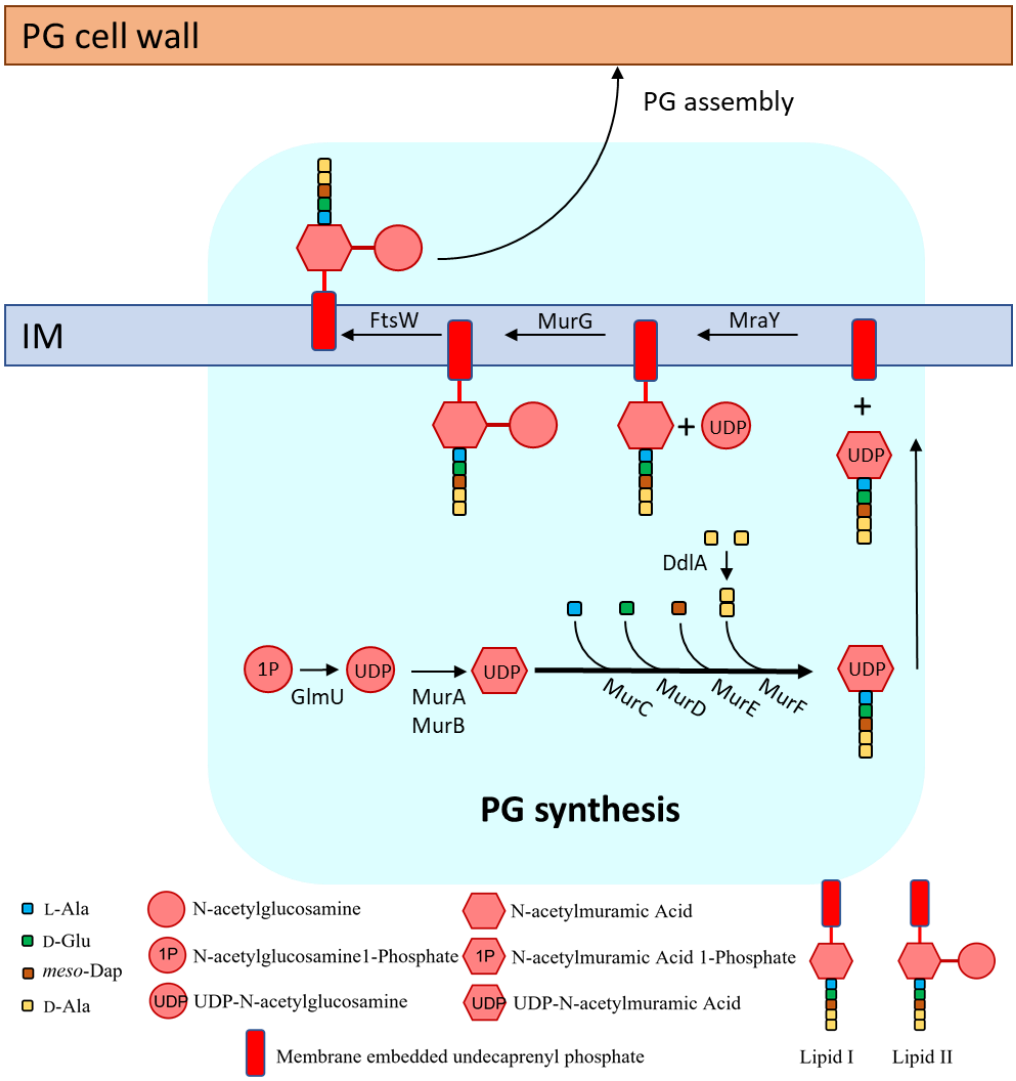

Figure 1.3. The peptidoglycan biosynthesis pathway as studied in *E. coli*. This cartoon shows the steps in the pathway for peptidoglycan synthesis. Glucosamine 1-phosphate is converted to uridine diphosphate (UDP) N-acetylglucosamine by GlmU, a bifunctional acetyltransferase/uridyltransferase. This is then converted to N-acetylmuramic acid (MurNAc) by MurA, a UDP-N-acetylglucosamine enolpyruvyl transferase, and MurB, a UDP-N-acetylenolpyruvoylglucosamine reductase. A pentapeptide stem is attached to the UDP-MurNAc in sequence; L-alanine by MurC (UDP-N-acetylmuramate--L-alanine ligase), a D-glutamine by MurD (UDP-N-acetylmuramoylalanine--D-glutamate ligase), a *meso*-diaminopilemic acid (Dap) by MurE (UDP-N-acetylmuramoyl-L-alanyl-D-glutamate--2,6-diaminopimelate ligase) and then two D-alanines, previously ligated by DdlA (D-alanine--D-alanine ligase A), by MurF (UDP-N-acetylmuramoyl-tripeptide--D-alanyl-D-alanine ligase). The MurNAc is then transferred to membrane bound undecaprenyl pyrophosphate, forming Lipid I, by MraY, a Phospho-N-acetylmuramoyl-pentapeptide-transferase. A

GlcNAc sugar is attached to the MurNAc by MurG, a UDP-N-acetylglucosamine--N-acetylmuramyl-(pentapeptide) pyrophosphoryl-undecaprenol N-acetylglucosamine transferase, forming a membrane bound disaccharide, Lipid II. A flippase, FtsW, transports this across the inner membrane, where it can be incorporated into the cell wall (Teo and Roper, 2015, Egan et al., 2020).

transferred to membrane bound undecaprenol, forming Lipid I. A GlcNAc sugar is attached to the MurNAc forming a membrane bound disaccharide. A flippase transports this across the inner membrane, where it can be incorporated into the cell wall.

B. bacteriovorus needs to have enough cell wall material to produce as many progeny as possible and to undergo successful septation. The traditional source of peptidoglycan in bacteria is through synthesis. The other source available to *B. bacteriovorus* is from the prey. Digested muropeptides could be taken up, potentially being used directly and incorporated into the cell wall, or fed back into the peptidoglycan synthesis pathway. It is currently unknown how this material is taken up by the predator, and what the pathway for its utilisation looks like. The timings of these processes are also unknown; the predator may only synthesise peptidoglycan at septation, while lateral growth is fuelled by host digestion products, or vice versa. This is explored further in chapter 5.

1.3.3 The *division and cell wall* cluster

The *division and cell wall* (*dcw*) cluster is a region of the genome highly conserved in rod-shaped bacteria that codes for many of the septal assembly and peptidoglycan synthesis proteins; in *E. coli*, the *dcw* cluster encodes fifteen genes in a single operon for these purposes (Vicente et al., 1998). Other rod-shaped bacteria have additional genes, such as *ylm* genes for sporulation in the *B. subtilis* cluster, which are usually linked to septation. The genes that are most conserved in bacterial *dcw* clusters are noted as “ancestral” in this thesis, and *B. bacteriovorus* has homologues for most of them. They also, however, have many novel gene insertions in this region. This is also investigated further in chapter 5.

1.3.4 Chromosome partitioning: ParAB

The ParABS system of chromosome segregation is highly conserved in most prokaryotes. This system regulates the partitioning of chromosomes during division to ensure that each daughter cell has a full copy of the genome. Mechanistically, the three elements of this system, ParA, ParB and *parS*, operate via a ratchet diffusion model (Jindal and Emberly, 2019). When bound to the *parS* element and cytidine triphosphate (CTP), the ParB homodimer, which is a CTP hydrolase, closes to form a ring structure around the *parS* element (Soh et al., 2019, Osorio-Valeriano et al., 2021). This changes the conformation of the *parS* binding region of ParB, resulting in reduced affinity to it, and allowing ParB to slide laterally while the DNA is held in the ring. CTP hydrolysis results in the opening of the ring and release of DNA, controlling the length of time ParB is associated to the DNA. ParA can dimerise and bind DNA without specificity when bound to ATP. The movement of ParB that leads to chromosome segregation is activated by its interaction with the DNA-bound ParA-ATP, also activating the ATPase activity of the latter complex and causing its dissociation from the chromosome. The resultant ParA-ADP can bind DNA again after a delay and phosphorylation. As ParB moves along the chromosome, it leaves behind a region of DNA not bound by ParA-ATP preventing any reversal of direction, hence the ratchet diffusion model.

1.4 MinCDE: septal site selection in *E. coli*

In *E. coli*, the MinCDE protein system is used to determine where the septum should form. This Gram-negative bacterium divides via binary fission, meaning that one septum is required and two identical progeny are produced. For there to be two daughter cells, each with a full genetic complement, septation must occur at the midcell. The MinCDE system is used to prevent Z-ring formation at the poles (Arumugam et al., 2014, Lutkenhaus, 2007).

An interesting aspect of this system is the oscillation of the MinCDE proteins, a phenomenon also now reported in the *B. subtilis* MinCD/DivIVA system discussed below. Originally thought to be a static system, MinD assembles on the membrane at the poles of the cell. MinC, an inhibitor of FtsZ ring

formation, is then recruited to MinD. MinE forms a ring at the site of MinD localisation, preventing the assembly of MinCD at the midcell by causing MinD to hydrolyse ATP, making it dissociate from the membrane. Mutants lacking these proteins undergo asymmetrical division, producing a large cell, containing the DNA, and a small cell, containing none.

With the use of fluorescent protein fusions, this system has been observed to oscillate from pole to pole. Since first being observed, this oscillation has also been characterised and reviewed (Martos et al., 2015, Arumugam et al., 2014, Lutkenhaus, 2007). MinE activates ATPase activity of MinD, causing it to disassemble at the pole. It can then be seen assembling at the opposite pole, followed by the MinE ring formation. MinC is recruited by MinD, but unlike MinD and MinE it cannot independently assemble at the poles. This leads to a two-protein system oscillating between the poles, preventing Z-ring formation at the poles.

1.4.1 Septation in *Bacillus subtilis*: MinCD and DivIVA

The system used for septal site selection in *Bacillus subtilis* is superficially very similar to *E. coli*. *B. subtilis* use the MinCD proteins and a third protein, DivIVA, which is paralogous to MinE from *E. coli* (Monahan et al., 2014). In this system, DivIVA forms a tetramer capable of sensing negative curvature in the cell. It was initially considered to be tethered at the poles; however, recent fluorescence microscopy has shown that the *Bacillus* system is dynamic (Bach et al., 2014). MinCD and DivIVA appear to migrate from the poles to the new septa during division. This has been suggested to prevent reinitiation of the division machinery, limiting the cell to one split per cell cycle. In addition, DivIVA in *Bacillus* has been implicated in sporulation where it determines the division site and coordinates relocating the chromosome into the prespore (Abhyankar et al., 2014, Perry and Edwards, 2006).

In *B. subtilis*, DivIVA has multiple roles through the cell cycle, evidenced by its interaction partners (Hammond et al., 2019). During sporulation, it interacts with RacA and the ParAB chromosomal segregation system to help localise the asymmetric position of the septum, as well as to facilitate compartment specific differential gene expression via sequestering SpoIIE, a regulatory

phosphatase. Another role is seen when the cell becomes competent; DivIVA sequesters the post-transcriptional regulator ComN, and stalls cell division via an interaction with transcription factor Maf. The importance of phosphorylation to the function of DivIVA has also been studied. PtkA, a tyrosine kinase that localises to the cell walls in a MinD-dependent manner, can phosphorylate DivIVA, with the likely possibility of other kinase interactions. The phosphorylation states of several DivIVA residues are thought to affect both vegetative growth and sporulation. In this system, null DivIVA mutants display inefficient cell division and sporulation.

Although initially studied in Firmicutes, DivIVA homologues have been seen in several other bacteria. It is present in Actinobacteria, such as *Streptomyces* and *Mycobacteria*, as well as in some Gram-negative bacteria, particularly in Deltaproteobacteria, such as *Geobacter* and *Myxococcus*. What is notable of these bacteria, is that their cell morphology and manner of division can vary greatly. Examples in Gram-negative bacteria are poorly studied, with most research focussing on Firmicutes and Actinobacteria, where DivIVA has very varied roles. Below are some examples of systems with a DivIVA homologue.

1.4.2 DivIVA in *Streptomyces*

Streptomyces coelicolor is a bacterium with a DivIVA homologue that is essential for survival (Hempel et al., 2008, Flardh, 2003, Hammond et al., 2019). DivIVA null mutants could not be produced, likely due to the unusual growth mode of *S. coelicolor*, but several partial DivIVA null mutants could be obtained, and showed varied growth phenotypes such as irregular hyphal growth and multiple branches. They conclude that DivIVA designates the growing pole of the hyphae, as well as observing the migration of DivIVA to determine new branching sites. DivIVA might be required to switch from vegetative hyphae to aerial hyphae, an essential function not required in the other discussed models. Despite the growth differences, DivIVA does share some roles that are seen with *B. subtilis* homologue. In, *S. coelicolor*, DivIVA is also phosphorylated by a serine/threonine kinase. It also interacts with the ParABS system to tether and segregate the chromosome during division, with a potential interaction between DivIVA and ParB (Kois-Ostrowska et al., 2016).

1.4.3 DivIVA in *Mycobacteria*

DivIVA has also been associated with growth in *Mycobacterium smegmatis*, a system without MinCD (Kang et al., 2008, Choukate and Chaudhuri, 2020). Fluorescent DivIVA was seen to be more concentrated at the sub-polar region of the growing pole, and interaction assays showed that DivIVA was interacting with enzymes responsible for integrating peptidoglycan into the cell wall (Meniche et al., 2014). This suggested that DivIVA was directing subpolar, lateral growth. Further studies also observed colocalisation, and direct interaction, between DivIVA and ParA (Ginda et al., 2013). More recently, it has been shown that elongation of the cell is modulated by competition between the nucleoid and DivIVA for the interaction of ParA (Pioro et al., 2019). As with other systems, DivIVA is phosphorylated in *M. smegmatis*. It is also implicated in the oxidative stress response where it protects FtsI, a division specific transpeptidase responsible for coordinating growth at the septum, from proteolysis when exposed to oxidative agents (Mukherjee et al., 2009).

1.5 Studied division homologues in *B. bacteriovorus*

Previous studies have identified several division protein homologues in *B. bacteriovorus*. David Milner (PhD, Sockett lab) has previously studied the *divIVA* homologue, *bd0464*, and the operon it is a part of, *bd0466-bd0463*. Like the Actinobacterial examples above, *B. bacteriovorus* does not have a MinCD system for septal site selection. Milner's investigation has provided a foundation for further study of the role of DivIVA in this system. Additionally, he identified three *parA* homologues and a single *parB* homologue, which he also investigated. His specific findings can be found in the introduction to chapter 3, followed by my continued investigation into *divIVA*, its genomic neighbours and its encoded protein interaction partners, as well as its connection to the *parAB* system in *B. bacteriovorus*.

B. bacteriovorus has most of the homologues for Z-ring and divisome assembly, largely transcribed from its *dcw* cluster; many of the homologues for cell wall synthesis are also transcribed from here. These are further discussed in chapter 5, where I bioinformatically investigate adaptations to the *dcw*

cluster, the whole peptidoglycan biosynthesis pathway and how *B. bacteriovorus* utilises digested prey peptidoglycan.

1.6 Research questions upon which my thesis is based:

- What are the interacting partners of DivIVA, and how do they relate to the host dependent cycle?
    - Does it interact with the other proteins encoded from the *divIVA* operon?
    - Do these include known division homologues such as ParA or septal assembly proteins?
    - Does DivIVA interact with any other systems, such as the response to reactive oxygen species (seen in *Mycobacterium*)? Why might these be connected to cell division?
- What roles do the other proteins encoded from the *divIVA* operon have, and how do they contribute to coordinating division and growth in the bdelloplast?
- How is the *dcw* cluster of *B. bacteriovorus* organised and adapted for an intracellular predatory lifestyle?
    - How does this relate to the progression of the HD lifecycle?
    - What signals are required for this progression?
- How does *B. bacteriovorus* utilise prey peptidoglycan, and how does this connect to the traditional biosynthesis of peptidoglycan?

2 Chapter 2: Materials and methods

2.1 Strains, plasmids, and primers

2.1.1 Bacterial strains

The subject of this study was the genome sequenced *B. bacteriovorus* HD100, originally isolated from soil, NCBI:txid264462 (https://www.ncbi.nlm.nih.gov/Taxonomy/Browser/wwwtax.cgi?id=264462) (Rendulic et al., 2004, Stolp, 1968).

Strain	**Description**	**Source**
HD100	Wild-type *Bdellovibrio bacteriovorus* strain, genome sequenced	(Rendulic et al., 2004)
HD100 DivIVA-mCherry	HD100 with pK18::DivIVA-mCherry integrated at *bd0464* (*divIVA*) locus	David Milner (former PhD) (Milner et al., 2020)
HD100 Δ*divIVA*	HD100 with *bd0464* markerless deletion	David Milner (former PhD) (Milner et al., 2020)
Hd100 Bd0465-mCherry	HD100 with single-crossover of pK18::Bd0465-mCherry; *bd0465* ORF fused to mCherry expressed from native promoter, and promoterless copy of *bd0465*	This study (Milner et al., 2020)
HD100 Bd0466-mTeal	HD100 with single-crossover of pK18::Bd0466-mTeal; *bd0466* ORF fused to mCherry expressed from native promoter, and promoterless copy of *bd0466*	This study (Milner et al., 2020)
HD100 Δ*divIVA*	HD100 with *bd0464* markerless deletion	David Milner (former PhD) (Milner et al., 2020)

HD100 pSUP404.2	HD100 with empty pSUP404.2 vector	David Milner (former PhD) (Milner et al., 2020)
Δ*divIVA* pSUP404.2	HD100 Δ*divIVA* with empty pSUP404.2 vector	David Milner (former PhD) (Milner et al., 2020)
Δ*divIVA* pSUP404.2 DivIVA	HD100 Δ*divIVA* with pSUP404.2 DivIVA complementation vector	David Milner (former PhD) (Milner et al., 2020)
Δ*divIVA* pSUP404.2 DivIVA(A78T)	HD100 Δ*divIVA* with pSUP404.2 DivIVA(A78T) complementation vector	David Milner (former PhD) (Milner et al., 2020)
HD100 pSUP404.2 DivIVA	HD100 with pSUP404.2 DivIVA complementation vector	David Milner (former PhD) (Milner et al., 2020)
HD100 pSUP404.2 DivIVA(A78T)	HD100 with pSUP404.2 DivIVA(A78T) complementation vector	David Milner (former PhD) (Milner et al., 2020)
HD100 *ParA1*-mCherry	HD100 with pK18 *parA1*-mCherry integrated at *bd1326* (*parA1*) locus	David Milner (former PhD) (Milner et al., 2020)
HD100 *ParA2*-mCherry	HD100 with pK18 *parA2*-mCherry integrated at *bd2331* (*parA2*) locus	David Milner (former PhD) (Milner et al., 2020)
HD100 *ParA3*-mCherry	HD100 with pK18 *parA3*-mCherry integrated at *bd3906* (*parA3*) locus	David Milner (former PhD) (Milner et al., 2020)
HD100 *Bd0064*-mCerulean	HD100 with pK18 *bd0064*-mCerulean integrated at *bd0064* locus	Provided by Paul Radford
HD100 *Bd0064*-mCerulean	HD100 with pK18 *bd0064*-mCerulean integrated at *bd0064*	(Milner et al., 2020)

DivIVA-mCherry	locus and single-crossover of pK18 DivIVA-mCherry.	
DH5α	F- *endA1 hsdR17* ($r_k^- mk^-$) *supE44* thi-1 *recA1 gyrA* (Nal^r) *relA1* Δ(lacIZYA-argF) U169 *deoR* (80dlacΔ(lacZ)M15); used as a cloning strain	(Hanahan, 1983)
S17-1	*thi*,*pro*,*hsdR*-,*hsdM*+,*recA*; integrated plasmid RP4-Tc::Mu-Kn::Tn7; used as donor for conjugating plasmids into *B. bacteriovorus*	(Simon et al., 1983)
BTH101	F-,Δ*cya*99, *gal*E15, *gal*K16, *rps*L1, *hsd*R2, *mcr*A1, *mcr*B1	(Karimova et al., 2005)
BTH101-G	F-,Δ*cya*99, *gal*E15, *gal*K16, *rps*L1, *hsd*R2, *mcr*A1, *mcr*B1	(Houot et al., 2012) Gift from the Tracy Palmer lab
MG1655	F- lambda- *ilvG*- *rfb*-50 *rph*-1	(Jensen, 1993)

Table 2.1. Bacterial strains used in this thesis.

2.1.2 Plasmids

Plasmid	**Description**	**Source**
pK18mobsacB	Kn^r suicide vector used for conjugation and recombination into *Bdellovibrio* genome	(Schafer et al., 1994)
pSUP404.2	Kn^r, Cm^r *Bdellovibrio* mobilizable vector, used for *in trans* complementation in *B. bacteriovorus*	(Roschanski and Strauch, 2011)
pZMR100	λ defective vector, Kn^r. Used to confer Kn^r to S17-1 used as prey	(Rogers et al., 1986)
pAKF56	Amp^r vector containing *mCherry* gene for cloning of ORFs for fluorescent tagging	(Fenton et al., 2010)

pAKF04	Amp^r vector containing *mTFP* gene for cloning of ORFs for fluorescent tagging	(Fenton et al., 2010)
pAKF56::bd0465	The *bd0465* ORF (plus 48 bp additional 5' DNA) was amplified from HD100 genomic DNA using primers Bd0465Fluo-CtagF and Bd0465Fluo-CtagR and the PCR product was cut with EcoRI and KpnI and ligated into pAKF56. The resulting plasmid had the *bd0465* ORF (minus the stop codon) upstream of *mCherry*.	This study
pAKF04::bd0466	The *bd0466* ORF (plus 48 bp additional 5' DNA) was amplified from HD100 genomic DNA using primers Bd0466Fluo-CtagF and Bd0466Fluo-CtagR and the PCR product was cut with EcoRI and KpnI and ligated into pAKF04. The resulting plasmid had the *bd0466* ORF (minus the stop codon) upstream of *mTeal*.	This study
pK18::bd0465-mCherry	The bd0465-mCherry fragment was cut out of the pAKF56::bd0465 plasmid using EcoRI and HindIII and ligated into pK18*mobsacB* using the same enzymes.	This study
pK18::bd0466-mTeal	The bd0465-mCherry fragment was cut out of the pAKF04::bd0466 plasmid using EcoRI and HindIII and ligated into pK18*mobsacB* using the same enzymes.	This study (Milner et al., 2020)

pK18::DivIVA-mCherry	The DivIVA-mCherry fragment was cut out of the pAKF56::DivIVA plasmid (see Milner's thesis) using EcoRI and HindIII and ligated into pK18*mobsacB* using the same enzymes.	This study (Milner et al., 2020)
pSUP404.2 DivIVA	The *divIVA* fragment was cut out of the pUC19 DivIVA plasmid (see Milner's thesis) using EcoRI and ligated into pSUP404.2 using the same enzyme.	David Milner (former PhD) (Milner et al., 2020)
pSUP404.2 DivIVA(A78T)	The *divIVA* A78T fragment was cut out of the pUC19 DivIVA(A78T) plasmid (see Milner's thesis) using EcoRI and ligated into pSUP404.2 using the same enzyme.	David Milner (former PhD) (Milner et al., 2020)
pK18::ParA1-mCherry	The ParA1-mCherry fragment was cut out of the pAKF56::ParA1 plasmid (see Milner's thesis) using EcoRI and HindIII and ligated into pK18*mobsacB* using the same enzymes.	David Milner (former PhD) (Milner et al., 2020)
pK18::ParA2-mCherry	The ParA2-mCherry fragment was cut out of the pAKF56::ParA2 plasmid (see Milner's thesis) using EcoRI and HindIII and ligated into pK18*mobsacB* using the same enzymes.	David Milner (former PhD) (Milner et al., 2020)
pK18::ParA3-mCherry	The Bd3906-mCherry fragment was cut out of the pAKF56::Bd3906 plasmid (David Milner) using EcoRI and HindIII and ligated into	David Milner (former PhD) (Milner et al., 2020)

	pK18*mobsacB* using the same enzymes.	
pKT25	Kn^r vector for fusion of gene to C-terminus of Cya-T25	David Milner (former PhD) (Karimova et al., 2001)
pUT18C	Amp^r vector for fusion of gene to C-terminus of Cya-T18 as a C-terminal tag	(Karimova et al., 2001)
pUT18	Amp^r vector for fusion of gene to C-terminus of Cya-T18 as an N-terminal tag	(Karimova et al., 2001)
pUT18+1	As above, with an additional nucleotide in the linker domain between the gene insert and the C-terminus of Cya-T18.	Tracy Palmer lab (Houot et al., 2012)
pKT25-zip	pKT25 containing the leucine zipper region from yeast GCN4	(Karimova et al., 2001)
pUT18C-zip	pUT18C containing the leucine zipper region from yeast GCN4	(Karimova et al., 2001)
pKT25-divIVA	The *bd0464* ORF was amplified from HD100 genomic DNA using primers divIVA_BTH_F and divIVA_BTH_R and the PCR product was cut with KpnI and XbaI and ligated into pKT25.	Constructed by Rob Till for this study
pUT18C-divIVA	As above but ligated into pUT18C.	Constructed by Rob Till for this study
pKT25-parA3	The *bd3906* ORF was amplified from HD100 genomic DNA using primers parA_BTH_F and parA_BTH_R and	Constructed by Rob Till for this study

	the PCR product was cut with KpnI and XbaI and ligated into pKT25.	
pUT18C-parA3	As above but ligated into pUT18C.	Constructed by Rob Till for this study
pKT25-parB	The *bd3905* ORF was amplified from HD100 genomic DNA using primers parB_BTH_F and parB_BTH_R and the PCR product was cut with KpnI and XbaI and ligated into pKT25.	Constructed by Rob Till for this study
pUT18C-parB	As above but ligated into pUT18C.	Constructed by Rob Till for this study
pKT25-bd0463	The *bd0463* ORF was amplified from HD100 genomic DNA using primers bd0463_BTH_F and bd0463_BTH_R and the PCR product was cut with KpnI and XbaI and ligated into pKT25.	Constructed by Rob Till for this study
pUT18C-bd0463	As above but ligated into pUT18C.	Constructed by Rob Till for this study
pKT25-bd0466	The *bd0466* ORF was amplified from HD100 genomic DNA using primers bd0466_BTH_F and bd0466_BTH_R and the PCR product was cut with KpnI and XbaI and ligated into pKT25.	Constructed by Rob Till for this study
pUT18C-bd0466	As above but ligated into pUT18C.	Constructed by Rob Till for this study

pKT25-bd0465	The *bd0465* ORF was amplified from HD100 genomic DNA using primers bd0465_BTH_F and bd0465_BTH_R and the PCR product was cut with KpnI and XbaI and ligated into pKT25.	Constructed by Rob Till for this study
pUT18C-bd0465	As above but ligated into pUT18C.	Constructed by Rob Till for this study
pKT25-ftsA	The *bd3190* ORF was amplified from HD100 genomic DNA using primers ftsA_BTH_F and ftsA_BTH_R and the PCR product was cut with KpnI and XbaI and ligated into pKT25.	Constructed by Rob Till for this study
pUT18C-FtsA	As above but ligated into pUT18C.	Constructed by Rob Till for this study
pKT25-ftsK	The *bd0041* ORF was amplified from HD100 genomic DNA using primers ftsK_BTH_F and ftsK_BTH_R and the PCR product was cut with KpnI and XbaI and ligated into pKT25.	Constructed by Rob Till for this study
pUT18C-ftsK	As above but ligated into pUT18C.	Constructed by Rob Till for this study
pKT25-bd0548	The *bd0548* ORF was amplified from HD100 genomic DNA using primers pKT25-Bd0548_BTH_gibF and pKT25-Bd0548_BTH_gibR, and the PCR product was ligated into KpnI/XbaI digested pKT25 using the Gibson Assembly kit.	This study

pUT18C-bd0548	The *bd0548* ORF was amplified from HD100 genomic DNA using primers pUT18C-Bd0548_BTH_gibF and pUT18C-Bd0548_BTH_gibR, and the PCR product was ligated into KpnI/XbaI digested pUT18C using the Gibson Assembly kit.	This study
pKT25-bd2107	The *bd2107* ORF was amplified from HD100 genomic DNA using primers pKT25-Bd2107_BTH_gibF and pKT25-Bd2107_BTH_gibR, and the PCR product was ligated into KpnI/XbaI digested pKT25 using the Gibson Assembly kit.	This study
pUT18C-bd2107	The *bd2107* ORF was amplified from HD100 genomic DNA using primers pUT18C-Bd2107_BTH_gibF and pUT18C-Bd2107_BTH_gibR, and the PCR product was ligated into KpnI/XbaI digested pUT18C using the Gibson Assembly kit.	This study
pKT25-bd3538	The *bd3538* ORF was amplified from HD100 genomic DNA using primers pKT25-Bd3538_BTH_gibF and pKT25-Bd3538_BTH_gibR, and the PCR product was ligated into KpnI/XbaI digested pKT25 using the Gibson Assembly kit.	This study
pUT18C-bd3538	The *bd3538* ORF was amplified from HD100 genomic DNA using primers pUT18C-Bd3538_BTH_gibF and pUT18C-Bd3538_BTH_gibR, and the PCR product was ligated into	This study

	KpnI/XbaI digested pUT18C using the Gibson Assembly kit.	
pUT18C-Lib	pUT18C plasmid ligated with random digested *B. bacteriovorus* genomic material between 500 and 2000 bp.	This study
pUT18-Lib	pUT18 plasmid ligated with random digested *B. bacteriovorus* genomic material between 500 and 2000 bp.	This study
pUT18+1-Lib	pUT18+1 plasmid ligated with random digested *B. bacteriovorus* genomic material between 500 and 2000 bp.	This study

Table 2.2. Plasmids used in this study.

2.1.3 Primers

Primer	**Sequence**	**Description**
Fluorescent construct		
Bd0465Fluo-CtagF	GTACTGGAATT CATGAATCCCT TGTTGAAATC	Has one random 5’ base for cutting efficiency, then an EcoRI site followed by a sequence 48 bp upstream of the *bd0465* ORF.
Bd0465Fluo-CtagR	AGTCAGGGTAC CTTTGATTTCCC GGGCCATTT	Has two random 5’ bases for cutting efficiency, then a KpnI site followed by a reverse complemented sequence at the 3’ of *bd0465* with the TAA stop codon deleted.
Bd0466Fluo-CtagF	GTACTGGAATT CATGGCATTAA AAGAGATCAC	Has one random 5’ base for cutting efficiency, then an EcoRI site followed by a sequence 48 bp upstream of the *bd0466* ORF.

Bd0466Fluo-CtagR	AGTCAGGGTACCCCCTTTGGCGGGACGTTCGC	Has two random 5’ bases for cutting efficiency, then a KpnI site followed by a reverse complemented sequence at the 3’ of *bd0466* with the TAA stop codon deleted.
Bacterial Two Hybrid		
divIVA_BTH_F	CCAGACTCTAGACATGAGAATTACTCCTATCGA	Has six random 5’ bases for cutting efficiency, then an XbaI site, followed by an additional C to keep ORF in frame and the first 20 bases of the *divIVA* (*bd0464*) ORF.
divIVA_BTH_R	AATGTGGGTACCTTATTCAGCAGAAAGAGGGG	Has six random 5’ bases for cutting efficiency, then a KpnI site followed by a reverse complemented sequence at the 3’ of *divIVA* (*bd0464*).
parA_BTH_F	CCAGACTCTAGACATGGCAAAAACAATCTGCAT	Has six random 5’ bases for cutting efficiency, then an XbaI site, followed by an additional C to keep ORF in frame and the first 20 bases of the *parA3* (*bd3906*) ORF.
parA_BTH_R	AATGTGGGTACCTTATGCCATTTGTTCTGTCT	Has six random 5’ bases for cutting efficiency, then a KpnI site followed by a reverse complemented sequence at the 3’ of *parA3* (*bd3906*).
parB_BTH_F	CCAGACTCTAGACATGTCTGATATTGCTGTAGA	Has six random 5’ bases for cutting efficiency, then an XbaI site, followed by an additional C to keep ORF in frame and the

		first 20 bases of the *parB* (*bd3905*) ORF.
parB_BTH_R	AATGTGGGTAC CTTACTGCCATC CTTCTTTAA	Has six random 5' bases for cutting efficiency, then a KpnI site followed by a reverse complemented sequence at the 3' of *parB* (*bd3905*).
Bd0463_BTH_F	CCAGACTCTAG ACATGATTGAA GCAACAAAAGG	Has six random 5' bases for cutting efficiency, then an XbaI site, followed by an additional C to keep ORF in frame and the first 20 bases of the *bd0463* ORF.
Bd0463_BTH_R	AATGTGGGTAC CTTAGGGAAGC CTCAGTGCTT	Has six random 5' bases for cutting efficiency, then a KpnI site followed by a reverse complemented sequence at the 3' of *bd0463.*
Bd0466_BTH_F	CCAGACTCTAG ACATGGCATTA AAAGAGATCAC	Has six random 5' bases for cutting efficiency, then an XbaI site, followed by an additional C to keep ORF in frame and the first 20 bases of the *bd0466* ORF.
Bd0466_BTH_R	AATGTGGGTAC CCTACCCTTTGG CGGGACGTT	Has six random 5' bases for cutting efficiency, then a KpnI site followed by a reverse complemented sequence at the 3' of *bd0466.*
Bd0465_BTH_F	CCAGACTCTAG ACATGAATCCC TTGTTGAAATC	Has six random 5' bases for cutting efficiency, then an XbaI site, followed by an additional C to keep ORF in frame and the first 20 bases of the *bd0465* ORF.

Bd0465_BTH_R	AATGTGGGTAC CTTATTTGATTT CCCGGGCCA	Has six random 5’ bases for cutting efficiency, then a KpnI site followed by a reverse complemented sequence at the 3’ of *bd0465.*
FtsA_BTH_F	CCAGACTCTAG ACATGAGTACA TCAAAACCCAA	Has six random 5’ bases for cutting efficiency, then an XbaI site, followed by an additional C to keep ORF in frame and the first 20 bases of the *ftsA* (*bd3190*) ORF.
FtsA_BTH_R	AATGTGGGTAC CTTAAAAAATC TGTCCAAAAA	Has six random 5’ bases for cutting efficiency, then a KpnI site followed by a reverse complemented sequence at the 3’ of *ftsA* (*bd3190*).
FtsK_BTH_F	CCAGACTCTAG ACATGAACCAA TTCCTTAAAAA G	Has six random 5’ bases for cutting efficiency, then an XbaI site, followed by an additional C to keep ORF in frame and the first 20 bases of the *ftsK* (*bd0041*) ORF.
FtsK_BTH_R	AATGTGGGTAC CTTATTGTTCTC TGTAACTAC	Has six random 5’ bases for cutting efficiency, then a KpnI site followed by a reverse complemented sequence at the 3’ of *ftsk* (*bd0041*).
pKT25-Bd0548_BTH_gibF	CACGCGGCGGG CTGCAGGGTCG ACTCAGATTGA AAAAAACCTGA AAG	Designed in NEBuilder for ligation into KpnI/XbaI cut pKT25 using the Gibson Assembly kit.

pKT25-Bd0548_BTH_gibR	GCCGAATTCTTAGTTACTTAGGTACTCATAGTTTTCTCCTCAGC	Designed in NEBuilder for ligation into KpnI/XbaI cut pKT25 using the Gibson Assembly kit.
pUT18C-Bd0548_BTH_gibF	AGTGGAACGCCACTGCAGGTCGACTCAGATTGAAAAAACCTGAAAG	Designed in NEBuilder for ligation into KpnI/XbaI cut pUT18C using the Gibson Assembly kit.
pUT18C-Bd2107_BTH_gibR	ATATCGATGAATTCGAGCTCGGTACTCATAGTTTTCTCCTCAGC	Designed in NEBuilder for ligation into KpnI/XbaI cut pUT18C using the Gibson Assembly kit.
pKT25-Bd2107_BTH_gibF	CACGCGGCGGGCTGCAGGGTCGACTTCCAAGTTCCTGCTTATC	Designed in NEBuilder for ligation into KpnI/XbaI cut pKT25 using the Gibson Assembly kit.
pKT25-Bd2107_BTH_gibR	GCCGAATTCTTAGTTACTTAGGTACTTACTTTTTCAATGTTTTATAAGCAG	Designed in NEBuilder for ligation into KpnI/XbaI cut pKT25 using the Gibson Assembly kit.
pUT18C-Bd2107_BTH_gibF	AGTGGAACGCCACTGCAGGTCGACTTCCAAGTTCCTGCTTATC	Designed in NEBuilder for ligation into KpnI/XbaI cut pUT18C using the Gibson Assembly kit.
pUT18C-Bd2107_BTH_gibR	ATATCGATGAATTCGAGCTCGGTACTTACTTTTTCAATGTTTTATAAGCAG	Designed in NEBuilder for ligation into KpnI/XbaI cut pUT18C using the Gibson Assembly kit.

pKT25-Bd3538_BTH_gibF	CACGCGGCGGGCTGCAGGGTCGACTCGTATTGTTCTGGTTCGC	Designed in NEBuilder for ligation into KpnI/XbaI cut pKT25 using the Gibson Assembly kit.
pKT25-Bd3538_BTH_gibR	GCCGAATTCTTAGTTACTTAGGTACCTAACGATTGCGGTTCTG	Designed in NEBuilder for ligation into KpnI/XbaI cut pKT25 using the Gibson Assembly kit.
pUT18C-Bd3538_BTH_gibF	AGTGGAACGCCACTGCAGGTCGACTCGTATTGTTCTGGTTCGC	Designed in NEBuilder for ligation into KpnI/XbaI cut pUT18C using the Gibson Assembly kit.
pUT18C-Bd3538_BTH_gibR	ATATCGATGAATTCGAGCTCGGTACCTAACGATTGCGGTTCTG	Designed in NEBuilder for ligation into KpnI/XbaI cut pUT18C using the Gibson Assembly kit.
RT-PCR		
RT-PCRBd0466F	GATTGGCCACCTTCAAAAGA	Forward primer to detect transcription of *bd0466* by RT-PCR; 89 bp product
RT-PCRBd0466R	CCAGTCCTGCCAGTACATCA	Reverse primer to detect transcription of *bd0466* by RT-PCR; 89 bp product
RT-PCRBd0465F	TCACGACGAGGATCAGTTTG	Forward primer to detect transcription of *bd0465* by RT-PCR; 91 bp product
RT-PCRBd0465R	CCAGTCCTGCCAGTACATCA	Reverse primer to detect transcription of *bd0465* by RT-PCR; 91 bp product

Table 2.3. Primers used in this study.

2.2 Bacterial growth media and conditions

2.2.1 Growth media

All formulae are for 1 L of medium.

2.2.1.1 YT broth and agar for growth of *E. coli* strains.

5 g NaCl, 5 g Difco Bacto Yeast Extract, 8 g Difco Bacto Tryptone, Adjusted to pH 7.5 with 2 M NaOH. Solidified with Sigma-Aldrich Select agar A5054 at 10 gL^{-1}

2.2.1.2 Mu broth for use in bacterial two hybrid assays

10 g Difco Bacto Tryptone, 5 g Difco Bacto Yeast Extract, 10 g NaCl, 2 ml 1 M NaOH (to pH ~7.0).

2.2.1.3 SOC broth for transformations of *E. coli*.

20 g Difco Bacto Tryptone, 5 g Difco Bacto Yeast Extract, 0.58 g NaCl, 0.186 g KCl, 2.03 g $MgCl_2$, 2.46 g $MgSO_4$, 3.6 g Glucose.

2.2.1.4 Calcium-HEPES (CaHEPES) buffer for host dependent *B. bacteriovorus* predatory cultures.

5.94g HEPES, 0.294 g $CaCl_2.2H_2O$, adjusted to pH 7.6 with 2 M NaOH.

2.2.1.5 YPSC agar for overlay plates.

1 g Difco Bacto Yeast Extract, 1 g Difco Bacto Peptone, 0.5 g Anhydrous Sodium Acetate, 0.25 g $MgSO_4.7H_2O$, adjusted to pH 7.6 with 2 M NaOH. Added sterile $CaCl_2$ from a 25 g L^{-1} stock to give 0.25 g L^{-1} after autoclaving.

YPSC-T agar solidified with Sigma-Aldrich Select agar A5054 at 6 g L^{-1}; YPSC-B agar solidified with Sigma-Aldrich Select agar A5054 at 10 g L^{-1}. For a lower percentage of agar in YPSC-T, the amount of agar added was adjusted accordingly.

2.2.1.6 Nutrient agar for bacterial two hybrid spot plates.

Made as per manufacturer's instructions: 28 g per L.

2.2.1.7 MacConkey agar for bacterial two hybrid library assays

Made as per manufacturer's instructions: 52 g per L

2.2.1.8 Supplements

Supplement	Stock concentration (mg/ml)	Final concentration (μg/ml)
Kanamycin (Kn)	50 (AnalaR)	25 (bacterial two hybrid) 50 (all other applications)
Ampicillin (Amp)	50 (AnalaR)	50

Isopropyl β-D-1-thiogalactopyranoside (IPTG)	200 (AnalaR)	20
5-bromo-4-chloro-3-indolyl-β-D-galactopyranoside (X-gal)	20 (Dimethylformamide, DMF)	40

Table 2.4. Supplements used in *B. bacteriovorus* and *E. coli* growth

2.2.2 Growth conditions

2.2.2.1 Host dependent *B. bacteriovorus* used for fluorescence microscopy (e.g. DivIVA-mCherry), time course microscopy and attack phase cell measurements.

HD *B. bacteriovorus* were regularly grown on overlay plates. For these, a bottom layer of YPSC-B was set in a plate. 5 ml of YSPC-T was mixed with 150 μl of prey culture, typically live stationary-phase *E. coli* S17-1 (~1 x 10^9 cfu ml^{-1}, see below for growth conditions), and poured over the YPSC-B and allowed to set. Regrowth of *B. bacteriovorus* frozen stocks would require 100 μl of the stock to be spotted over the top of the overlay plate. In other circumstances, such as with ex-conjugants, the *B. bacteriovorus* predatory culture could be mixed with the YPSC-T and poured. Plates were incubated upside down at 29 ^oC for 3-10 days.

B. bacteriovorus could be grown in CaHEPES buffer in the presence of live *E. coli* prey, termed a predatory culture. To do so, a "plug" of cleared overlay plate, extracted with a pipette, could be added to 2 ml of CaHEPES mixed with 150 μl of prey culture. This was incubated at 29 ^oC, 200 RPM shaking, until prey were completely lysed, confirmed by microscopy, in ~24 hours. HD strains could be maintained by subculturing every 24 hours using an inoculum from the previous predatory culture. These were typically 10 ml (10 ml CaHEPES, 600 μl prey culture, 200 μl previous predatory culture) or 50 ml predatory culture (50 ml CaHEPEs, 3 ml prey culture, 1 ml previous predatory culture), at 29^oC, 200 RPM shaking.

2.2.2.2 *E. coli* growth conditions, for use in predatory cultures, bacterial two hybrid assays, transformations, and conjugations into *B. bacteriovorus*

E. coli strains were grown as prey for *B. bacteriovorus* or for the purposes of cloning and conjugation. To isolate single colonies of frozen stocks, they were streaked onto YT agar and incubated at 37 ºC for 16 hours. Colonies were grown in liquid culture using YT broth and incubated at 37 ºC, shaking at 200 RPM. This typically yields around 1 x 10^9 cfu ml^{-1}.

For bacterial two hybrid assays, the BTH101 strain was used. These were grown from frozen stocks on YT agar, incubated at 29 ºC. BTH101 liquid cultures were grown in Mu broth, at 29 ºC shaking at 200 RPM. All steps for generating chemically competent cells or in transformations that were originally incubated at 37 ºC were instead incubated at 29 ºC.

2.3 Bacterial manipulations

2.3.1 Generating chemically competent cells for transformations

To make chemically competent *E. coli* strains DH5α and S17-1, 10 ml cultures were grown 16 hours in YT broth under standard conditions. This culture was diluted 1:100 with YT and grow to an OD_{600} of 0.4-0.6 and transferred to 50 ml falcon tubes. These were centrifuged at 5525 x *g* for 5 minutes at 4 ºC. Pellets were resuspended in 20 ml of 4 ºC TFB1 and incubated on ice for 5 minutes before being centrifuged again, with the same conditions as before. Pellets were then resuspended in 2 ml TFB2 and incubated on ice for 1 hour. These were divided into 200 µl aliquots in microcentrifuge tubes and snap frozen in liquid nitrogen for storage at -80 ºC. Before use, these were thawed on ice.

2.3.1.1 TFB1

To make 1 L

30 mM potassium acetate	2.94 g
10 mM $CaCl_2.2H_2O$	1.47 g
50 mM $MnCl_2.4H_2O$	9.90 g

100 mM RbCl	12.08 g
15% (v/v) Glycerol	187.5 ml 80% added After pH

Adjust pH to 5.8 using 1M acetic acid. Sterilise through a 0.2 μl filter.

2.3.1.2 TFB2

To make 1 L

10 mM MOPS	2.10 g
75 mM CaCl2	11.02 g
10 mM RbCl	1.2 g
15% (v/v) Glycerol	187.5 ml 80% added After pH

2.3.2 Transforming plasmids into *E. coli* strains

Chemically competent cells were thawed on ice. 1 μl of plasmid was added to the competent cells and incubated on ice for 30 minutes before being heat shocked at 42 ^{o}C for 1 minute. Cells were placed back on ice for 5 minutes. 1 ml of SOC medium was added to the cells which were then incubated at 37 ^{o}C, shaking at 200 rpm for 1 hour. Cells were then centrifuged at 17,000 x *g* for 1 minute and then resuspended in 100 μl of YT medium. Cells were then plated onto YT agar with any appropriate supplements and incubated for 16 hours at 37 ^{o}C.

2.3.3 Plasmid extraction from *E. coli* strains

For high-throughput screening of many *E. coli* transformants, a standard protocol was used based of alkaline-SDS lysis (Dong et al., 2007). 300 μl of each transformant culture, grown under standard conditions for 16 hours and with appropriate supplements, was transferred to a microcentrifuge tube, to which 300 μl of alkaline SDS was added and mixed by inversion. The reaction was neutralised with 300 μl of 3M potassium acetate, mixed by inversion. This was then centrifuged at 17,000 x *g* for 5 minutes. The supernatant was transferred to a microcentrifuge tube containing 700 μl of isopropanol and mixed by inversion. This was again centrifuged as above, and the supernatant removed. The remaining pellet was washed with 100 μl 70% ethanol, and centrifuged for a further minute. The supernatant was removed and the pellets

resuspended in 25 µl TE (10 mM Tris-HCl pH 8, 1 mM EDTA) containing 10 µg ml-1 RnaseA.

For high purity and yield of plasmids, the Sigma-Aldrich GenElute™ Plasmid Miniprep Kit was used, as per manufacturer's instructions. In short, a culture of *E. coli* cells was lysed using alkaline-SDS lysis. This was absorbed into a silica column, washed with ethanol, and eluted, typically into 50 µl of elution solution although smaller elutions were used for a greater concentration of plasmid. For larger elutions, typically 1 ml, the Sigma-Aldrich GenElute™ Plasmid Midiprep Kit was used with a similar manufacturer's protocol.

2.3.3.1 Alkaline SDS (1% SDS / 0.2M NaOH)

1 ml 10% SDS

1 ml 2M NaOH

8 ml water

2.3.4 Isolating genomic DNA from *B. bacteriovorus*

Isolating chromosomal DNA from *B. bacteriovorus* required the Sigma-Aldrich GenElute™ Bacterial Genomic DNA kit. A 10 ml predatory culture of *B. bacteriovorus*, grown for 16 hours and containing roughly 2.5 x 10^8 plaque forming units ml^{-1}, was centrifuged and processed according to manufacturer's instructions. This produces roughly 200-250 ng/µl of genomic material.

2.3.5 Conjugating plasmids into host dependent *B. bacteriovorus*

Conjugations are the most efficient method for transferring a plasmid into *B. bacteriovorus*, typically in the vector pK18*mobsac*B or PSUP404.2. A 50 ml predatory culture of wild type *B. bacteriovorus* HD100 was grown under standard conditions, of which 10 ml was centrifuged at 5525 x *g* for 20 minutes at 29 ºC. The pellet was resuspended in 100 µl CaHEPES and pipetted onto a sterile piece of Nytran SuPerCharge 0.45 µm Nylon Transfer Membrane immobilised on SPY agar. This was allowed to dry.

A 50 ml culture of the donor strain *E. coli* S17-1 was grown under standard condition with appropriate supplements (typically kanamycin^{50} for pK18*mobsac*B. 10 ml of the culture was centrifuged at 5525 x *g* for 10 minutes before the pellet was resuspended in 100 µl of YT. This was then pipetted onto

the membrane with the dry *B. bacteriovorus* and incubated at 29 ºC for 16 hours.

The membrane was removed using sterile forceps and the membrane placed into 1 ml CaHEPES. Cells were resuspended by repeatedly pipetting the medium over the membrane. The cells were then mixed with 100 µl of host cells (*E. coli* S17-1 containing plasmid pZMR for kanamycin resistance) grown under standard conditions. These were then added to 5 ml melted YPSC-T agar and poured over dry YPSC-B agar containing kanamycin[50]. These were incubated upside down for 3 to 10 days at 29 ºC until plaques had formed (clear areas in the agar). Using a pipette, a "plug" of plaque could be picked and suspended in a predatory culture.

2.3.6 Synchronous predatory cultures

For time course microscopy and RNA extraction, attack phase *B. bacteriovorus* and prey cells are mixed such that all the predator cells are at the same stage in the HD lifecycle for imaging and comparison. To do this, *B. bacteriovorus* were grown predatorily on stationary-phase *E. coli*, typically S17-1, for 16 hours at 29 ºC, until all prey had been lysed. These were then passed through a 0.45 µm filter (yielding ~2 x 10^8 pfu ml^{-1}) and centrifuged at 5525 x *g* for 20 minutes. Cells were resuspended in 0.5 ml CaHEPES.

A 50 ml stationary-phase prey culture (standard growth conditions, incubated at 37 ºC for 16 hours, yielding ~1 x 10^9 cfu ml^{-1}) was back-diluted to OD_{600} nm 1 in fresh YT broth. 10 ml of the back-diluted culture was centrifuged at 17,000 x *g* and the pellet resuspended in 700 µl of CaHEPES. At time 0, the 500 µl of *B. bacteriovorus* was mixed with 700 µl of *E. coli*, making the synchronous predatory culture. This was incubated at 29 ºC shaking at 200 RPM.

At the appropriate timepoints, samples could be taken from the synchronous predatory lysate for microscopy (slide preparation is described below). For RNA extraction, multiple synchronous lysates were made, also described below.

2.3.7 RNA extraction from HD *B. bacteriovorus.*

For RT-PCR and RNA-seq, RNA had to be extracted from *B. bacteriovorus*. The RT-PCR assays and RNA-seq analysis I performed used RNA extracted by other lab members (Carey Lambert and Simona Huwiler kindly allowed me to use their RNA and RNA-seq data). RNA was extracted from synchronous predatory cultures at the appropriate times in the lifecycle. A summary of the process follows.

A synchronous predatory culture is set up using a 1 L predatory culture, grown under standard conditions, and 100 ml of prey culture (*E. coli* S17-1), with predatory culture synchrony being checked by microscopy at early time points. *E. coli* and *B. bacteriovorus* only controls were made alongside the predatory culture for enumeration. After starting the infection (when predator and prey are mixed), samples were taken from the predatory culture at the appropriate time points (0, 15, 30, 45, 60, 120, 180, 240 and (optionally) 300 minutes) and placed in a phenol/ethanol solution (5% phenol, 95% ethanol). These samples were then held on ice before centrifugation and pellets stored at -80 ^{o}C.

To extract the RNA, the Promega SV total RNA Purification kit was used. Pellets were resuspended in 100 µl of TE (100mM Tris, 1mM EDTA) and 50 g/ml lysozyme solution, and incubated at room temperature for a maximum of 5 minutes. 75 µl of the RNA lysis buffer was added followed by 350 µl of RNA dilution buffer. Samples were heated to 70 ^{o}C for 3 minutes and then centrifuged at 17000 x *g* for 10 minutes. 400 µl of supernatant was transferred into a clean tube containing 200 µl of 100% ethanol. All of this was then transferred to a spin column, which was centrifuged as above for 1 minute.

50 µl of DNAse mix was added to the column matrix and incubated at room temperature for 15 minutes. 200 µl DNAse stop solution was added to this and then centrifuged at 17000 x *g* for 1 minute. Columns were washed twice, once with 600 µl and then 250 µl of RNA wash solution, centrifuged as above for each time. Columns were transferred to sterile microcentrifuge tubes and 50 µl of RNAse-free water added. This was centrifuged as above and the eluate transferred to a 0.5 ml RNAse-free microcentrifuge tube, before being stored at

-20 ^{o}C. The RNA could then be used for RT-PCR assays or to send for RNA-seq analysis.

2.4 DNA manipulations

2.4.1 Polymerase Chain Reaction (PCR)

For DNA amplification Phusion® High-Fidelity DNA polymerase was used in a typical 50 µl reaction, although this could be scaled appropriate to need. The standard reaction is as follows.

Buffer (including $MgCl_2$)	10 µl (5x)
10 mM dNTPs	2 µl
Primers (100 pmol μl^{-1})	1 µl
Template genomic DNA	1 µl
DNA Polymerase	0.5 µl
AnalaR water	34.5 µl
TOTAL	*50 µl*

2.4.2 Restriction digests

Restriction digests typically used Fermentas FastDigest restriction endonucleases with a universal buffer. Standard reactions were typically 20 µl, with no greater than 5% glycerol content (v/v) to reduce star activity. Reactions ran for 2 hours at the optimal temperature for the enzyme.

2.4.3 Purifying restriction digests and PCR products

Following restriction digests, products were purified via agarose gel electrophoresis and the desired fragment manually excised from the gel with a scalpel. This was then processed with the Sigma-Aldrich GenElute™ Gel Extraction kit as per manufacturer's instructions. Purifying PCR products that were not visualised on an agarose gel required the Sigma-Aldrich GenElute™ PCR Clean-up kit.

2.4.4 Gibson assembly

Primers for Gibson assembly cloning were designed in web tool NEBuilder (nebuilder.neb.com). The ligation reaction required a PCR amplified gene and any inserts, such as a fluorescent tag, and a vector digested with the appropriate restriction enzymes (PCR and restriction digest as standard). These were ligated with the Gibson Assembly® Master Mix as per manufacturer's instructions.

2.4.5 Ligations

All ligations used Fermentas T4 DNA ligase in a 1/10 dilution. In a typical 20 µl reaction, 2 µl of ligase was used with a 3:1 ratio of insert to vector. Reaction time would be 1-2 hours at room temperature or 16 hours at 16 ^{o}C.

2.5 Microscopy

2.5.1 Fluorescence and phase contrast microscopy

Microscopy images were acquired using a Nikon Eclipse Ti-E widefield inverted microscope equipped with an Andor Neo sCMOS camera, as previously described (Kuru et al., 2017). Images were processed in either SimplePCI software (HCImage.com) or FIJI (ImageJ) (Schneider et al., 2012).

For timecourse microscopy, synchronous predatory cultures were used (see above for conditions) and samples taken for imaging at the appropriate time points in the predatory cycle. To do so, CaHEPES containing 1% agar was applied as a thin layer to a glass microscope slide. This was allowed to set before 10 µl of the synchronous predatory culture was applied and a glass cover slip placed over the top. The synchronous predatory culture was returned to the incubator immediately after the sample was taken.

The below table shows the excitation and emission values of the fluorophores used in this study.

Fluorophore	**Excitation (nm)**	**Emission (nm)**
mCherry	550-600	610-665
mTFP	420-454	458-500
mCerulean	433-445	475-503

Table 2.5. Excitation and emission values for fluorophores used in this study.

2.5.2 MicrobeJ

2.5.2.1 Attack phase morphology analysis

To take measurements of attack phase cells, images were taken from predatory cultures. These were prepared under standard conditions (CaHEPES buffer, above) with either *E. coli* S17-1 or MG1655 as prey. These were incubated for 24 hours and checked for complete lysis of prey before images were taken. Slides were prepared as in section 2.5.1. This resulted in images containing only attack phase *B. bacteriovorus*.

The plugin MicrobeJ for the programme FIJI was used to analyse the images for the measurements of individual attack phase cells (Schindelin et al., 2015, Schindelin et al., 2012). To detect HD attack phase cells, the following parameters were used: length was set between 0.5 and 2.5, width between 0.3-1.2 and area 0.2 to 0.8. All other parameters were set to default. Manual inspection was required to see that most cells were correctly assigned before analysis. The shape measurements including the angularity, area, aspect ratio, circularity, curvature, length, roundness, sinuosity, solidity and width were measured for each type of cell.

2.5.2.2 Fluorescent foci and heatmaps

A synchronous predatory culture was prepared for timecourse microscopy as in section 2.3.6 and images taken as in section 2.5.1. After image acquisition, cell measurements were generated using MicrobeJ, a plugin for the FIJI software, as described previously in Kuru et al., 2017 (Schindelin et al., 2012; Ducret et al., 2016, Kuru et al., 2017). To detect fluorescent foci of DivIVA-mCherry; the rounded, invaded, *E. coli* prey cells (bdelloplasts) were detected in the phase channel by defining circularity as 0.96-max and length as 1-max, with all other parameters as default. *B. bacteriovorus* cells (with cytoplasmic Bd0064-mCerulean) were detected by the medial axis method in the mCerulean channel as maxima 1, by defining area as 0.15-max, with all other parameters as default. They were associated with the bdelloplasts with a tolerance of 0.1. Fluorescent foci of DivIVA-mCherry were detected as maxima 2 in the red channel by the “fit shape to circle” method by defining area as 0-0.25, with all other parameters as default. These were associated to maxima 1 with a tolerance of 0.1. Manual inspection of the analysed images

confirmed that most cells were correctly assigned. In cases where bdelloplasts appeared to be infected by two *Bdellovibrio*, these were manually removed from the analysis. The shape measurements including the angularity, area, aspect ratio, circularity, curvature, length, roundness, sinuosity, solidity and width were measured for each type of cell.

2.6 Reverse Transcription PCR

RNA extraction and Reverse Transcriptase PCR (RT-PCR) assays were performed as previously described (Lambert et al., 2006, 2016). Using a Promega SV total RNA isolation kit, total RNA was extracted from samples taken throughout the time course. RT-PCR assays were performed using the Qiagen One-step RT-PCR kit. Reaction conditions are as follows: One cycle of 50 ℃ for 30 min then 95 ℃ for 15 min, followed by 25-30 cycles of 94 ℃ for 1 min, 48 ℃ for 1 min, 72 ℃ for 2 min, and then a 10 min extension at 72 ℃ after the 25-30 cycles, and ultimately held at 4 ℃ prior to gel analysis of products.

For cotranscription RT-PCR, RNA from one time point was used with a forward primer from the first gene and reverse primer from the second gene. The protocol for the assay was the same, but as the product was much longer than a standard RT-PCR the extension time was 30 minutes.

2.7 Bacterial Two Hybrid

2.7.1 Pairwise bacterial two hybrid assay

Pairwise Bacterial Two Hybrid (BTH) assays were performed to test for interactions between DivIVA, ParA3 and other *B. bacteriovorus* proteins using protocols previously described (Battesti and Bouveret, 2012). Competent BTH101 cells were thawed on ice, and 1 μl of each plasmid (pKT25- and pUT18C-derived) was added. These were incubated on ice for 30 minutes and then heat shocked for 1 minute at 42 ºC, before returning to ice for 5 minutes. 1 ml of SOC broth was then added and the cells incubated at 29 ºC, shaking at 200 RPM, for 1 hour. The culture was then centrifuged at 17,000 x *g* for 1 minute, the supernatant removed, and the cells resuspended in 100 μl Mu broth. This was diluted to 10^{-1} and 10^{-2} before all dilutions were plated on

Nutrient Agar supplemented with Amp_{50}, Kn_{25}, $Xgal_{40}$ and $IPTG_{20}$. Plates were incubated for 48 hours at 29 ^{o}C.

Following incubation, three representative colonies were picked from the plates to inoculate 5 ml Mu broth with the above supplements, such that each interaction had three discrete cultures, and grown for 16 hours at 29 ^{o}C, shaking at 200 RPM. 5 µl of each culture was then spotted onto a NA plate (with above supplements) and incubated for a further 48 hours (29 ^{o}C). After this, the plates could be scanned, with blue spots indicating an interaction. All assays included controls: positive controls used plasmids pKT25-zip and pUT18C-zip and negative controls using plain pKT25 and pUT18C plasmids. Additionally, untransformed BTH101 cells were used as a further negative control.

2.7.2 Manual β-galactosidase activity assay

Initially, pairwise BTH assays were further assessed using the manual β-galactosidase activity assay. This is based on work by Miller (Miller, 1972). This assay utilises ortho-nitrophenyl β-D-galactopyranoside (ONPG), an artificial chromogenic substrate of β-galactosidase. When cleaved, colourless ONPG becomes ortho-nitrophenol (ONP) which is yellow.

The 5 ml cultures from the pairwise BTH assay, used to produce spot plates, are used for this protocol. 1 ml of the culture was centrifuged at 3275 x *g* for 10 minutes before removing supernatant and resuspending in 2 ml of Z-buffer (see below), keeping the cells at 4 ^{o}C. 0.5 ml of this resuspension was mixed with 0.5 mls of Z-buffer in a new 15 ml tube. 100 µl of 0.1% SDS solution and 100 µl of chloroform were added to permeabilise cells, which were then incubated at 29 ^{o}C, shaking at 200 RPM, for 10 minutes. At this time, OD_{600} readings were taken for the remaining 1.5 ml of the original culture/Z-buffer mix.

To start the reaction, 0.2 ml of ONPG solution (see below) was added and a timer started. When the reaction turned sufficiently yellow, it was quenched with the addition of 0.5 ml 1M Na_2CO_3. While waiting for the colour to develop, reactions were kept in the incubator conditions above.

Once quenched, 1.5 ml was transferred to a microcentrifuge tube and centrifuged at 17,000 x *g* for one minute. Using 1 ml of this, OD_{420} and OD_{550} readings were taken for each reaction. The below equation could then be used to determine the enzyme activity in Miller units:

Miller Units = $1000 \times [(OD_{420} - 1.75 \times OD_{550})] / (T \times V \times OD_{600})$

OD_{420} and OD_{550} are read from the reaction mixture. OD_{600} reflects cell density in the washed cell suspension. T = time of the reaction in minutes. V = volume of culture used in the assay in ml.

2.7.2.1 ONPG solution (100 ml)

4 mg/ml ONPG in 0.1M phosphate buffer.

To make 0.1M phosphate buffer: 0.85 g Na_2HPO_4, 0.55 g $NaH_2PO_4.H_2O$ in 100 ml water.

2.7.2.2 Z-buffer (per litre)

8.348 g Na_2HPO_4 (anhydrous), 5.6 g $NaH_2PO_4.H_2O$, 5 ml 2M KCl solution, 1 ml 1M $MgSO_4$ solution, 2.7 ml β-mercaptoethanol. Make up to 1 L with water and adjust pH to 7.

Make up to 1 l and adjust pH to 7.0, store at 4^{o}C.

2.7.3 One-step β-galactosidase assay

While the manual method above was initially used for pairwise BTH screening, another protocol was used for testing BTH library interactions, as well as reconfirming the pairwise interactions. This method for liquid β-galactosidase assays were performed using the single-step protocol (Schaefer et al., 2016). The reactions use a 96 well plate and measurements are taken with a FLUOstar Omega Microplate Reader.

80 µl of the spot plate culture was added per well, to which was added 120 µl of "β-gal mix" (see below). The plate was then inserted into the reader and the program, available with Schaefer *et al*., was run for an hour. The MARS Data Analysis software then calculated the activity in Miller Units.

2.7.3.1 β-gal mix (1.2 ml / 10 reactions)

800 µl Z buffer with 2.7 µl/ml β-mercaptoethanol, 300 µl Z buffer with 4 mg/ml ONPG, 80 µl PopCulture reagent (Millipore), 20 µl lysozyme stock solution (10 mg/ml lysozyme in 10mM Tris-HCl pH8 or water).

2.7.4 Bacterial two hybrid library construction protocols

The construction process can be seen in Chapter 4. Below are the specific conditions for the protocols mentioned in that chapter.

2.7.4.1 Genomic digest

B. bacteriovorus HD100 genomic material was digested using NEB restriction enzyme *Sau3A1* in a 1/50 dilution. 20 µl reactions were more efficient than larger reactions, and had the following constituents:

0.4 µl NEB *Sau3A1*

2 µl NEBuffer 10x (supplied with enzyme)

5 µl genomic material, 250 ng/µl

12.6 µl H_2O

2.7.4.2 Ligation into library vectors

Standard ligations were set up for all three library vectors with a 3:1 ratio of insert (average size 1kb) to vector. Reaction ran for 16 hours at 16 ºC.

2.7.4.3 Transformation into *E. coli* DH5α and extraction of plasmids

Transformations were as standard with the following edits. The whole 20 µl ligation reaction was mixed with the competent cells, rather than 1 µl. Instead of centrifuging after the 1 hour incubation, the undiluted culture in SOC medium was plated onto 150 mm round plates with YT agar supplemented with ampicillin[50] and incubated for 16 hours at 37 ºC.

Following incubation, all colonies on the plates were washed off with 2ml YT medium and collected into a single 50 ml tube. Plates were washed as many times as necessary to remove all cells. The collected cells were centrifuged at 5525 x *g* for 10 minutes, and the pellet resuspended into 8 ml of YT medium. This was split into two 4 ml cultures and the plasmids extracted with the

Sigma-Aldrich GenElute^{TM} Plasmid Midiprep Kit as per manufacturer's instructions, eluting to 500 µl each and pooled to 1 ml total.

2.7.4.4 Ethanol precipitation

To concentrate the library plasmid mix, an ethanol precipitation was performed. The 1 ml of each library produced by the plasmid Midiprep was split into three microcentrifuge tubes, to which was added 2.5x volume of 100% ethanol and 0.1x volume of sodium acetate and placed in a freezer for 1 hour. These were centrifuged at 17,000 x *g*, 4 ^{o}C for 30 minutes. The supernatant was removed and the pellet washed with 100 µl of 100% ethanol. This was centrifuged, as above, for a further 5 minutes. The ethanol was removed and the pellet allowed to dry. The pellet from one of the three tubes was resuspended in 50 µl TE, which was then used to resuspend the other two pellets, resulting in a 50 µl concentrate.

2.7.5 Bacterial two hybrid library assay

This is detailed in chapter 4. Briefly, to screen against the libraries a candidate bait gene is ligated into pKT25 and transformed into BTH101G. These cells were then made competent for the assay. 1µl of each library was transformed into individual aliquots of competent cells containing the bait plasmid as per protocol. These were then plated onto 150mm round petri dishes containing MacConkey agar, supplemented with ampicillin, kanamycin, Xgal and IPTG, without dilution and incubated for 48 hours. Any blue colonies at the end of the incubation were then picked and streaked out so that individual colonies can be taken after another 48 hours incubation. Once picked into broth supplemented with ampicillin and kanamycin, and incubated for 24 hours, plasmids were extracted via Sigma miniprep. This resulted in a mix of pKT25 and library (pUT18 etc.) plasmids.

The mix of plasmids were then transformed into DH5α and plated onto YT agar with ampicillin, so that the pKT25 plasmid, which is kanamycin resistant, could be cured out of the cells. Three colonies for each potential interaction were picked into YT broth with ampicillin, incubated for 24 hours and then spotted onto two plates; one with ampicillin and one with kanamycin. Cultures that grew on ampicillin but not kanamycin had been fully cured of the pKT25

bait plasmids, and the library plasmid could be extracted via Sigma miniprep and sequenced to determine the gene coding for the interacting partner.

2.8 Bioinformatics

2.8.1 Gene and protein sequences

Gene and protein sequences for *B. bacteriovorus* HD100 were acquired from Xbase (Chaudhuri et al., 2008). Gene and protein homologues were found with the NCBI BLAST program suite (Altschul et al., 1990).

2.8.2 Alignments

Pairwise alignments were generated in EMBOSS Needle and multiple alignments in EMBOSS ClustalO (Rice et al., 2000; Sievers and Higgins, 2018). For multiple alignments, an identity matrix could be taken showing the percentage homology of each sequence to the others. Alignments were further processed in Microsoft Powerpoint.

2.8.3 Promoter prediction

Promoter predictions were made using the online tool BProm by Softberry (Solovyev, 2011). This predicts transcription start positions for bacterial genes regulated by Sigma70 promoters. Softberry note that it is around 80% accurate with *E. coli* promoters when using sequences between ORFs. It must be noted that accuracy decreases when the sequence is intragenic, as is the case with many promoters predicted in this thesis. Therefore, predicted promoters were only reported with an LDF (Linear discriminant function) above 2.5.

2.8.4 Protein topology prediction

Protein topology searches were made using online tool Topcons (Tsirigos et al., 2015). By inputting an amino acid sequence, this tool uses several algorithms to predict the presence of a signal sequence as well as any transmembrane regions, and whether parts of the sequence are cytoplasmic or periplasmic. The multiple algorithms are combined into a consensus prediction.

2.8.5 Protein domain search

Protein domain predictions were made using online tool Interpro (Blum et al., 2021). With an amino acid sequence input, this tool uses several protein

databases to classify the protein family, specific domains and important sites, where available.

2.8.6 Phylogenetic analysis

B. bacteriovorus HD100 protein sequences were from the genome published by Rendulic *et al*. (European Molecular Biology Laboratory accession no. BX842601) (Rendulic et al., 2004). Homologues to the *B. bacteriovorus* sequence were found in NCBI BLAST, using full length *B. bacteriovorus* sequences and default settings (NCBI BLAST. Bethesda (MD): National Library of Medicine (US), National Center for Biotechnology Information – [cited 25.08.2021.]. Available from: https://www.ncbi.nlm.nih.gov/blast/) (Altschul et al., 1990). Analysis was performed in MEGA-X software, version 10.0.05 (Kumar et al., 2018). In this software, alignments were made with ClustalW (Thompson et al., 1994). Phylogenetic analysis was made using the Maximum Likelihood method (Sullivan, 2005) with the Jones – Taylor – Thornton substitution model (Jones et al., 1992). All trees were bootstrapped with either 500 or 1000 replications. Trees were visualised in Figtree, version 1.4.4 (1977, Figtree et al., 2019). **Swissmodel structural search**

Structural searches were made with online tool Swissmodel (Waterhouse et al., 2018). Using an amino acid sequence, the program searches for proteins with a homologous structure from a repository of annotated structural models. Where results have been used in this thesis, the PDB (Protein Data Bank) number and citation have been included.

2.8.8 RNA-seq data

Unpublished RNA-seq data was kindly provided by Simona Huwiler. These included data for individual time points (0, 15, 30, 45, 60, 120, 180, 240 and 300 minutes). To visualise data, Rockhopper software was used (McClure et al., 2013, Tjaden, 2015, Tjaden, 2020). This displayed tracks for each time point for both positive and negative strands based on the *B. bacteriovorus* HD100 annotated genome from GenBank (Sayers et al., 2021). Reads are overlaid onto these tracks and visualised as a graph. Rockhopper also has a prediction for multi-gene operons based on the RNA reads provided.

3 Chapter 3: Investigating the interaction of the DivIVA and ParAB division systems

3.1 Chapter 3 introduction

3.1.1 DivIVA

As discussed in chapter 1, *divIVA* has been shown to encode a protein with several cell growth and septation related roles in Gram-positive bacteria, including septal site selection and chromosome segregation (Thomaides et al., 2001; Hammond et al., 2019). In Gram-negative bacteria, few studies have focused on the function of DivIVA homologues, which are typically limited to some Oligoflexia and Deltaproteobacteria (Akiyama et al., 2003).

Other bacterial genomes containing DivIVA homologs can have non-conventional methods for septation. Mycobacteria are reported to have both symmetrical septation, producing two identical daughter cells, and asymmetric septation, where one daughter cell is significantly larger than the other (Kieser and Rubin, 2014; Vijay et al., 2014). In contrast, *Streptomyces* growth and division is characterized by polar (apical) growth of branched hyphae and the dispersion of spores, much like fungi (Flardh et al., 2012). The background of other proteins in addition to DivIVA (such as Noc and MinCD which are involved in the co-ordination of division site), can vary between Gram-positive bacteria so there is clearly no “one size fits all” scenario (Monahan et al., 2014; Hammond et al., 2019). In addition, in Streptococci, which like *B. bacteriovorus* lack MinCD, it was noted that post translational modifications of the DivIVA protein can also occur, and in Streptococci that a conserved alanine residue A78 is important for mediating DivIVA protein-protein interactions, suggesting a different regulatory network for septation control (Fadda et al., 2007). In these and other Gram-positive bacterial systems, DivIVA has been at least partially characterized as having varied roles, from regulating septation to polar cell wall growth (Hempel et al., 2008; Kang et al., 2008, Flardh et al., 2012; Ginda et al., 2013, Hammond et al., 2019). Fenton *et al.* observed apical growth in the *B. bacteriovorus* filament during the HD cycle, making this a possible role for DivIVA in this system (Fenton et al., 2010).

In *Bacillus subtilis*, the coiled-coil DivIVA protein is localized to negatively curved membranes by an N-terminus membrane-binding domain (Lenarcic et al., 2009). This localization allows DivIVA to interact with partner proteins to facilitate septum formation at mid-cell and chromosome segregation (Edwards and Errington, 1997; Marston and Errington, 1999, Thomaides et al., 2001). In other species the DivIVA protein directs hyphal tip extension, such as in *Streptomyces coelicolor* (Flärdh, 2003; Hempel et al., 2008), and regulates polar growth in *Corynebacterium glutamicum* and *Mycobacterium smegmatis* (Kang et al., 2008; Letek et al., 2008, Donovan and Bramkamp, 2014; Kieser and Rubin, 2014, Meniche et al., 2014). However, in the cyanobacterium *Synechococcus elongatus*, the DivIVA homolog Cdv3 does not contain the conserved residues linked to negative curvature sensing (MacCready et al., 2017).

Previous work has shown DivIVA and ParA directly interact in *M. smegmatis* (Ginda et al., 2013; Ramirez et al., 2013), establishing a link between the functions of both proteins. In other bacteria, DivIVA interacts with MinD, a ParA-like ATPase that functions in division site selection, either directly, such as in *Listeria monocytogenes* (Kaval et al., 2014), or indirectly, such as in *B. subtilis* where the interaction occurs via MinJ (Patrick and Kearns, 2008; Van Baarle and Bramkamp, 2010, Eswaramoorthy et al., 2011). In the *M. smegmatis* model, DivIVA directs subpolar addition to the cell wall during division (Kang et al., 2008), suggesting there is coordination between cell elongation and chromosome segregation. Given these roles across bacteria, DivIVA is a strong candidate to provide this type of coordination in B. bacteriovorus where complex, multi-septa division occurs along a filamentous cell (Fenton et al., 2010a).

3.1.2 ParAB

Pre-divisional partitioning is a process required for the organization of bacterial cellular components, including chromosomes, plasmids, individual proteins [such as *E. coli* proteins UidR (transcriptional repressor), HisG (ATP phosphoribosyltransferase) and MalI (transcriptional repressor)], chemotaxis clusters and carboxysomes (Bignell and Thomas, 2001; Ringgaard et al., 2011, Roberts et al., 2012; Cho, 2015, Kuwada et al., 2015). The partitioning of

DNA ensures that cell division does not occur across nucleoids, whilst the partitioning of proteins ensures that each daughter cell receives the prerequisite components for optimum fitness. Whilst some partitioning events may be stochastic, other events require active organization (Huh and Paulsson, 2011). A major checkpoint in the division cycle is the segregation of chromosomes, such that each progeny has a complete copy of the genome. In many bacteria chromosome segregation is driven by a three component ParABS system which guides newly replicated chromosomes to bacterial cell poles, facilitating DNA segregation (Hui et al., 2010; Mierzejewska and Jagura-Burdzy, 2012, Espinosa et al., 2017).

Bacterial chromosomes often also encode orphan ParA-like proteins, which are additional ParA homologues not encoded from a canonical parAB locus. These ParA-like proteins perform roles distinct from ParA, for example PldP determines division sites in *Corynebacterium glutamicum* (Donovan et al., 2010; Donovan and Bramkamp, 2014), a ParA/Soj-like protein in *M. tuberculosis* interacts with the MzF6 protein regulating cell growth (Ramirez et al., 2013), and PpfA is involved in partitioning cytoplasmic chemotaxis clusters in *Rhodobacter sphaeroides* (Thompson et al., 2006; Roberts et al., 2012). These orphan *parA*-like genes are often, but not exclusively, found within operons containing genes for the processes in which they are involved. For example, *parC* (partitioning of chemotaxis) genes have been identified in chemotaxis operons in numerous bacterial species (Ringgaard et al., 2011). In *Vibrio cholerae*, ParC is involved in partitioning chemotaxis proteins, thus playing a role in chemotaxis itself, and influencing swimming and swarming (Ringgaard et al., 2011).

3.1.3 Previous study and publication of DivIVA in *B. bacteriovorus*

Previous work on DivIVA was performed by David Milner (PhD, Sockett lab). Prior to this, very little was known of the division systems in *B. bacteriovorus.* His studies, as well as significant contributions from other researchers, and work from this thesis culminated in a publication (Milner et al., 2020). Much of this chapter and chapter 4 are featured in the publication. In this section, other researchers' work will feature to maintain a coherent sequence and will be credited appropriately. This chapter continues from the work in David

Milner's PhD thesis, specifically chapter 3, which focussed on the DivIVA homologue in *B. bacterivorus*, and chapter 4, on the ParA homologues. I will summarise his findings here.

Milner found that the *divIVA* homologue, *bd0464*, of *B. bacteriovorus* was transcribed from a four gene operon, *bd0466-463.* RT-PCR results showed it was constitutively expressed throughout the HD cycle; this did not match the transcription patterns of *bd0466* or *bd0463*. The first gene in the operon *bd0466*, showed low expression through most of the cycle, with upregulation at 180 and 240 minutes. The ultimate gene in the operon, *bd0463*, showed expression throughout the cycle, with peaks at 15-, 120- and 180-minute time points.

Imaging of a fluorescent strain showed that DivIVA-mCherry localised to the poles of attack phase cells. Bipolar localisation at the poles of the growing filament continued through the elongation phase of the HD cycle. Once septated, every daughter cell also showed bipolar distribution; he could not capture the migration of DivIVA-mCherry to the new poles, so it is uncertain whether the protein migrated to the constricting septa before division was complete, or if migration occurred after division and the new pole was formed.

Milner also constructed a *divIVA* null mutant. This was found to be shorter and wider than wild type when analysing images taken from transmission electron microscopy. Complementation partially rescued this phenotype, with cells significantly longer and thinner than the *ΔdivIVA* strain, though still shorter and wider than wild type. The predation rates for both the fluorescent and null strains was the same as wild type, but the null mutant produced a small number of "doublet" cells. These appeared to be two daughter cells connected by a pinched septum, which Milner hypothesised to be due to incomplete constriction.

In his thesis, Milner also characterised the three ParA homologues found in *B. bacteriovorus*. These were termed ParA1 (Bd1326), ParA2 (Bd2331) and ParA3 (Bd3906). Of these, *parA3* is the only encoding gene to neighbour a *parB* homologue (*bd3906*), and so was considered the canonical homologue.

Milner showed that *parA3, bd3906,* was the first gene in a three gene operon, which included *parB* and *bd3904*. It was not possible to clone null mutants of *parA3* but a fluorescent strain, ParA3-mCherry, had an aberrant phenotype. Attack phase cells were longer and had a more variable nucleoid size. These were ascribed to potential septation and chromosome segregation defects.

Milner found that *parA1* was transcribed as the first gene in a three gene operon, followed by hypothetical gene *bd1327* and *bolA*-like gene *bd1328*. When imaging a fluorescent strain expressing ParA1-mCherry, most attack phase cells (~70%) did not show fluorescence. The ones that did had variable localisation; some were cytoplasmic, while others had one or two foci. In HI strains, there was no association of fluorescence with the septa. A *parA1* null mutant was obtained, however its morphology and predation rate did not differ from wild type.

A fluorescent ParA2-mCherry strain also showed varied fluorescence in attack phase. Most had a central, non-polar distribution (~86%), but a smaller number had one or more foci, and a small number had bipolar foci (0.77%). The number of bipolar foci increased (~10%) following incubation on a 1% agarose surface. This led Milner to find a correlation between bipolar foci and cells that were not engaged in gliding motility. A null mutant strain showed that *ΔparA2* cells reversed their gliding direction more frequently than wild type but did not have any changes to morphology or predation rate. Milner concluded that these data showed ParA2 as a regulator of gliding motility. He predicted that bipolar ParA2 prevents the gliding complex from associating with the cell poles, thus preventing this motility. When central, however, ParA2 allows the gliding machinery to reach the pole and initiate movement. When *parA2* was deleted, the gliding complex was free to associate with either pole, leading to increased direction switching.

Bacterial gliding is a process characterized by the non-flagellar movement of a single cell on a solid surface and has been previously observed in many bacterial species, including *B. bacteriovorus* (Spormann, 1999; Mendez et al., 2008, Lambert et al., 2011; Asada et al., 2012, Zhu and McBride, 2016). Gliding motility can be subdivided into two categories; social (S)-motility,

surface movement using pilus retraction in *Myxococcus xanthus*; and adventurous (A)-gliding motility, characterized by the movement of individual cells (McBride and Zhu, 2013; Jakobczak et al., 2015, Zhu and McBride, 2016). *B. bacteriovorus* is known to exhibit a form of A-motility which uses gliding engines and is independent of pili (Lambert et al., 2011). Abolition of gliding (for example, in a diguanylyl cyclase (*dgcA*) mutant), renders the *Bdellovibrio* cells unable to glide out and exit a prey cell after lysis (Hobley et al., 2012a). Thus, gliding may be particularly relevant when *Bdellovibrio* prey upon bacteria within biofilms.

This chapter continues study of these division elements in *B. bacteriovorus.* I have used the bacterial two hybrid system to determine pairwise interactions for these known division homologues. I also further characterise the *divIVA* operon and its encoded proteins, as well as continue Milner's morphological studies of the fluorescent and null mutants that he constructed for *divIVA* and the *parA* homologues. Additionally, I have reanalysed some of Milner's microscopy for publication, and used his DivIVA-mCherry plasmid to produce a cofluorescent strain that makes it easier to determine the localisation of DivIVA in the growing filament while obscured by the bdelloplast.

3.1.4 Bacterial Two Hybrid for use with *B. bacteriovorus* proteins

One of the key experimental systems used in this thesis is the Bacterial Two Hybrid (BTH) assay. This is a procedure used to determine protein-protein interactions in a living model.

In 1989, Fields and Song published a method for determining protein-protein interactions in *Saccharomyces cerevisiae*, which they named Yeast Two Hybrid (YTH) (Fields and Song, 1989). Two plasmids are used in this system, each coding for a discrete half of the GAL4 protein. GAL4 is a transcription regulatory protein which binds to UAS_G motifs in DNA, causing expression of the regulated gene.

Genes coding for candidate interacting proteins can be inserted into these plasmids creating a fusion gene, resulting in the expressed candidate proteins having one half of the GAL4 protein attached to them. Should the candidate proteins interact, both halves of the GAL4 protein are united and can bind the

UAS_G DNA elements. These fusion proteins are expressed in a *S. cerevisiae* strain with deletions of both *GAL4* and its negative regulator *GAL80*, which also contains a *GAL1-lacZ* fusion reporter gene. Activation of this gene by the reconstituted GAL4 results in β-galactosidase activity which can be measured, with the degree of activity showing how strongly the two candidate proteins are interacting.

This system has been successfully used with bacterial proteins but there are limitations due to the differences between the eukaryotic test system and the bacterial system from which the proteins originate. These include issues with protein translocation to the yeast nucleus and a lack of cofactors, ligands and chaperones that are not present in the eukaryotic system; ultimately, this leads to low sensitivity and many false negative results. To address this, Karimova *et al.* produced a similar bacterial system; Bacterial Two Hybrid (Karimova et al., 1998, Karimova et al., 2000a, Karimova et al., 2000b).

This system follows a similar principle to YTH; two plasmids code for discrete halves of an adenylate cyclase from *Bordetella pertussis*, with genes inserted to make fusions. Should the proteins coded by these genes interact, both halves of the adenylate cyclase form a functional catalytic domain that produces cyclic AMP (cAMP). This product interacts with Catabolite Activator Protein (CAP) and induces expression of certain operons; the lactose and maltose catabolic operons being relevant to this assay. This system is expressed in the BTH101 strain of *E. coli*, which lacks its own adenylate cyclase. When an interaction occurs on indicator media, the colonies will be coloured. In this thesis, the medium contains Xgal (5-bromo-4-chloro-3-indolyl-β-D-galactopyranoside) so that when an interaction occurs and the lactose catabolic operon is induced, β-galactosidase activity cleaves the Xgal which results in the formation of a dark blue compound, 5,5'-dibromo-4,4'-dichloro-indigo. Therefore, blue colonies are indicative of an interaction.

This system has obvious advantages over YTH when using bacterial proteins. Their expression in *E. coli* means that any cofactors, ligands, or chaperones absent in the yeast system are more likely to be present. Additionally, the structure of the cell and the contents of the cytoplasm will be closer to the

system the candidate proteins are native to. This will result in proteins far more likely to fold correctly, and maintain their intended conformation, and no issues regarding nucleus translocation.

For these reasons, BTH was chosen as the primary assay for determining protein-protein interactions in this study. However, as this study is primarily focussed on division related proteins, there were some initial concerns. The two halves of the adenylate cyclase are expressed in the cytoplasm. As division is a process that requires interaction between cytoplasmic, periplasmic, and outer membrane elements, it was unknown if this system could accurately assess interactions in these other bacterial compartments.

3.1.5 Assaying *B. bacteriovorus* proteins in *E. coli* BTH101

B. bacteriovorus and *E. coli* are both proteobacteria and the BTH system has been used successfully with genes from *B. bacteriovorus*. The most recent publication found an interaction between RomR, a response regulator, and the remnants of a sensor histidine kinase (Lowry et al., 2019). The GC content of both bacteria is very similar (51% for *B. bacteriovorus* HD100 and 52% for *E. coli* MG1655 coding DNA), with similar codon usage (as seen on www.kazusa.or.jp). Additionally, this system has been used extensively with more distantly related Gram-positive bacteria such as *Bacillus subtilis* (Van Baarle et al., 2013, Sharma et al., 2020a).

Some *B. bacteriovorus* proteins may be lethal when expressed in *E. coli*, such as digestive proteins or proteins whose overexpression could be deleterious. These cases should be obvious as, during plasmid construction, the host *E. coli* transformant will have impeded growth. This could be expected with some division related proteins; for example, the *B. bacteriovorus* FtsZ homologue may share high identity with the *E. coli* homologue, and constant expression could lead to potentially fatal septation abnormalities.

3.1.6 BTH for periplasmic proteins

Another issue is the use of secreted, periplasmic proteins. Division and septation are processes that extend from the cytoplasm to the periplasm and outer membrane. Expressing these in the cytoplasm could lead to misfolding, particularly if the protein has a *Sec* signal and would typically undergo folding

in the periplasm. For these proteins, the *Sec* signal must be removed, preventing them from crossing the inner membrane to the periplasm.

Despite this, there are studies that have used proteins that are localised to the periplasm. A recent example is in *Pseudomonas aeruginosa*, where bacterial two-hybrid was used to test for interactions between proteins involved in pyoverdine synthesis (Bonneau et al., 2020). The initial stages of this pathway occur in the cytoplasm, but the product is matured in the periplasm before secretion into the extracellular medium. This study successfully explored the interaction network of the periplasmic proteins using the cytoplasmic BTH system. The BTH plasmids have also been used successfully with transmembrane proteins, such as interactions between PhoQ and SafA in *E. coli* (Eguchi et al., 2012).

3.1.7 Examples of BTH used for division proteins in bacteria.

This system has already been used extensively for division related proteins in Gram-positive and Gram-negative models, due to many of these proteins being potential targets for antibiotics. Examples of FtsZ interaction networks can be seen for *Mycobacterium tuberculosis, Streptococcus suis* and *Neisseria gonorrhoeae* (Tan et al., Mir et al., 2019, Zou et al., 2017). These typically include many other proteins expressed from the *dcw* cluster, which are known interactors from other models, several of which are membrane bound or periplasmic. DivIVA can also be seen in many BTH studies. Example models include *Bacillus subtilis*, *Listeria monocytogenes* and *Deinococcus radiodurans* (Van Baarle et al., 2013, Sharma et al., 2020a, Kaval et al., 2014, Sharma et al., 2020b, Maurya et al., 2016). The success of these studies validates the use of BTH with the *B. bacteriovorus* homologues of these division proteins in this thesis.

3.2 Specific research aims

- Use pairwise BTH assays to determine:
    - If DivIVA interacts with the proteins encoded from the *bd0466-bd0463* operon.
    - If DivIVA interacts with other division related proteins, such as the ParA homologues, and septal proteins.

- Further investigate the *divIVA* operon bioinformatically.
- Investigate the localisation of Bd0466 and Bd0465 via fluorescence microscopy.
- Continue Milner's work on the morphology of *divIVA* null mutants and fluorescently tagged ParA homologues, using larger sample sizes and automatic cell measurements.
- Phylogenetically analyse the ParA homologues to gain insight into their evolutionary origins.

3.3 Chapter 3 Results

3.3.1 *B. bacteriovorus* DivIVA may not inherently sense negative curvature like the *B. subtilis* homologue Soj

Features critical to the function of DivIVA in *Bacillus subtilis* were shown when the crystal structure of the N terminus was resolved (Oliva et al., 2010). Of particular note were residues S16, F17, R18, G19 and Y20, which are located between two alpha helices, forming a crossed-loop that exposes them to the substrate. The N terminus is where dimerisation occurs. The crossed-loop residues were determined to be essential for membrane association, as the structure of DivIVA senses the negative curvature in that bacterium. Null phenotypes were observed in *B. subtilis* upon mutation of F17, R18 and G19 (Oliva et al., 2010).

In the *B. bacteriovorus* DivIVA homologue, Bd0464, four of these residues are different from those in *B. subtilis*, although the alpha helices either side are conserved and predicted to keep the same structure; the sequence in Bd0464 is KMMGL, **figure 3.3.1**. The study publishing the crystal structure of DivIVA in *B. subtilis* also showed that none of these residues are essential for dimerisation (Oliva et al., 2010). Therefore, the conservation of the alpha helices suggests that Bd0464 can still dimerise.

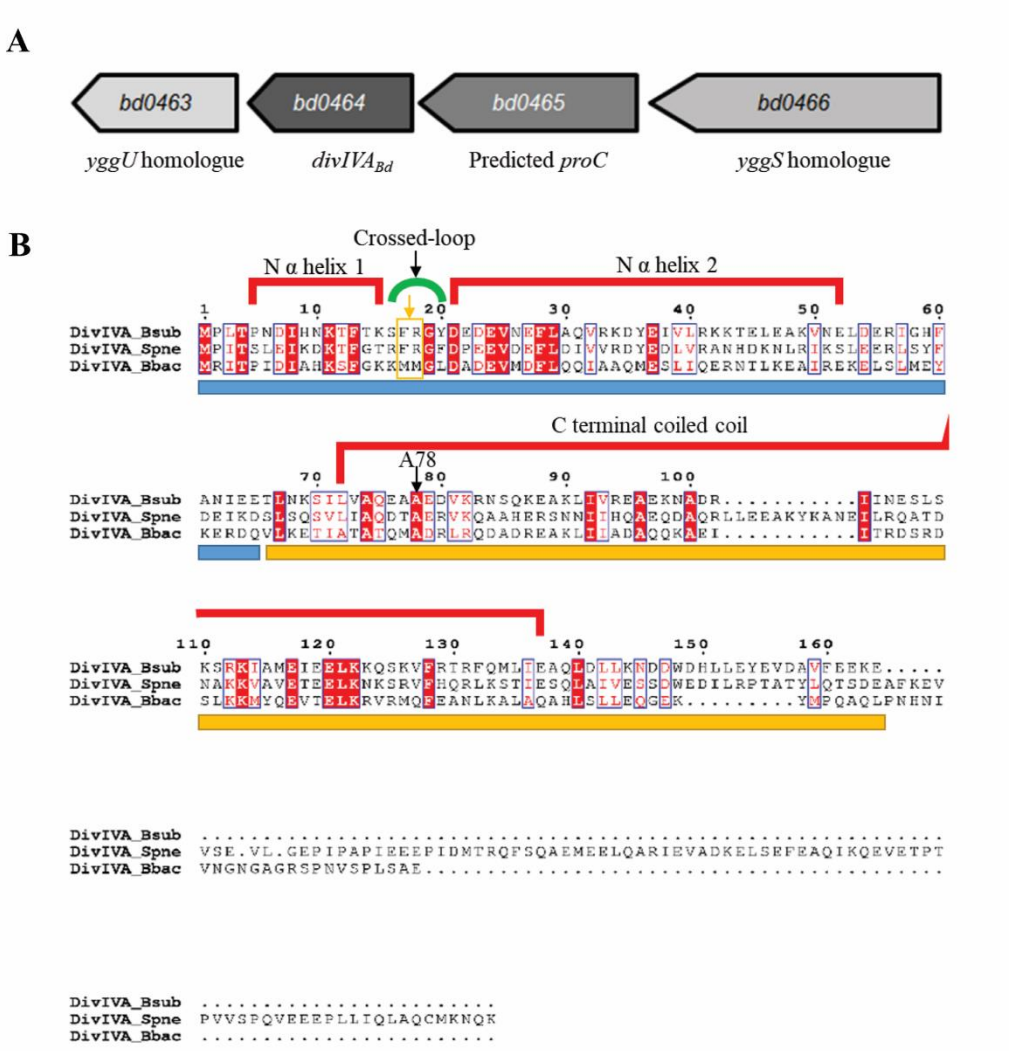

Figure 3.3.1. A representation of the *divIVA* operon and an alignment of DivIVA homologues from *Bacillus subtilis, Streptococcus pneumoniae* and *B. bacteriovorus*. (a) A representation of the *divIVA* operon in *B. bacteriovorus* and the putative roles of the genes. (b) An alignment of DivIVA homologues. Bars below the sequence indicate the N (blue) and C (yellow) terminal domains. Red, square brackets above the sequence indicate helices, and the green, curved bracket indicates the crossed-loop region. The residues with the yellow arrow and box (*B. subtilis* F17 and R18) are essential to membrane sensing in *B. subtilis* but are not conserved in the *B. bacteriovorus* homologue (Oliva et al., 2010). Also indicated is residue A78, which is phosphorylated in *S. pneumoniae* (Ni et al., 2018).

BLAST analysis of the N terminal domain of Bd0464 showed that many DivIVA homologues have substitutes for S16 and F17. In Firmicutes this is commonly KM, although not exclusively. Indeed, the closest similarity to the N terminal domain (residues 1-36) of Bd0464 was found in members of *Bacillus* and *Lactobacillus* (up to 63% identity). In *B. subtilis*, F17A mutants showed diffuse cytoplasmic localisation, suggesting this residue is necessary for negative curvature sensing (Oliva et al., 2010).

Milner first noted the importance of residue R18 to localisation of DivIVA homologues, and that the *B. bacteriovorus* protein has this substituted with methionine. This substitution is very rare in other homologues. Even the Firmicute DivIVA homologues with the highest sequence identity to the Bd0464 N terminal domain all have a conserved R18. This residue is clearly exposed to the surrounding solvent, and the R18A mutant in *B. subtilis* localised to spots in the cytoplasm (Oliva et al., 2010). That *B. bacteriovorus* lacks these residues, both substituted with methionine, suggests it cannot inherently sense negative curvature. Therefore, polar localisation of Bd0464 is likely to require further protein interactions.

Apart from in the BALOs, two other exceptions without R18 were noted, the first published for the cyanobacterial *Synechococcus elongatus* DivIVA-like protein Cdv3 (MacCready et al., 2017). In this context, Cdv3 does not have the first conserved alpha helix, and each of the five crossed-loop residues had been substituted, the crossed-loop sequence becoming ENDLL. As with *B. bacteriovorus*, negative curvature sensing may not occur due to the loss of residues F17 and R18. Despite this, Cdv3 was observed at the midcell recruiting MinC, suggesting another method of localisation. This could be via protein interaction. ZipN has previously been found to bind Cdv3 and many Fts proteins, and is a candidate for recruiting them to the divisome (Marbouty et al., 2009), though *B. bacteriovorus* does not contain a ZipN homologue. The second exception is the Deltaproteobacterium *Geobacter*. All *Geobacter* DivIVA crossed-loops have a similar sequence. An alignment shows that both alpha helices are conserved and K16 is highly conserved, but the RGY motif from Bd0464 has been substituted with (I/L)GG(I/L). As with Bd0464, this

suggests a loss of function for negative curvature sensing, but conservation of amino acids required for dimerisation.

Prime candidates for interaction include the proteins encoded from the *divIVA* operon, Bd0466, Bd0465 and Bd0463. These may interact with Bd0464 to localise it, or to connect its division functions to other cellular processes. First, I investigated these proteins bioinformatically to assess their potential functions.

3.3.2 The ultimate gene in the *divIVA* operon encodes for a YggU homologue

The last gene of this operon is *bd0466*. Protein domain predictions show that it encodes for a YggU homologue. These small proteins are very poorly studied but are conserved among bacteria and eukaryotes. There is currently no indication of what their function may be. Milner briefly studied this, finding it to be cotranscribed with *divIVA.* A fluorescent tag of the protein showed no detectable fluorescence at attack phase. Given the lack of information on this protein, it has not been a focus of this thesis, however, it was included in the interaction assays used later.

3.3.3 The first gene of the *divIVA* operon, *bd0466,* encodes a YggS homologue for pyridoxal phosphate homeostasis

The first gene, *bd0466*, of the four gene operon encoding DivIVA in *B. bacteriovorus* is a pyridoxal homeostasis protein homologue, *yggS*. Initially, this gene was annotated as an alanine racemase (Alr), as it is referred to in David Milner's thesis, due to the shared structure of YggS proteins and the barrel domains of these enzymes. The barrel domain binds cofactor pyridoxal 5'-phosphate (PLP), a B6 vitamer, which facilitates the racemase action of the second domain of Alr proteins; YggS does not have this second domain, consisting only of the barrel structure.

Recent studies, predominantly in *E. coli*, have elucidated some functions of this protein. Initially, *yggS* null mutants were found to excrete valine into the medium, with increased concentrations of valine and isoleucine, as well as their metabolic enzymes, found in the cells (Ito et al., 2013). The authors

showed that this was due to reduced availability of coenzyme A (CoA). This phenotype was rescued with complementation of YggS homologues from *E.*

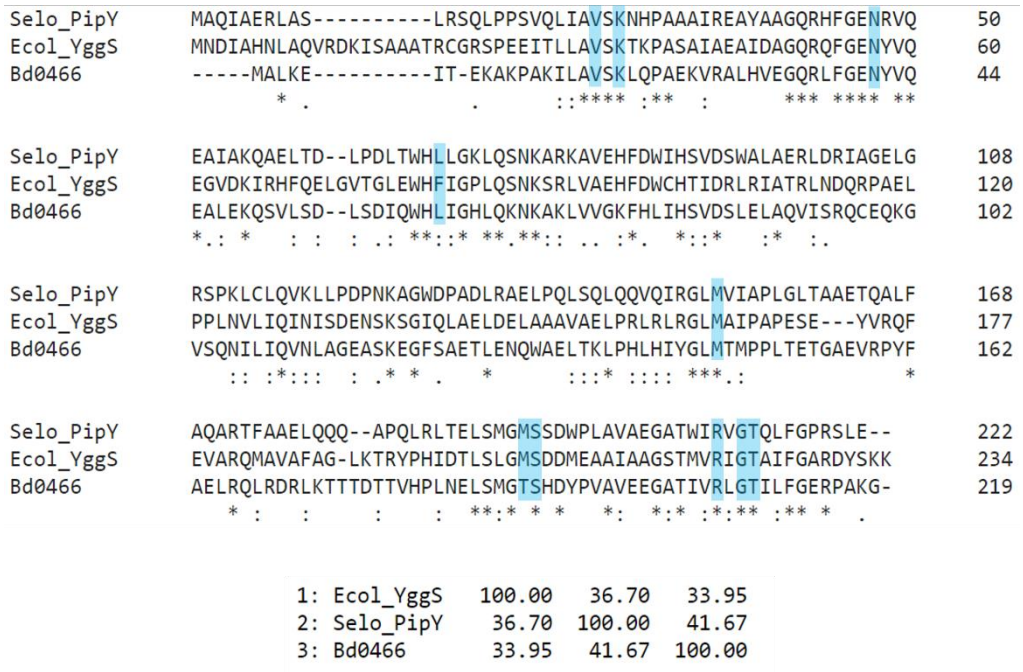

Figure 3.3.2. An alignment of YggS homologues from *Synechococcus elongatus*, *Escherichia coli* and *B. bacteriovorus* suggest Bd0466 has conserved function. Blue highlighted residues indicate those found to be important for pyridoxal 5-phosphate binding in the *S. elongatus* protein. Nine of ten are conserved in Bd0466, as is the case with the *E. coli* homologue. Below the alignment is an identity matrix. Bd0466 shares slightly higher sequence identity with the *S. elongatus* homologue than the *E. coli* homologue.

coli, *B. subtilis*, *Saccharomyces cerevisiae* and humans. Following this, YggS was shown to affect PLP homeostasis, with mutants also accumulating PLP precursor pyridoxine 5'-phosphate (PNP) and exhibiting pyridoxine sensitivity (Ito et al., 2016, Ito et al., 2019). These studies show that YggS is an important regulator of the essential cofactor PLP and amino acids valine and isoleucine.

Aligning Bd0466 and the YggS from *E. coli* shows 31.2% identity, **figure 3.3.2**. A Swissmodel structural search shows the closest protein to Bd0466 is a PipY (PDB ID 5nm8) from *Synechococcus elongatus*, with 43% identity; PipY are confirmed YggS homologues (Tremino et al., 2017). Nine of the ten identified residues for binding PLP in the *S. elongatus* PipY are conserved in

Bd0466; for comparison, nine are also conserved in the *E. coli* YggS. This suggests that Bd0466 retains PLP binding.

If Bd0466 retains the functions of other studied YggS homologues, its role could be regulatory, connecting its PLP and amino acid homeostasis functions with the role of DivIVA in septation. The abundance of PLP and amino acids could be an indicator of the stage of digestion of the host bdelloplast, contributing to the switch from replication to division.

3.3.4 PLP synthesis pathways in *B. bacteriovorus*

There are two main synthesis pathways in bacteria: the deoxyxylulose-5-phosphate (DXP)-dependent pathway present in α- and γ-proteobacteria, studied primarily in *E. coli*, and the DXP-independent pathway, studied in *B. subtilis* (Rosenberg et al., 2018, Mukherjee et al., 2011, Richts et al., 2019, Ito and Downs, 2020). The DXP-dependent pathway is a seven-step process converting erythrose 4-phosphate (E4P), an intermediate product in the pentose phosphate pathway, to PNP, using the substrate DXP. Epd (erythrose 4-phosphate dehydrogenase), PdxB (4-phosphoerythronate dehydrogenase), and SerC (3-phosphoserine aminotransferase) convert E4P to 4-phosphohydroxy-L-threonine (4HTP). PdxA converts this to 2-amino-3-oxo-4-(phosphohydroxy)butyric acid, which is spontaneously decarboxylated to 3-phosphohydroxy-1-aminoacetone. DXP is generated from glyceraldehyde 3-phosphate and pyruvate by DXP synthase Dxs. PNP synthase PdxJ produces PNP from both substrates, which can be converted by PLP synthase PdxH to PLP in the final step. The DXP-independent pathway involves only the PdxST enzyme complex, which converts glutamine to PLP. Searching for homologues shows that *B. bacterivorus* has putative protein homologues for enzymes in the DXP-dependent pathway, **figure 3.3.3**, but none for PdxS or PdxT of the DXP independent pathway. This suggests that it can synthesis PLP through the DXP-dependent pathway, as seen in *E. coli*.

In addition to synthesis, some bacteria can also salvage B6 vitamers pyridoxal (PL), pyridoxine (PN) and pyridoxamine (PM) through phosphorylation. In *E. coli*, some identified salvage proteins are PdxK and PdxI (Mukherjee et al., 2011, Ito and Downs, 2020). Neither of these have homologues in *B.*

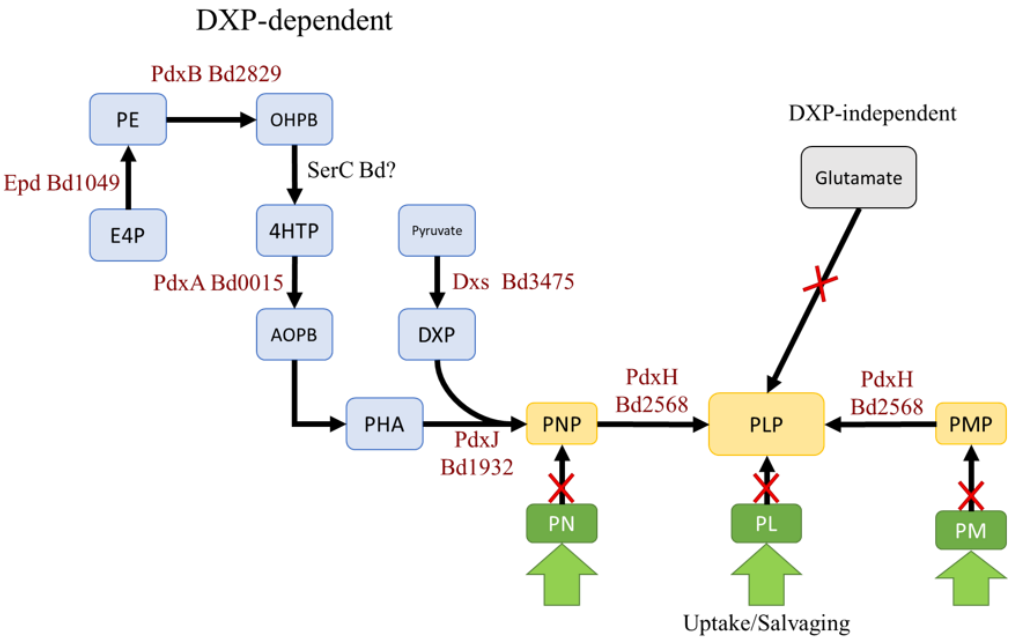

Figure 3.3.3. Analysis of pyridoxal 5'-phosphate synthesis pathways suggests *B. bacteriovorus* only use the DXP-dependent pathway. This cartoon shows the pathways for pyridoxal 5-phosphate (PLP) biosynthesis and uptake. In *B. bacteriovorus*, no homologues were found for the deoxyxylulose 5-phosphate (DXP)-independent pathway or for the salvaging pathway. It does, however, have homologues for the DXP-dependent pathway. In this pathway Epd (erythrose 4-phosphate dehydrogenase), PdxB (4-phosphoerythronate dehydrogenase), and SerC (3-phosphoserine aminotransferase) convert E4P to 4-phosphohydroxy-L-threonine (4HTP). PdxA converts this to 2-amino-3-oxo-4-(phosphohydroxy)butyric acid, which is spontaneously decarboxylated to 3-phosphohydroxy-1-aminoacetone. DXP is generated from glyceraldehyde 3-phosphate and pyruvate by DXP synthase Dxs. PNP synthase PdxJ produces PNP from both substrates, which can be converted by PLP synthase PdxH to PLP in the final step (Mukherjee et al., 2011).

bacteriovorus. To prevent PLP from reaching toxic levels, *E. coli* can also reverse this by dephosphorylating PLP and PNP to PL and PN respectively, with enzyme PdxP, a PLP phosphatase that can also catalyse the reverse reaction. This, too, has no homologue in *B. bacteriovorus*.

This shows that *B. bacteriovorus* has a pathway for PLP synthesis, the DXP-dependent pathway of *E. coli*, but does not have a recognisable pathway for the salvage of B6 vitamers or for reducing the level of cellular PLP should it become toxic. Either an alternative method of reducing PLP exists in *B. bacteriovorus*, or it strictly controls the synthesis pathway. A lack of salvaging proteins could also mean that uptake of B6 vitamers from prey is also not possible.

3.3.5 Second operonal gene *bd0465* encodes a putative ProC, which catalyses the final step in proline synthesis

The second gene in this operon, *bd0465*, is annotated as encoding a ProC, pyrroline-5-carboxylate reductase (P5CR), which catalyses the final step in proline synthesis. The proline synthesis pathway from glutamate consists of three enzymes that convert glutamate to L-proline. ProB, glutamate 5-kinase, synthesises glutamyl-γ-phosphate. ProA, glutamyl-γ-phosphate reductase, converts this to glutamate 5-semialdehyde. This undergoes spontaneous cyclisation to become pyrroline-5-carboxylate, which is acted upon by ProC (Fichman et al., 2015). Interestingly, a pBlast of ProA and ProB from *E. coli* shows there are no homologues for these proteins in *B. bacteriovorus*.

An alternative pathway sees the conversion of proline from ornithine, which requires an ornithine δ-aminotransferase (δOAT) to convert ornithine to glutamate 5-semialdehyde. One candidate for this protein is Bd3449, found from a pBlast using an *Arabidopsis* δOAT with this role. Bd3449 is annotated as a HemL, glutamate-1-semialdehyde 2,1-aminomutase, homologues of which are part of the porphyrin synthesis pathway (Ilag et al., 1991). A domain search suggests Bd3449 has an OAT-like domain but is more likely a HemL than δOAT. Further work would be required to determine if there is δOAT in *B. bacteriovorus*. If lacking both pathways, this could mean that *B. bacteriovorus* is dependent on external sources of proline.

A Swissmodel search identifies a ProC homologue from β-proteobacterium *Neisseria meningitidis* (PDB ID 2ag8) as the closest structural homologue to Bd0465, with which it shares 32% identity (Nocek et al., 2005). This paper also studied the ProC homologue of *Streptococcus pyogenes*. Seen in the

alignment **figure 3.3.4**, Bd0465 contains the NADPH binding motif GxGxx(A/G) as well as nine of ten key proline binding residues.

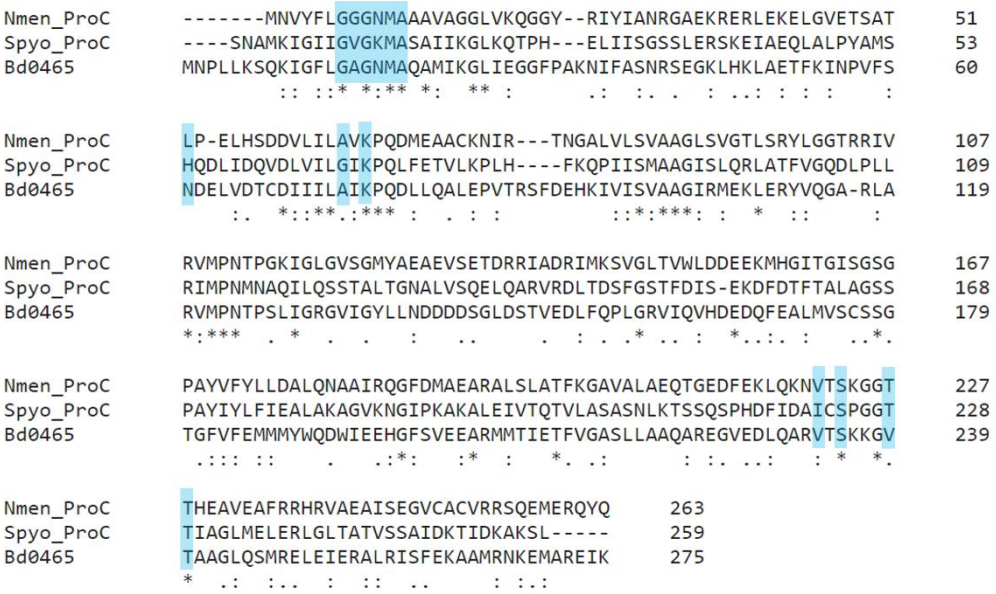

Figure 3.3.4. An alignment of proline synthesis ProC homologues from *Neisseria meningitidis*, *Streptococcus pyogenes* and *B. bacteriovorus* suggest that Bd0465 retains NADPH and proline binding functions. Blue highlighted residues are important for the function of the *N. meningitidis* protein. Specifically, the 7GxGxxA12 is for NADPH binding, conserved in Bd0465, while the others are for proline binding. Only one proline binding residue is not at least partially conserved.

As a homologue of the enzyme responsible for the final catalytic step in proline synthesis from both glutamate and ornithine, a full synthesis pathway would be expected. However, a lack of enzymes for the conversion of glutamate, and potentially arginine, to proline could mean that this protein has an altered function in *B. bacteriovorus*, or that its substrate P5C may be taken from alternative sources, such as media or from the host during the HD cycle. It could also have a sensory role; as proline binding is likely conserved in Bd0465, this could be another signal, dependent on the abundance of proline, for triggering division. If Bd0466 and Bd0465 were to both signal to DivIVA, they would have to be localised together in the *B. bacteriovorus* cell.

3.3.6 Bd0465-mCherry is localized in the cytoplasm

Milner found that DivIVA-mCherry fluorescence was seen at the cell poles. Therefore, I assessed the localization of Bd0465 and Bd0466 through fluorescent microscopy to see if they colocalise. To do so Bd0465-mCherry and Bd0466-mTFP constructs, **figure 3.3.5**, were conjugated separately into wild type *B. bacteriovorus* HD100. As seen in **figure 3.3.6,** in contrast to the polar foci of DivIVA-mCherry, Bd0465-mCherry was ubiquitously expressed in the cytoplasm in attack phase cells. Bd0466-mTeal was too faint to accurately determine its cellular location. Images were taken throughout the predatory life cycle, but the fluorescence was too faint to accurately determine localization when *B. bacteriovorus* was within the bdelloplast. Diffuse localisation in the cytoplasm means that Bd0465 would be able to interact with DivIVA at the poles.

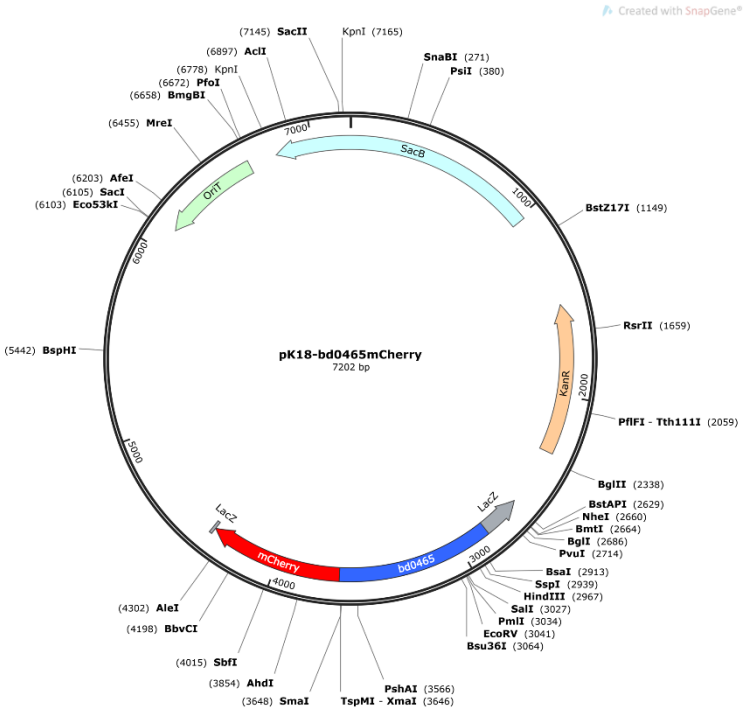

Figure 3.3.5. pK18 plasmid construct containing mCherry tagged bd0465. DNA for *bd0465* was amplified with primers Bd0465Fluo-CtagF and Bd0465Fluo-CtagR which include EcoRI and KpnI restriction enzyme recognition sites. PCR product and

plasmid pAKF56 were digested with these enzymes and then ligated, making plasmid pAKF56::bd0465, adding a C-terminal *mCherry* tag to the gene. This plasmid was digested with EcoRI and HindIII to remove bd0465-mCherry and ligated into plasmid pK18*mobsac*B, digested with the same enzymes.

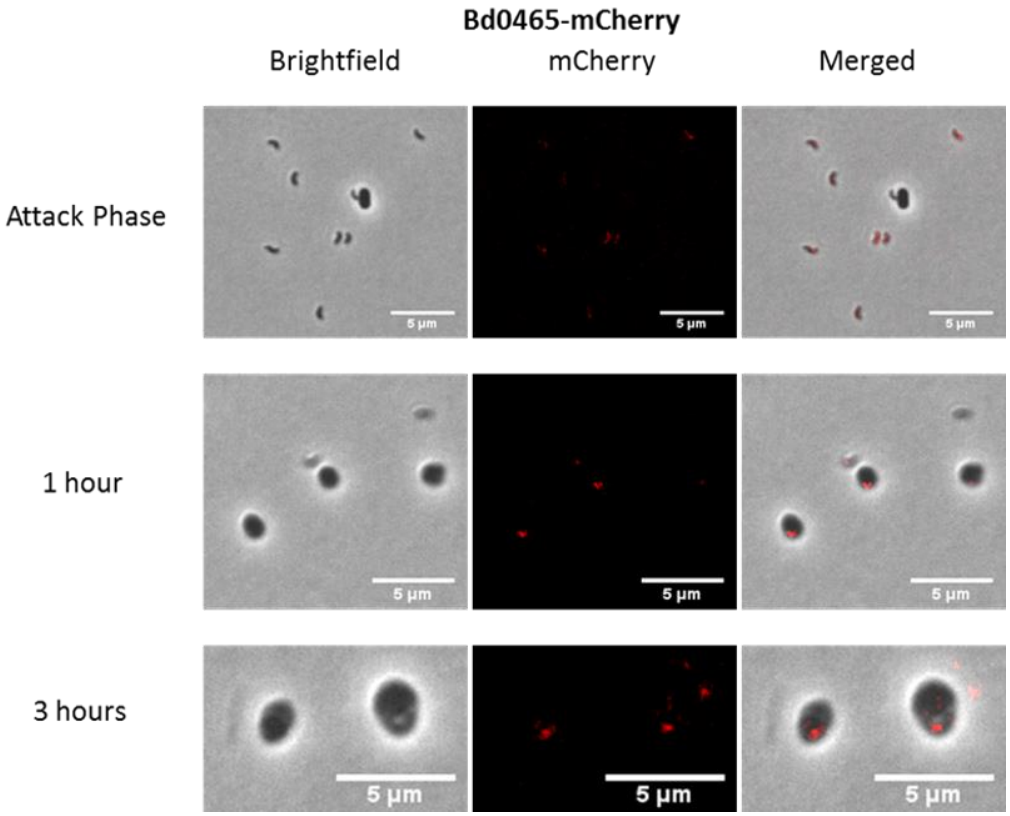

Figure 3.3.6. Phase contrast and epifluorescence microscopy displaying the faint expression of Bd0465 tagged with mCherry in the cytoplasm. Localisation was observed in a synchronous predatory culture preying upon *E. coli* S17-1. The first panel is at time 0, directly following the mix of predator and prey cultures. Further panels are shown at 60 minutes, when the *B. bacteriovorus* cell is established and growing, and at 180 minutes, when replisomes have dissipated, and the filament preparing to septate. At all timepoints, fluorescence is localised cytoplasmically, although it is difficult to discern location precisely in the bdelloplast due to it being faint and the host cell masking it. Images are representative of three biological repeats.

3.3.7 RNA-seq data and RT-PCR assays show varying expression patterns for genes in the *divIVA* operon

RT-PCR assays of *bd0466* and *bd0465* show that they are constitutively expressed throughout the HD cycle, **figure 3.3.7**. In his thesis, Milner confirmed that *bd0465* and *divIVA* are cotranscribed and that *divIVA* has its own promoter, using promoter walking. This was also evidenced in his RNA-seq data, which only accounts for attack phase cells, as *divIVA* had an expression level above the baseline operon expression.

Shown in **figure 3.3.8**, Rockhopper analysis of the unpublished RNA-seq data used in this thesis confirms the promoter before *divIVA*, but also shows there is potentially an additional promoter before *bd0465*, located in *bd0466*. This data shows that *bd0466* expression is very low compared to the rest of the operon; the only discernible expression is at the 120- and 180-minute time points. However, RT-PCR analysis of *bd0466* expression shows that it is expressed throughout the HD cycle. This could suggest that its expression is conditional, or that it just has a very low level of expression. Also using RT-PCR, **figure 3.3.7**, I confirmed that there is readthrough from *bd0466* to *bd0465* at the 180 minute time point.

Genes *bd0465* and *bd0464* are most highly expressed at attack phase, although they are expressed throughout the rest of the HD cycle, too. As noted by Milner, there is a marked increase in expression of *divIVA* compared to its neighbours. Ultimate gene *bd0463*, like *bd0466*, has a much lower expression level, with expression mainly occurring at attack phase and 180 to 300 minutes. Gene *bd0463* does not appear to have its own promoter. Discrepancies in expression patterns of these genes shows that while there is a base level of readthrough for the operon, genes *bd0465* and *bd0464* have their own level of independent regulation. It also shows that full operon expression is only likely to occur at low expression, and potentially only at the 180 minute time point. Following this, I investigated DivIVA itself to further clarify its expression and localisation in the growing filament.

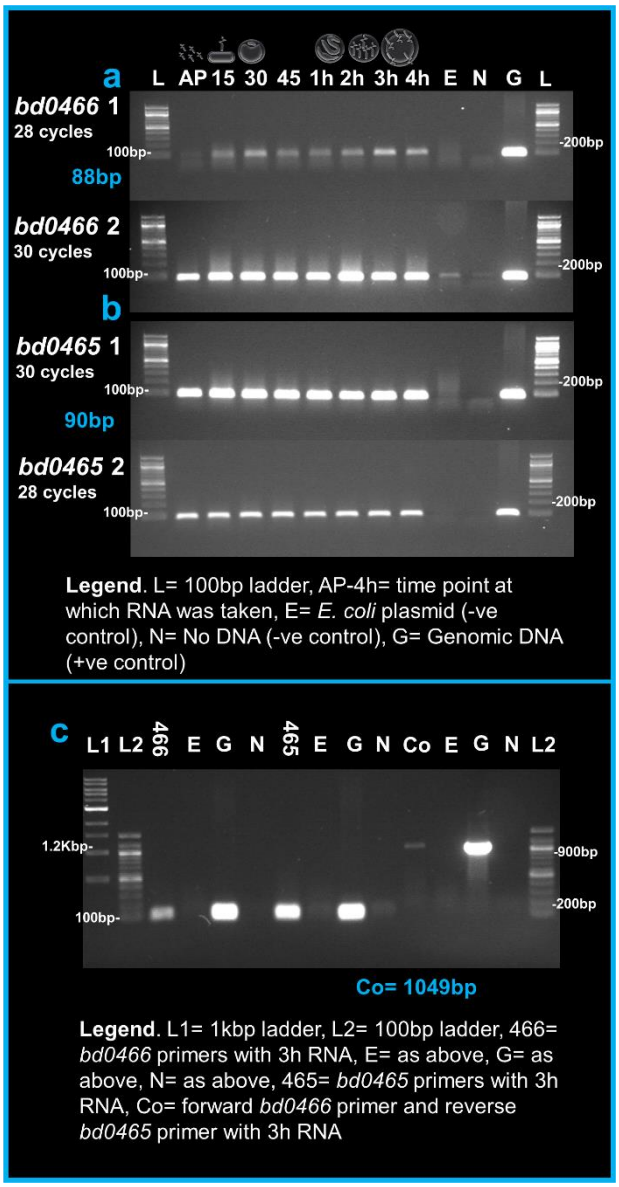

Figure 3.3.7. RT-PCR results showing constitutive expression for *bd0466* and *bd0465*, as well as cotranscription across the two genes, on RNA extracted from host dependent *B. bacteriovorus*. (a) two replications of a timecourse RT-PCR for *bd0466* using primers RT-PCRBd0466F and RT-PCRBd0466R. (b) shows the same for *bd0465* using primers RT-PCRBd0465F and RT-PCRBd0465R. RNA was extracted from HD *B. bacteriovorus* at the time points shown with positive controls of *E. coli* genomic DNA and no RNA/DNA, and negative control of *B. bacterivorus* genomic DNA. (c) Cotranscription RT-PCR showing expression for *bd0466* and *bd0465* with RNA extracted from the 3h (180 minute) time point using the above primers, as well as a cotranscription test using the forward primer for *bd0466* and reverse primer for *bd0465*. This produces a faint band confirming cotranscription at this time point.

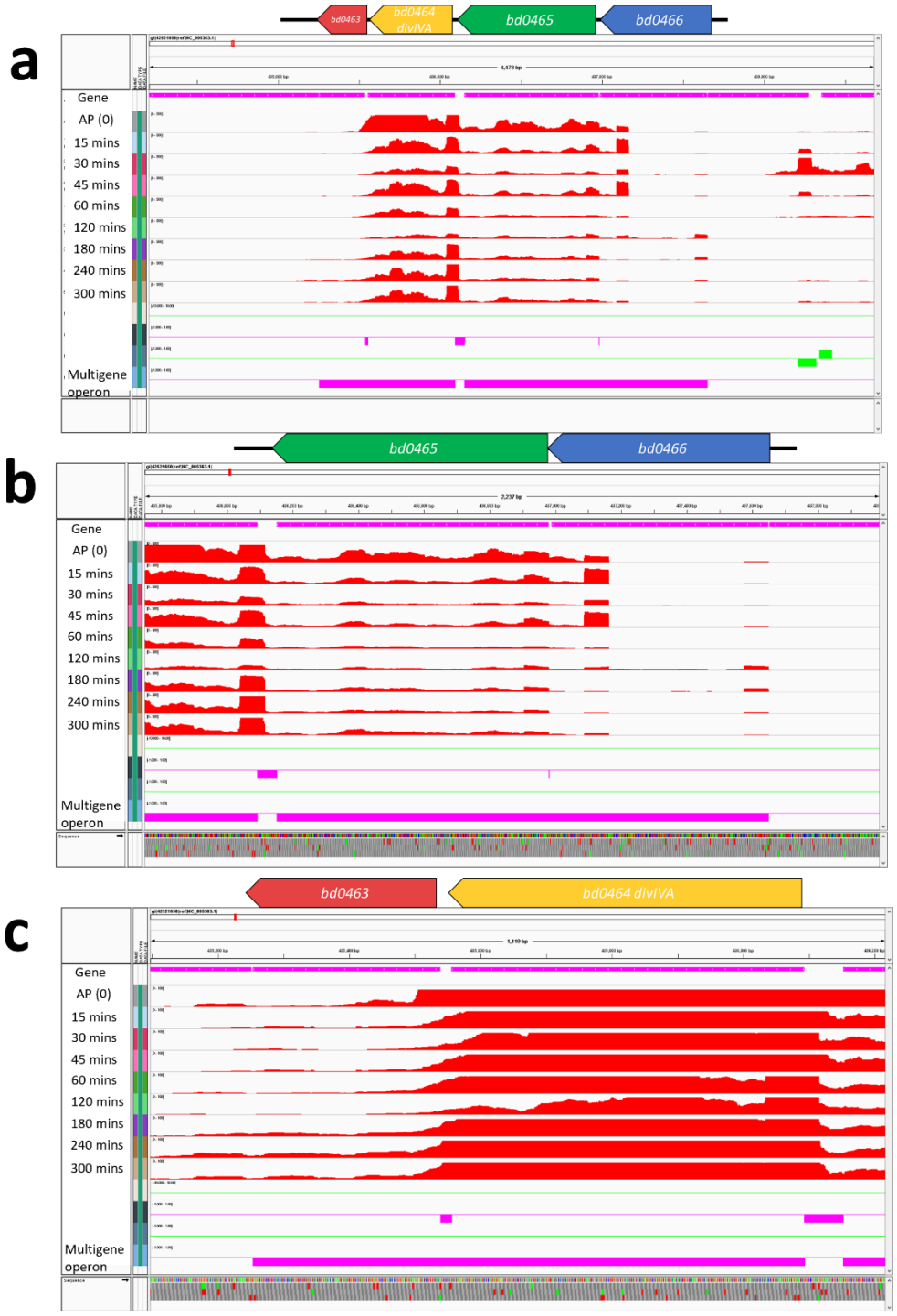

Figure 3.3.8. RNA-seq data for the *divIVA* operon shows different levels of expression across the genes, with *divIVA* highest. Screenshots were taken from Rockhopper. (a) This shows a zoomed out image for the expression of the whole operon. Lower expression is seen for *bd0466 and bd0463*. Gene *divIVA* is expressed throughout the cycle. Range 0-500 reads. (b) This is a closer image of genes *bd0466* and *bd0465* to show that expression of *bd0466* is much lower than that of *bd0465*. (c) This shows genes *divIVA* and *bd0463*. Range is 0-100 to show readthrough of *bd0463*

at attack phase and 180-300 minute time points. To the left, the tracks are labelled with times representing the timepoint at which the RNA was extracted from the *B. bacteriovorus* predatory culture (AP = attack phase). Above, the cartoon shows the location and designation of the genes in relation to the Rockhopper screenshot. The gene track shows the location of the genes, the operon track is where Rockhopper predicts a multigene operon.

3.3.8 Heatmaps of DivIVA-mCherry in a Bd0064-mCerulean background strain show bipolar fluorescence until septation

Milner had previously constructed a *B. bacteriovorus divIVA-mCherry* merodiploid strain and saw that the fluorescence had a bipolar distribution. While he did perform time course microscopy over the whole of the HD cycle, due to the difficulty of visualising the growing filament in the bdelloplast I wanted to have a clearer analysis of the localisation of DivIVA-mCherry at the later time points. To do this, I conjugated Milner's pK18::DivIVA-mCherry plasmid into a *B. bacteriovorus* HD100 strain, kindly provided by Paul Radford, with a ubiquitously expressed, cytoplasmic Bd0064-mCerulean as a background. For microscopy, this produced a channel for the background fluorescence of the whole filament upon which the mCherry channel could be overlaid.

Once conjugated, I performed time course fluorescent microscopy to acquire images at the standard time points in the lifecycle of *B. bacteriovorus*; representative images are shown in **figure 3.3.9a**. Images were then processed in MicrobeJ, a plugin for FIJI, which detected the bdelloplasts in the phase channel and the *B. bacteriovorus* cells in the mCerulean channel, allowing the mCherry foci to be overlaid and seen in the bdelloplast (see methods for detection parameters). Once detected, a heatmap of the *B. bacteriovorus* cells could be made to show where the DivIVA-mCherry foci were inside the bdelloplast, seen in **figure 3.3.9b**.

These images clearly show bipolar DivIVA-mCherry fluorescence from attack phase, 0 minutes, up to 120 minutes, when there are multiple replisomes. However, at 180 minutes, when replisomes have dissipated and the filament is

preparing to septate, DivIVA-mcherry fluorescence is no longer focussed and is instead seen throughout the cytoplasm. This could signify the point at which DivIVA is moving to the new poles that are being formed. As DivIVA does not have the negative curvature sensing residues conserved, there must be an interaction, or multiple interactions, that facilitate its position at the pole followed by its release and transition to the septa.

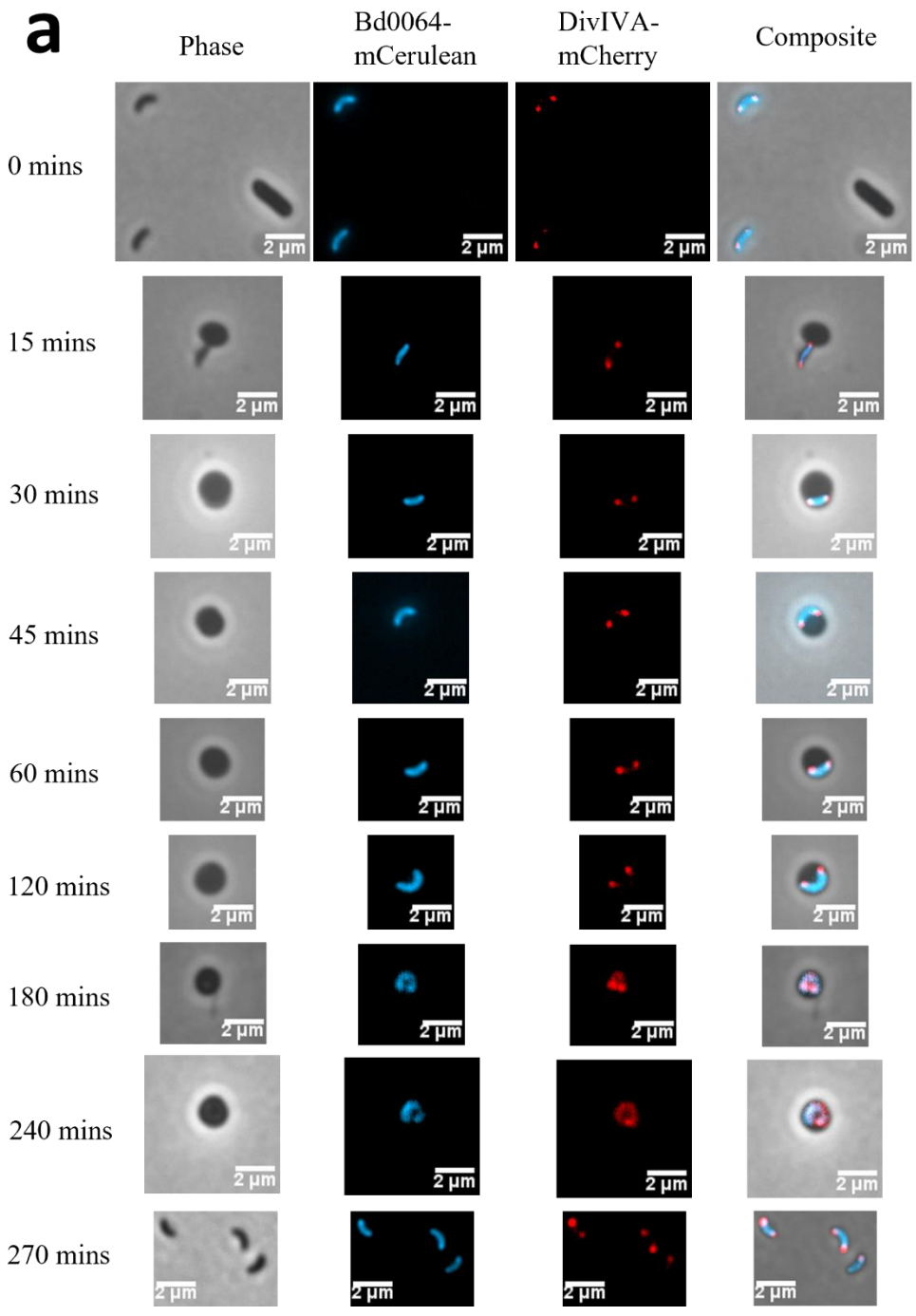

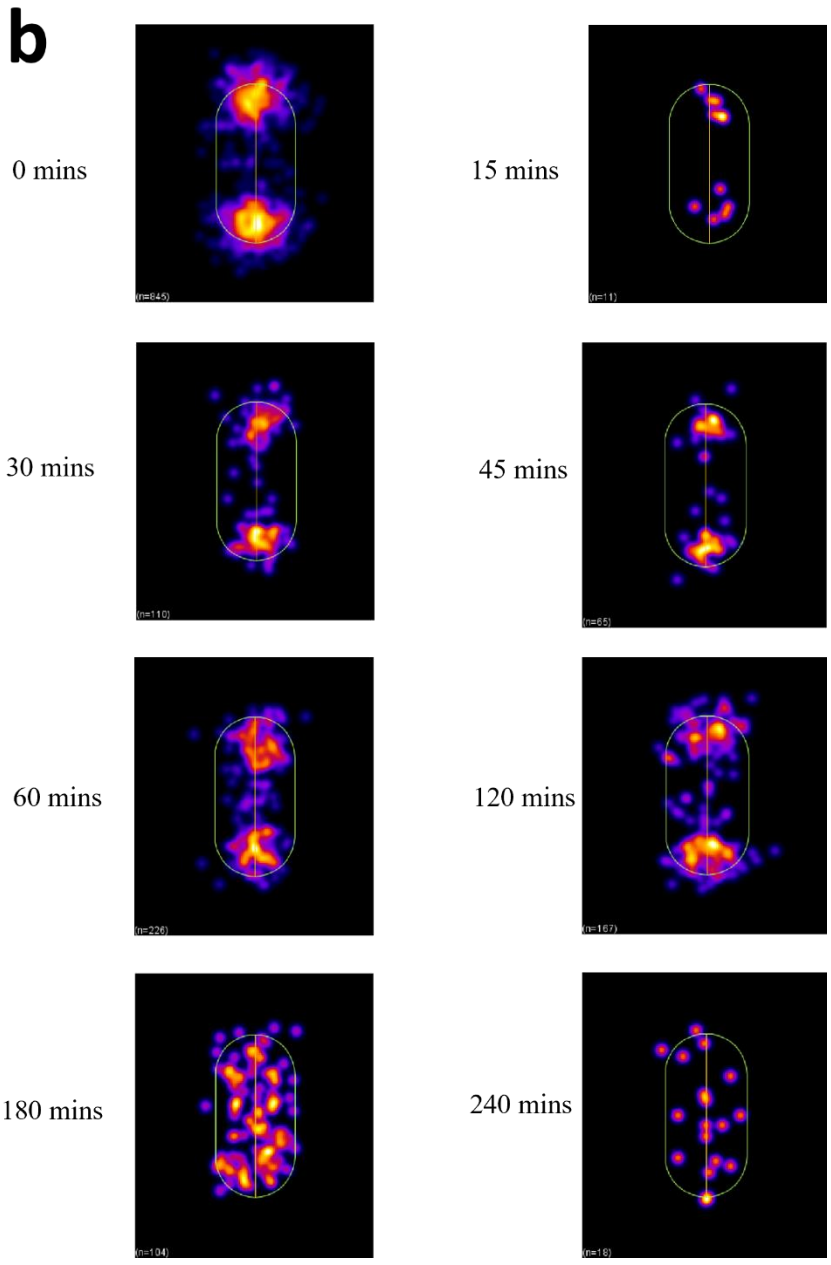

Figure 3.3.9. Timecourse microscopy with heatmaps showing bipolar localisation of DivIVA-mCherry from attack phase to septation. (a) Timecourse microscopy of the *B. bacteriovorus* HD100 Bd0064-mCerulean DivIVA-mCherry strain at the time points shown to the left of the panels. To make this strain, DivIVA-mCherry was conjugated into the HD100 Bd0064-mCerulean double crossover strain, such that it was merodiploid for DivIVA-mCherry. Channels are shown at the top: from left to right are phase contrast, mCerulean, and mCherry channels with a composite of all three. These show the bipolar fluorescence of the DivIVA-mCherry in the Bd0064-mCerulean background up until 180 minutes. These images are indicative of three biological repeats. (b) Using the timecourse microscopy images in MicrobeJ,

heatmaps were made of the DivIVA-mCherry foci using the mCerulean fluorescence to define the *B. bacteriovorus* cell (n varies by time point due to some timepoints being experimentally more difficult to capture: 0 mins – 845, 15 mins – 11, 30 mins – 110, 45 mins – 65, 60 mins – 226, 120 mins – 167, 180 mins – 104, 240 mins – 18). These also show bipolar foci up to 180 minutes.

3.3.9 Using phase contrast microscopy and MicrobeJ to analyse the morphological phenotype of *ΔdivIVA*

Milner showed that deletion of *divIVA* was possible in predatory *B. bacteriovorus*, demonstrating that DivIVA is not essential for predatory growth and division. He did, however, find a morphological phenotype for this strain. Via transmission electron microscopy of attack phase cells recently emerged from bdelloplasts, Milner found that the *B. bacteriovorus ΔdivIVA* strain had a morphological defect resulting in shorter, wider cells. Wild-type *B. bacteriovorus* HD100 pSUP404.2 (empty vector) cells had a mean length of 1.40 ± 0.04 μm and mean width of 0.36 ± 0.01 μm (n = 75). The Δ*divIVA*$_{Bd}$ mutant had a shorter mean length of 1.01 ± 0.03 μm (T test, $p<0.001$; n = 75) and larger mean width of 0.42 ± 0.01 μm (T test, $p<0.01$; n = 75) (Figure 4). Additionally, rare doublet cells were observed in the attack phase population (at less than 1%). These appeared to have an incompletely divided septum, which pinched in between the non-divided cells, resulting in a single longer cell. Milner found that complementation partially restored cell length and width of attack phase cells when imaged by TEM (T test, $p<0.001$, n = 75). He also found that complementation with mutant DivIVA(A78T) only partially restored the width and not length of the cells. Fixing cells for TEM imaging may alter the morphology of the cells, and the sample sizes were small, so, I repeated this analysis using phase contrast microscopy, with the the MicrobeJ plugin for analysis of the images (Ducret et al., 2016).

Initially, I used the *ΔdivIVA* strain constructed by Milner and WT HD100 as a control to see whether Milner's results were replicable without the presence of the PSUP404.2 plasmid. Additionally, I used two strains of *E. coli* as prey, S17-1 and MG1655; Milner's analysis only used S17-1. This was to see whether the size of the prey affects the size of the *B. bacteriovorus* progeny; S17-1 are typically longer than MG1655, with greater variability in length. Larger host cells may exacerbate defects arising from septation due to the increased number of septa and progeny. All results are indicative of three biological repeats.

Firstly, I characterised the morphology of the prey strains. S17-1 cells were longer, with higher variability in length, at 2.92 ± 0.28 μm (n = 3379),

compared to MG1655 cells, at 2.22 ± 0.12 μm (n = 4287). MG1655 cells were marginally wider, 0.82 ± 0.001 μm, than S17-1, 0.79 ± 0.001 μm, but width variability was similar. This characterised MG1655 strain as shorter cells with less variable lengths.

As shown in **figure 3.3.10**, for WT *B. bacteriovorus*, the mean length of attack phase cells was not affected by the prey strain; 1.221 ± 0.004 μm for S17-1 and 1.212 ± 0.002 μm for MG1655. However, attack phase cells were significantly wider (T test, P<0.001, n = 5782 (HD100 w/ S17-1), 9234 (HD100 w/ MG1655)), on average, when preying upon MG1655 (0.548 ± 0.001 μm, n = 5782) than with S17-1 (0.386 ± 0.001 μm, n = 9234). The width difference could be due to the available space in the bdelloplast. The longer S17-1 cells form a larger bdelloplast, with ample space for elongation; if the filament can no longer extend, as may be the case in the smaller MG1655, the resources could instead be used to expand the width of the filament.

A further effect of prey strain is seen in the variance of lengths between *B. bacteriovorus* preying on the different strains. While mean length of *B. bacteriovorus* remained the same, variance was much higher for those preying upon S17-1 (0.71), a strain with a higher variance in length, than for MG1655 prey (0.53). The distribution of both length and width results can be seen in **figure 3.3.11**. This, with the difference in width between prey, suggests that *B. bacteriovorus* can adapt to the morphology of its prey. With more room, *B. bacteriovorus* can extend further, resulting in longer prey. In smaller prey, with limited room for extension, excess resources could go towards expanding width. Therefore, cells could be of a similar overall size, containing everything required to continue the cycle, irrespective of how far they can extend in the bdelloplast.

The mutant strain *ΔdivIVA* had significantly lower mean length than its WT counterpart when preying on either *E. coli* strains, agreeing with Milner's analysis; 1.062 ± 0.004 μm for S17-1 (T test, P<0.001, n = 4051) and 1.027 ± 0.004 μm for MG1655 (T test, P<0.001, n = 3540). When preying upon S17-1, the *ΔdivIVA* was wider than WT, at 0.503 ± 0.001 μm (T test, P<0.001, n = as above), but with MG1655 prey there was minimal difference for average

width, at 0.54 ± 0.002 μm. Interestingly, variance in length for *ΔdivIVA* was similar with both S17-1 (0.57) and MG1655 prey (0.58). In the *ΔdivIVA* strain, the higher variance seen with WT preying upon S17-1 is no longer present. This could be due to this strain no longer being able to adapt to prey

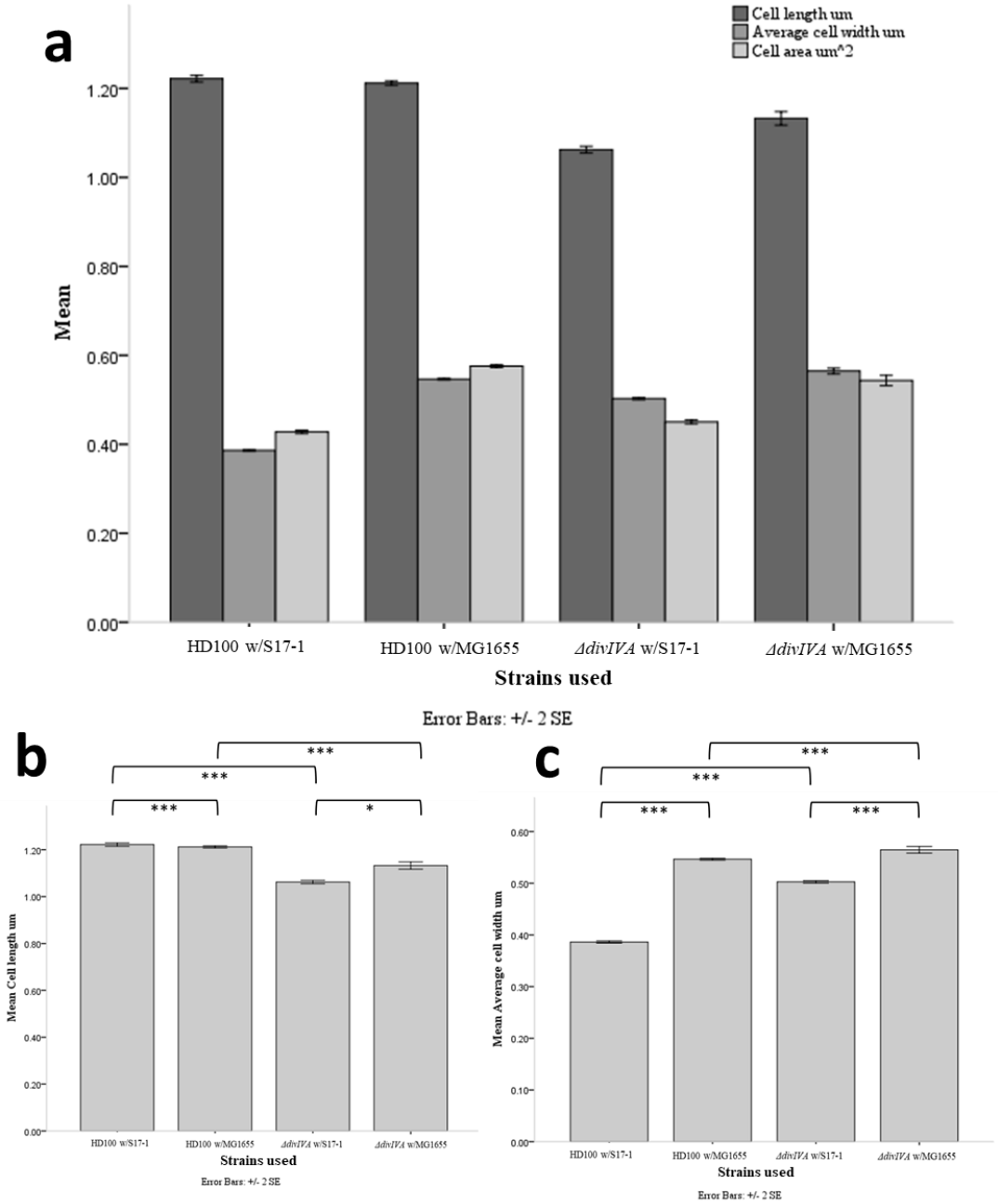

morphology, as hypothesised above.

Figure 3.3.10. Graphs showing decreased mean length and increased width of strain *ΔdivIVA*, and morphological differences of attack phase cells based of prey strain. Graph (a) shows the collected data for length, width and area of attack phase

cells. Graph (b) shows significance between mean cell lengths. With both prey, cells were shorter for the *ΔdivIVA* strain (T test, P<0.001, n = 5782 (HD100 w/ S17-1), 9234 (HD100 w/ MG1655), 4051 (*ΔdivIVA* w/ S17-1), 3540 (*ΔdivIVA* w/ MG1655)). (c) This shows the significance between mean cell widths. In WT, preying upon *E. coli* MG1655 prey produced wider AP cells (T test, P<0.001). Additionally, *ΔdivIVA* strain AP cells were wider than their WT counterparts (T test, P<0.001). Together, these agree with Milner's previous analysis that *ΔdivIVA* attack phase cells are shorter and wider than WT. They also show that for WT HD100, cell width, but not cell length, varies with prey size. In the *ΔdivIVA* strain, both length and width vary. All results are representative of three biological repeats. SE represents standard error of the mean.

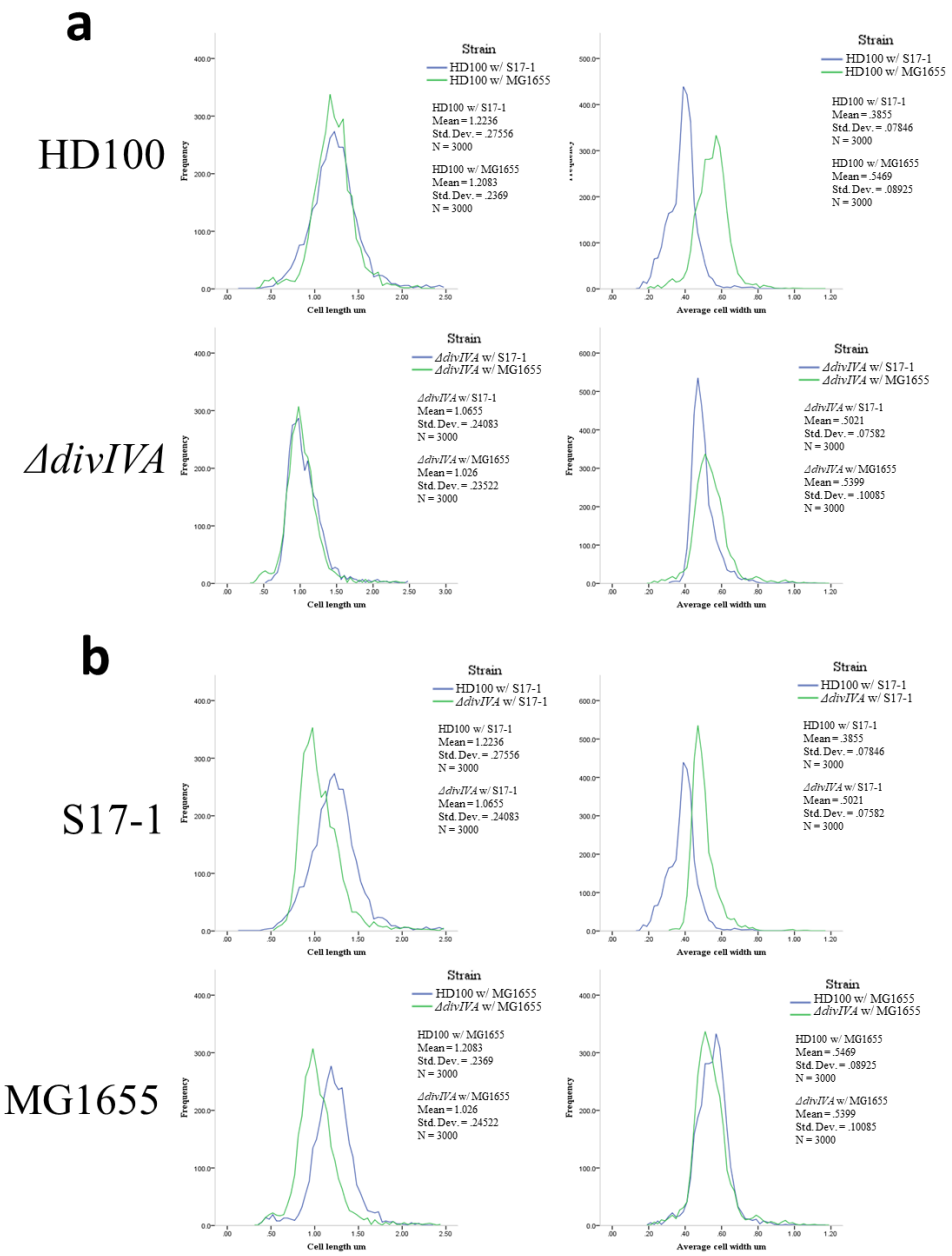

Figure 3.3.11. Frequency histograms for the distribution of length and width measurements for *B. bacteriovorus* WT and *ΔdivIVA* strains, showing increased variation of width when preying on *E. coli* MG1655, and loss of variation in the *ΔdivIVA* strain. Histograms in (a) show the distribution of length (left) and width (right) for WT (top) and *ΔdivIVA* (bottom) strains. Overlaid distributions are shown for predatory cultures with *E. coli* S17-1 (blue) and MG1655 (green). These show a greater width difference between prey strains with WT *B. bacteriovorus* than there is for the *ΔdivIVA* strain. Histograms in (b) also show length (left) and width (right) distributions but show these for both *B. bacteriovorus* strains when preying up S17 (top) or MG1655 (bottom). Overlaid distributions are shown for WT (blue) and *ΔdivIVA* (green). To generate histograms, 1000 random samples were taken for each experiment.

WT with either prey and *ΔdivIVA* with MG1655 had a significant positive correlation ($P<0.001$ for all) between length and width, whereas there was no correlation found in *ΔdivIVA* with S17-1, **figure 3.3.12**. This could indicate that the variable, long prey cells have a greater morphological effect on the *ΔdivIVA* strain, possibly due to an increased number of progeny. With MG1655, fewer septa may lead to a lower risk of this defect occurring. This could be due to DivIVA having a role in width control, or because of a role in septal site selection. It could also be a result of not receiving metabolic signals that would normally indicate how many progeny can be made from available resources. There could be enough room in the S17-1 bdelloplast for overextension of the filament, resulting in thinner progeny, while the smaller MG1655 bdelloplast may limit this mechanically.

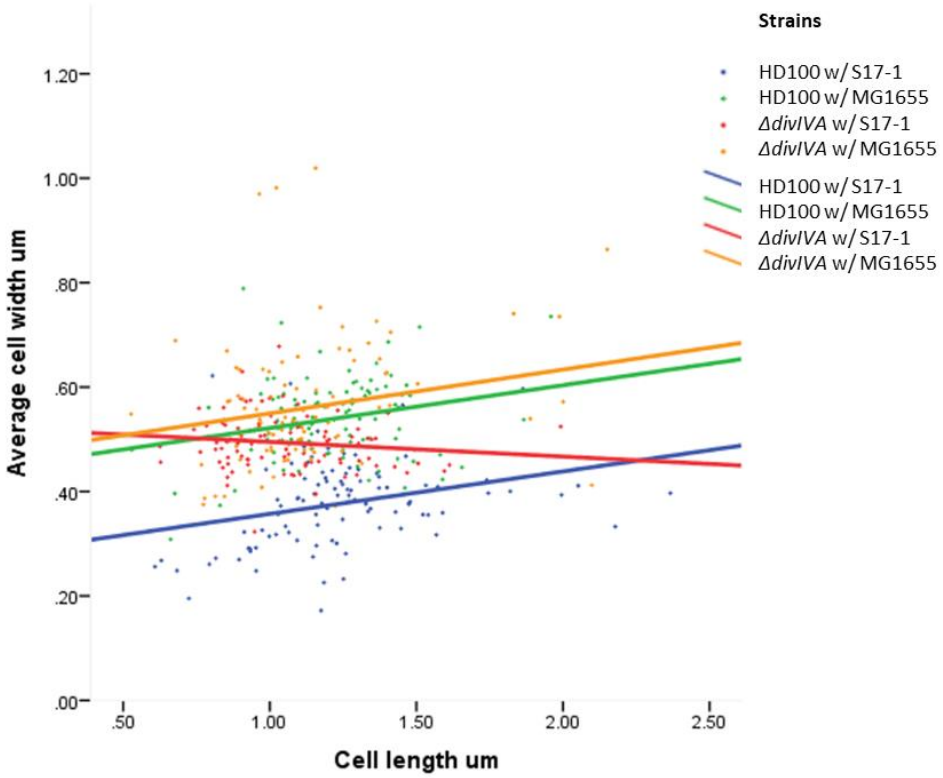

Figure 3.3.12. Scatter graph showing the significant correlation between cell length and width for WT *B. bacteriovorus* strains, with either prey strain, and in the *ΔdivIVA* strain, only with *E. coli* MG1655 prey. This scatter graph plots the cell length with the average cell width of WT *B. bacteriovorus* and the *ΔdivIVA* in attack phase, having been grown in a lysate containing either *E. coli* prey strain S17-1 or MG1655. 100 random samples were taken from three biological repeats to generate this graph. The lines represent a line of best fit. Using the full data set, positive correlations (Pearson's correlation coefficient) were found for *B. bacteriovorus* HD100 when preying upon *E. coli* S17-1 (PCC 0.293, $p<0.001$, n = 5782) and MG1655 (PCC 0.207, $p<0.001$, n = 9234), as well as for strain *ΔdivIVA* when preying upon *E. coli* MG1655 (PCC 0.214, $p<0.01$, n = 3540). No significance was found for *B. bacteriovorus* strain *ΔdivIVA* when preying up *E. coli* S17-1 (PCC -0.003, $p > 0.05$, n = 4051).

Following this, I repeated Milner's complementation analysis with the PSUP404.2 strains in the presence of kanamycin. This consisted of six strains,

three each of WT and *ΔdivIVA*. The plasmid was either empty, as a control, or contained a copy of either *divIVA* or the *divIVA-A78T* mutant. This was repeated with both S17-1 and MG1655 prey strains.

As with Milner's results, all *ΔdivIVA* strains were shorter than WT with both prey strains, shown in **figure 3.3.13**. Width was also higher in *ΔdivIVA* but the effect size was small. Complementation results were variable. With S17-1 prey, complementation of the *ΔdivIVA* with the PSUP404.2 *divIVA* plasmid resulted in partial restoration of length, but did not rescue width, of the attack phase cells. With MG1655 prey, the width was restored by introduction of PSUP404.2 *divIVA*, and partially restored by PSUP404.2 *divIVA-A78T*.

An interesting effect was found when looking at the distribution of *B. bacteriovorus* sizes for the WT strain with the PSUP404.2 *divIVA-A78T* plasmid introduced. In this population, there were increased rates of smaller and longer cells, shown in **figure 3.3.14**, while the mean length was similar to the WT strain with the empty PSUP404.2 plasmid. While further work is needed, this introduces the possibility that expression of this mutant in WT cells results in morphological changes even in the presence of WT DivIVA.

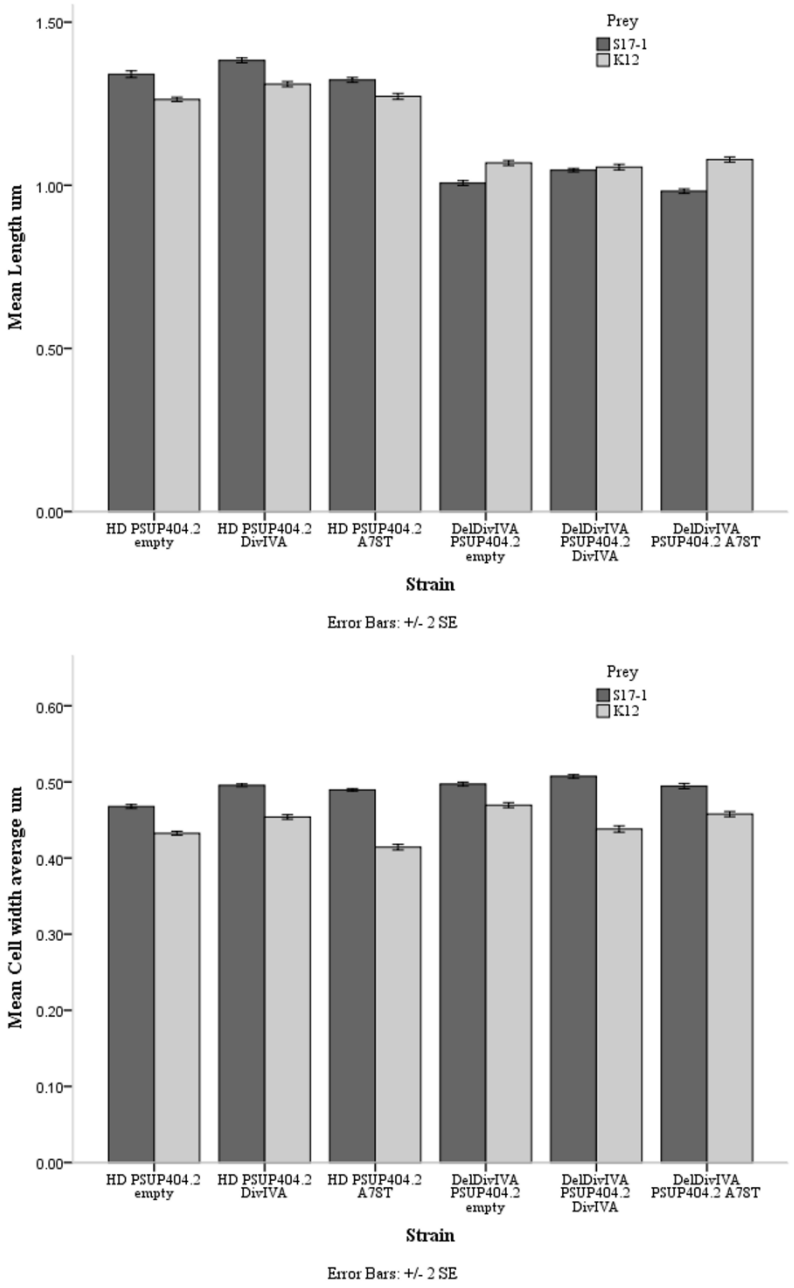

Figure 3.3.13. Graphs showing mean length decrease and slight width increase for *ΔdivIVA* strains containing PSUP404.2 plasmids, with limited or no rescue from complementation. Mean lengths (top) and widths (bottom) are shown for attack phase *B. bacteriovorus* WT and *ΔdivIVA* strains containing PSUP404.2 plasmids. The plasmids either had no insert, WT *divIVA*, or *divIVA* mutant A78T. Two *E. coli* prey strains were used: S17-1 (dark) and MG1655 (light). These results agree with Milner's in that *ΔdivIVA* strains are shorter and, marginally, wider. Complementation with WT or A78T *divIVA* had variable results. All results are representative of three biological repeats.

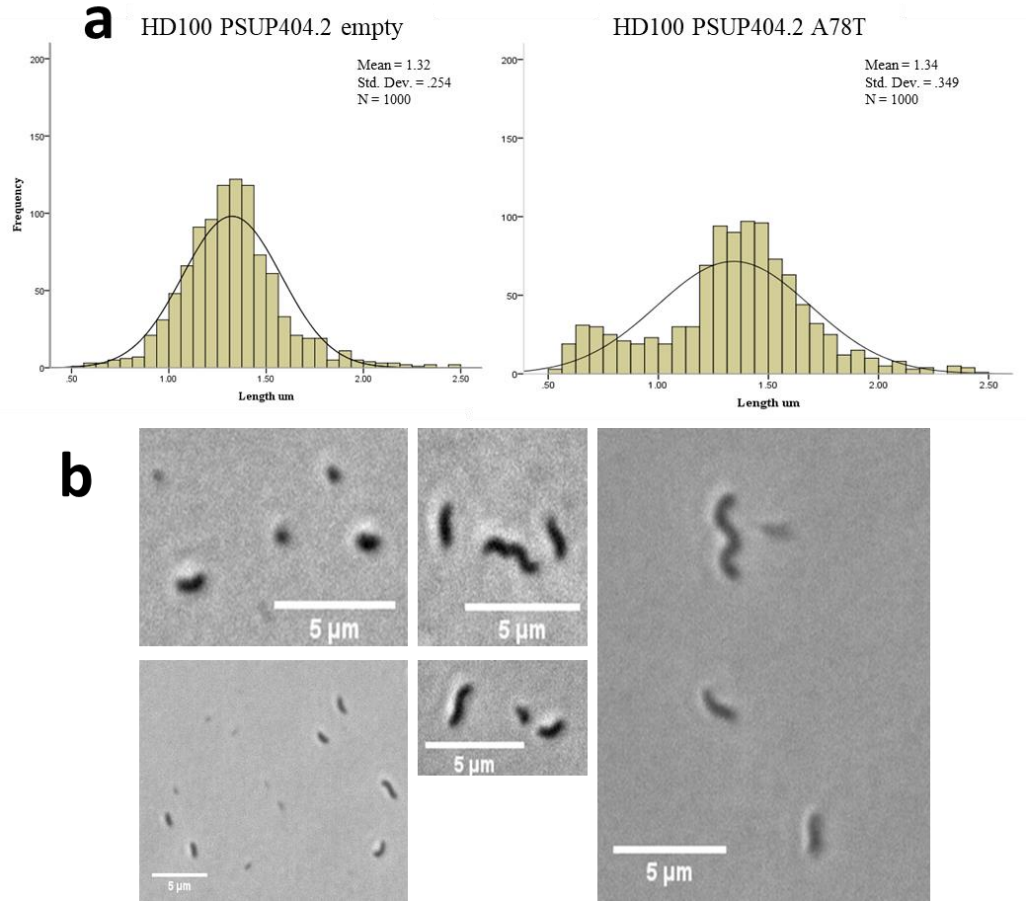

Figure 3.3.14. B. bacteriovorus HD100 WT containing plasmid PSUP404.2-*divIVA*(A78T) shows an increase in shorter and longer cells but has the same mean length as wild type. (a) A distribution graph for the cell lengths of HD100 containing empty plasmid PSUP404.2 and HD100 containing PSUP404.2 expressing *divIVA* mutant A78T. Expression of the mutant in the presence of WT *divIVA* has a dominant effect that shows an increase in shorter cells. The mean length between the strains is the same, suggesting an increase in longer cells, too. (b) Phase contrast images of the HD100 strain expressing A78T mutant *divIVA*. These show the longer and shorter cells seen in the distribution graph.

3.3.10 Pairwise BTH testing shows Bd0465 interacts with DivIVA, Bd0466, and ParA3

To determine if DivIVA interacts with the other protein products of the *divIVA* operon, we used the Bacterial Two Hybrid assay. In addition, we also tested a selection of known *B. bacteriovorus* cell division related proteins, largely cloned by other lab members before my project started (see acknowledgements). BTH assays were performed in a pairwise manner between candidate proteins. For confirmation and quantification, the positive interactions were subjected to β-galactosidase activity assays. These assays showed significant results (Mann-Whitney U test, $p<0.05$, $n = 9$, three biological repeats) for interactions between Bd0465-DivIVA, Bd0465-Bd0466 and Bd0465-ParA3, **figure 3.3.15**. No interaction was detected between DivIVA-Bd0463, and for DivIVA with ParA1, ParA2 or ParA3. This shows a potential network of interactions focussed around Bd0465, which interacts with DivIVA and Bd0466, as well as ParA3, the canonical ParA homologue. This could connect amino acid regulation and cofactor PLP homeostasis with division and partitioning.

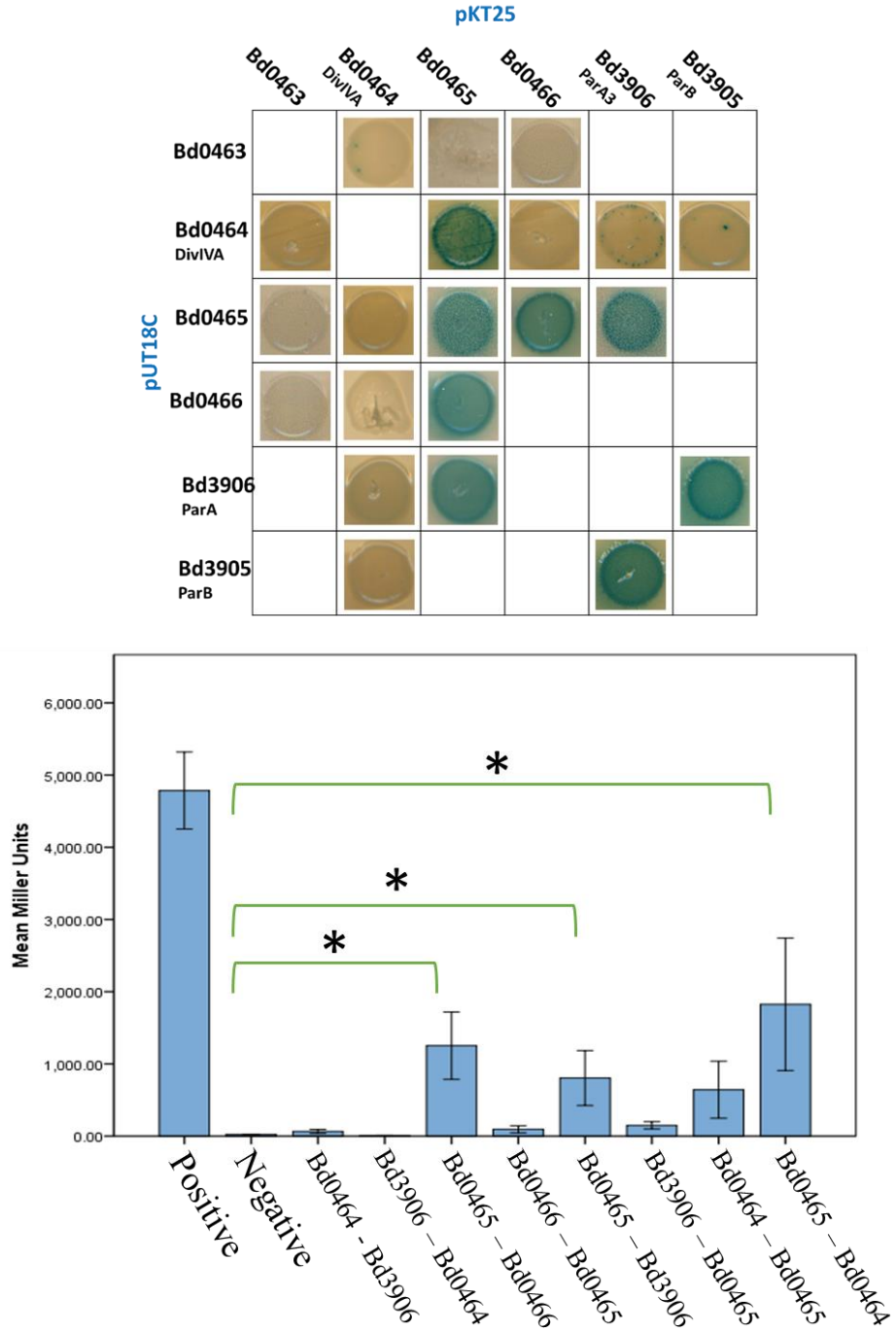

Figure 3.3.15. Pairwise Bacterial Two Hybrid spot result and associated β-galactosidase assays show positive interactions for Bd0465 with DivIVA, Bd0466 and ParA3. (Above) The result matrix shows scanned images of positive blue spots and negative white spots for pairwise BTH assays. These show positive interactions for plasmid pKT25-bd0465 with pUT18C-bd0464 (DivIVA), -bd0466 and -bd3906 (ParA3). Additionally, Bd0465 is shown to interact with itself, and Bd3906 (ParA3) is shown to interact with Bd3905 (ParB) in this system. (Below) A graph of manual β-galactosidase activity assay results for the pairwise interactions in (a). Significant

results (Mann-Whitney U test, $p<0.05$) were attained for pKT25-bd0465 with pUT18C-bd0466, -bd0464 and -bd3906.

Interaction was also confirmed between ParA3 and ParB. No interactions were found between Bd0463 and all other proteins encoded from the *divIVA* operon. Additionally, there were no interactions seen between DivIVA and division homologues FtsA (Bd3190), FtsK (Bd0043), PBP1A (Bd0160) and PBP2 (Bd2460). There was also no interaction between DivIVA and putative kinase Bd3148, which Milner identified as a candidate for phosphorylating DivIVA.

These results led to the connection between DivIVA and ParA3. Following this, I wanted to find unknown interactors of DivIVA. This is addressed with the BTH library in chapter 4. The BTH results also led into an investigation of the ParA homologues in *B. bacteriovorus* which were also previously studied by Milner.

3.3.11 The *parA1* operon is expressed from 120 minutes of the HD cycle

Milner used RT-PCR analysis to show the expression of the *parA* homologues through the HD cycle. He found that *parA1* expression peaks at 180/240 minutes. Expression of *parA2* had a peak at 15 minutes, and then a stronger peak from 120- to 240-minutes. Expression of *parA3* was found to peak at 60 minutes. Using unpublished RNA-seq data, I have further analysed the expression of the *parA* homologues and any genes that are cotranscribed.

Rockhopper predicts that *parA1 bd1326* is the first gene in a three gene operon. Using RT-PCR, Milner previously showed that these genes are cotranscribed. This RNA-seq analysis shows that these three genes are expressed from 120 minutes, peaking at 180 minutes but still expressed through to 300 minutes, **figure 3.3.16**. There is currently no known function for ParA1, but this expression pattern does suggest a role during growth and/or division.

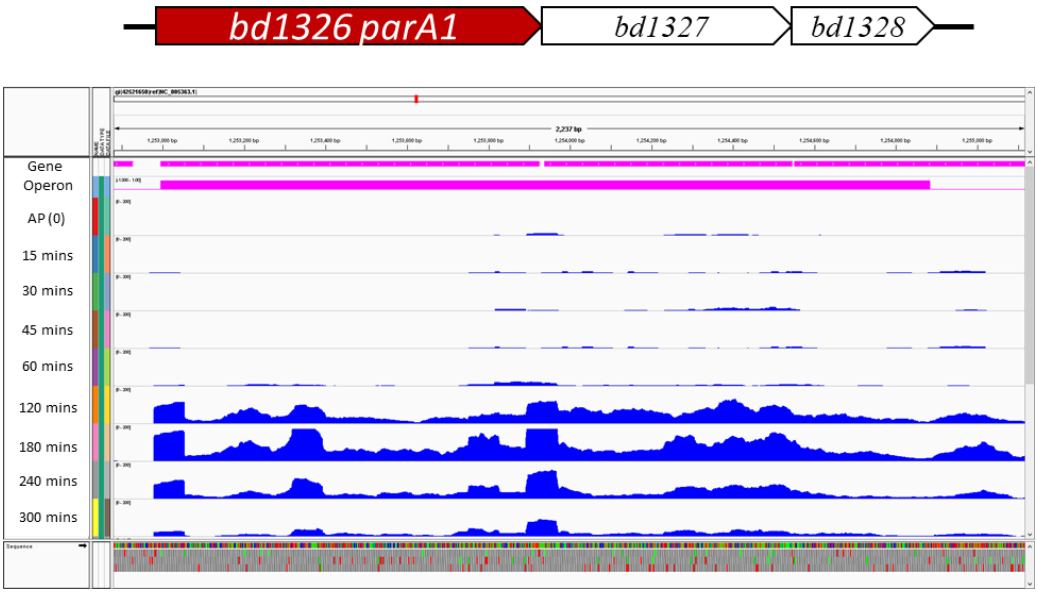

Figure 3.3.16. RNA-seq data for the *parA1* operon shows upregulation from 120 minutes to 300 minutes in the HD cycle. Screenshot taken from Rockhopper showing the positive strand at the parA1 operon. This shows increased expression at 120 minutes, the time at which multiple replisomes are present. This continues through septation, maturation and lysis (180-240 minutes) with decreased, but still present expression, in the newly released attack phase progeny (300 minutes). The range is 0-200 reads for all tracks. To the left, the tracks are labelled with times representing the timepoint at which the RNA was extracted from the *B. bacteriovorus* predatory culture (AP = attack phase). Above, the cartoon shows the location and designation of the genes in relation to the Rockhopper screenshot. The gene track shows the location of the genes, the operon track is where Rockhopper predicts a multigene operon.

3.3.12 Genes *parA2* and *bd2329* are predicted to be cotranscribed and are expressed from 120 minutes

Rockhopper predicts that *parA2* is cotranscribed with *bd2329*, as Milner showed using RT-PCR. The peak seen in Milner's RT-PCR assay for *parA2* expression is not reflected in the RNA-seq data used here, however its expression from 120 minutes is apparent. This peaks at 180 minutes but is still seen at a lower level at the 300-minute time point, **figure 3.3.17**.

Protein domain predictions and structural searches for Bd2329 do not return any result and a pBLAST of the protein shows that homologues are only

present in *Bdellovibrio* species, but not *B. exovorus*. This suggests it is specific to intracellular predation, however its function cannot be discerned without further work.

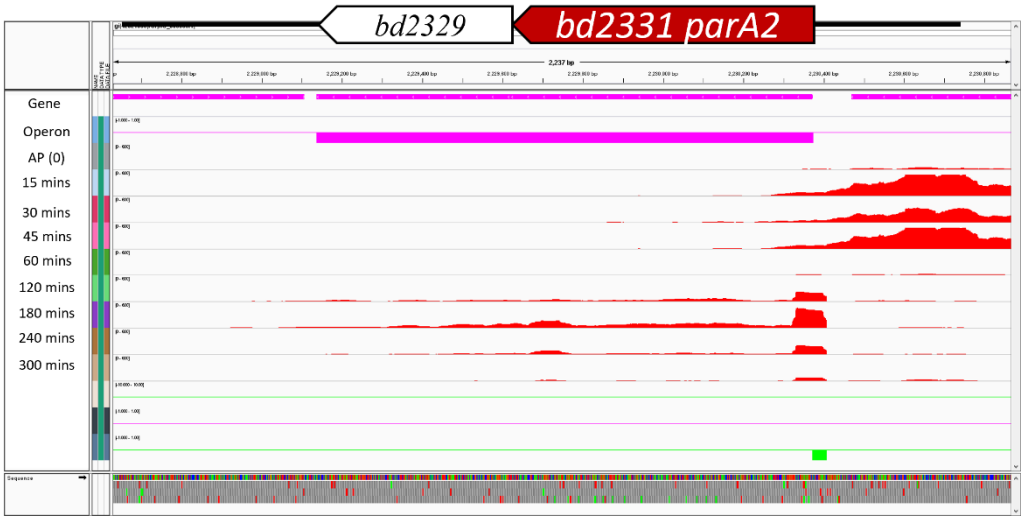

Figure 3.3.17. RNA-seq data for the *parA2* operon shows upregulation from 120 to 300 minutes in the HD cycle. This operon shows upregulation at 120 minutes, when multiple replisomes are present in the growing filament, with expression peaking at 180 minutes, when the replisomes are gone and septation is beginning. Expression continues at 240 minutes when the bdelloplast is being lysed with decreased expression in the released progeny at 300 minutes. Range is 0-800 reads. To the left, the tracks are labelled with times representing the timepoint at which the RNA was extracted from the *B. bacteriovorus* predatory culture (AP = attack phase). Above, the cartoon shows the location and designation of the genes in relation to the Rockhopper screenshot. The gene track shows the location of the genes, the operon track is where Rockhopper predicts a multigene operon.

3.3.13 The *parA3* operon is expressed from 60 to 300 minutes

As Milner previously showed, *parA3* is predicted to be the first of a three gene operon by Rockhopper. This includes *parB* and *bd3904*, the latter of which was identified as a bactofilin (Lin et al., 2017). This operon is expressed from 60 minutes, peaking at this time point with continuing expression through to 300 minutes, **figure 3.3.18**.

At the 60-minute time point of the HD cycle, the first replisome is seen, and by 180 minutes, the replisomes have become diffuse and the filament prepares to septate. This shows that ParAB, and the cotranscribed bactofilin, are present for this whole process, as would be expected.

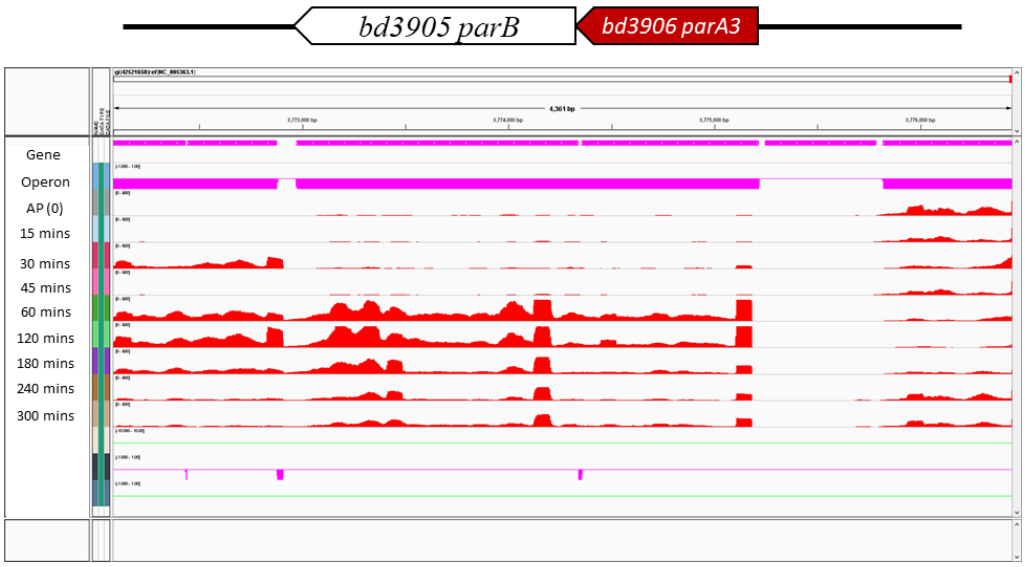

Figure 3.3.18. RNA-seq data for the *parA3* operon shows upregulation from 60 to 300 minutes in the HD cycle. The canonical *parA3* and neighbour *parB* are expressed from 60 minutes, at which time a single replisome can be seen. This continues through to 300 minutes, covering the generation of multiple replisomes, septation and bdelloplast lysis. This expression pattern suits the roles of *parA3* and *parB* chromosomal partitioning. Range is 0-1000 reads. To the left, the tracks are labelled with times representing the timepoint at which the RNA was extracted from the *B. bacteriovorus* lysate (AP = attack phase). Above, the cartoon shows the location and designation of the genes in relation to the Rockhopper screenshot. The gene track shows the location of the genes, the operon track is where Rockhopper predicts a multigene operon.

3.3.14 Analysing the effect of fluorescently tagging ParA homologues on morphology of attack phase cells

Milner originally found that *parA3* (*bd3906*, the canonical *parA* homologue) could not be deleted in *B. bacteriovorus*. Upon fluorescently tagging it, he saw that the mean length of these cells increased compared to wild type. In his

analysis, he used TEM imaging to determine that the population had an increased number of very long cells. He also found that fluorescently tagged *parA1* and *parA2* did not change the morphology of the cells.

As with his *ΔdivIVA* strain, I have repeated his analysis with phase contrast microscopy and a larger sample size. This used Milner's mCherry tagged strains of each ParA homologue and the control strain *bd0064-mcherry*. Two *E. coli* prey strains were used, containing empty plasmids to confer kanamycin resistance. These were S17-1 with pZMR100 and MG1655 with PSUP404.2.

With S17-1 prey, my analysis showed no significant difference between the mean lengths of *parA3-mCherry* and control strains, seen in **figure 3.3.19**. Contrasting Milner's results, the mean length of *parA1-mCherry* and *parA2-mCherry* strains were significantly longer than the control. The mean width of cells was similar for the control, *parA1-mCherry* and *parA2-mCherry*, while *parA3-mCherry* cells had a slightly higher average width. A similar effect was seen with MG1655 prey, except that the *parA3-mCherry* strain was marginally longer than the control, and all three *parA* strains were marginally wider, although effect sizes are minimal.

The discrepancy between mine and Milner's analyses could be methodological. His images were taken on a TEM, requiring the cells to be treated and fixed prior to imaging. In contrast, the phase contrast images from this study used live cells with a much larger sample size.

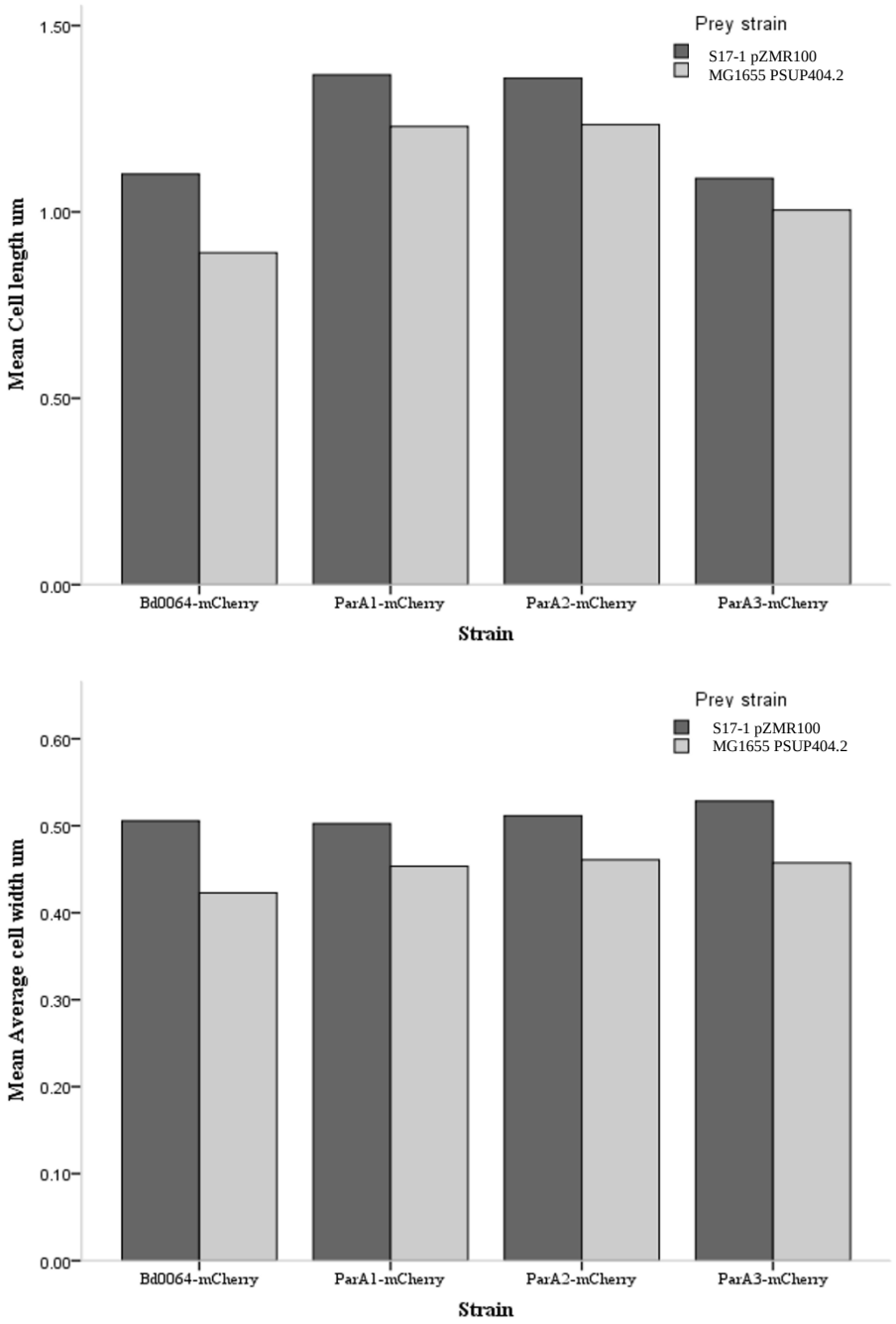

Figure 3.3.19. Graphs showing increased cell length for HD100 strains expressing tagged ParA1 and ParA2, but not for ParA3. In contrast to Milner's results, based on TEM images, attack phase cells for strains expressing ParA1-mCherry and ParA2-mCherry had significantly increased mean length (top) compared to control strain Bd0064-mCherry (T test, $P<0.001$, n = 2361 (Bd0064-mCherry w/ S17-1), 2681 (ParA1-mCherry w/ S17-1), 1498 (ParA2-mCherry w/ S17-1), 1707 (ParA3-mCherry w/ S17-1), 9859 (Bd0064-mCherry w/ MG1655), 22895 (ParA1-mCherry w/

MG1655), 20966 (ParA2-mCherry w/ MG1655), 9225 (ParA3-mCherry w/ MG1655)). This was the case when either *E. coli* prey strain was used (dark: S17-1, light: MG1655). While mean widths (bottom) of all mCherry strains preying on MG1655 were significantly higher than the control ($P<0.001$) the effect size was marginal. Results are from three biological repeats.

3.3.15 Phylogenetic protein tree of canonical ParA3 shows relationship to Firmicute homologues

I also wanted to gain further insight into the evolution of the ParA homologues in *B. bacteriovorus*. To do so, I constructed phylogenetic trees for each of the homologues.

For Bd3906, ParA3, sequences were found via pBLAST, excluding Bdellovibrionales. The top 100 non-redundant sequences were used, with the highest e-value being 3e-104. Low e-values are expected given that this is the canonical homologue. To these were added the canonical ParA homologues of *B. bacteriovorus* Tiberius, *B. exovorus* and *Halobacteriovorax marinus*, as well as *Geobacter, Myxococcus* and *E. coli* homologues. Using MEGA software, a maximum likelihood tree was processed, with 1000 bootstrap replications.

This tree clearly shows two main clades, one with Deltaproteobacteria and *Bdellovibrio,* and another with Firmicutes, **figure 3.3.20**. The Firmicutes were largely made of the genera *Paenibacillus* and *Listeria*. The specific Firmicutes are interesting; while both are facultatively anaerobic, *Paenibacillus* forms endospores, a process in Bacilli for which Soj (DivIVA) plays a major role, while *Listeria* do not. The Deltaproteobacteria include homologues from *Syntrophaceae, Desulfuromonas* and *Geobacter*, as well as several unclassified Deltaproteobacteria. This could indicate a horizontal gene transfer event between the ancestor of these Deltaproteobacteria/Oligoflexia and this clade of Firmicutes.

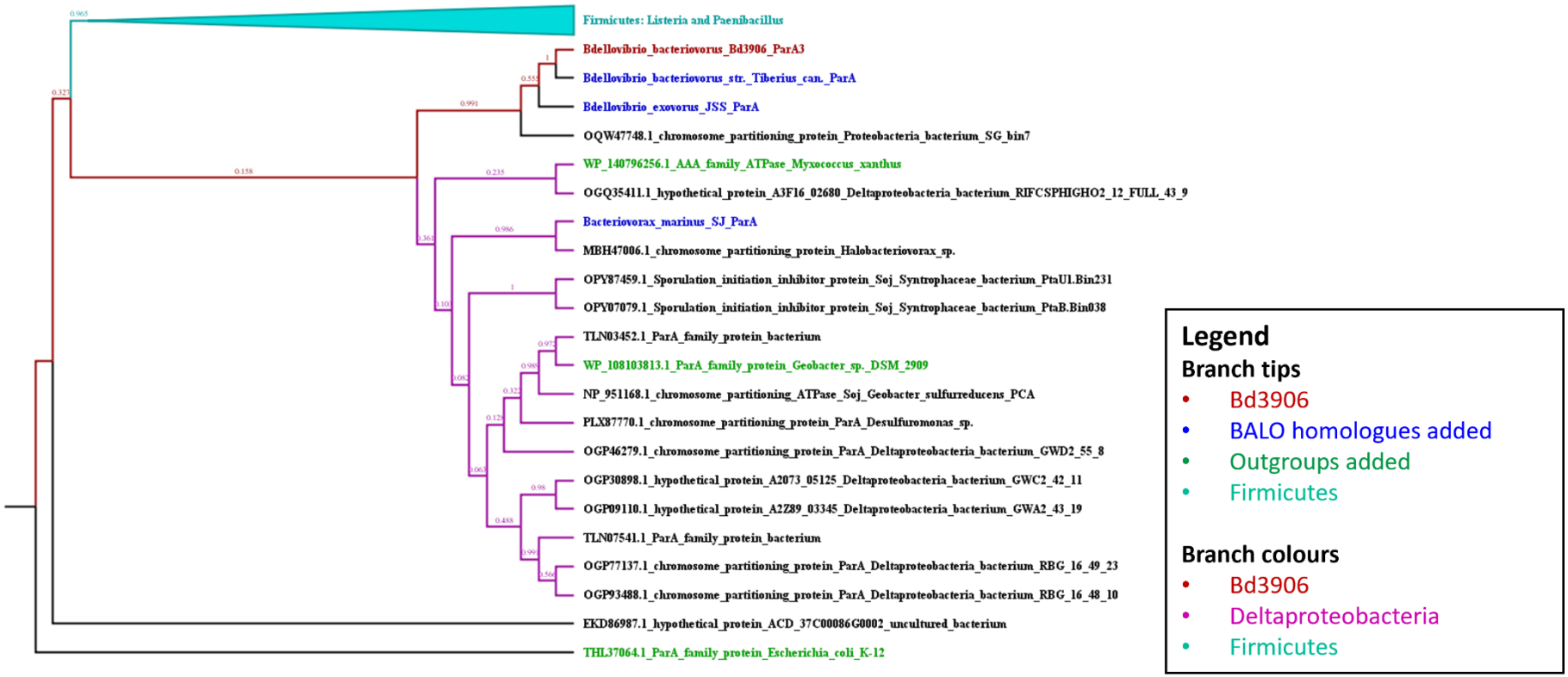

Figure 3.3.20. A protein tree showing that ParA3 (Bd3906) is most homologous to other, select δ-proteobacteria homologues, followed by ParA proteins in Firmicute genera *Listeria* and *Paenibacillus*. The blue entries indicate BALO sequences and green show outgroup sequences manually added to the analysis. All other entries were found in pBLAST using default settings. This shows a BALO/δ-proteobacteria clade and a related group of Firmicutes. Sequences were analysed in MEGA-X software using the maximum likelihood method with 1000 bootstrap replications and visualised in Figtree.

3.3.16 ParA1 phylogenetic tree shows its similarity to γ-proteobacterial *Piscirickettsia* and *Legionella* homologues

The same process as with ParA3 was used to generate a phylogenetic tree for Bd1326, with different outgroups used. These were the other ParA homologues in *B. bacteriovorus* HD100 and Tiberius, as well as the homologues in *B. exovorus* and *H. marinus* (these only have a single homologue for ParA). These clearly formed a separate clade to the ParA1 homologues.

The tree shows a few close homologues in Flavobacteria and a large group of Gammaproteobacteria, comprised mostly of *Piscirickettsia* and *Legionella* sequences, **figure 3.3.21**. This indicates another potential horizontal gene transfer event between these groups.

3.3.17 ParA2 phylogenetic tree indicates very few homologues outside of *Bdellovibrio* species

When searching for sequences homologous to Bd2331, ParA2, most were found to be more closely related to the canonical ParA3. These were discounted, leaving only a few sequences that shared higher similarity to ParA2. The addition of the other ParA homologue outgroups shows that ParA2 has higher similarity to Bd3906, ParA3, than to Bd1326, ParA1. Due to very few homologous sequences being returned in pBLAST, Bdellovibrionales were not excluded from the search.

As seen in **figure 3.3.22**, there were three homologous sequences outside of BALOS, two from *Omnitrophica* and one from *Planctomycetes*. These are from the PVC group of bacteria, so named for the inclusion of Planctomycetes, Verrucomicrobia, and Chlamydiae (Rivas-Marin et al., 2016). This poorly studied group represents bacteria with diverse modes of growth and division, with many having no FtsZ homologue. There are also several PVC bacteria whose use of peptidoglycan is in question, such as certain Chlamydiae, or where there are no biosynthetic enzymes present at all, like in the budding Planctomycetes which are instead thought to employ a proteinaceous cell wall. Given that ParA2 has a role in gliding motility, it may be that these homologues in PVC bacteria share the same function.

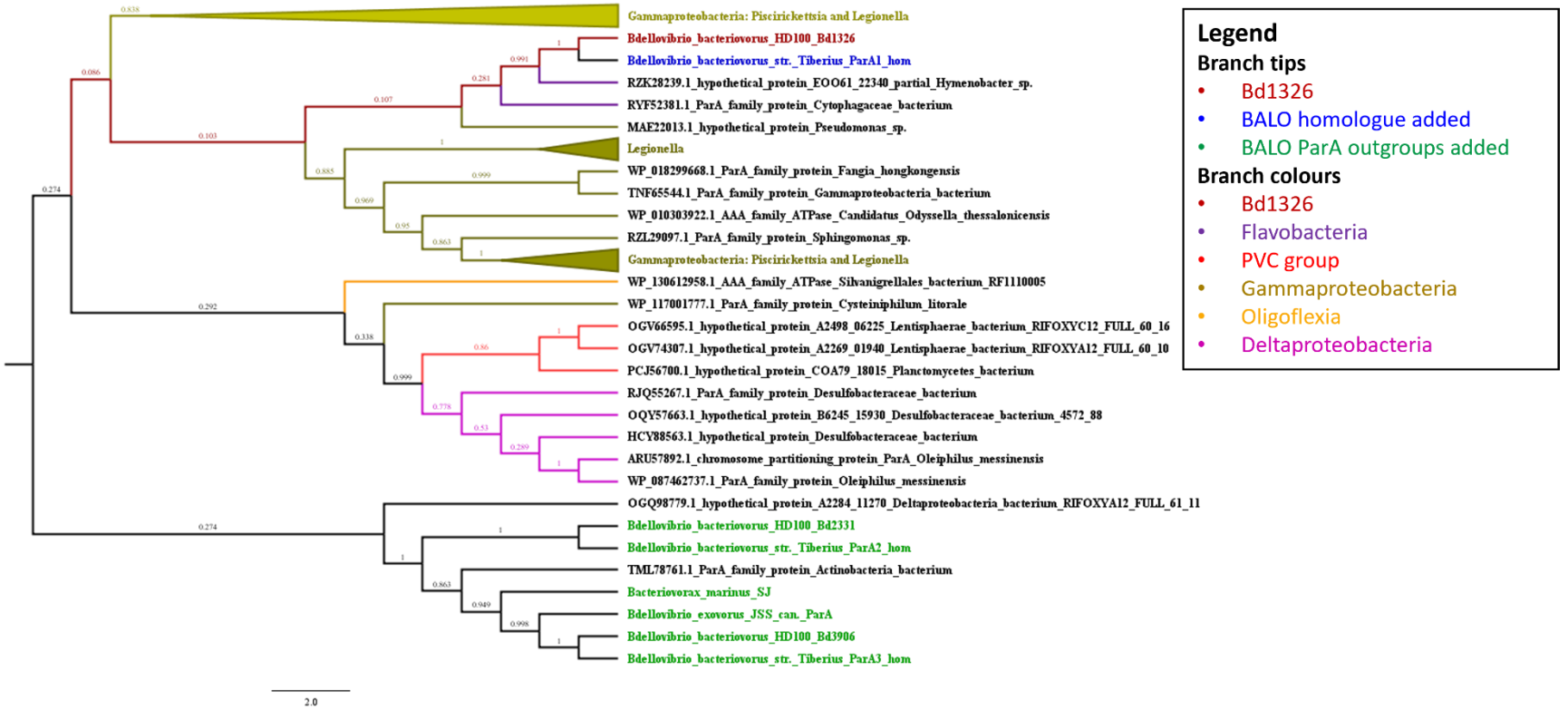

Figure 3.3.21. A protein tree showing that ParA1 (Bd1326) is most homologous to proteins in γ-proteobacteria genera *Piscirickettsia* and *Legionella*. The blue entries indicate BALO sequences specifically homologous to ParA1 and green show BALO outgroup sequences for ParA2 and ParA3, manually added to the analysis. All other entries were found in pBLAST using default settings. These sequences were added to show that the sequences returned from pBLAST are more homologous to ParA1 than to canonical ParA3 This shows ParA1 shares highest homology with proteins from Flavobacteria as well as *Piscirickettsia* and *Legionella*, both of which are γ-proteobacteria. There is also a clade containing homologues from Oligoflexia, the PVC group and δ-proteobacteria. Sequences were analysed in MEGA-X software using the maximum likelihood method with 1000 bootstrap replications, and visualised in Figtree.

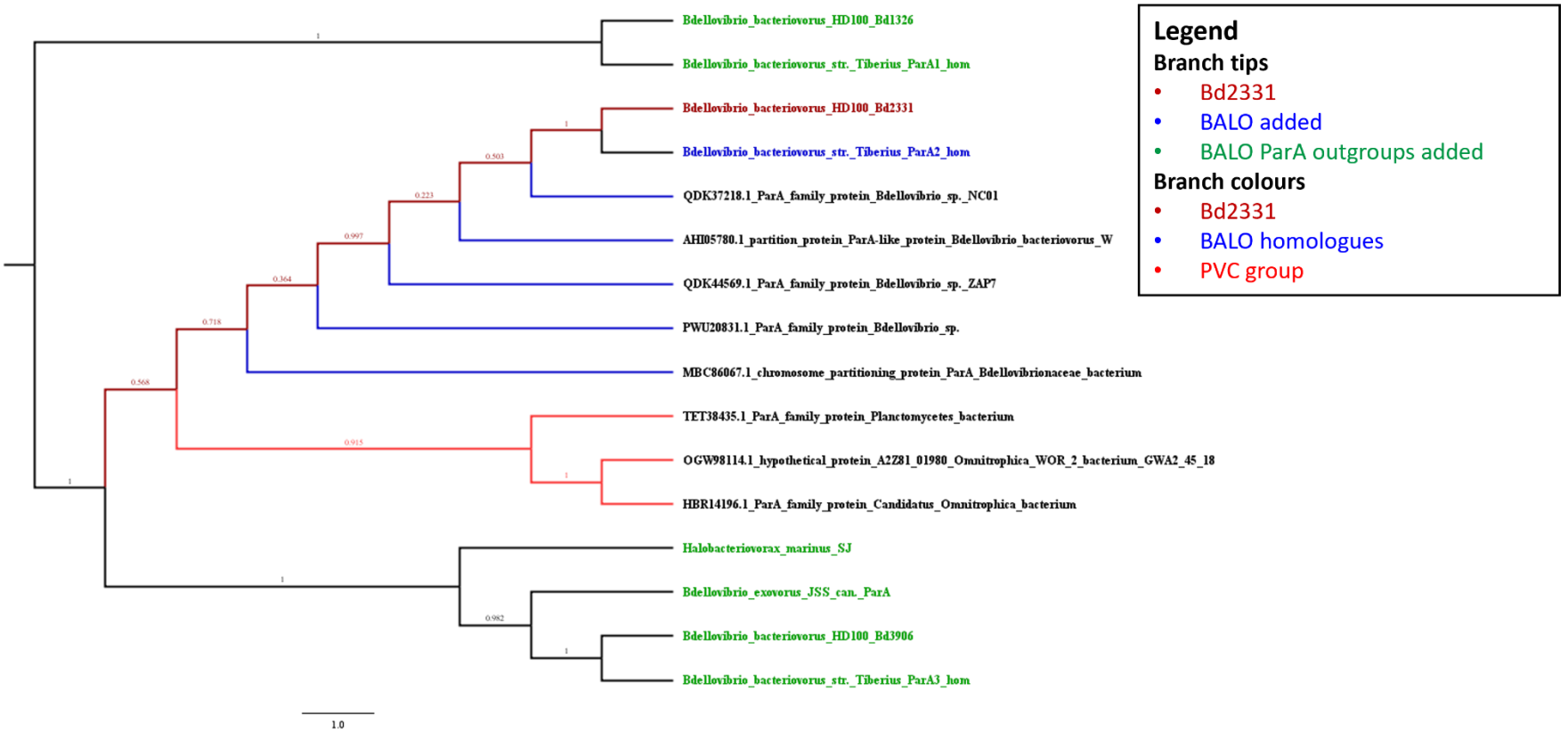

Figure 3.3.22. A protein tree showing that ParA2 (Bd2331) is homologous to PVC group proteins. The blue entries indicate BALO sequences specifically homologous to ParA2 and green show BALO outgroup sequences for ParA1 and ParA3, manually added to the analysis. All other entries were found in pBLAST using default settings. Only sequences that were more homologous to ParA2 than to canonical ParA3 were included in this tree. This shows very few non-BALO protein homologues were found, with only three PVC group homologues, annotated as ParA family proteins. Sequences were analysed in MEGA-X software using the maximum likelihood method with 100 bootstrap replications, and visualised in Figtree.

3.4 Chapter 3 Discussion

3.4.1 BTH interactions show DivIVA interaction network

The interaction between Bd0465, a ProC homolog, and Bd0466, an YggS homolog, has not been recorded in any other bacteria. It is possible that this interaction is a part of a signaling pathway that continues from Bd0466 to both ParA3 and DivIVA. YggS proteins bind pyridoxal phosphate (PLP), a highly regulated cofactor, and a change in the level of this molecule may signal to the division machinery to coordinate growth and septation. Recent work has suggested that changes in PLP levels are associated with changes in flux through the biosynthetic pathways for amino acids (Ito et al., 2013; Prunetti et al., 2016, Ito et al., 2019). One can see the necessity for such a signal due *to B. bacteriovorus* producing progeny at a timepoint when prey cell resources have been depleted. At a critical point in the predatory life cycle, the invading *B. bacteriovorus* cell must detect when remaining nutrients from the inside of the single prey cell are insufficient to produce another progeny cell. At this time septation must occur and the *B. bacteriovorus* cell must switch from growth and biosynthesis to the less metabolically active, prey-hunting attack phase progeny. The Bd0466 interaction with Bd0465 may represent a pivotal part of this signalling pathway. This is further supported by the constitutive expression of both *bd0465* and *bd0466*, as is the case with DivIVA, and the diffuse, cytoplasmic localization of the Bd0465/0466 proteins in the predator cells.

This may lead to a specific association between Bd0466 and Bd0465 occurring when PLP levels change; then in turn this could affect the Bd0465 association with ParA3, possibly releasing ParA3 for partitioning which may lead to Bd0465 association with DivIVA. Therefore, the DivIVA- Bd0465 -ParA3 interaction could synchronize the actions of DivIVA with chromosome segregation, as is thought to be the case in *M. smegmatis*, albeit through an indirect interaction (Kang et al., 2008; Ginda et al., 2013, Vijay et al., 2014). It may also possibly relate to *Corynebacterium glutamicum*, where DivIVA was shown by protein-protein studies to interact with ParB (Hammond et al., 2019).

This hypothesis focuses on metabolic signals, specifically, levels of PLP, proline and potentially other amino acids, being key to the switch from growth to division. Initial searches of biosynthesis pathway homologues suggest that *B. bacteriovorus* may not have a proline synthesis pathway. This has significant implications, as proline has several roles in bacteria, such as in osmoregulation and stress response (Pandhare et al., 2009, Szabados and Savoure, 2010, Hoffmann et al., 2012, Liang et al., 2013, Fichman et al., 2015, Zhang et al., 2015, Zaprasis et al., 2015, Christgen and Becker, 2019). Not having this pathway would mean that *B. bacteriovorus* must rely on exogenous sources, typically from the prey bdelloplast. As such, proline may have more limited use for these roles, which requires the ability to increase proline levels via synthesis in response to environmental conditions. If proline from prey is abundant, *B. bacteriovorus* would only require the catabolic pathway and could use proline intake as a metabolic indicator of the state of digestion of the prey. As such, Bd0465 may not retain its enzymatic function, but may have the ability to bind proline as a sensor, with its ability to bind to DivIVA and ParA3 regulated by its binding state.

Initial searches indicate the PLP can be synthesised by *B. bacteriovorus* in a pathway homologous to *E. coli*. However, I could not identify any salvaging proteins or enzymes responsible for converting PLP to its thioester PL. It could be the case that the substrates for the salvaging proteins may not be abundant enough in the prey cell to warrant the salvaging machinery. Of more interest is the lack of enzymes for converting PLP to PL. PLP is highly regulated in other bacteria due to its toxicity, therefore requiring a method of lowering cellular levels of the cofactor. *B. bacteriovorus* may have an alternative method of disposing of PLP or it may strictly regulate synthesis and uptake, which could also be the reason why the salvaging machinery is not present. As a part of this signalling network, Bd0466 could also be a sensor for the levels of PLP in the growing *B. bacteriovorus*, indicating to the division machinery that the cofactor can no longer be synthesised due to exhausted substrates.

3.4.2 Further insights into DivIVA and cell morphology

Continuing from Milner's preliminary comparison of cell morphology of wild type and *ΔdivIVA* strains, I analysed attack phase cells that had emerged from

two different *E. coli* strains; the longer, more variable S17-1, and the shorter, less variable MG1655. Interestingly, wild type *B. bacteriovorus* had different morphological profiles dependent on the prey strain. Attack phase cells were significantly wider when preying upon the shorter MG1655 strain, and length variability was higher with S17-1.

My results agreed that *ΔdivIVA* cells were shorter and wider, on average, than wild type with either prey strain, and also showed that the variability in length seen with wild type preying on S17-1 was no longer seen with the *ΔdivIVA* strain. This could be due to DivIVA having a role in the sensing of extension room in the bdelloplast. In the wild type, DivIVA could direct apical growth when there is excess space in the bdelloplast. The filament could then mechanically sense when there is no longer space to extend and prevent DivIVA from further increasing the filament. In the absence of space in a smaller bdelloplast, this growth could instead be directed towards the width of the filament. Such a mechanism would result in bigger bdelloplasts having longer cells emerge, while smaller bdelloplasts would have wider cells. In a prey strain such as S17-1, with higher variability in cell length but not width and thus higher variability bdelloplast size, this would result in a higher variance in the emerging cell length.

In this scenario, the *ΔdivIVA* strain would not be capable of the apical extension even when there is excess space in the bdelloplast but may still direct excess growth to the width. Therefore, this would result in emerging cells that are both shorter and wider than wild type. Application of different prey cells with varying morphologies may confirm this hypothesis. The use of other rod shaped bacteria could show if this effect is universal and cocci prey may also show if this effect is purely reliant on overall bdelloplast size.

3.4.3 Evolutionary insights into the three ParA homologues

The phylogenetic trees show a different array of bacterial homologues for each ParA in *B. bacteriovorus*. Canonical ParA3 is homologous to a ParA proteins in a group of δ-proteobacteria and Oligoflexia, as well as a clade of Firmicutes *Listeria* and *Paenibacillus*; these are both of the Order Bacillales. Interestingly, *Listeria* form endospores, for which a DivIVA homologue is involved, while

Paenibacillus do not. This suggests a lateral gene transfer event between the ancestors of the Firmicutes and the Gram-negative groups.

The tree for ParA1 suggests its closest homologues are from Flavobacteria and γ-proteobacteria, suggesting a different origin to that of ParA3. A lack of close homologues in Oligoflexia and δ-proteobacteria could be due to a more recent gene transfer event, although there is a clade of this bacteria with homologues that are more distantly related. As this is not canonical, not essential to growth, and has the lowest identity to ParA3 of the two orphan homologues, it is harder to determine the evolutionary origins. However, its homology to γ-proteobacterial ParA homologues could be further investigated while its function is also being determined in future work.

When acquiring sequences for ParA2, most of the results in the pBLAST tool had a higher homology to ParA3. Therefore, I chose to include only sequences whose homology was closer to ParA2, resulting in only three homologues outside of *Bdellovibrio* species. These were all PVC group bacteria, and two were from *Omnitrophica* species, which are poorly studied. *Omnitrophica* are closely related to *Planctomycetes*, for which a homologue is included in the ParA2 tree, which are slightly better studied. These have a diverse range of morphologies and some have been seen to divide by budding (Lage et al., 2013, Wiegand et al., 2018). Additionally, they have been shown to have a peptidoglycan cell wall, which has been questioned in other PVC group bacteria (Jeske et al., 2015). As ParA2 has been shown to have a role in intracellular predation, specifically in gliding motility and exiting the bdelloplast, it would appear to have been adapted by intracellular *Bdellovibrio* species for this task. Its transfer to these PVC bacteria may relate to their lifestyles, which, for planctomycetes, is often found in biofilms with marine microorganisms. In such an environment, gliding motility may be preferable compared to using flagella.

3.4.4 Future considerations: expressing the BTH system in *B. bacteriovorus*

Although *E. coli* is a useful model system for BTH assays, future work in this area could include the development of a *B. bacteriovorus* strain for native

assays. This would, of course, come with several obstacles. Any adenylate cyclase genes would have to be deleted from the strain. A pBlast of the *E. coli* adenylate cyclase protein does not return any homologues in *B. bacteriovorus*. However, a pBlast using a *Leptospira* CyaK suggests two candidates for such genes, *bd1116* and *bd2640*. A domain prediction of protein products suggests that both have transmembrane regions; two in Bd1116 and four in Bd2640. Although both have a predicted C terminal adenylate cyclase domain, it is predicted to be in the periplasm for Bd1116 and in the cytoplasm for Bd2640. Additionally, this domain is preceded by a HAMP domain in Bd1116, which is often seen in two component messenger systems. In *M. tuberculosis* it has been found to modulate the activity of the cyclase domain it is fused to (Linder et al., 2004).

Both proteins also have an N terminal domain but, again, they occupy different spaces; cytoplasmic for Bd1116 and periplasmic for Bd2640. This is a CHASE2 domain in Bd2460, another domain often seen in signal transduction pathways. The domain in Bd1116 does not have a prediction and a pBlast of this region suggests it is only seen in homologous adenylate cyclase proteins from oligoflexia, deltaproteobacteria and spirochaetes.

Both proteins show considerable differences to the adenylate cyclase, encoded by *cyaA*, that is deleted in the *E. coli* BTH101 strain. This is considered a Class I adenylate cyclase, a wholly cytoplasmic protein whose regulation is tied to glucose metabolism, found in *E. coli* and similar Gram-negative bacteria (Peterkofsky, 1981). An alignment of this with Bd1116 and Bd2640 shows very low identity (17-18%). The *B. bacteriovorus* proteins may have more in common with Class III adenylate cyclases, which are characterised as having multiple transmembrane regions (Shenoy and Visweswariah, 2004). These are found in a range of bacteria, as well as eukaryotes and archaea. Additionally, the HAMP domain in Bd1116 is also found to accompany Class III adenylate cyclase domains in *M. tuberculosis* (Linder et al., 2004).

A Swissprot structural scan suggests that both Bd1116 and Bd2640 are most similar to a photoactivated adenylate cyclase from a Cyanobacteria, *Oscillatoria acuminata* (PDB 4yut), although it should be noted that the only

homologous region was the adenylate cyclase domain itself (Ohki et al., 2016). The N terminal regions of Bd1116, Bd2640 and the *Oscillatoria acuminata* protein are not homologous. The authors of the study state that the adenylate cyclase domain is Class III, suggesting the same for the *B. bacteriovorus* proteins. A comparison of key catalytic residues for this domain shows that both proteins contain the aspartate residue required to coordinate the catalytic metal ion. All other key residues are conserved in Bd1116 and partially conserved in Bd2640; Phe180 and Phe197, required for dimerisation, are replaced with a leucine and a tyrosine in Bd2640.

Although the pathways are unknown, these data suggest both proteins function in signal transduction pathways, with cAMP synthesis tied to the signal; the N terminal domains are likely key to regulating their activity. For the BTH system to be used in *Bdellovibrio bacteriovorus*, both proteins would have to be deleted. Any cAMP synthesis outside of the introduced system would result in blue colonies. This could pose problems for the strain as both proteins appear to function in as yet unknown signal transduction pathways; deletions could be deleterious to the strain potentially negating its use for this system.

There are additional putative adenylate cyclase genes annotated in the *B. bacteriovorus* HD100 genome, as many as three more, although their encoded proteins do not appear in the pBlast searches used above. It is possible that these are not true adenylate cyclases, potentially being other nucleotide cyclases, however they would have to be investigated to determine this. If they have any adenylate cyclase activity, they would also need to be deleted in addition to the two I have investigated above.

Additionally, a *B. bacteriovorus* BTH strain would have to be grown as an HI strain, as the presence of a host and the products of digestion being transported into the predator, which may include cAMP, could interfere with the assay. As HI *B. bacteriovorus* take considerably longer to grow than the *E. coli* BTH strain, this would severely depreciate the value of the assay. Added to the difficulties in making the multiple deletion strain, using *B. bacteriovorus* to host the assay may not be viable but, if successful, could provide more accurate results for future researchers.

3.5 Further experiments

Pairwise BTH could be expanded further to include a wider range of division proteins. As Bd0465 seems to connect DivIVA to the ParAB system, Bd0465 could be tested for further interactions with the proteins that did not interact with DivIVA. This could also be repeated with Bd0466.

Mutagenesis of Bd0465 could also prove interesting. By mutating the residues responsible for NADPH binding (the GxGxx(A/G) motif) or any of the nine proline binding residues, this could determine if either are required for the interaction with Bd0465, Bd0466 or ParA, as well as seeing if Bd0465 has any enzymic function as a ProC, despite being the only identifiable homologue in this pathway in *B. bacteriovorus*.

4 Chapter 4: Using a BTH library to probe unknown DivIVA interactions

4.1 Chapter 4 introduction

In chapter 3, BTH results suggest the possibility of a sensory network that uses metabolic signals to coordinate growth, chromosome partitioning and septal site selection. DivIVA has diverse roles in bacteria, and often multiple roles in a single system. Therefore, I wanted to investigate the possibility of unknown interactions of DivIVA in *B. bacteriovorus*. There are examples of DivIVA having roles less obviously connected to division and, given the unique lifestyle of *B. bacteriovorus*, this could also be the case in this system.

4.1.1 DivIVA and oxidative stress

As well as its primary division and growth roles, DivIVA has also been shown to influence the oxidative stress response in certain systems. This was initially seen in *M. smegmatis* strains expressing a mutant of *M. tuberculosis* DivIVA homologue Wag31 (Mukherjee et al., 2009). Wag31 is essential in Mycobacteria but overexpression of the mutant Wag31(Δ^{46}NSD^{48}) from *M. tuberculosis* in the *M. smegmatis* system led to an interesting phenotype. The authors suggest that the three deleted residues form a loop crucial to its interaction with PBP3, the D,D-transpeptidase otherwise known as FtsI. Expression of the mutant caused the cells to become more susceptible to oxidative stress, with further experiments showing that the Wag31-PBP3 interaction protected PBP3 from oxidative stress-induced proteolytic degradation.

Another study also found links between DivIVA and oxidative stress in *Streptococcus suis* (Ni et al., 2018). The authors showed that DivIVA is phosphorylated by a Ser/Thr protein kinase (STK), and that deletion strains of both DivIVA and the STK had increased susceptibility to reactive oxygen species (ROS). They show that the STK phosphorylates and activates SodA, a manganese-dependent superoxide dismutase which removes ROS. However, they were uncertain as to the mechanism for susceptibility to ROS seen in strains that are only *ΔdivIVA*.

While this link has only been observed in these systems, it does introduce the possibility that other bacteria have connections between DivIVA and resistance to ROS. In *B. bacteriovorus*, there has been limited study on the conditions in the bdelloplast, and none relating to the prevalence of ROS, which may accumulate in the bdelloplast due to the respiration of the predator and the digestion of the prey. To investigate this connection in *B. bacteriovorus*, and to find additional unknown interactions between DivIVA and other systems, a BTH library was developed.

4.1.2 BTH library; principles and use in other bacteria

While many studies have shown success with pairwise BTH assays, genomic fragment libraries have also been used successfully to find interacting partners with a single bait protein. The BTH101 strain is transformed with the pKT25 bait plasmid containing the known bait gene. These are then cotransformed with a genome fragment library in the pUT18 family of plasmids. Once plated, cotransformants with interacting proteins will form blue colonies. These are harvested and the library fragment sequenced to determine the protein, or portion of protein, that interacts with the bait. Examples of these libraries can be seen in *E. coli* (Handford et al., 2009), *Pseudomonas aeruginosa* (Houot et al., 2012) and *Salmonella typhimurium* (Qin et al., 2016). Using these studies as a basis, a library for *B. bacteriovorus* HD100 was constructed for this thesis. Construction and use of this library were greatly aided by Grant Buchanan and the Tracy Palmer lab.

4.1.3 Using a BTH library with *B. bacteriovorus*

As has been seen when cloning *B. bacteriovorus* genes into *E. coli* strains, there are proteins in the predator that can have deleterious effects. This could also be the case when expressing the library in the *E. coli* BTH101 strain. Plasmids containing enzymes for the digestion of prey may lead to non-viable host cells. The same could be true of some division proteins if overexpression leads to a lethal phenotype, as is predicted to be the case with the *B. bacteriovorus ftsZ* homologue. Therefore, the BTH library constructed for this bacterium may not include plasmids containing these genes, several of which DivIVA might interact with. However, it is hoped that many of the interactions

I am probing for will still be represented as they are not necessarily division or digestion specific.

4.1.4 Phylogenetic analysis of the three deacetylases in *B. bacteriovorus*

In addition to my work on DivIVA, I have also contributed to a study on deacetylases expressed by *B. bacteriovorus* (Harding et al., 2020). It has previously been shown that the host peptidoglycan is extensively modified, including N-deacetylation of the amino sugars, as well as the addition of long chain fatty acids (Thomashow and Rittenberg, 1978b, Thomashow and Rittenberg, 1978a). This converts the lysozyme-vulnerable cell wall to being lysozyme-resistant, as well as softening the wall and preventing invasion by other attack phase *B. bacterivorous*. The study by Harding *et al*. focussed on four lysozymes, deacetylases DslA (Bd0314), DslB (Bd1413) and DslC (Bd1440), as well as Bd1411 which is a more distantly related lysozyme. Mutational study showed that lysozymes DslA, DslB and DslC target deacetylated GlcNac in the prey cell wall, but only DslA, which was upregulated at prey exit (240-300 minutes into the cycle), is responsible for lysing the bdelloplast at the end of the cycle. In contrast, DslB and DslC were not upregulated at any specific point in the cycle and their function could not be determined. Bd1411, however, was upregulated for prey entry and a deletion mutant had significantly increased entry time. My contribution to this work was a phylogenetic analysis of these lysozymes, focussing on DslA.

4.2 Specific research aims

- Construct a BTH library for *B. bacteriovorus* as a resource for future studies.
- Use the BTH library to probe for unknown DivIVA interactions.
- Investigate potential interacting partners bioinformatically.
- Produce a phylogenetic analysis the deacetylases

4.3 Chapter 4 results

4.3.1 Constructing the *B. bacteriovorus* BTH library

Firstly, genomic material from *B. bacteriovorus* had to be randomly digested to produce fragments of 500-2000 bps. Restriction enzyme *Sau3A1* was chosen for this digest due to its compatibility with the pUT18 derived plasmids and

because its recognition sequence is 50% GC, matching *B. bacteriovorus* HD100 GC content of coding DNA (as seen on https://www.kazusa.or.jp/codon/cgi-bin/showcodon.cgi?species=264462). To determine the best concentration of restriction enzyme *Sau3A1*, three dilutions were made; 1/10, 1/25 and 1/50 (see methods for the digest). These were mixed with *B. bacteriovorus* genomic material and samples removed every 5 minutes for an hour. 0.1 µl, 10 mM EDTA was added to the samples to stop the reaction and then they were immediately placed on ice. Once all samples had been collected, they were run on a 0.8% agarose gel, **figure 4.3.1**. Given the results of the digest, the 1/50 *Sau3A1* dilution digest for 40 minutes was selected (protocol in methods).

Ten more of these digests were prepared and the reaction stopped after 40 minutes with 0.5 µl EDTA. These were then pooled. After being run on a 0.8% agarose gel, **figure 4.3.2**, material between 500 and 2000 bps was excised and extracted using the Sigma-Aldrich GenElute^{TM} Gel Extraction kit to produce a 100 µl elution. 50 µl of this was concentrated to 10 µl in the SpeedVac.

The digested and concentrated material was then ligated into three plasmids: pUT18, pUT18+2 and pUT18C. The plasmids were digested with restriction enzyme BamHI, which produces identical sticky ends to *Sau3A1*, in a standard reaction. Plasmids pUT18C and pUT18 were used, as well as plasmid pUT18+2 which was provided by the Tracy Palmer lab. This has two additional nucleotides in the linker between the adenylate cyclase and inserted fragment sequences. This accounts for frame shifted fragments, increasing the likelihood that fragments are expressed correctly. For unknown reasons, a pUT18+1 plasmid could not be obtained by the Tracy Palmer lab. Ligations were made at a 3:1 ratio of insert to vector in a standard 20 µl ligation reaction.

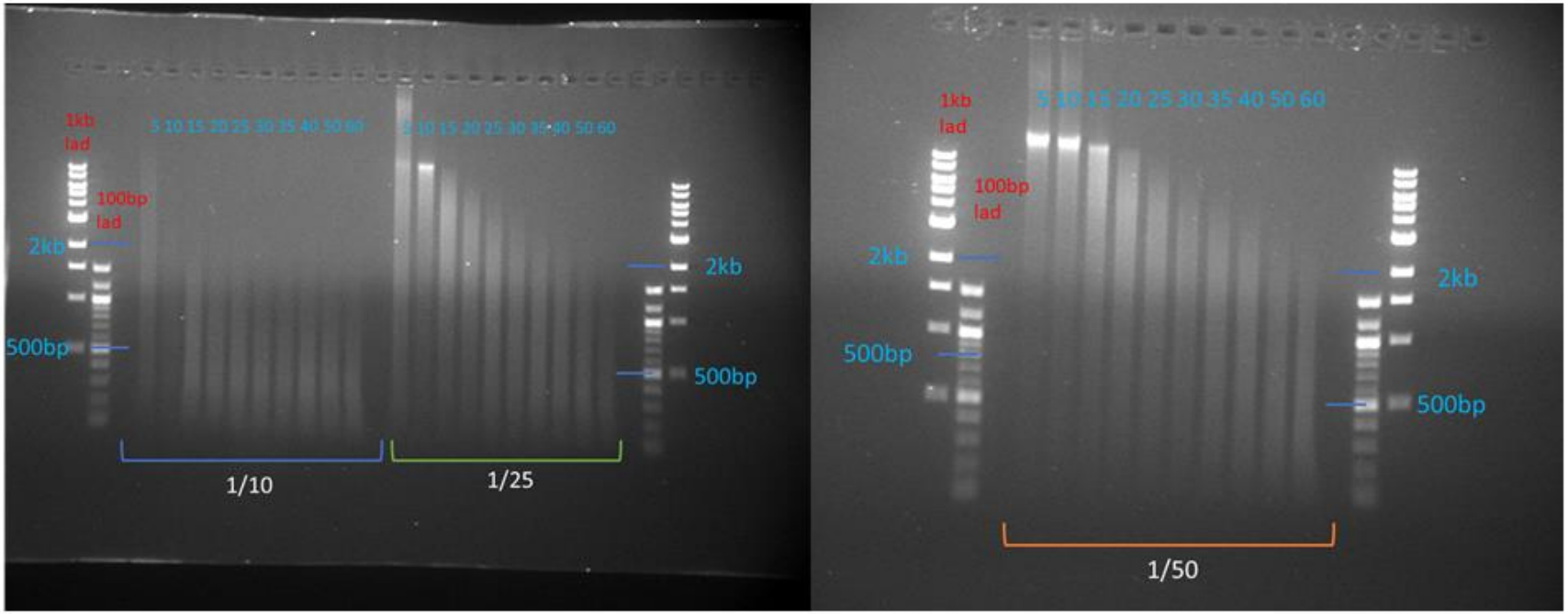

Figure 4.3.1. Agarose gels with test digests of *B. bacteriovorus* genomic material and restriction enzyme *Sau3A1* used to determine the conditions for further digests in BTH library construction. Shown are test digests with varying dilutions of SauA3 (bottom bracket); a 1/10 dilution (blue), 1/25 (green) and 1/50 (orange). Samples were taken and the reaction stopped at 5 minute intervals using 0.5 ul EDTA (interval in minutes shown in top numbers). 3x Orange G added to each sample, then run on 0.8% agarose with ethidium bromide. 1 kb and 100 bp ladders are marked at 2 kb and 500 bp to show the region of interest. Based on these results, the 1/50 dilution for 40 mins was chosen for further digests.

Whole ligations were then transformed into *E. coli* DH5α, as standard protocol, but instead of centrifuging after the 1-hour incubation, they were spread onto YT agar plates, with ampicillin, without dilution. After 24 hours of growth, each plate was washed with YT medium to remove the colonies, using as much medium as necessary to remove all colonies. These were pooled by plasmid and each pooled culture was centrifuged at 5525 x *g* for 10 minutes. Each pellet was resuspended in 8 ml of YT medium and split into two 4 ml cultures. Plasmids were extracted using the Sigma-Aldrich GenElute^{TM} Plasmid Midiprep Kit, producing two 500 µl elution per plasmid, combined into 1 ml. 1 µl and 5 µl of the pUT18C-library elution are shown on the left in **figure 4.3.3**, compared with the original stock of pUT18C plasmid. The eluted library plasmids were very faint, and so an ethanol precipitation was performed (see methods) to concentrate the 1 ml to 50 µl, shown on the right in **figure 4.3.3b**. This was then ready to use in a library screening assay.

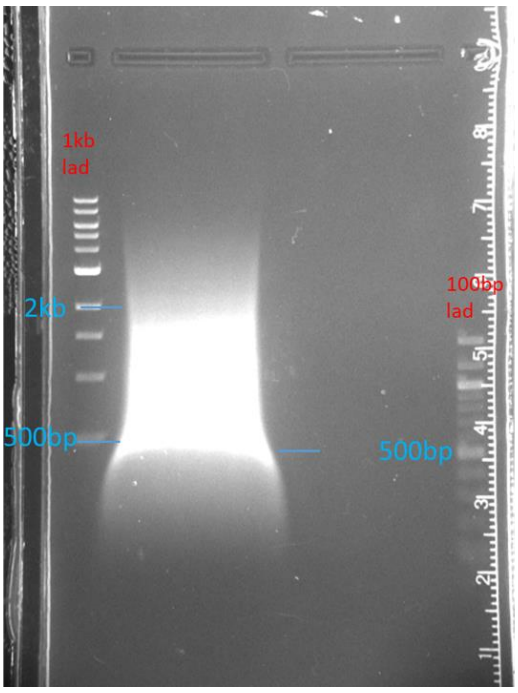

Figure 4.3.2. Digested and pooled genomic material before extracting 500-2000 bp fragments. Ten 1/50 *Sau3A1* dilution digests of *B. bacteriovorus* HD100 genomic material were prepared and stopped after 40 minutes with the addition of 0.5 µl EDTA. These were pooled and 100 µl 3x Orange G buffer was added. This was run on 0.8% agarose with 1 kb and 100 bp ladders (red). 2 kb and 500 bp (blue) are shown; this contains fragments sizes wanted for ligation into the library plasmids. This region was excised from the gel for continued construction of the BTH library.

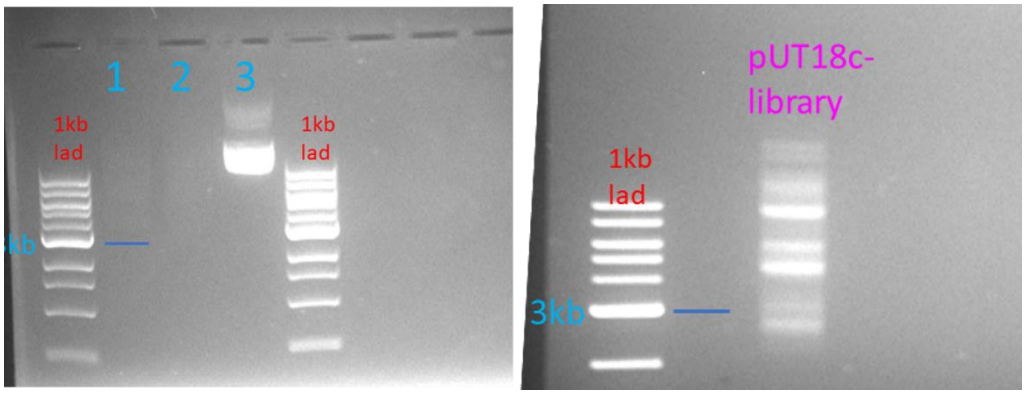

Figure 4.3.3. Samples of the pUT18C BTH library before and after concentration. Shown on the left is a comparison of (1) 1 µl and (2) 5 µl of the pUT18C BTH library, with (3) plain pUT18C plasmid. Library plasmids are very faint. On the right, the library plasmids have been concentrated with ethanol precipitation. All ladders are 1 kb.

4.3.2 BTH library screening

As with the pairwise procedure, screening for the library uses the *cyaA*-MG1655 strain BTH101. Before the assay, this strain is transformed with the bait plasmid as per transformation protocol, with all incubations at 29 ^{o}C.

Initially, the protocol for library screening is like the pairwise BTH protocol. *E. coli* BTH101 containing the bait plasmid is transformed with 1 µl of a plasmid library (see methods for the full protocol). For screening, this required three transformations per bait plasmid, one for each plasmid library. However, after the 1 hour incubation, rather than resuspending the cells in a small amount of medium and creating dilutions, the cells are resuspended in 1 ml of YT medium and spread across seven large MacConkey plates containing Amp_{50}, $Kan_{25,}$ $IPTG_{20}$ and $Xgal_{40}$ and incubated for 48 hours, as per protocol.

The plates have a lot of growth, and it can be difficult to collect single colonies, so blue colonies are picked and streaked onto a separate MacConkey plate. After another 48-hour incubation, individual blue colonies can then be used to inoculate 2 ml of Mu broth and incubated for 16 hours, shaking at 200 RPM. Cultures are then extracted with the Sigma-Aldrich GenElute^{TM} Plasmid

Miniprep Kit. At this stage, the extract contains both the bait plasmid and the library plasmid.

To remove the bait plasmid, *E. coli* DH5α are transformed with the extract, as per standard protocol, and grown for 16 hours with only Amp_{50} on YT agar. As the pKT25 bait plasmid is not needed for kanamycin resistance, the host cells should lose it. Three colonies per transformation are picked into YT broth which, after 16 hours incubation, can be spotted onto two plates, one containing Amp_{50} and one containing Amp_{50} and Kan_{25}. The bait plasmid has been successfully removed in colonies that grow on ampicillin but not on kanamycin. The spots from the ampicillin plates can be used to inoculate more YT broth and grown under standard conditions for plasmid extraction. To confirm the interaction, extracted plasmids were used in pairwise BTH and β-galactosidase activity assays with the bait plasmid, as per protocols. Plasmids can then be sequenced to determine the fragment present in the library plasmid.

4.3.3 Four potential interacting partners found for DivIVA

Library screens using bait plasmid pKT25-divIVA resulted in the identification of four library plasmids encoding potentially interacting protein fragments, with confirmation plates shown in **figure 4.3.4**. Sequencing showed these to be internal gene fragments of *bd0548* (encoding 328 of 358 total residues), a fragment running across *bd2106* and *bd2107* (encoding the first 100 residues of Bd2106 and the first 133 residues of Bd2107), and *bd3538* (encoding residues 37 to 141 of 261 total).

Full-length copies of these four genes were tested in a pairwise fashion with the BTH plasmids. Example constructs are shown for *bd0548* in **figure 4.3.5**. Potential interactions were measured with the one step β-galactosidase assay. Compared to the negative control, all three library fragment products showed a significant interaction with a large effect (Miller units>500, Mann-Whitney U test, $P<0.001$, $n = 18$, indicative of three biological repeats), **figure 4.3.6**. The full-length products, however, showed significant interactions with a small effect size (Miller units for significant interactions range between 13 and 37).

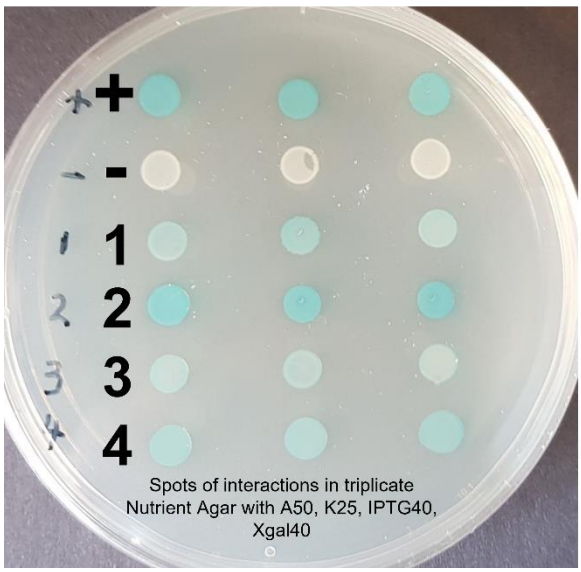

+ pKT25-Zip : pUT18C-Zip (+con)
- pKT25 : pUT18C (-con)
1 pKT25-DivIVA : pUT18CLib-15
2 pKT25-DivIVA : pUT18Lib-12
3 pKT25-DivIVA : pUT18Lib-21
4 pKT25-DivIVA : pUT18+2Lib-2

Sequenced:
pUT18CLib-15 – Bd3538 TrmJ
pUT18Lib-12 – Bd2106/2107
pUT18Lib-21 – Bd3538 TrmJ
pUT18+2Lib-2 – Bd0548 MenE

Figure 4.3.4. Interaction plates for pKT25-divIVA bait plasmid show four positive interactions. This shows the interaction spot plates. These show the positive (+) and negative (-) controls followed by interactions between BTH101 strains containing pKT25-divIVA bait plasmid and four library fragments. Analysis showed that library plasmids contained fragments for (1) bd3538, (2) bd2106/2107, (3) bd3538 and (4) bd0548. Note that bd3538 fragments interacted from both pUT18C and pUT18 libraries.

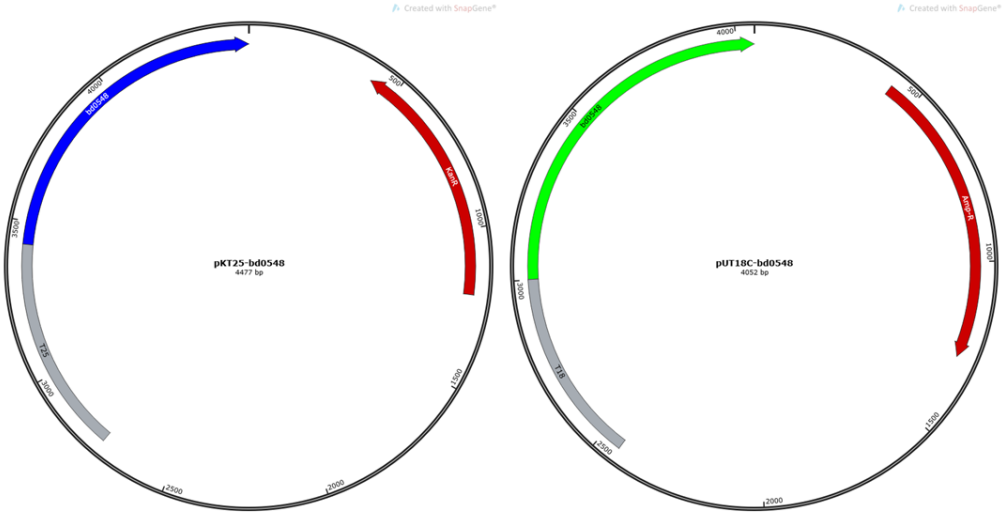

Figure 4.3.5. Example constructs of pKT25-bd0548 and pUT18C-bd0548 used in pairwise BTH assays to confirm library interactions. These show plasmid maps for two constructs made following identification of four potential interacting partners in the DivIVA BTH library screen. Similar constructs were made for *bd2107* and *bd3538*. Left is show the pKT25 plasmid, with an N-terminal T25 tag. Right is shown the pUT18C plasmid, with an N-terminal T18 tag.

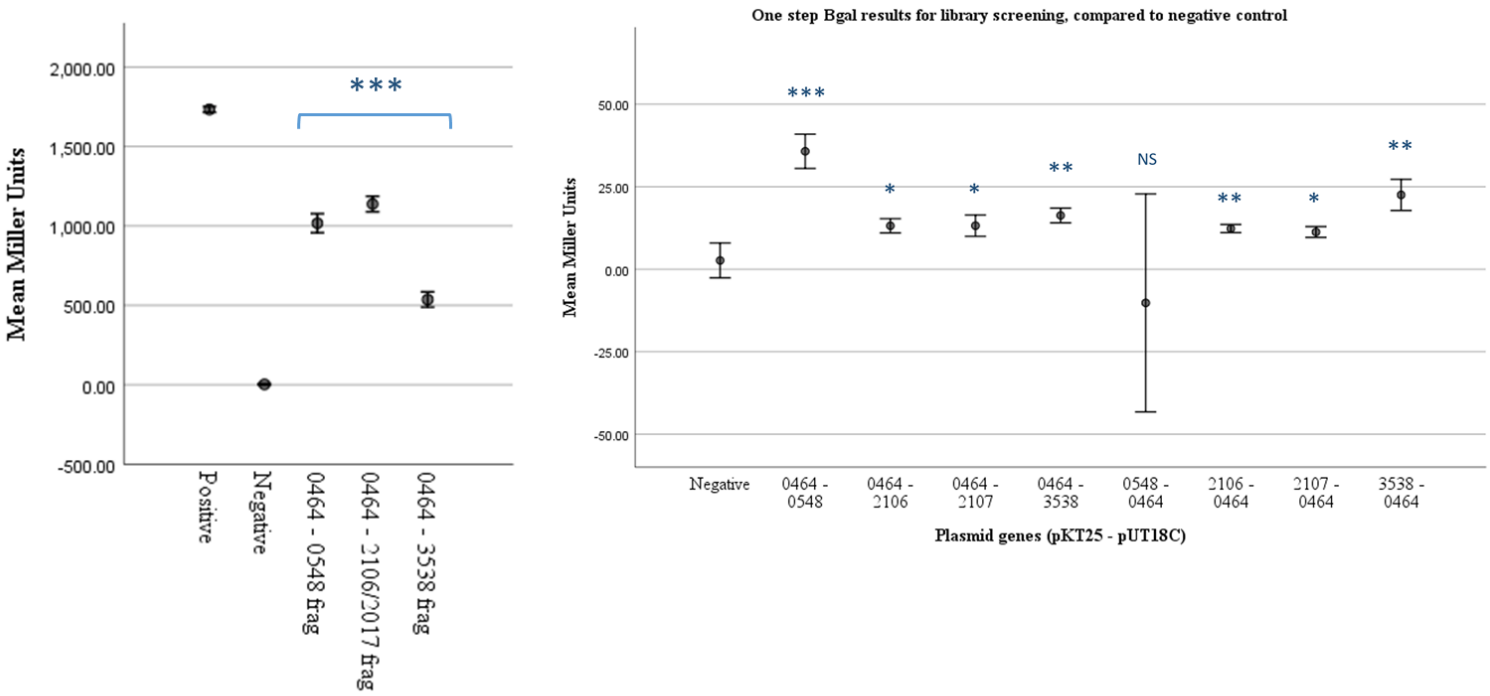

Figure 4.3.6. β-galactosidase activity assay results for positive BTH library fragments with pKT25-divIVA to confirm interactions. The left graph shows one-step β-galactosidase activity assay results for interactions using pKT25-divIVA and the library fragment plasmids that gave positive spot tests. Right are whole genes of the library fragments cloned into BTH assay plasmids and tested pairwise with BTH plasmids containing *divIVA*. All interactions were significant except for pKT25-bd0548 with pUT18C-divIVA. Miller units were much higher for library fragment plasmids than for the whole genes tested pairwise. All significance tests were Mann-Whitney U tests, with n = 18, over three biological repeats.

4.3.4 Interaction between DivIVA and TrmJ connects division with resistance to oxidative stress

Bd3538 is annotated as a TrmH but it shows greater homology to TrmJ, as confirmed by protein domain prediction, which in *E. coli* is a cytoplasmic S-adenosyl-L-methionine (SAM)-dependent tRNA (cytidine/uridine-2'-O-)-methyltransferase. TrmJ catalyses the formation of 2'O-methylated cytidine (Cm32) or 2'O-methylated uridine (Um32) at position 32 in tRNA. Deletion of this gene in *Pseudomonas aeruginosa* increases susceptibility to oxidative stress from hydrogen peroxide (Jaroensuk et al., 2016). Interestingly, in *Streptococcus suis*, deletion of divIVA leads to the same phenotype (Niet al., 2018).

A Swissmodel structural search shows that the closest known protein structure is the *Zymomonas mobilis* TrmJ homologue (PDB ID 5GRA) (Gu et al., 2017). *Z. mobilis* is an anaerobic, rod shaped Alphaproteobacterium. I aligned this with Bd3538 and a TrmJ homologue from *E. coli* whose structure has also been solved (PDB ID 4XBO), and the *P. aeruginosa* homologue stated above, for which the authors solved the crystal structure (PDB ID 5GMC), **figure 4.3.7**. From this alignment, Bd3538 shares the highest identity with the *P. aeruginosa* homologue (27.4%) and the lowest with the *Z. mobilis* TrmJ (23.2%).

Key dimerisation residues from *E. coli* are largely conserved in Bd3538; F199, E225, I228 and L229 are all conserved, while G231 is replaced by a threonine. Two distinct regions were linked to tRNA binding. Key residues from the first region, R82 and R84, are conserved. From the second region, R213 and R214 are conserved, while R218 is partially conserved as a glutamine, while K211 is not conserved. It should be noted that the TrmJ from *Z. mobilis* also has only one residue fully conserved, and one partially conserved. Catalytic residues identified in *P. aeruginosa,* R23 and S143, are both conserved in Bd3538.

To date, there is no evidence for the effect of deleting the *E. coli* and *Z. mobilis* homologues. As stated, the *P. aeruginosa* homologue has been linked to the oxidative stress response (Jaroensuk et al., 2016). The authors showed that in a *trmJ* deletion strain, catalase activity was significantly lower than wild type.

This became even more pronounced when the cells were exposed to H_2O_2. *P. aeruginosa* have three catalase genes, *katA*, *katB* and *katE*. Expression of *katB* and *katE* was found to be reduced in the absence of TrmJ. They then showed that TrmJ modulates the expression of *oxyR*, which is known to regulate catalase *katB.* Deletion of another gene, *ttcA*, which encodes a tRNA-thiolating enzyme, has been found to have a similar effect in this system (Romsang et al., 2018). In contrast to the TrmJ findings, this was found to be due to a reduction in *katA* expression. Together, these results show that modifications to tRNA are used to modulate the oxidative stress response in this system. A pBLAST predicts *bd2064* is a homologue of *ttcA*, and further experiments in *B. bacteriovorus* could confirm a similar role for both this and TrmJ.

Figure 4.3.7. An alignment of TrmJ homologues suggest Bd3538 has conserved function. Aligned TrmJ (cytoplasmic S-adenosyl-L-methionine (SAM)-dependent tRNA (cytidine/uridine-2'-O-)-methyltransferase) homologues from *Zymomonas mobilis* (PDB ID 5GRA), *Escherichia coli* (PDB ID 4XBO), *Pseudomonas aeruginosa* (PDB ID 5GMC) and *B. bacteriovorus* (Bd3538). Catalytic residues from *P. aeruginosa* are highlighted in yellow (R23 and S143, both conserved). Two regions were identified for tRNA binding in *E. coli*, highlighted green (R82 and R84, both conserved) and purple (K211, R213, R214, R218; 3 of 4 conserved). Highlighted blue are *E. coli* dimerisation residues (F199, E225, I228, L229, G231; 4 of 5 conserved).

4.3.5 Interacting partner MenE connects DivIVA to menaquinone synthesis

Bd0548 is annotated as MenE O-succinylbenzoate CoA ligase, an enzyme in the Men pathway for menaquinone synthesis (Sharma et al., 1996), which is a molecule involved in the respiratory electron transport chain of Gram-positive bacteria, and low oxygen respiration of Gram-negative bacteria. In Gram-negative bacteria this is used as a low oxygen alternative to uniquinone, which is used for aerobic respiration.

MenE is an intermediate step in the menaquinone biosynthesis pathway, which converts it from chorismate. A cursory search suggests that *B. bacteriovorus* has the complete pathway, with encoding genes located in several putative operons. The operon containing *menE* also has *menA* (*bd0546*) and *menC* (*bd0547*), as well as *bd0550* which is unknown in function. Another operon encodes the first three enzymes in the pathway, *menF* (*bd3485*), *menD* (*bd3484*) and *menH* (*bd3483*). Gene *menG* (*bd3487*: otherwise called *ubiE*) is the second in a three gene operon neighbouring this, with an *aroAG* (*bd3486*), which is part of chorismate synthesis, and a *htrA* (*bd3488*), which is used in the heat shock response for degradation of denatured proteins. Gene *menB* (*bd3492*) occurs at the end of an operon containing further chorismate synthesis genes, including *aroA*, *aroB*, *aroC* and *aroK*. RNA-seq data shows that all these operons are upregulated from 60 minutes, typically peaking at 180/240 minutes, covering the growth and division phases of the HD cycle.

MenE proteins catalyse two reactions to convert o-Succinylbenzoyl (OSB) to o-Succinylbenzoyl-CoA (OSB-CoA); The first is an adenylation reaction, forming OSB-AMP, and the second is thioesterification resulting in the final product. A protein domain scan of Bd0548 shows an AMP-dependent synthetase/ligase domain, as is also seen in the *E. coli* MenE. A structural scan finds the most similar solved structure is a MenE homologue from *Bacillus subtilis* (PDB ID 5X8F) (Chen et al., 2017). This study focussed on the thioesterification reaction, identifying three crucial residues for the active site, and two that lower the activity when mutated. Of these, two are partially conserved in Bd0548, **figure 4.3.8**.

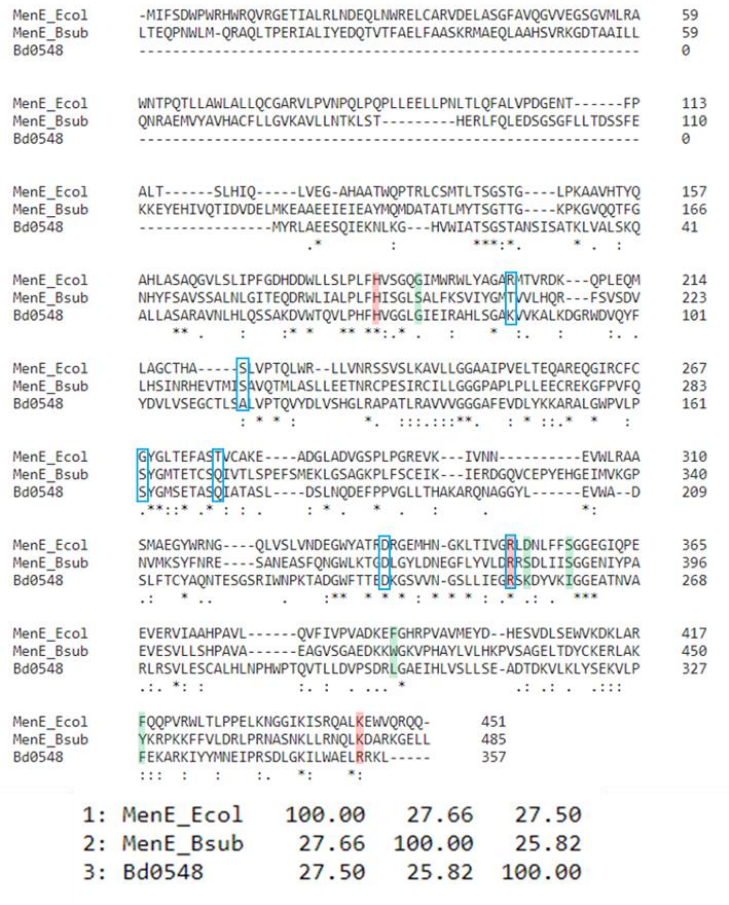

Figure 4.3.8. An alignment of MenE homologues from *E. coli* and *B. subtilis* show that functional residues are largely conserved in Bd0548. Aligned MenE (O-succinylbenzoate CoA ligase) homologues from *E. coli, B. subtilis* and *B. bacteriovorus* bd0548. Highlighted red are key residues for the adenylation reaction, studied in the *E. coli* homologue, two of which are conserved and the third partially conserved, as well as green highlighted residues which are non-essential. The six blue boxed residues are involved in the thioesterification reaction, of which five are at least partially conserved in Bd0548.

A previous paper investigated the adenylation reaction, solving the structure of the enzyme when bound to the intermediary product OSB-AMP (Chen et al., 2016). In this they found three crucial active site residues, all of which are conserved in Bd0548. Many of the other active site residues which have a more subtle role are also conserved or semi-conserved. Despite lower conservation for the thioesterification reaction, the presence of complete

pathways for chorismate and menaquinone synthesis suggest that this protein retains its function in the pathway.

Interestingly, a search for proteins in the pathway for ubiquinone biosynthesis, which *E. coli* use for aerobic respiration, is not present in *B. bacteriovorus*. This could reflect the potentially low oxygen environment of the bdelloplast, particularly towards the end of the cycle after several hours of respiration. The peak expression of the menaquinone pathway at 180 minutes could act as a signal to determine the end of replication. In *E. coli*, the redox state of menaquinone has been shown to be crucial to the sensing of oxygen availability via the ArcBA signalling system. A similar system in *B. bacteriovorus* could be involved in progressing the cycle from growth to division.

4.3.6 Bd2107 is a potential fusion protein that interacts with menaquinone to form disulphide bonds in newly synthesised periplasmic proteins

The last interacting library fragment covered the start of both *bd2106* and *bd2107*. Bd2106 is classed as a Cofac_haem_bdg domain containing protein, thought to be involved in haem uptake. Bd2107 is a DsbA homologue, required for the formation of disulphide bonds in some proteins as they enter the periplasm (Heras et al., 2009, Zapun et al., 1993). Given the orientation of the fragment, the protein encoded must be Bd2107. In *E. coli*, DsbA/B system introduces disulphide bonds into newly synthesised proteins that have been exported into the periplasm. Membrane bound DsbB partners with ubiquinone to generate a disulphide bond, which is then passed to DsbA, a thiol disulphide oxidoreductase, which donates it to the folding protein (Inaba and Ito, 2008). If *B. bacteriovorus* do not have ubiquinone, as suggested when investigating MenE, I would expect Bd2107 to be, at least, modified and possibly incorrectly annotated. A pBLAST of an *E. coli* DsbB does not return any results in *B. bacteriovorus*, suggesting *B. bacteriovorus* does not have the same system as *E. coli*.

A topology scan of Bd2107 shows that this is a transmembrane protein, with the N terminal half of the protein containing five transmembrane regions. The

C terminal half of the protein is in the periplasm. The region coded for in the library fragment covers the first 289 bases of the 1209 bp gene. This accounts for the first two cytoplasmic regions. If this interaction is true, then it is most likely one of these regions that interacts with DivIVA.

Domain and structural scans suggest that only the C terminal domain is homologous with DsbA homologues, and an alignment with an *E. coli* DsbA shows only 12% identity, with the homologous region at the C terminus. The *E. coli* protein, which is 208 residues, is entirely aligned with the C terminus of the larger, 402 residue Bd2107. This region in Bd2107 is predicted to have a thioredoxin-like fold. Additionally, the *E. coli* protein does not have any predicted transmembrane regions, instead being entirely periplasmic.

The domain scan of Bd2107 suggests that there is an N terminal vitamin K epoxide reductase (VKOR) domain. Typically studied in Actinobacteria, VKOR proteins also form disulphide bonds, and complements deleted *dsbB* in *E. coli*, restoring oxidation to DsbA (Ke et al., 2018). Instead of quinone, these proteins use menaquinone (vitamin K), which does appear to be synthesised in *B. bacteriovorus*, to generate the disulphide bonds. An alignment of Bd2107 with a *Mycobacterium smegmatis* VKOR shows that the 210 residue VKOR is aligned to the N terminus, **figure 4.3.10**. Thus, Bd2107 appears to be a fusion of a VKOR and a thiol disulfide oxidoreductase. In *E. coli*, DsbA, DsbB and ubiquinone form a complex (Inaba, 2008, Inaba et al., 2009); it could be that Bd2107 binds with menaquinone to form a complex with a similar role. This further supports the potential interaction of DivIVA with menaquinone biosynthesis protein MenE.

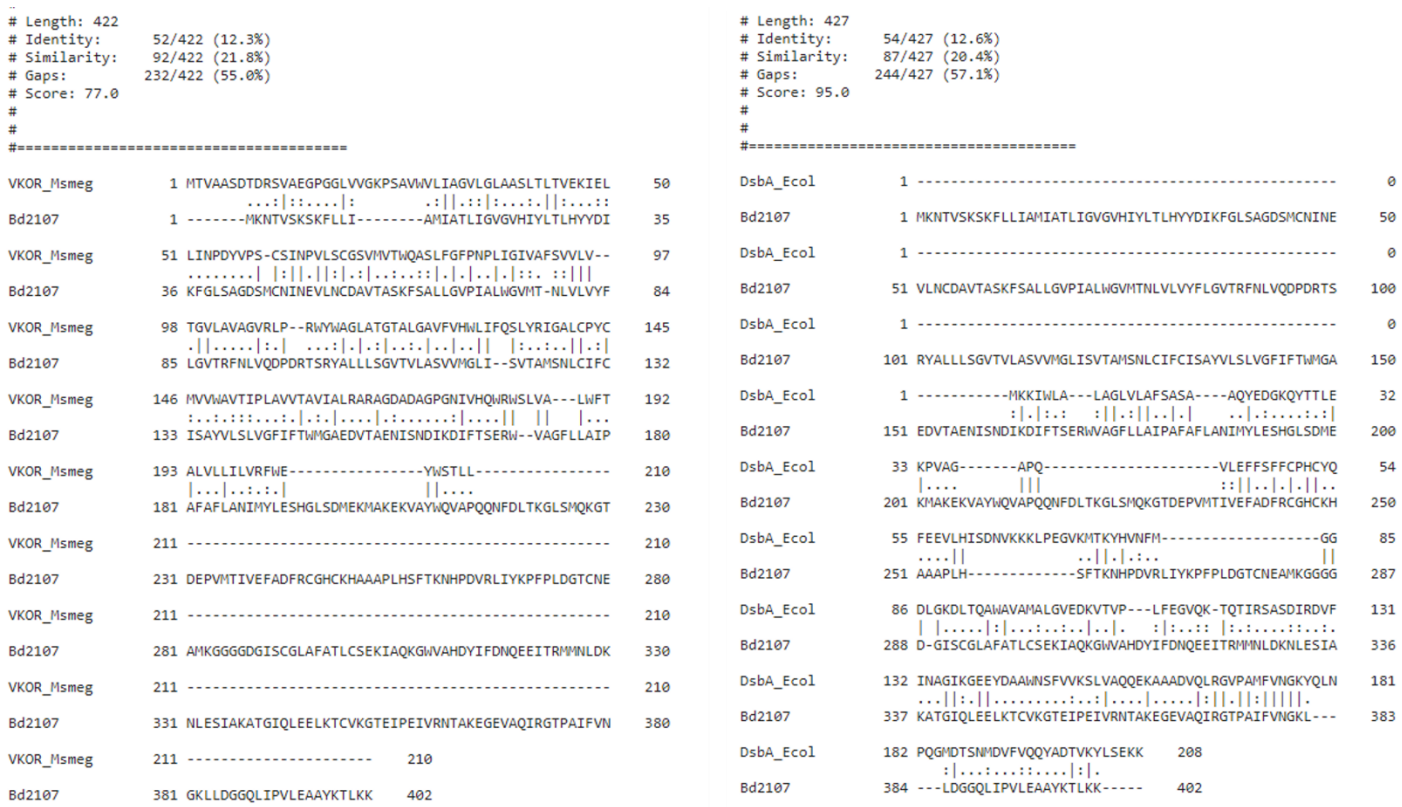

Figure 4.3.10. Alignments of Bd2107 show that the N terminal domain is a VKOR and the C terminal a DsbA. Two alignments are shown, both containing Bd2107. Left, an *M. smegmatis* vitamin K epoxide reductase (VKOR) is aligned to Bd2107, showing that the VKOR is homologous to the N terminal region. Right, an *E. coli* DsbA is shown to align with the Bd2107 C terminal region. This suggests that Bd2107 is a fusion of VKOR and DsbA proteins.

4.3.7 DslA, the deacetylase responsible for prey exit, is phylogenetically distinct from other deacetylases in *B. bacteriovorus*

As mentioned in the introduction, I contributed a phylogenetic analysis to the deacetylases of *B. bacteriovorus* to a recent publication seen in **figure 4.3.11**. (Harding et al., 2020). This clearly showed two distinct clades. One contained DslB and DslC, very closely related, as well as Bd1411, more distantly related. The other clade contained DslA, showing clear distance between this lysozyme and the others in *B. bacteriovorus*. The most closely related non-BALO homologue to DslA was found in *Oceanospirillum beijerinckii* (Satomi et al., 2002). This is a spiral-shaped, heterotrophic γ-proteobacterium isolated from marine environments. They are 7-15 μm long, motile with tufts of bipolar flagella, and divide via binary fission.

More distantly related bacterial homologues include α-proteobacteria. The environments these have been isolated from vary, with representatives from soil, freshwater, and marine environments, as well as a group isolated from plant root tissue. The latter grouping was the most closely related α-proteobacteria to the *Caulobacter vibrioides* homologue, which was added to the analysis. *Caulobacter* are notable for their asymmetric division, a product of the two stages of their life cycle, with non-motile stalked cells producing motile swarmer cells through budding.

There are also a few β-proteobacteria, such as *Variovorax*, *Achromobacter* and *Limnohabitans*, and γ-proteobacteria from genera *Rheinheimera* and *Pararheinheimera* in this grouping. The final group of homologues in this clade are the eukaryotic C-type lysozymes, which are used as antimicrobials that target bacterial peptidoglycan. These are found only in animals, with representatives in the protein tree being human, mouse and fruit fly proteins.

Despite the presence of many α-proteobacteria, there are no homologues from the predatory bacteria of this class, *Micavibrio*, as well as other predatory bacteria, such as δ-proteobacterium *Myxococcus xanthus*. It should be noted, however, that these are non-invasive predators, as is *B. exovorus* which does not have a homologue for DslA. It would therefore seem that this deacetylase has been specifically adapted by invasive *Bdellovibrio* species.

a

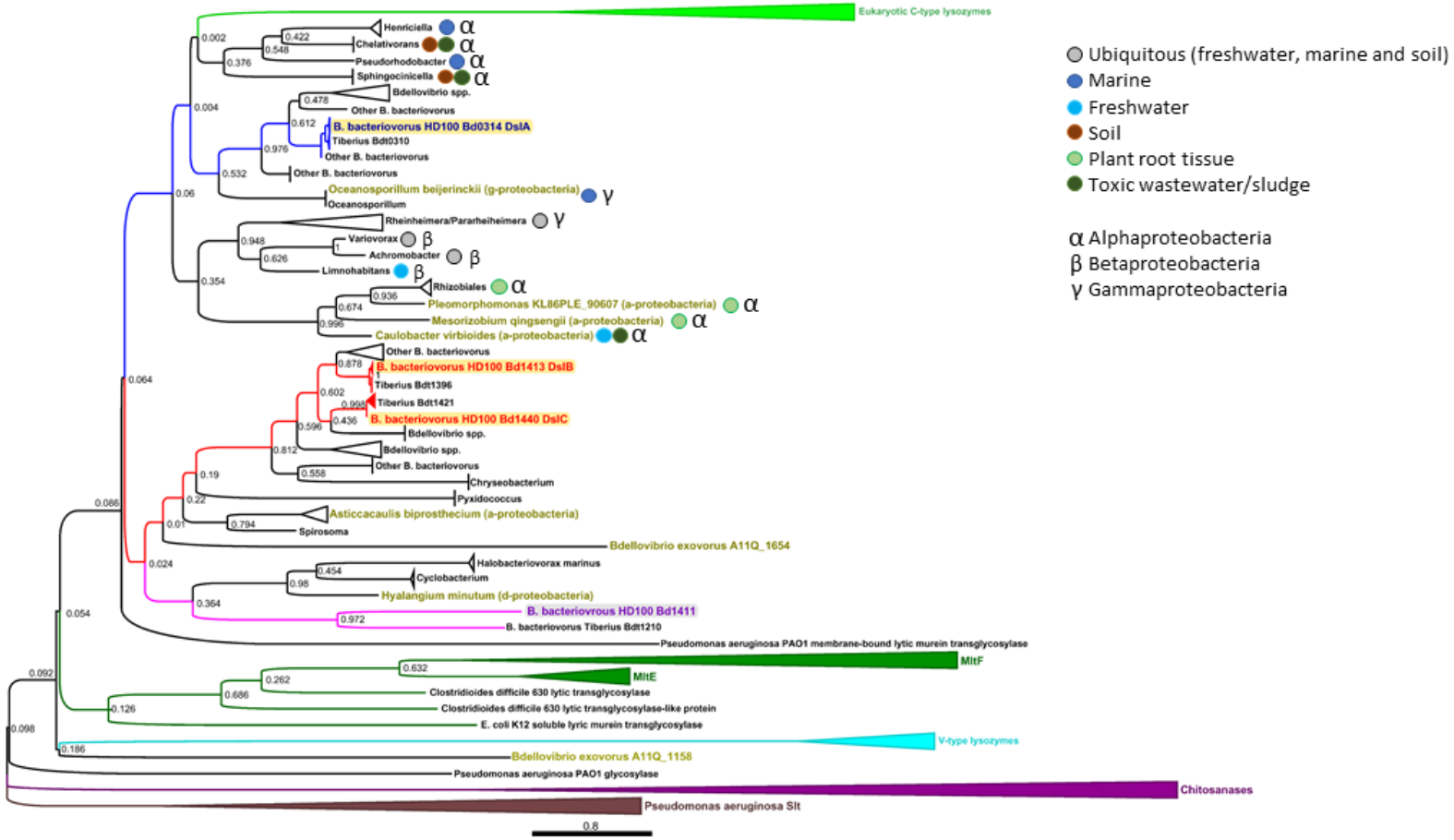
Eukaryotic C-type lysozymes
Henriciella
Chelativorans
Pseudorhodobacter
Sphingocinicella
Bdellovibrio spp.
Other B. bacteriovorus
B. bacteriovorus HD100 Bd0314 DslA
Tiberius Bdt0310
Other B. bacteriovorus
Other B. bacteriovorus
Oceanosporillum beijerinckii (g-proteobacteria)
Oceanosporillum
Rheinheimera/Pararheiheimera
Variovorax
Achromobacter
Limnohabitans
Rhizobiales
Pleomorphomonas KL86PLE_90607 (a-proteobacteria)
Mesorizobium qingsengii (a-proteobacteria)
Caulobacter virbioides (a-proteobacteria)
Other B. bacteriovorus
B. bacteriovorus HD100 Bd1413 DslB
Tiberius Bdt1396
Tiberius Bdt1421
B. bacteriovorus HD100 Bd1440 DslC
Bdellovibrio spp.
Bdellovibrio spp.
Other B. bacteriovorus
Chryseobacterium
Pyxidococcus
Asticcacaulis biprosthecium (a-proteobacteria)
Spirosoma
Bdellovibrio exovorus A11Q_1654
Halobacteriovorax marinus
Cyclobacterium
Hyalangium minutum (d-proteobacteria)
B. bacteriovrous HD100 Bd1411
B. bacteriovorus Tiberius Bdt1210
Pseudomonas aeruginosa PAO1 membrane-bound lytic murein transglycosylase
MltF
MltE
Clostridioides difficile 630 lytic transglycosylase
Clostridioides difficile 630 lytic transglycosylase-like protein
E. coli K12 soluble lyric murein transglycosylase
V-type lysozymes
Bdellovibrio exovorus A11Q_1158
Pseudomonas aeruginosa PAO1 glycosylase
Chitosanases
Pseudomonas aeruginosa Slt
0.8
Ubiquitous (freshwater, marine and soil)
Marine
Freshwater
Soil
Plant root tissue
Toxic wastewater/sludge
α Alphaproteobacteria
β Betaproteobacteria
γ Gammaproteobacteria

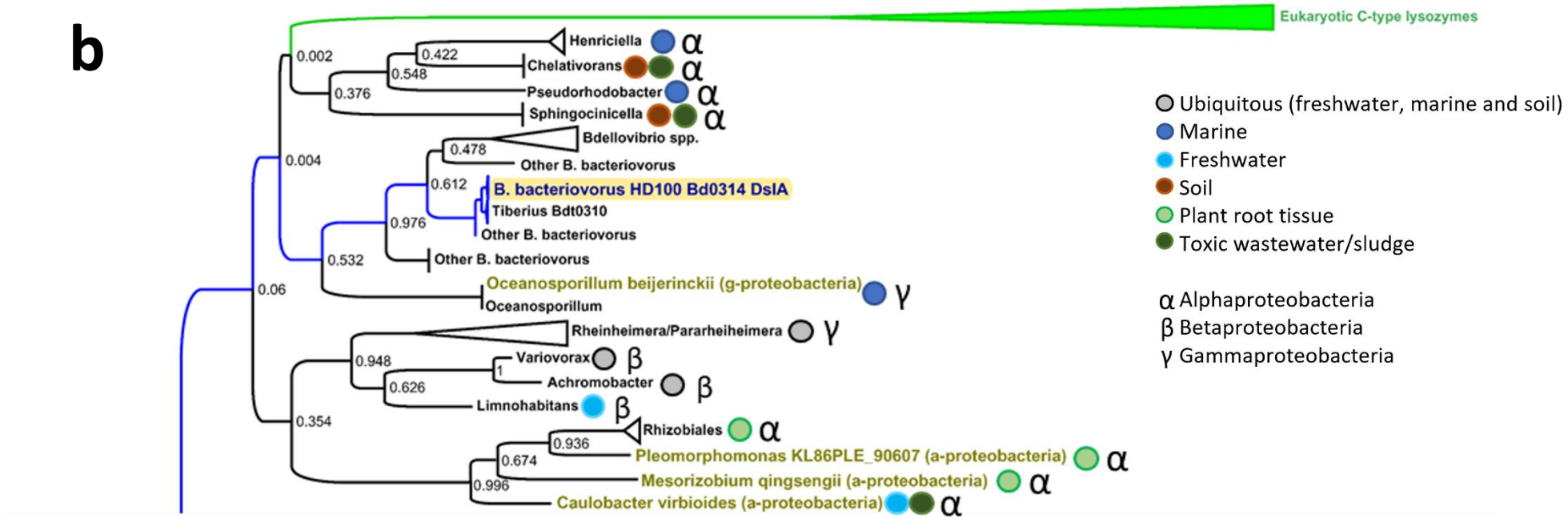

Figure 4.3.11. A protein tree showing DslA (Bd0314) is homologous to proteins in γ-, β- and α-proteobacteria. Phylogenetic analysis performed in MEGA-X and Figtree software with 213 total sequences using the maximum likelihood method with 500 bootstrap replications. (a) These include: (highlighted) *B. bacteriovorus* HD100 DslA (Bd0314), DslB (Bd1413), DslC (Bd1440) and their *B. bacteriovorus* Tiberius homologues, (pink) lysozyme Bd1411, (yellow writing) previously identified bacterial homologues of DslA. Also added were a selection of other lysozymes such as 23 eukaryotic C-type lysozymes, 2 V-type lysozymes from Phage T4, *P. aeruginosa* chitosanases, G-type lysozymes and Slt homologues and *E. coli* MltE homologues. This tree shows that exit-specific DslA is related to homologues in γ-, β- and α-proteobacteria from various environments. This suggests ancestral lateral gene transfer events. (b) This is a zoomed copy of the DslA region.

4.4 Chapter 4 discussion

4.4.1 Pairwise and library BTH results link DivIVA to menaquinone synthesis and utilisation, as well as oxidative stress

Although preliminary, several potential interacting partners with DivIVA have been identified and have been highlighted (**figure 4.3.6**) for future investigation. Probing a *B. bacteriovorus* BTH library identified four putative DivIVA-interacting proteins beyond those encoded by the *divIVA* operon. Although diverse, all these proteins would be expected to change in levels in a *B. bacteriovorus* filament that has been growing for a long period in a bdelloplast, consuming oxygen and nutrients.

Bd0548 MenE is a cytoplasmic protein associated with synthesis of a menaquinone to allow electron transport in more anaerobic conditions, such as those generated by continued enclosed growth of *B. bacteriovorus* inside the bdelloplast (Sharma et al., 1996). While some other Gram-negative bacteria, such as *E. coli*, produce ubiquinone for aerobic respiration and menaquinone for low oxygen respiration, *B. bacteriovorus* does not appear to encode for any other quinones. This is also the case for Gram-positive bacteria, which rely solely on menaquinone. This could reflect the conditions in which *B. bacteriovorus* respire. The enclosed bdelloplast may be a low oxygen environment, and the use of menaquinone over ubiquinone could be advantageous.

Also linked to menaquinone is Bd2107, which I hypothesise to be a DsbA/VKOR fusion protein capable of performing the same role as the DsbA/DsbB/ubiquinone system of *E. coli* to form disulphide bonds in newly synthesised proteins in the periplasm. Rather than using DsbB, the N terminus of Bd2107 wholly aligns with *M. smegmatis* VKOR, which is paralogous to DsbB, using menaquinone instead of ubiquinone. As stated, VKOR from Actinobacteria can complement *E. coli dsbB* deletion strains. The C terminus of Bd2107 wholly aligns with *E. coli* DsbA. Should both domains function, and if they bind to menaquinone, the Bd2107-menaquinone complex could be responsible for the formation of disulphide bonds in periplasmic proteins. This

supports the interaction between DivIVA and MenE, presenting crosstalk between division and menaquinone biosynthesis and utilisation.

The final DivIVA interactor identified by BTH was Bd3538, a TrmJ homolog. This is a potential oxidative stress responsive protein in Gram-negative bacteria, which is intriguing as deletion of *divIVA* in Streptococci leads to an oxidative stress phenotype (Jaroensuk et al., 2016; Ni et al., 2018). Again, this could be associated with oxidative changes in the bdelloplast toward the end of filamentous growth of *B. bacteriovorus* and could signal the need to divide and exit the dead prey cell. While the β-galactosidase assays for interaction of the library fragments were strongly positive, whole protein interactions were less substantial, prompting future work to determine the strength and extent of these protein interactions.

4.4.2 DslA homologues in various Proteobacteria suggests lifestyle adaptations and multiple lateral gene transfer events.

My DslA protein tree analysis highlighted several bacterial homologues for DslA in several proteobacteria, including α-, β- and γ-proteobacteria from varying environments, but not other Oligoflexia or δ-proteobacteria. Homologues for DslA may be present in these non-predatory bacteria seen in this analysis as a form of protection, much as eukaryotes use the C-type lysozymes to protect against bacteria. This is certainly plausible with the α-proteobacterial order Rhizobiales, otherwise called Hyphomicrobiales, which are extracted from plant root tissue, typically legumes (Friesen, 2012, Walker et al., 2020). These have a symbiotic relationship with their host legume plants, fixing nitrogen and contributing to protecting the root system, for which antimicrobials would be useful.

Plants themselves do not encode for a C-type lysozyme, such as that seen in the phylogenetic analysis. The group of these enzymes in the protein tree are predominantly encoded from human, mouse, and fruit fly genomes. The presence of a deacetylase in the plant symbiotes could therefore serve a function that the plant root cannot, allowing the bacteria to be engulfed by the root hair with a lower chance of infection by bystander bacteria in the soil, a beneficial outcome for the symbiotic bacteria (Rhizobiales), who eliminate

competition, and the plant, which may otherwise take in a pathogen. Ultimately, this reduces competition and potential infection at the root.

Another possible function for a DslA homologue in a plant root symbiote would be to act upon the plant itself. DslA in *B. bacteriovorous* targets the link between the two elements of the peptidoglycan backbone after they have been deacetylated, cleaving apart muramic acid (MurN) and glucosamine (GlcN). Plants do not produce peptidoglycan, and the cellulose in their cell walls are a D-glucose polymer. However, N-acetylglucosamine (GlcNAc) and GlcN have been detected in the arabinogalactan-proteins (AGPs) of carrot plants (*Daucus carota*) (van Hengel et al., 2001). AGPs are proteoglycans with a small protein backbone, which is around 10% of the molecule by mass, bound by carbohydrates which make up to 90% of the mass of the molecule (Nothnagel, 1997). The sugars in these polysaccharides are typically arabinosyl and galactosyl. AGPs are ubiquitous in plants, abundant in all tissues including the root as well as secreted in the root exudate and have been shown to have varying signalling functions in tissue and organ development (Rumyantseva, 2005, Su and Higashiyama, 2018). Importantly, there is also evidence for their role in the attraction and attachment of members of Rhizobiales, with most research focussing on *Rhizobium* species (Nguema-Ona et al., 2013).

The presence of GlcNAc and Glc had been detected in these proteoglycans before, but as single molecule anchor points for the protein backbone; none had been observed in the carbohydrates. Hengel *et al*. found that the AGPs of carrot plants contained GlcNAc and Glc oligomers and additionally found these oligomers to be activated upon cleavage by endochitinases.

Chitin, which is typically found in the cell walls of fungi, is a GlcNAc polymer. Endochitinases are enzymes that cleave this polymer into multimers of GlcNAc (Malik and Preety, 2019). These enzymes are secreted from plant tissues, including from the root, as one facet of plant antifungal resistance (Ceasar and Ignacimuthu, 2012, Singh and Arya, 2019). Hengel *et al*. found that the endochitinases secreted from the carrot plant acted upon the GlcNAc and GlcN oligomers in the AGPs as well, thus activating them. Their study concluded that these AGPs reactivated cells, promoting division and

elongation, as well as influencing somatic embryogenesis, the process whereby somatic cells convert to totipotent stem cells capable of developing into a new embryo (Raemakers et al., 1995, Lakshmanan and Taji, 2000, Guan et al., 2016).

Therefore, a modified DslA homologue in symbiotic Rhizobiales species may be capable of acting upon these AGPs, much as the secreted plant endochitinase would, stimulating growth of the root tissue. A comparison of the structures of peptidoglycan, GlcNAc-deacetylated peptidoglycan and chitin, as well as where DslA and endochitinases act on them, can be seen in **figure 4.4.1**.

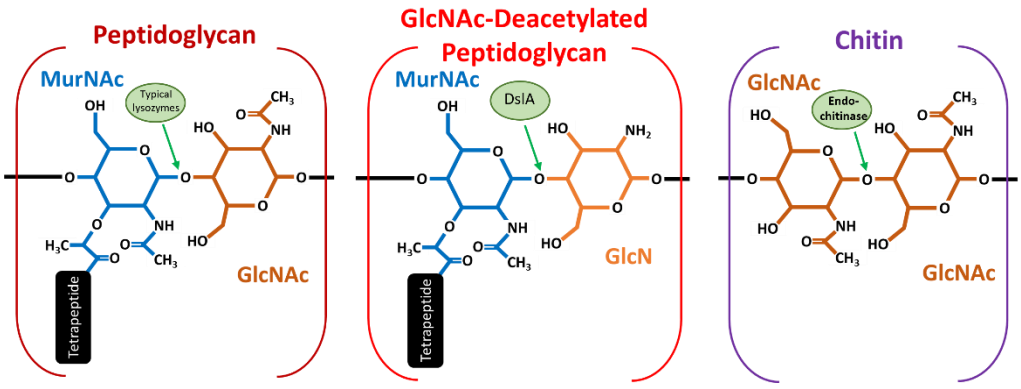

Figure 4.4.1. A comparison of the molecular structure of peptidoglycan, GlcNAc-deacetylated peptidoglycan and chitin. The left panel shows a disaccharide subunit of peptidoglycan, comprised of MurNAc-pentapeptide and GlcNAc. The green circle and arrow indicate where typical lysozymes act. The middle panel shows peptidoglycan with deacetylated GlcNAc, as is seen in the modified cell walls of the bdelloplast. The green arrow indicates where DslA acts. The right panel shows chitin, a GlcNAc polymer. The green arrow shows where endochitinases act. These illustrations show the similarity in the molecular structures of these polymers and the possibility that a DslA homologue could be adapted to target chitin (Harding et al., 2020, Malik and Preety, 2019).

This could be a part of the interaction between AGPs and symbiotic bacteria that has already been studied, helping the bacteria to attach to the root and stimulating the curling of the root hair, followed by the engulfment of the

beneficial bacterium. It could additionally even promote somatic embryogenesis to further develop the environment to favour the symbiotic bacteria, an act that would aid the propagation of the plant and therefore the symbiotic bacteria. Isolation of the DslA homologue and application to their symbiotic plant tissues could confirm this. While evidence exists for AGP microbe interactions, and the effect of AGP cleavage by secreted plant endochitinases, the action of a bacterial deacetylase on plant AGP has yet to be studied but could be an important factor in plant-microbe interactions.

When considering similarities of DslAs, we must consider how the homologues arose in these particular bacteria**.** As stated by Gophna *et al*., there is evidence of substantial ancient lateral gene transfer (LGT) events into the *B. bacteriovorus* genome, with 41% of coding ORFs having homologues only in bacteria outside of Oligoflexia and δ-proteobacteria (Gophna et al., 2006). They also showed that the three largest modern groups with such homologues were γ-, β- and α-proteobacteria in that order, the three classes seen in the DslA clade of the protein tree, followed closely by other groups such as Firmicutes and Spirochaetes. Pan *et al*. also provided evidence of more recent LGT events with the same classes of prey bacteria shown here (Pan et al., 2011). This strongly suggests that the deacetylase has had at least one LGT event directly involving *B. bacteriovorus*, or an ancestor, with further events spreading it between these three Gram-negative classes. While the presence of DNAses prevents the uptake of prey DNA by the invading predator cell, there is certainly opportunity to either conjugate while in attack phase with a bacterium not currently being preyed upon, or for other bacteria to have taken up the DNA of lysed *B. bacteriovorus* cells, shown in **figure 4.4.2**. *Bdellovibrio* species have previously been shown to prey upon a range of Proteobacteria, but earlier studies did not include α-proteobacteria (Markelova, 2010).

However, there is now evidence of *Bdellovibrio* species preying upon bacteria found in wastewater environments and activated sludge (Feng et al., 2017, El-Shanshoury et al., 2016, Ozkan et al., 2018). An abundance of α-proteobacteria is specifically noted in these studies, and Feng *et al.* showed that levels of all Proteobacteria were reduced with *Bdellovibrio* treatment. Therefore, contact

between ubiquitous *Bdellovibrio* species and the marine γ-proteobacterial *Oceanospirillum*, ubiquitous β-proteobacteria, and marine, wastewater and soil based α-proteobacteria seen in my DslA analysis is entirely plausible.

The exact LGT events that occurred are hard to determine, as they could be transferred to or from *Bdellovibrio* species, and my DslA analysis only included the protein sequences. Although beyond the scope of this publication, further study, needing more diverse *Bdellovibrio* genomes, could elucidate the relationship between the encoding genes, and how they might have propagated through these bacteria and how much evolutionary distance there is between them.

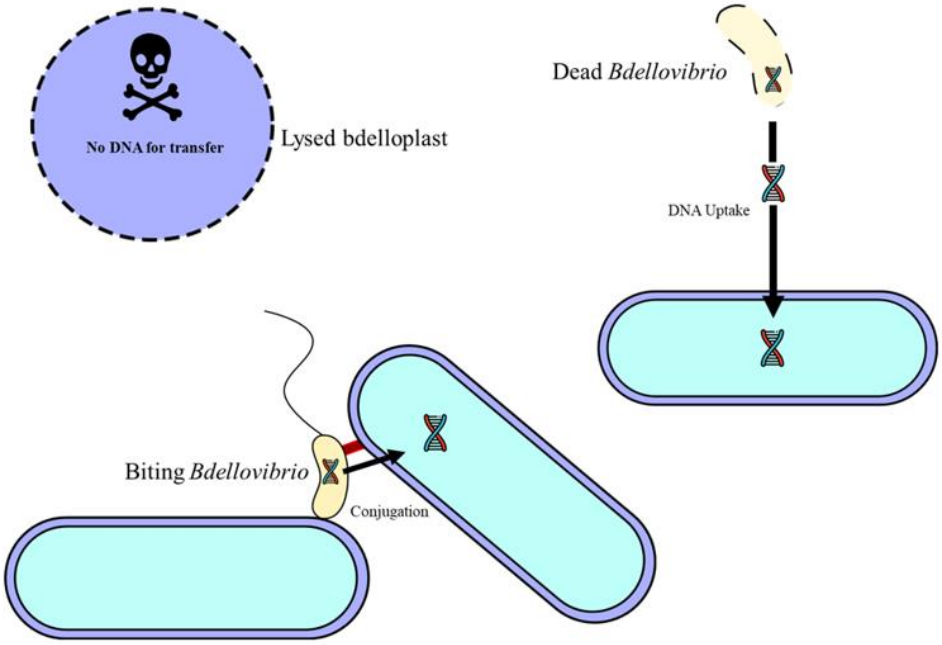

Figure 4.4.2. A cartoon showing the possible ways that lateral gene transfer may occur between *B. bacteriovorus* and other Gram-negative bacteria. Top left is a depiction of a lysed bdelloplast, in which DNA could not be recovered by *B. bacteriovorus*. Below is an attack phase *B. bacteriovorus* cell attached to one prey bacterium while conjugating with another. On the right, a bacterium is shown to take up DNA from a lysed B. bacteriovorus cell. These serves to show the possible pathways for lateral gene transfer with a predatory bacterium such as *B. bacteriovorus* (Gophna et al., 2006, Pan et al., 2011).

4.5 Further experiments

Further library screenings could be beneficial, using bait plasmids containing some of the genes highlighted in this thesis. Specifically, finding interactions with Bd0465 could expand the putative signalling network to which it links DivIVA. Bd0466 would also be a candidate for this, potentially showing further amino acid or PLP related signals. Library assays for ParA1 may also help to resolve what function it may perform, as this is currently unknown.

It is also possible to determine whether DivIVA has a protective effect against reactive oxygen species. This could be done with the addition of H_2O_2 at varying concentrations during the HD cycle, or with the application of other ROS, to both *B. bacteriovorus* WT and *ΔdivIVA* strains. Lower numbers of plaque forming units in *ΔdivIVA* would suggest susceptibility.

When DivIVA was tested in a pairwise fashion with whole proteins for Bd0548, Bd2107 and Bd3538, the β-galactosidase assay showed less activity than with the library fragment plasmids. To further confirm these interactions, his-tagging DivIVA and performing a pull down and coprecipitation assay could be performed.

5 Chapter 5: bioinformatic investigation of the *division and cell wall* cluster

5.1 Chapter 5 introduction

5.1.1 Shielding from Covid

As I am considered vulnerable, I have spent the past two years of my research shielding at home. This interrupted my practical work, leaving certain areas I would have liked to have investigated unfinished or unexplored. While I have not been able to attend the lab, I have worked from home to complete my thesis. The work in this chapter has all been done during this time.

5.1.2 The ancestral division and cell wall cluster

The *division and cell wall* (*dcw*) cluster is a group of genes, often in a singular operon, that encode for septal assembly and peptidoglycan synthesis and incorporation proteins (Vicente et al., 1998). This cluster is highly conserved in rod shaped bacteria, both Gram-negative and -positive. While there is some variation between bacteria as to which genes are present in their cluster, there is a set of genes that are commonly found in all bacterial clusters; I refer to these as "ancestral" *dcw* cluster genes, seen in **figure 5.1.1**.

Figure 5.1.1. A cartoon representation of the genes considered to be in the ancestral *dcw* cluster. From left to right, these are: *mraZ* (transcriptional regulator), *mraW* (Ribosomal RNA small subunit methyltransferase H), *ftsL* (cell division gene), *ftsI* (Peptidoglycan D,D-transpeptidase), *murE* (peptidoglycan synthesis gene), *murF* (peptidoglycan synthesis), *mraY* (peptidoglycan synthesis), *murD* (peptidoglycan synthesis), *ftsW* (cell division gene and Lipid II flippase), *murG* (peptidoglycan synthesis), *murC* (peptidoglycan synthesis), *murB* (peptidoglcyan synthesis), *ddlB* (peptidoglycan synthesis), *ftsQ* (cell division gene), *ftsA* (Z-ring stabilisation/cell division gene) and *ftsZ* (Z-ring and cell division gene). These are largely conserved in rod-shaped bacteria, with genes removed or inserted depending on the mode of division and lifestyle of the bacterium (Vicente et al., 1998, Mingorance et al., 2004).

The *E. coli dcw* cluster consists of fifteen genes in a single operon. These are all commonly found in other bacterial *dcw* clusters beginning with cluster regulator *mraZ*. The fourteen other genes code for septal assembly proteins, including FtsZ, and peptidoglycan synthesis proteins. The cluster of *B. subtilis* sees several additional genes for the process of sporulation, which is tied to the division process (Real and Henriques, 2006). In all cases, the genes are transcribed in the same direction. Exclusively in Gram-positive bacteria, the *ylm* operon can be found immediately downstream of *ftsZ*, and contains between five and seven genes, typically *ylmDEFGH* and ending with *divIVA* (White and Eswara, 2021). While *B. bacteriovorus* do have *divIVA*, they do not have the *ylm* operon, as is the case with other Gram-negative bacteria.

While highly conserved in rod-shaped bacteria, the *dcw* cluster is far less conserved in other bacteria, such as those with a different shape. An extreme example are *Mycoplasma* species, which do not produce a cell wall (Alarcon et al., 2007, Lluch-Senar et al., 2010). In *Mycoplasma genitalium* the *dcw* cluster is limited to four genes: *mraZ, mraW, MG_223* and *ftsZ*. Recently, the whole cluster has been shown to be non-essential to growth (Martínez-Torró et al., 2021). The complete absence of these genes is not surprising given that this bacterium does not synthesise peptidoglycan.

Other examples of less conserved *dcw* clusters can be seen in cocci or helical bacteria. *Staphylococcus aureus* and *Enterococcus faecalis* both have smaller *dcw* clusters, with genes for both division and cell wall biosynthesis no longer conserved, as does *Helicobacter pylori* (Pucci et al., 1997, Kamran et al., 2018). Genes that are no longer seen in the cluster are typically elsewhere in the genome as these bacteria still produce peptidoglycan.

This raises the question as to whether *B. bacteriovorus* will also have a less conserved *dcw* cluster. In attack phase the cells are curved, however, during growth and division in the bdelloplast, the cell grows as a filament and has multiple, simultaneous septa with a variable number of progeny based on host biomass. *Streptomyces coelicolor* also grow as a filament, and their *dcw* cluster resembles that of *Bacillus subtilis*, largely due to them both having sporulation specific genes (Zhang et al., 2018). The unique lifecycle of *B. bacteriovorus*

may have reduced the conservation of the *dcw* cluster, or there could be additional genes in the cluster to coordinate growth and division with other cellular processes. This could include metabolic signals or sensory pathways for detecting the stage of digestion of the host.

5.1.3 The Peptidoglycan biosynthesis pathway

Many of the genes in the *dcw* cluster encode for peptidoglycan biosynthesis enzymes. Of the ancestral genes, this includes *mraW, mraY, ddlB* and genes *murBCDEFG*. Genes *murA* and *murJ* are not typically found in the *dcw* cluster.

The many-stepped process of peptidoglycan synthesis has been studied most extensively in *E. coli* and has been recently reviewed (Egan et al., 2020). As seen in general introduction, synthesis starts in the cytoplasm. Initially, UDP-MurNAc is synthesised from UDP-GlcNAc by MurA (UDP-GlcNAc enolpyruvyl transferase) and MurB (UDP-MurNAc dehydrogenase). The stem peptide is then attached to this in stages. MurC (UDP-MurNAc ʟ-Ala ligase) attaches an ʟ-Ala and MurD (UDP-MurNAc-ʟ-Ala-ᴅ-Glu ligase) extends this with a ᴅ-Glu synthesised by MurI (Glu racemase). MurE then adds a *meso*-Dap unit (UDP-MurNAc-ʟ-Ala-ᴅ-Glu-*meso*-Dap ligase). DdlA (ᴅ-Ala-ᴅ-Ala ligase A) joins two ᴅ-Ala units which are then attached by MurF (UDP-MurNAc-tripeptide-ᴅ-alanyl-ᴅ-Ala ligase), completing the pentapeptide chain. The whole unit is attached to membrane embedded undecaprenyl phosphate by MraY (phospho-*N*-acetylmuramoyl-pentapeptide transferase) creating Lipid I. Lipid II is then made by MurG (undecaprenyldiphospho-muramoylpentapeptide beta-*N*-acetylglucosaminyltransferase) attaching a GlcNAc onto the MurNAc. This is then flipped across the membrane by MurJ and FtsW (Lipid II flippases). From there, Lipid II becomes a substrate for incorporation into the cell wall. In this process, septal assembly and cell wall synthesis intersect at FtsW, which has roles as both the Lipid II flippase and in recruiting further periplasmic septal components.

B. bacteriovorus also has another potential source of peptidoglycan in the host. Digestion and incorporation of the host cell wall would be a way to circumvent much of the synthesis pathway. However, the integrity of the host bdelloplast

is also paramount to the success of the predatory lifestyle. Weakening the cell wall may risk the bdelloplast overly leaking or breaking open when the filament is growing and vulnerable, leaving the predator without further nutrients or a sheltered environment. As such, use of the bdelloplast wall may be very limited, at least until the progeny are matured. While there is substantial evidence for modification of prey cell wall, there is currently no evidence as to any potential pathways for the uptake and incorporation of prey peptidoglycan into the *B. bacteriovorus* cell wall.

5.1.4 The *dcw* cluster of *B. bacteriovorus*: adaptations for a host dependent lifestyle

There are many potential pathways and systems in *B. bacteriovorus* that may feasibly have been associated with the *dcw* cluster, just as *B. subtilis* and other Firmicutes have with sporulation specific genes. The link between DivIVA, PLP and amino acid homeostasis, and ROS resistance already shows novel methods for regulating growth and cell division. Similarly, these or other systems with an input into regulating growth and its transition to division could be associated with the *dcw* cluster. Given previous evidence of lateral gene transfer events, both ancient and more modern, and its environmental ubiquity, it is possible that *B. bacteriovorus* has acquired genes from other bacteria, or developed novel genes specifically for intracellular predation. In this chapter, I will investigate the possible adaptations to the *B. bacteriovorus dcw* cluster and their implications on the regulation of growth and division in this predator. In addition, I will investigate the full peptidoglycan synthesis pathway and the putative pathways for utilisation of prey cell wall.

5.2 Specific research aims

- Investigate the *B. bacteriovorus dcw* cluster including:
    - The structure and novel operons of the HD100 *dcw* cluster
    - The ancestral genes of the cluster, including those that have moved to another locus
    - The novel inserted genes in the HD100 cluster and how they relate to division and cell wall roles
    - Use RNA-seq data to compare transcription profiles

- Compare the HD100 *dcw* cluster to that of other BALOs, such as *B. bacteriovorus* Tiberius and *B. exovorus*.
- Investigate the peptidoglycan biosynthesis pathway and alternative sources of peptidoglycan and how they relate to the *B. bacteriovorus* lifecycle.

5.3 Chapter 5 Results

5.3.1 The *dcw* cluster in *B. bacteriovorus HD100* has multiple operons and gene insertions

As previously stated, both the genes in the *dcw* cluster and the order in which they are transcribed is highly conserved across many bacteria, both Gram-negative and -positive. Systems in which this is not the case are often bacteria that are not rod shaped (cocci or helical) or where no cell wall is made (*Mycoplasma*) (Pucci et al., 1997, Alarcon et al., 2007).

In *B. bacteriovorus*, the *dcw* cluster contains most of the ancestral genes in the conserved order, **Figure 5.3.1**, as is seen in the many bacteria with a homologous cluster (Mingorance et al., 2004); only three are missing. Two are absent from the genome entirely; they are *mraZ,* a transcriptional regulator for the cluster, and *ddlB*, a D-alanine--D-alanine ligase. While absent from the cluster, *murB* is positioned downstream in the genome at *bd3233*. There are a striking number of insertions in the *B. bacteriovorus dcw* cluster, a total of fifteen additional genes of interest, numbered as shown in **Table 5.3.1**. Twelve of these are inserted within the cluster, of which eight are transcribed in the opposite direction to the ancestral genes, and three of them follow *ftsZ*.

In the *E. coli* cluster, genes *ftsL* to *ddlB* are transcribed from four promoters at the start of the cluster: one before *mraZ* (mraZp), one before *mraW* (mraWp1) and two within *mraW* (*ftsLp1, ftsLp2*), as shown in **Figure 5.3.2.** (Vicente et al., 1998, de la Fuente et al., 2001). Other systems, however, have additional promoters in their cluster. *B. subtilis*, a sporulating, rod shaped Firmicute, has several more promoters, preceding *spoVD*, *murE*, *spoVE* and *divIB* (Real and Henriques, 2006). In *Neisseria gonorrhoeae*, a coccal intracellular pathogen, the cluster has three hypothetical, non-ancestral genes inserted, as well as 6 transcriptional terminators (Francis et al., 2000). In both systems, all of the genes are oriented in the same direction as the ancestral genes. Clearly, the *dcw*

cluster can be adapted to account for variation in cell shape and the specific lifestyle of bacteria.

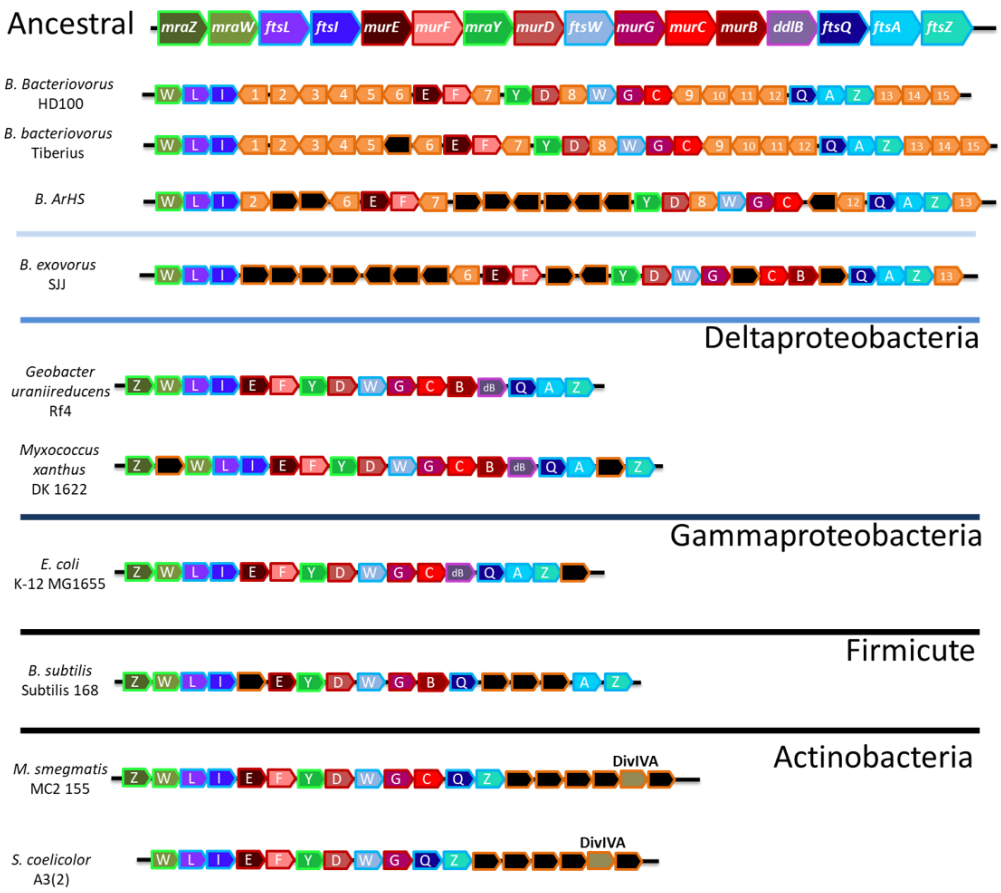

Figure 5.3.1. A cartoon representation of the genes present in the *dcw* clusters of various bacteria. The first cluster, labelled "Ancestral", shows genes that are commonly found and conserved in the *dcw* clusters of rod-shaped bacteria. The following clusters use an abbreviated and colour coded system, based on the ancestral cluster, to represent the genes. Orange, numbered genes in the *B. bacteriovorus* HD100 genome represent inserted genes. Homologues of these in other clusters are numbered the same, whereas orange bordered but black filled genes are insertions in that cluster that are not seen in the *B. bacteriovorus* HD100 *dcw* cluster. See Table 1 for the gene numbers and annotations.

Gene tag	Gene name	Insertion number	Predicted product function/features	15min/AP	30min/AP	45min/AP	60min/AP	120min/AP	180min/AP	240min/AP	300min/AP
bd3215	*mraW*		Ribosomal RNA Methyltransferase protein MraW	0.82	0.44	0.51	0.21	0.35	0.44	0.47	0.40
bd3214	*ftsL*		Cell division protein FtsL	0.55	0.40	0.36	0.44	0.36	2.09	2.56	1.43
bd3213	*ftsI*		Cell division protein FtsI	0.46	0.38	0.46	0.51	0.27	2.38	2.89	1.54
bd3212		1	β-lactamase-/transpeptidase-like protein	0.43	0.36	0.64	0.71	1.00	2.93	3.00	2.21
bd3210		2	DNA helicase RecQ homologue	1.00	2.00	11.00	22.00	63.00	27.00	15.00	8.00
bd3209		3	LpxH-like metallophosphatase	0.83	0.42	0.33	0.58	0.17	2.25	3.17	2.00
bd3208		4	Sugar metabolism and outer membrane integrity	0.60	0.35	0.30	0.28	0.13	1.53	2.15	1.30
bd3207		5	Unknown	1.00	1.00	1.00	1.00	2.00	8.00	5.00	1.00
bd3206		6	Outer membrane modifying acyl-protein thioesterase	1.00	1.00	2.00	2.00	10.00	14.67	12.00	4.00
bd3205	*murE*		Peptidoglycan synthesis protein MurE	0.57	0.57	1.29	1.43	6.71	11.71	10.14	3.29
bd3204	*murF*		Peptidoglycan synthesis protein MurF	0.50	0.33	0.83	0.83	4.33	8.83	7.83	3.17
bd3203		7	CBS domain, AMP/ATP sensing protein	0.39	0.19	0.20	0.18	0.14	0.10	0.13	0.39
bd3201	*mraY*		Peptidoglycan synthesis protein MraY	2.09	3.18	2.36	3.09	5.55	7.00	5.18	3.55
bd3200	*murD*		Peptidoglycan synthesis protein MurD	1.75	3.50	3.00	2.88	6.25	7.00	5.25	2.88
bd3199		8	Lipoprotein associated - invasion specfic	0.18	0.12	0.10	0.32	0.05	0.33	0.41	0.39
bd3198	*ftsW*		cell division protein FtsW	0.69	0.36	0.31	0.40	0.23	1.13	1.37	0.91
bd3197	*murG*		Peptidoglycan synthesis protein MurG	0.78	0.54	0.63	0.61	0.41	1.73	2.17	1.24
bd3196	*murC*		Peptidoglycan synthesis protein MurC	0.70	0.49	0.51	0.58	0.58	1.86	2.14	1.21
bd3195		9	Glyoxylate hyrdroxypyruvate reductase	6.50	1.00	0.50	1.00	3.50	7.00	6.00	2.00
bd3194		10	Caspase of unknown function - invasion specific	10.00	1.13	0.33	0.20	0.07	0.33	0.33	0.47
bd3193		11	Universal stress protein	0.25	0.50	0.25	0.50	4.75	8.25	7.00	2.75
bd3192		12	Methyl-accepting chemotaxis protein, CheW interaction domain	0.89	0.78	0.67	0.33	0.11	1.67	3.11	3.33
bd3191	*ftsQ*		cell division protein FtsQ	0.30	0.16	0.18	0.27	0.08	0.84	1.18	0.76
bd3190	*ftsA*		cell division protein FtsA	0.62	0.38	0.71	0.71	3.83	9.62	7.98	3.05
bd3189	*ftsZ*		cell division protein FtsZ	0.35	0.23	0.29	0.42	1.84	7.65	6.42	2.58
bd3188		13	Lipid X synthesis, LpxH homologue	0.50	0.13	0.38	0.88	2.38	8.50	6.75	3.50
bd3187		14	Unknown	0.20	0.20	0.20	0.80	2.60	10.00	8.40	3.20
bd3186		15	methyltransferase	0.50	0.50	0.50	0.50	0.50	5.00	4.00	2.00

Table 5.3.1. An overview of RNA-seq data for the *dcw* cluster of *B. bacteriovorus* with gene numbers, insertion numbers and relative expression compared to attack phase.

In this table, the genes of the *dcw* cluster are listed in the first column. The second column has the annotation for ancestral genes. The third column has the insertion number as seen in figure 5.3.1. The fourth column is the predicted function of these genes as annotated with the genome, before my investigation. The following columns show Simona Huwiler's unpublished RNA-seq data. These show the reads at each timepoint compared to attack phase (for example, a value of 1 is the same, 0.5 is half and 2 is twice as many). Cells are colour coded to show if the reads are significantly fewer (red) or higher (green).

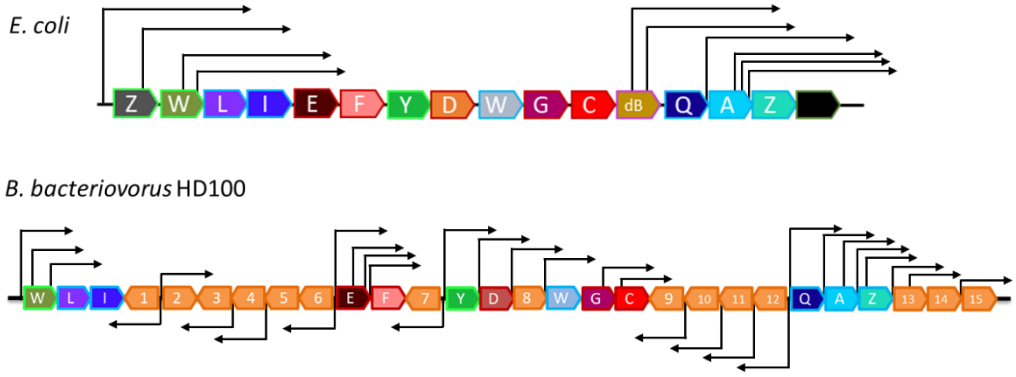

Figure 5.3.2. A cartoon representation of the dcw clusters of *E. coli* and *B. bacteriovorus* HD100 showing promoters for the ancestral genes. Arrows indicate the position of a known promoter (for *E. coli*) or a predicted promoter (for *B. bacteriovorus*). Predicted promoters were found with Bprom predictor online tool (http://www.softberry.com/berry.phtml?topic=bprom&group=programs&subgroup=gfindb). To reduce the number of false promoters, only those with a score above 2 are shown (Vicente et al., 1998, de la Fuente et al., 2001).

As the HD100 cluster is fragmented, with inserted genes transcribed opposite to the ancestral genes, there must be numerous additional promoters to express the novel insertions, as well as the ancestral homologue operons and genes which cannot be transcribed from these initial promoters. This introduces the possibility of increased complexity in regulation of the cluster, with each operon potentially being transcribed via different transcription factors.

The addition of so many inserted genes, and the fragmentation of the cluster, is striking, and it must be considered within the context of the bdelloplast. As the prey is systematically degraded and the materials transported into the growing *B. bacteriovorus* filament, there will be many potential metabolic and physiological cues for determining the extent of growth and transition to septation. Working on the novel nature of the HD100 *dcw* cluster will give insight to the relationship between the growth and division processes, such as filamentous growth, both of the inner and outer membranes and the cell wall, genome replication and DNA synthesis, and partitioning, to name a few. One would expect tight regulation, synchronisation and control of these processes

to efficiently use the biomass available to produce as many progeny as possible, in as short a time as possible.

5.3.2 Investigating the ancestral gene homologues of the *dcw* cluster

In this section, I will bionformatically investigate the *dcw* cluster in *B. bacteriovorus* HD100; my objectives are to consider the overall structure of the cluster, the potential cotranscription of genes, the patterns of expression, and the function of individual proteins encoded from this operon. All these points are considered with reference to the defined HD cycle earlier in this thesis**.** When these genes are expressed could be an insight into which specific process, or processes, they are synchronised and interact with. This data should give an overview of the cluster in *B. bacteriovorus* HD100 and make a basis for further investigation.

5.3.2.1 Operon *mraW – ftsL – ftsI* retains the same promoter structure as *E. coli*

The first putative operon is *mraW-ftsL-ftsI* (*bd3215-bd3214-bd3213*). As with the *E. coli* cluster, there are several promoters in this grouping, shown in **figure 5.3.2**. These I have labelled in the same fashion as the *E. coli* promoters discussed. One promoter is predicted preceding *mraW*, *mraWp*, with two situated in the gene itself, *ftsLp1* and *ftsLp2*; these roughly correspond to the positions of the *E. coli* promoters. Promoter *mraWp* is predicted to have recognition sequences for transcription factors LexA, SoxS and ArgR; only LexA has a homologue in HD100. Promoter *ftsLp1* is predicted to be dependent on RpoD (σ70) and IHF (Integration host factor), while there are no predicted sequences for *ftsLp2*.

Using RNA-seq data, shown in **appendix 8.1.1a**, gene *mraW* is shown to be expressed from 120 to 300 minutes into the cycle, with a much lower expression than *ftsL* and *ftsI*. Expression at 120 minutes and 300 minutes is low, with much higher expression at 180 to 240 minutes. This means that it is expressed after digestion of the prey is underway and multiple replisomes are present. However, its expression is highest after replication is complete and the filament is preparing for septation. This could mean that MraW function relates specifically to septation, a process that begins at 120 minutes, with

upregulation of *ftsZ*, with the septation event occurring after 180 minutes; at this time, *mraW* expression is at its highest, through to 240 minutes when septation has been completed and progeny are maturing, and dropping at 300 minutes when lysis and escape is initiated. This shows a focussed window in which MraW, a methyltransferase acting on and regulating rRNA, is acting to promote septation.

The expression of *ftsL* and *ftsI* is highest at 180 to 300 minutes, additionally with pronounced expression at attack phase, but showed much lower expression from 15 to 120 minutes. FtsL forms part of the divisome structure, in complex with FtsQ and FtsB, that connects the cytoplasmic processes, such as Z-ring formation, with the periplasmic, such as peptidoglycan synthesis. Increased expression at 180 minutes coincides with the septation event but being expressed throughout the cycle also means that lower amounts of FtsL may be ready for assembly into the divisome as soon as the Z-ring is being stabilised. High expression through to 300 minutes and attack phase covers septation, maturation and lysis of the bdelloplast and the progeny becoming free swimming, processes that might not be immediately associated with FtsL which is thought to link the cytoplasmic division proteins to the periplasmic; once septation has occurred, FtsL has fulfilled its traditional role (Guzman et al., 1992, Buddelmeijer and Beckwith, 2004). This data, therefore, may show a role for it in newly released progeny and attack phase cells. FtsI is a peptidoglycan D,D-transpeptidase shown to catalyse cross-linking at the septal cell wall and is one of the proteins that the FtsL complex is connecting to the cytoplasmic divisome (Dai and Lutkenhaus, 1992, Vicente et al., 1998, Karimova et al., 2005). As both have the same expression, it could mean that they are active beyond the septation event, modifying the cell wall of the newly released progeny. Indeed, Fenton *et al.* showed that newly released progeny do extend their cell length, but not width, after leaving the bdelloplast (Fenton et al., 2010). This could be directed by the divisome if elements of it stay assembled following the septation event. Following septation, this assembly would now be located at the cell poles and could be directing peptidoglycan growth post-division and lysis.

5.3.2.2 Ancestral homologues *murE* and *murF* are cotranscribed and could be regulated by convergent, antisense RNA

The second potential operon of ancestral *dcw* homologues is *murE-murF* (*bd3205-bd3204*). These appear to have a single promoter and are upregulated from 180 to 300 minutes into the cycle, with almost no transcription before. Promoter predictions show two high scoring promoters, one before *murE* (*murEp*) and one starting 130 bps into *murF* (*murFp1*), as well as two lower scoring promoters within *murE* (*murFp2* and *murFp3*). Of these, *murFp1* shows transcription recognition sequences for RpoD (σ70) and CRP (cyclic AMP receptor protein), *murFp2* shows recognition sequences for RpoD, and *murFp3* for ArgR (note that *argR* is not present in HD100; section 5.3.2.1). Again, this expression coincides with the septation event through to newly released attack phase cells; however, unlike *ftsI* and *ftsL*, expression drops at 300 minutes with no transcription at attack phase, giving a profile more like *mraW*, shown in **appendix 8.1.1b**. Both genes encode enzymes that function in the cytoplasmic stages of peptidoglycan synthesis. This expression is therefore surprising, as filament growth has been observed before their expression, and peptidoglycan would be required to elongate. It could be that the prey provides a source of peptidoglycan fragments when digestion starts after invasion and synthesis is not required until the resources are nearly depleted; the final amount that is synthesised by the predator may be just what is needed to complete septation. If this is not the case, then an alternate source or pathway for earlier synthesis may exist that bypasses the early stages catalysed by the enzymes.

Immediately downstream of this operon and transcribed in the opposite direction is *bd3203*, labelled 7 in **Figure 5.3.1/Table 5.3.1**. This gene has a transcription profile opposite that of *murE-murF*; higher transcription from attack phase and 300 minutes, with much decreased transcription at 120 to 240 minutes, also shown in **appendix 8.1.1b**. RNA-seq also suggests that transcription of *bd3203* overlaps with the end of *murF*, displaying increased reads on both plus and minus strands. Rockhopper designates a 172 bp region following *bd3203* as a UTR (untranslated region) suggesting this could be an indication of 3'-overlapping, or convergent, antisense RNA (asRNA) (Georg

and Hess, 2011). This asRNA would regulate *murE-murF* post-transcriptionally, preventing translation during the time points at which growth and division do not occur. Additionally, just the process of transcribing *bd3203* could interfere with the transcription of *murE-murF*, as any RNA polymerase transcribing one would block the transcription of the other. This additional level of regulation may act as a hard stop on the canonical peptidoglycan synthesis pathway at non growth and division times. This would prevent the products of MurABCD from being further processed and inserted into the cell wall. It may be the case that the material available for cell wall growth is higher than for other processes, such as genome duplication, and that this regulation stops an excess of wall growth that would ultimately require more energy usage for the same number of progeny.

5.3.2.3 Homologues *mraY* and *murD* are cotranscribed and expressed throughout the HD cycle

Ancestral homologues *mraY-murD* are also predicted to be cotranscribed, with a predicted promoter preceding *mraY* (*mraYp*). Interestingly, their transcription suggests that they are active during the whole cycle, **appendix 8.1.1c**. While transcription does peak at 180 minutes, both genes show significant activity at all points except for attack phase. Both genes encode proteins that act in the cytoplasmic part of the peptidoglycan synthesis pathway. Activity before invasion of the prey, and a potential lack of exogenous biomass for growth, raises questions as to the availability of the substrates they act upon and for what purpose peptidoglycan precursors are being synthesised. This is explored later in the thesis. Promoter prediction suggests an additional, high-scoring promoter in this operon (*murDp*) preceding *murD*. Both promoters have predicted transcription factor recognition sequences; PhoB, LRP and FIS (factor for inversion stimulation) for *mraYp*, and IHF and GlpR for *murDp*.

Again, this speaks to increased complexity in the regulation of cluster genes; in *E. coli*, neither genes have their own promoter. It could be that the first promoter, *mraYp*, cotranscribes both genes for division whereas *murDp* allows transcription of *murD* at other points in the cycle, or under different conditions. It should also be noted that an additional *murD* homologue is found in the *B. bacteriovorus* genome, *bd0052*. While this is explored later, its transcription

profile differs to *bd3200*, and could indicate two pathways; one for canonical peptidoglycan synthesis, and another for an as yet unknown product synthesised at non-growth time points.

5.3.2.4 Operonal transcription predicted for *ftsW – murG – murC* but with additional promoters within *murC*

The next predicted operon is *ftsW-murG-murC* (*bd3198-bd3197-bd3196*), with four predicted promoters. The first precedes *ftsw* (*ftsWp*), the second preceding *murG* (*murGp*), the third near the end of *murG* (*murCp1*) and the fourth 184 bps into *murC* (*murCp2*). Promoters *ftsWp, murCp1* and *murCp2* all have predicted recognition sequences for RpoD. The transcription profiles for all three genes show expression throughout the cycle, with a peak at three hours, **appendix 8.1.1d**. As with *mraY* and *murD, murG* and *murC* encode enzymes active in the cytoplasmic stages of the peptidoglycan synthesis pathway. FtsW is the flippase responsible for transporting Lipid II, the ultimate product of these cytoplasmic peptidoglycan synthesis steps, across the inner membrane into the periplasm for integration into the peptidoglycan wall (Pastoret et al., 2004). Activity during pre-invasion time points raises the same questions as with *mraY-murD*; what is the source of the substrates they act upon? As above, this is explored later in the thesis in section 5.3.6.

5.3.2.5 Homologues for *ftsQ* and *ftsA* are not predicted to be cotranscribed with *ftsZ*

Interestingly, Rockhopper does not predict *ftsQ, ftsA* and *ftsZ* to be an operon in the *B. bacteriovorus* cluster, and their transcription profiles do differ. In *E. coli, ftsZ* is transcribed from three dedicated promoters within *ftsA*, as shown in **figure 5.3.2** (de la Fuente et al., 2001). If the *B. bacteriovorus* prediction is correct, transcriptional regulation of *ftsZ* has not been conserved. This would also make *ftsA* and *ftsQ* the only non-operonal ancestral homologues in the cluster. Previous studies, before the divisome was fully characterized, showed that septation in *E. coli* requires the right balance of FtsA to FtsZ (Dai and Lutkenhaus, 1992, Dewar et al., 1992). Increases in FtsA will inhibit the function of FtsZ, until expression of FtsZ is also increased. However, this is a system in which FtsZ is also stabilised by ZipA, a protein absent in *B. bacteriovorus*. The FtsZ/FtsQ/ZipA assembly is also influenced by the

MinCDE system, which determines the site of septum formation. Again, this system is absent in *B. bacteriovorus* (Lutkenhaus, 2007, Arumugam et al., 2014, Martos et al., 2015). Producing several septa, depending on the biomass provided by the prey, clearly requires a different method of determination and Z-ring stabilization. This would tie into the dynamic determination of septa number based on prey resources, requiring input from other sources; potentially, DNA synthesis, nucleotide metabolism, genome duplication, peptidoglycan synthesis and other metabolic pathways.

The gene *ftsQ* is predicted to have a single preceding promoter (*ftsQp*), with predicted recognition sequences for CRP and FadR. Transcription occurs predominantly at 180 to 300 minutes, with some expression at attack phase and minimal expression at other time points, **appendix 8.1.1e**. This matches the transcription of *ftsL*, whose product binds with FtsQ. FtsQ and FtsL form a complex with FtsB in the divisome in *E. coli*. Interestingly, while FtsB is essential in *E. coli*, it is absent in HD100. How this affects the function of the complex during division has yet to be determined. In *E. coli*, localisation of FtsL to the divisome only requires FtsQ, which itself only requires FtsK to localise at the septum (Buddelmeijer and Beckwith, 2004). Therefore, a complex of only FtsQ/L will likely still form at the divisome in *B. bacteriovorus*. Again, as with *ftsL* and *ftsI*, expression after the septation event and at attack phase may suggest that the FtsQ/L complex is still assembled and directing periplasmic proteins, possibly as a way of continuing to modify the cell wall in the transition from newly released to matured attack phase cells.

Gene *ftsA* has a predicted promoter preceding it (*ftsAp*), and one intergenic promoter (*ftsZp1*). Both have RpoD recognition sites, and ftsZp1 also has CarP and FNR sites. Despite the lack of cotranscription prediction, it is possible that there is a small amount of cotranscription, or there are conditions in which it will occur that were not met when collecting this data. Gene *ftsA* shows transcription from 120 to 300 minutes, peaking at 180 minutes, with minimal transcription in the rest of the cycle, **appendix 8.1.1e**. As with previous genes, the peak coincides with the start of the septation event, as would be expected. Upregulation at 120 minutes indicates that the formation of Z-ring, and thus septation site selection, is at least beginning at this time point.

5.3.2.6 Putative cotranscription of *ftsZ* with *lpxH* and a gene of unknown function

ftsZ is predicted to be in an operon as the first of three genes, with *bd3188*, annotated as a *lpxH*, and *bd3187*, a protein of unknown function. Promoter prediction for *ftsZ* shows one preceding the gene (*ftsZp2*) and one 233 bps into the gene (*bd3188p1*), both with predicted RpoD recognition sites. There are two more promoters in the operon, both within *bd3188*; one starting 30 bps in (*bd3188p2*), with a TorR recognition sequence, and another 412 bps in (*bd3187p*), with PhoB and NagC recognition sequences. NagC does not appear to have a homologue in *B. bacteriovorus.* A search for TorR with the *E. coli* homologue shows a very highly conserved protein Bd1017, annotated as PhoB.

Transcription of *ftsZ* occurs from 120 to 300 minutes into the cycle, peaking at 180 minutes, **appendix 8.1.1f**. This is the same as *ftsA*, above, with which *ftsZ* directly interacts in other systems. Its expression at 120 mins also shows that septa site selection begins at this time point (Dai and Lutkenhaus, 1992, Azzolina et al., 2001, de la Fuente et al., 2001). Transcription for *bd3188* and *bd3187* is much lower, although it does occur at the same time points. Readthrough of these two genes appears to be very low but being cotranscribed with *ftsZ* would suggest a strong link between their function and formation of the Z-ring. This could be to synchronise these processes or for regulating the timings between them.

LpxH, also known as YbbF, is an UDP-2,3-diacylglucosamine hydrolase. These synthesise Lipid X in the lipopolysaccharide (LPS) biosynthesis pathway, specifically Lipid A synthesis (Babinski et al., 2002, Cho et al., 2020). Lipopolysaccharides are found on the outer membrane of Gram-negative bacteria where Lipid A acts as an anchor, holding the LPS in the membrane. An *lpxH* sharing an operon with *ftsZ* suggests crosstalk between the LPS biosynthesis pathway and the division process; as the divisome is assembling, LPS is being synthesised for the growth of the cell membranes and for the septa. Outer membrane integrity of *B. bacteriovorus* is especially important; not only are they growing in a rapidly changing environment, as prey resources are broken down and used up, but they are also using a range of lytic enzymes to do this. Self-susceptibility to these would be catastrophic, so

protecting the growing *B. bacteriovorus* would require the outer membrane to be monitored and supported both structurally, with LPS synthesis, and with a range of self-protection proteins.

Protein predictions do not identify any potential domains in Bd3187, other than it being a predicted to have an N terminal signal peptide with no transmembrane regions. Its secretion could suggest that it acts in the same region as Bd3188, the predicted LpxH. A pBlast also shows that there are no homologues in other bacteria, including other BALOs. Again, cotranscription with *ftsZ* suggests a role in septation, possibly in modifying LPS as with the predicted LpxH.

5.3.2.7 Transcription factors for ancestral homologue operons

As shown in **Table 5.3.2**, several promoter predictions were run for the ancestral *dcw* cluster genes. While a range were found, there are some common transcription factor recognition sites among the promoters. Of the 17 documented, 8 of the promoters had a recognition sequence for RpoD, or sigma factor 70 (σ^{70}); *ftsL*/*ftsI, murF, ftsW, murC, ftsA* and *ftsZ* are all transcribed from at least one predicted promoter with a σ^{70} recognition sequence. Additionally, each of these genes has a transcription pattern that peaks at 180 minutes. Among bacteria, σ^{70} is considered the primary, housekeeping sigma factor, responsible for the expression of unconditionally essential genes, which certainly includes divisome proteins (Davis et al., 2017). Some bacteria code for multiple σ^{70} family proteins, however only one homologue is found in *B. bacteriovorus*: Bd0242. This is expressed throughout the HD cycle, though it is most highly expressed at 30 minutes, and is downregulated at 180 minutes on, a pattern adverse to the genes above with recognition sequences in their promoters. However, sigma factors are often regulated post-transcriptionally by anti-sigma factors, which could mean that σ^{70} is expressed early in the cycle but is still present at these later points. Regulation by an anti-sigma factor could mean that it is only active later in the cycle, perhaps at 180 minutes, when these genes show the highest expression.

Two gene promoters have recognition sequences for CRP (cyclic-AMP binding receptor protein): *ftsQ* and *murF*. In *E. coli*, CRP is a global

transcription regulator that binds, and is activated by, cAMP. It regulates many processes but is notable for its major role in carbon catabolite repression (CCR) and the system that controls the preferential consumption of glucose over other carbon sources (Escalante et al., 2012). There is a single CRP homologue in *B. bacteriovorus*: Bd3056. Interestingly, it is only upregulated at attack phase and from 180 to 300 minutes, a similar pattern to *ftsQ* and *murF*. This connects divisome assembly and peptidoglycan synthesis pathways to the regulation of sugar metabolism, possibly synchronising division to the availability of certain carbon sources.

Associated Gene	Promoter name	Promoter Score	TF prediction - Score
mraW	mraWp	3.43	LexA - 7
ftsL	ftsLp1	3.48	RpoD15 - 12 IHF - 6
	ftsLp2	1.60	NP
murE	murEp		NP
murF	murFp1	3.28	RpoD15 - 14 CRP - 10
	murFp2	1.83	RpoD - 6
	murFp3	2.48	NP
mraY	mraYp	5.99	PhoB - 8 LRP - 6 FIS - 18
murD	murDp	3.70	IHF - 6 GlpR - 6
ftsW	ftsWp	3.14	RpoD18 - 9
murG	murGp	2.96	NP
murC	murCp1	1.84	NP
	murCp2	3.78	RpoD18 - 5
ftsQ	ftsQp	4.07	CRP - 6 FadR - 5
ftsA	ftsAp	6.60	RpoD15 - 14 RpoD17 - 11 RpoD18 - 12
ftsZ	ftsZp1	3.94	FNR - 5 CarP - 7 RpoD17 - 11
	ftsZp2	2.26	RpoD19 - 6

Table 5.3.2. Promoter and transcription factor predictions for ancestral *dcw* cluster gene homologues.
This table shows prediction results for ancestral *dcw* gene promoters found with BProm (http://www.softberry.com/berry.phtml?topic=bprom&group=programs&subgroup=gfindb). The gene (first column) plus the 200bp upstream of the gene start were submitted with default settings. The first column shows the gene name and the second column the name given to the promoter in this study based on the gene. The third column is the score given by the BProm promoter prediction and the fourth column shows predicted transcription factors and their associated score.

5.3.2.8 Overview of ancestral *dcw* gene homologues

This section shows that the *dcw* cluster of *B. bacteriovorus* contains a set of ancestral homologue genes conserved in order. Despite this, they are fragmented by inserted genes, breaking the cluster into smaller gene groups. The consequence of this is that, while the ancestral genes are conserved, their method of regulation is not. Promoter predictions show that many of the novel promoters likely require σ^{70} for initiating transcription, there are also a host of other transcription factors that seem unique to the various promoters. The lifecycle of *B. bacteriovorus* could be the cause of this. The obvious difference to other bacteria, and most likely explanation for this increased level of regulatory complexity, is the lifecycle of *B. bacteriovorus*; this bacterium must consume the bdelloplast biomass, grow and replicate, and finally septate and lyse the bdelloplast, in as efficient a manner as possible. The above evidence clearly shows that many of the processes, such as wall and membrane growth, divisome assembly and SOS response pathways, are linked to one other and that crosstalk between these systems could be how the sequence of events in the HD lifecycle are synchronised.

There are further avenues to explore. Investigating the inserted genes could produce even more evidence of crosstalk between various pathways. This could be further evidence for those related to the ancestral genes, such as the peptidoglycan synthesis or divisome assembly, or they may show other pathways. Certainly, one would expect to see an input from metabolic pathways, as state of digestion in the bdelloplast will be a major indication for when to switch from growth to septation. These are investigated in the next section.

There are also other pathways that could be explored. The *dcw* cluster contains many of the genes of the *de novo* peptidoglycan synthesis pathway, but there are still several genes yet to be accounted for that would complete the pathway. Additionally, some genes in this pathway are activated at seemingly unnecessary time points, suggesting a role outside of peptidoglycan synthesis during the growth phase. Gene *murD* (*bd3200*) is expressed throughout the

cycle, and there is also a second *murD* (*bd0052*) that has yet to be investigated. Exploring the peptidoglycan synthesis genes distal to the cluster (here meaning outside of gene locus *bd3186* to *bd3215*) would help to show if the pathway is complete, and if there is any more evidence of crosstalk between this pathway and others.

5.3.3 Investigating the *dcw* cluster gene insertions

There are fifteen genes associated with the HD100 *dcw* cluster that I do not consider to be ancestral; genes whose homologues are not commonly found in bacterial *dcw* clusters, shown in **figure 5.3.1/table 5.3.1**. Many of these are inserted between the ancestral homologues, meaning that although the ancestral homologues are in the ancestral order and orientation, cotranscription of the cluster is broken up by these insertions, many of which are transcribed in the opposite direction to the canonical cluster genes. Many of these inserted genes are annotated as hypothetical and some appear to be unique to *B. bacteriovorus*.

In this section I will investigate the inserted *dcw* cluster genes; depending on the predicted function of these genes, such analysis could help to link other cellular processes to those related to the *dcw* cluster, as well as give a view into any novel methods of regulating and coordinating the many processes involved in the unique environmental conditions of the bdelloplast.

5.3.3.1 Gene *bd3212* encodes a putative β-lactamase-/transpeptidase-like protein

The first inserted gene is *bd3212*, annotated as a β-lactamase, and this is transcribed counter to the ancestral cluster; end to end with *bd3213, ftsI*. This is labelled 1 in **Figure 5.3.1**. Further domain prediction suggests that Bd3212 is a signal peptide-containing protein with a β-lactamase-/transpeptidase-like homology (Pares et al., 1996). Unpublished RNA-seq data, **appendix 8.1.2a** suggests *bd3212* transcription is primarily from 180 to 300 minutes of the predation cycle, covering when replisomes are gone and the filament is preparing to septate, through to the release of matured progeny. A promoter prediction shows a preceding promoter with an RpoD recognition sequence. This is seen in many of the ancestral genes.

It is unknown whether Bd3212 is a β-lactamase or transpeptidase, and further work would be needed to determine this. If the latter, it would not be the only transpeptidase at this locus, as *bd3213 ftsI*, its genomic neighbour, also encodes a D, D- transpeptidase, and is transcribed at the same time points. However, the proteins differ significantly, sharing less than 10% identity. Another transpeptidase active during division could be involved in the construction of new cell wall at the septa.

If Bd3212 acts as a β-lactamase, it stands to reason that it is expressed at the same time as the transpeptidases. As there is no cell wall growth before invasion, with possibly only maintenance activity, it may be a waste of resources to express the protective enzyme. β-lactamase enzymes are thought to have evolved from D, D- transpeptidases, as these are the targets of β-lactam antibiotics, which closely resemble the D-ala-D-ala substrate (Peimbert and Segovia, 2003). As such, these families overlap in homology and further functional studies would be required to ascertain the activity of Bd3212.

5.3.3.2 Gene *bd3210* encodes a putative RecQ, DNA response protein

Upstream of *bd3212*, and transcribed in the direction of the ancestral cluster, is *bd3210*, annotated as a *recQ* DNA helicase, labelled 2 in **figure 5.3.1**. These are ubiquitous in bacteria and eukaryotes with a range of roles in DNA replication, recombination, and repair. In *E. coli* it acts with other proteins in the RecF recombination pathway, repairing stalled replication forks at damaged DNA and repressing aberrant recombination events (Dou et al., 2004). Bd3210 contains the expected domains; an N terminal ATP binding helicase domain, a RecQ helicase domain, and the C terminal HRDC (helicase and RNaseD C-terminal) domain.

Another *recQ* homologue is annotated in the HD100 genome: *bd0988*. While proteins encoded from both homologues are predicted to have the RecQ domain, they differ at their C terminals; the final 90 residues of Bd3210 and 120 residues of Bd0988. As above, Bd3210 has the HRDC terminal, but Bd0988 has a winged helix domain, predicted as potentially binding zinc ions. In *E. coli*, a recent paper has modelled how the HRDC domain is crucial to modulating the activity of the RecQ domain in relation to the way the DNA

structure has been unwound and unfolded (Teng et al., 2020). A Swissmodel structural search shows that Bd3210 is similar to the human Bloom's syndrome protein (pdb 4cdg); this is a RecQ with a C terminal HRDC domain that, when not functioning correctly, leads to multiple symptoms including chromosomal instability (Newman et al., 2015). This all suggests that Bd3210 functions similarly to the *E. coli* RecQ; further functional and interaction studies could confirm this.

The *bd3210* promoter is predicted to have a MetR recognition site. MetR, originally identified in *E. coli*, was found to activate genes that synthesise methionine, such as *metE* and *metH (Maxon et al., 1989, Weissbach and Brot, 1991)*. Recently, in *Serratia marcescens*, it has also been shown to regulate other important processes; cell motility, stress tolerance, exopolysaccharide synthesis and biofilm formation were positively regulated by MetR, while repressing prodigiosin synthesis (Pan et al., 2020). If the *B. bacteriovorus* homologue also regulates methionine synthesis, this could further suggest crosstalk between DNA replication and amino acid synthesis, two processes that will occur at similar times in the cycle, as the *B. bacteriovorus* filament grows and the genome is replicated. Transcription of *bd3210* occurs from 60 minutes onwards, dropping at 240 to 300 minutes, **appendix 8.1.2b**. Expression at 60 minutes coincides with the appearance of the first replisome, which agrees with the function of a RecQ homologue in DNA repair. Repairing stalled replication forks, along with other maintenance and repair activities, will be a necessity for quickly producing the required number of genome copies whilst synthesising *de novo* mononucleotides, and/or importing them in from the prey. Simultaneously, the *B. bacteriovorus* cell will be synthesising a multitude of enzymes and other proteins, requiring newly synthesised amino acids; synchronisation of these growth processes is to be expected. Replisomes have dissipated at 180 minutes, suggesting that *bd3210* is expressed shortly after this, possibly to maintain the genome copies before septation, which is imminent. At 240 minutes, the filament has septated and the genomes separated, hence downregulation at this time.

5.3.3.3 Gene *bd3207* may be the first in an operon of inserted genes and has unknown function

Inserted genes *bd3207-bd3208-bd3209*, labelled 5, 4 and 3 in **figure 5.3.1**, are unique in the cluster, as they form the only predicted operon comprised solely of inserted genes. Transcription of *bd3207* is low, but is seen at 180 to 240 minutes, the period in which septation occurs and the bdelloplast is lysed. Gene *bd3207* has no promoter predicted upstream. If so, this gene has a start site further into the gene than is annotated, or it is cotranscribed with *bd3206*; the RNA seq data supports readthrough of this putative operon from 180 to 240 minutes, once replisomes have dissipated and septation is occurring, **appendix 8.1.2b**.

Bd3207 has unknown function, with predictions only showing that it has an N terminal signal peptide. This could mean it is cell wall related, or possibly sensory with further regard to environmental cues within the bdelloplast. Another possibility is that it is outer membrane related, as is evidenced in *bd3188* above.

A promoter is predicted 360 bps into *bd3207*, bd3208p1, with recognition sequences for RpoD, ArcA and PurR. This could mean that the start site for *bd3207* is incorrect or that this promoter is solely for the expression of *bd3208* and *bd3209*. If the latter, *bd3207* is only expressed through cotranscription with *bd3206*.

Although they are predicted to be cotranscribed with *bd3207*, transcription for *bd3208* and *bd3209* is much higher. Additionally, transcription is active throughout the HD cycle, though it is highest from 180 to 240 minutes. The promoter for this higher level of transcription is predicted to be 295 bps into this 743 bp *bd3208*, bd3209p, but whether this indicates a shorter gene or if this promoter is solely for transcription of *bd3209* is unknown. This promoter has recognition sites for IHF and CRP, which have been seen before in the novel promoters of ancestral genes, above. This suggests that the transcription of *bd3207-bd3208-bd3209*, and potentially *bd3206*, is like many of the ancestral gene clusters; multiple genes transcribed from a common promoter, with additional promoters within.

5.3.3.4 Bd3208 may have a role in outer membrane integrity or cAMP signalling

The second gene in the operon is *bd3208*. Protein domain predictions for Bd3208, also annotated with unknown function, show a predicted superfamily for an RmlC-like jelly roll fold. RmlC is a dTDP-sugar isomerase enzyme involved in L-rhamnose synthesis, primarily studied for its role in the virulence of some Gram-negative bacteria, such as *Salmonella enterica*, *Vibrio cholerae* and pathogenic strains of *E. coli*, and Gram-positive bacteria, such as *M. tuberculosis* and pathogenic *Streptococcus* species (Giraud et al., 2000). L-rhamnose is important as a residue of the O-antigen in the LPS of the Gram-negative bacteria, which gives resistance to serum killing and aids colonisation, and is incorporated in the capsule of Gram-positive bacteria, promoting adherence to surfaces (Samuel and Reeves, 2003, Kalynych et al., 2014, Liu et al., 2020, Giraud et al., 2000, Ma et al., 2002, van der Beek et al., 2019). However, the RmlC-like jelly roll fold superfamily includes several other proteins. This includes other enzymes for sugar metabolism, such as glucose-6-phosphate and mannose-6-phosphate isomerases which convert glucose-6-phosphate and mannose-6-phosphate, respectively, to fructose-6-phosphate; these have homologues in all three Kingdoms (Hansen and Schonheit, 2005, Miles and Guest, 1984, Sato et al., 1993, Vorobjeva et al., 2020). The growing *B. bacteriovorus* filament must maintain its outer membrane to remain resistant to its own lytic enzymes; Bd3208 could provide a link between the *dcw* cluster division functions and maintaining the outer membrane as it grows with the *B. bacterivorus* filament. Again, linking division to outer membrane synthesis/maintenance has already been seen with Bd3188.

Another family of proteins with similar structure are CRP proteins (cyclic-AMP binding receptor proteins), specifically the beta-barrel architecture. This is a transcription factor that has recognition sequences in several of the

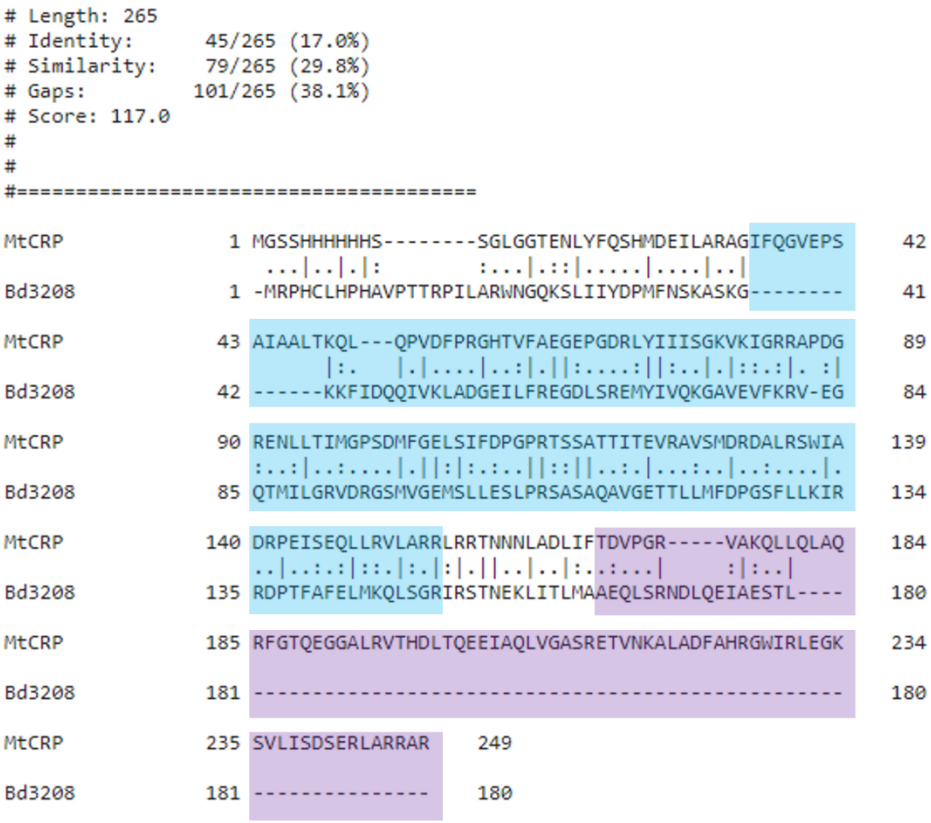

Figure 5.3.3. An alignment between Bd3208, encoded from an inserted gene in the *dcw* cluster, and a cAMP receptor protein from *Mycobacterium tuberculosis* shows homology at the N terminal domain. A Swissmodel search found that the *M. tuberculosis* CRP (PDB ID: 3I54) was the closest known structure to Bd3208. The blue highlight indicates the cAMP binding domain from the *M. tuberculosis* protein, and the purple highlight shows the DNA binding domain. Bd3208 aligns with the cAMP binding domain but does not align with the DNA binding domain.

promoters already discussed in this chapter. A Swissmodel search for structural homologues of Bd3208 returns a *M. tuberculosis* CRP (PDB ID: 3I54) (Reddy et al., 2009). In *E. coli*, CRP responds to increases in intracellular cAMP, binding to it and mediating the expression of many genes (Gosset et al., 2004). Those activated typically include genes encoding ribosomal proteins and tRNA. Some few enzymes are also activated, including the pyruvate dehydrogenase E2 component *aceF*, acetate kinase *ack* and

adenylate kinase *adk*. The Factor for Inversion Stimulation gene *fis* was also highly upregulated.

Many genes were also downregulated, largely enzymes in central pathways of carbon catabolism, including many genes of the Krebs cycle; nearly half of these accounted for the initiation of their pathways. Additionally, 18 stress response genes were also repressed.

The *M. tuberculosis* CRP has two domains, the cAMP binding domain and a Helix-Turn-Helix (HTH) DNA binding domain. **Figure 5.3.3** shows that Bd3208 aligns to the cAMP binding domain and does not have the DNA binding domain, suggesting Bd3208 is not a transcriptional regulator like the *M. tuberculosis* CRP. Of the eleven residues they identified as important to binding cAMP, five are conserved and four are semi-conserved in Bd3208, suggesting that it may retain cAMP binding. While it is clearly unable to bind DNA, it is possible that it still senses cAMP levels in the filament.

This gene is upregulated at 180 to 240 minutes, which could mean it is involved with switching from growth and replication, to septation and lysis, based upon the cellular concentration of cAMP.

5.3.3.5 Bd3209 is a predicted LpxH, similar to Bd3188, but with lower conservation

Domain predictions for Bd3209 suggest an LpxH-like metallophosphatase (Babinski et al., 2002, Cho et al., 2020). This is like *bd3188*, which is mentioned above as being a *lpxH* cotranscribed with *ftsZ*. An alignment of Bd3188, Bd3209 and an LpxH from *Klebsiella pneumoniae*, identified as a structural homologue to Bd3209 through Swissmodel (PDB ID: 6PH9), shows that Bd3188 has a higher identity to $LpxH_{Kpne}$ (26%) than Bd3209 (19%), as shown in **Figure 5.3.4** (Cho et al., 2020). Additional homologous structures were found for Bd3209, one from *Haemophilus influenzae* (PDB ID: 5k8k) and another from *Pseudomonas aeruginosa* (PDB ID: 5b49) (Cho et al., 2016, Okada et al., 2016). When aligned, Bd3209 is found to have conserved all the manganese ion binding residues and three of four key lipid X binding residues, with the fourth being partially conserved (Arg132). In comparison, all these residues are conserved in Bd3188. Additionally, Bd3188 has a higher overall

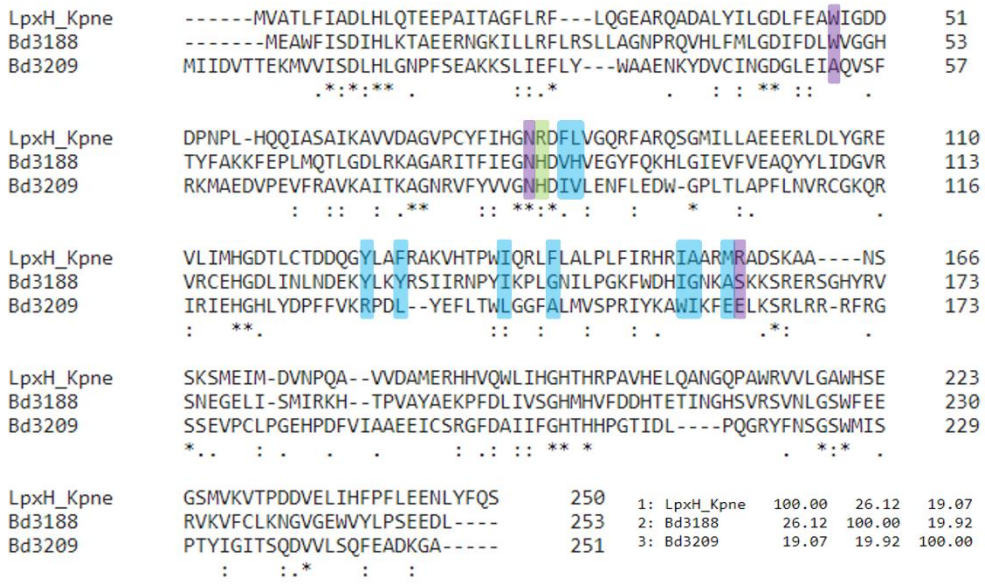

Figure 5.3.4. An alignment between *Klebsiella pneumoniae* LpxH, Bd3188 and Bd3209 shows higher conservation for the former protein. Both *B. bacteriovorus* proteins are predicted to be LpxH proteins, and the *K. pneumoniae* LpxH (PDB ID: 6PH9) was found to have a similar structure in a Swissmodel search. The highlights show key residues for the function of this LpxH, as discussed in Cho *et al.,* 2020, and their conservation in the *B. bacteriovorus* sequences. The green highlight shows the cation-π stacking interaction arginine; this is partially conserved as a histidine in the *B. bacterivorus* proteins. The purple highlights show the three residues that make hydrogen bonds with the substrate; Bd3188 has two conserved, Bd3209 has only one. The blue highlights show hydrophobic residues that surround the substrate and interact with van der Waals interactions; three are conserved in Bd3188 and none are conserved in Bd3209. In the lower right is a table comparing the identities of the sequences.

identity with the other LpxH sequences, 23-26%, than Bd3209 does, 18-20%. This could indicate that they produce different outer membrane lipids; Bd3188 could produce lipid X, while Bd3209 produces a slightly different product. The purpose of this may be protection for the growing *B. bacteriovorus* from its own digestive enzymes, which cannot act on the modified outer membrane.

There are some differences in the expression patterns of these two *lpxH* homologues, seen in **appendix 8.1.2b**. Expression for both is low from attack phase to 60 minutes, the period leading up to the start of filamentous growth

and chromosome replication. As growth is not yet occurring, the need for outer membrane lipids is low at this point. At 120 minutes, when growth and chromosome replication are high, *bd3188* expression increases, peaking at 180 minutes but continuing through to 300 minutes. For *bd3209*, expression remains low at 120 minutes, but increases at 180 minutes and peaks at 240. This further suggests that Bd3188 is the canonical LpxH, producing lipid X at the time of filamentous growth, whereas Bd3209 is producing a modified lipid that is incorporated later into the outer membrane. Alternatively, it may produce lipids for the purpose of incorporation into the septa as the filament divides, a process starting from 180 minutes. This analysis further implicates the connection between outer membrane synthesis and other division processes associated with the *dcw* cluster.

5.3.3.6 Bd3206 is similar to an EstB and may modify outer membrane lipids

The gene *bd3206* has already been mentioned as potentially being cotranscribed with *bd3207*, as seen in the RNA-seq data, between the 120 and 240 minute points in the cycle. This gene is labelled 6 in **figure 5.3.1**. A promoter prediction indicates a promoter preceding this gene but no recognition sequences were identified. Bd3206 is annotated as an EstA esterase. Homologues in *Pseudomonas aeruginosa* act in the synthesis pathway of rhamnolipids (Wilhelm et al., 2007). Bd3206 is much shorter than $EstA_{Paer}$, however, and shows minimal homology (5% identity).

A Swissmodel structural search found a homologous serine hydrolase in *Francisella tularensis* (PDB ID: 4F21) and aligning them, **figure 5.3.5**, showed higher similarity (21%) and had ten of fourteen residues conserved that were identified in the active site, binding pocket, and membrane binding loop, including the catalytic serine (Filippova et al., 2013). The identified enzyme is homologous to human acyl-protein thioesterase (hAPT1), and in *Francisella tularensis* has been linked to the virulence of the bacterium through modification of outer membrane lipids (Filippova et al., 2013). A promoter prediction did not return any results.

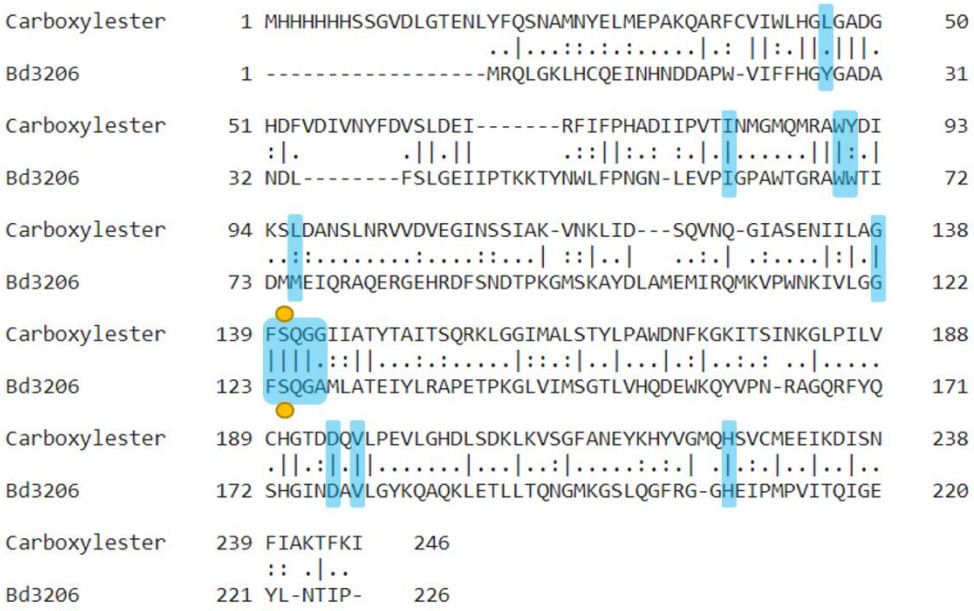

Figure 5.3.5. An alignment between an EstB carboxylesterase from *Francisella tularensis* and Bd3206 show high conservation in functional residues. The *F. tularensis* carboxylesterase (PDB ID: 4F21) was found from a Swissmodel structural search. The blue highlights show residues involved in the active site, the substrate binding pocket, and the membrane binding loop. The catalytic serine is marked with the yellow circle. Ten of the fourteen highlighted residues are conserved in Bd3206, including the catalytic serine.

The domain conservation and transcription profile of *bd3206* suggests that it codes for an acyl-protein thioesterase that modifies the outer membrane lipids during the growth phase, 120 minutes, through to septation, before downregulation after septation. Not only does the outer membrane need to grow with the rest of the filament, but it must also be carefully maintained and protected to avoid the *B. bacteriovorus* lytic enzymes acting upon itself. Altering the outer membrane so that it is different to prey lipids may reduce the chance that these enzymes will target the *B. bacteriovorus* filament in the bdelloplast. This finding also suggests further crosstalk between growth, septation and cell wall synthesis, as performed by proteins coded from the *dcw* cluster, with LPS synthesis and outer membrane modification.

5.3.3.7 Bd3203 may sense intracellular energy levels by monitoring AMP/ATP

Inserted gene *bd3203,* labelled 7 in **figure 5.3.1** has already been discussed above regarding the asRNA regulation of *murE* and *murF*. The gene itself is annotated as hypothetical, but domain prediction suggests Bd3203 contains a pair of CBS domains, named for the protein they were first identified in, cystathionine beta synthase, which was first, and still is, studied primarily in eukaryotes as catalysing the first step in the synthesis of cysteine from homocysteine via the intermediate cystathionine (Pajares and Perez-Sala, 2018). When paired these domains join to form a single, stable domain, sometimes referred to as a Bateman domain, that has been shown to bind adenosyl carrying ligands, such as AMP and ATP (Kemp, 2004). Some proteins with tandem CBS domains and an associated domain have been shown to be regulated by the adenosyl ligands, and studies in humans have found that CBS pairs are used to sense intracellular energy levels (Scott et al., 2004). Several proteins with the Bateman domain have been characterised in bacteria, including pyrophosphatases in *Clostridium* and IMP dehydrogenases in *E. coli* (Anashkin et al., 2015, Pimkin et al., 2009). Following the CBS domains of Bd3203 is a region of about thirty residues without a predicted function, which could be used to interact with other proteins.

A Swissmodel structural search of Bd3203 shows that an AcuB protein from *V. cholerae* has the highest homology (PDB ID: 2O16), however the study on this protein has not been published. Acetoin utilisation protein AcuB is involved in acetoin degradation, and has mainly been studied in *B. subtilis* where it is encoded from a three gene operon; *acuABC* (Gardner and Escalante-Semerena, 2008). However, while the activities of AcuA and AcuC have been determined in postranscriptionally regulating acetyl-coenzyme A synthetase (AcsA) activity, the function of AcuB has yet to be determined (Gardner and Escalante-Semerena, 2009). Bd3203 does not occur as part of an operon, and a pBlast using *B. subtilis* proteins show no predicted homologues for AcuA and AcuC in the *B. bacteriovorus* genome.

A promoter prediction shows a single preceding promoter, bd3203p, with recognition sequences for CRP, ArcA and Tus. CRP has been seen in two

ancestral gene promoters, ftsQp and murFp1, and ArcA in bd3208p. RNA-seq data for *bd3203*, shown with *murE* and *murF* in **appendix 8.1.1b**, shows that its highest expression occurs at attack phase, with downregulation occurring as early as 15 minutes, during attachment and invasion. Lowest expression occurs from 120 to 240 minutes, when the filament is growing, and multiple replisomes are active, through to the end of replication and subsequent septation. It is then upregulated at 300 minutes, when the progeny lyse the bdelloplast and are released. As its highest expression occurs before invasion, it is unlikely that this protein senses changes in intracellular energy levels due to digestion. It may, however, suppress proteins at attack phase that function once invasion has occurred and the HD100 cell has established. Its downregulation following invasion would allow these to become active. Several of the *dcw* cluster genes have shown low levels of transcription at attack phase, making the encoded proteins potential interaction partners with Bd3203.

5.3.3.8 Bd3199 is a putative lipoprotein

Between *murD* (*bd3200*) and *ftsW* (*bd3198*) and transcribed in the same direction as the ancestral cluster genes, is *bd3199*, another hypothetical gene, labelled 8 in **figure 5.3.1**. As shown in **appendix 8.1.2c**, its highest expression occurs at attack phase, with lower expression seen through the rest of the cycle; downregulation is greatest at 120 minutes, with upregulation at 180 minutes. Domain predictions only indicate that it either has an N terminal signal peptide or has a membrane lipoprotein lipid attachment site. Interestingly, there are no homologues found in a pBlast outside of *Bdellovibrio* species, and there is no homologue in *Bdellovibrio exovorus*. This is discussed later, along with the phylogeny of the rest of the cluster, but it does suggest with transcription at attack phase that this protein is uniquely used for invasion and may have been inserted at this locus in a relatively recent event, or that it has subsequently been lost in *B. exovorus*. Its function can only be speculative without further study, but as a short protein with a signal peptide it could be sensory, detecting environmental cues in attack phase, and potentially the rest of the cycle, for when the *B. bacteriovorus* cell is inside, or is in the process of invading, the prey. This could also be true as a lipoprotein,

if associated to the outer membrane. No homologue in *B. exovorus* suggests that it is specifically for intracellular predation; it could have been acquired recently in *B. bacteriovorus* or it may have been removed from *B. exovorus*.

It has a single predicted promoter bd3199p, with RpoD and TyrR recognition sites. TyrR is a transcription factor capable of both repressing and activating transcription (Pittard et al., 2005). It has three amino acid cofactors, tyrosine, phenylalanine, and tryptophan, which, when bound, allow it to interact with RNA polymerase to activate transcription. The *E. coli* TyrR regulon includes genes involved in the metabolism of these amino acids, and particularly with their transporters and permeases. The presence of these amino acids could be used as a signal in *B. bacteriovorus*, to indicate the state of digestion and/or whether there is enough material for their synthesis. A drop in the cellular levels of amino acids might indicate the need to change from growth to septation. A pBlast shows several potential homologues in *B. bacteriovorus*, though none are annotated as a TyrR. Further work would be required to identify this regulator.

5.3.3.9 Bd3195 is a putative glyoxylate hydroxypyruvate reductase.

There are four genes located between the *ftsW-murG-murC* cluster and *ftsQ*. These are not predicted to be in an operon and have differing transcription profiles, **appendix 8.1.2e-f**. The first is *bd3195*, labelled 9 in **figure 5.3.1**, annotated as encoding an hydroxypyruvate reductase, otherwise called glyoxylate hydroxypyruvate reductase (GRHPR) (Njau et al., 2001). These enzymes are found in most known organisms, including bacteria, and have a dual function; the reduction of glyoxylate into glycolate and the conversion of hydroxypyruvate into D-glycerate (Hullin, 1975, Rumsby and Cregeen, 1999, Yoshikawa et al., 2007, Lassalle et al., 2016). GRHPR enzymes have largely been studied in humans; a lack of this enzyme causes hyperoxaluria type II characterised by a toxic buildup of glyoxylate (Cramer et al., 1999).

In bacterial systems, such as *E. coli* and *Pseudomonas*, glyoxylate was originally found to be a carbon source (Bailey and Hullin, 1966, Hansen and Hayashi, 1962). Glyoxylate has also been found to be an important intermediate in several metabolic pathways, including amino acid metabolism

(serine, glycine and threonine) and purine metabolism, as well as the glyoxylate cycle, a process studied in plants, fungi, protists and bacteria whereby the organism can utilise acetate as a carbon source (Dolan and Welch, 2018, Dunn et al., 2009). There is also now evidence to suggest that glycolate could counteract reactive oxygen species (ROS). In *Caenorhabditis elegans*, paraquat treatment produces a toxic effect through the production of superoxide radicals, reducing the membrane potential of mitochondria (Diez et al., 2021). This was reportedly rescued through the supplementation of glycolate. The authors determined that glycolic acid proffers a protective effect against hydrogen peroxide, produced by the superoxide radicals, restoring the membrane potential of mitochondria. While this has not been documented in bacteria, the parallels between bacteria and eukaryotic mitochondria could mean that the same reaction occurs in bacterial systems. In the enclosed system of the bdelloplast, accumulation of ROS elements due to hydrolysis of prey biomass may increase the risk of damage to the developing HD100 filament, and the production of glycolate and other antioxidant molecules could counteract this.

Hydroxypyruvate reductase activity produces D-glycerate, a function studied in Alphaproteobacterial, or type II, methanotrophs. In these bacteria, the serine cycle is used to utilise C_1 compounds, with glyoxylate and hydroxypyruvate as intermediates (Anthony, 2011). In other systems, the D-glycerate formed through reduction of hydroxypyruvate can be fed into gluconeogenesis. A cursory search for HD100 homologues of enzymes known to function in the serine cycle suggests that three of the nine typical enzymes, as outlined in Anthony, 2011 review, are not encoded in the *B. bacteriovorus* genome. Serine-glyoxylate aminotransferase is considered a key marker for this pathway and while a homologue is found in Bd1462, domain and structural predictions suggest this is a serine-pyruvate aminotransferase. It is unlikely that *B. bacteriovorus* has a functional serine cycle. This may mean that any hydroxypyruvate reductase activity of this enzyme could be to feed into gluconeogenesis.

A Swissmodel search for Bd3195 showed the closest, homologous solved structure is from an archaeon, *Pyrococcus yayanosii* (PDB ID: 6BII) (Lassalle

et al., 2016). This study solved the structures of two archaeal glyoxylate hydroxypyruvate reductase (GRHPR) proteins, the other homologue being from *Pyrococcus furiosus*. Alignment of these with Bd3195 shows 39% identity to the *P. yayanosii* homologue and 36% to the *P. furiosus* protein, **Figure 5.3.6**. The NADP(H) binding motif, a glycine rich loop (GxGxxR), is conserved in Bd3195, as are seven of the eight residues identified for substrate binding. Bd3195 is therefore likely to act as a glyoxylate hyrdroxypyruvate reductase.

The above study found that the GRHPR affinity for hydroxypyruvate was much greater than for glyoxylate, leading the authors to characterise the proteins solely as hydroxypyruvate reductases. There are, however, other studied Archaeal homologues with a greater affinity for glyoxylate, and while structural homology for Bd3195 is closest to the *P. yayanosii* protein, further study would be required to determine its affinity for these other substrates (Ohshima et al., 2001, Yoshikawa et al., 2007).

The highest expression for *bd3195*, shown in **appendix 8.1.2d**, occurs at 180- and 240-minute time points, when chromosome replication is complete, replisomes have dissipated, and the filament is septating. This may be to utilise the remaining carbon from the bdelloplast, as the filament still requires the energy and materials to septate and for the progeny to mature. There is currently no evidence that it functions in an alternative pathway, such as the serine cycle. A promoter prediction shows a low scoring promoter before this gene, bd3195p, with no predicted recognition sequences. There is a higher scoring intergenic promoter predicted, bd3194p1, however it also has no recognition sequence predictions.

Figure 5.3.6. An alignment with glyoxylate/hydroxypyruvate reductases from two archaea, *Pyrococcus yayanosii* and *Pyrococcus furiosus* show Bd3195 has high conservation of functional residues. The blue highlight shows the dinucleotide binding motif and the purple highlights show glyoxylate/D-glycerate binding residues, all of which are conserved in Bd3195. The orange highlight marks the catalytic arginine. All residues are conserved. The *P. yayanosii* protein (PDB ID: 6BII) was found in a Swissmodel search.

5.3.3.10 Bd3194 is a putative caspase of unknown function

Gene *bd3194*, labelled 10 in **figure 5.3.1**, is annotated as a hypothetical gene. Domain predictions of Bd3194 only show that it has an N terminal signal peptide with one small domain like a caspase P20 subunit domain. Caspases are proteases, specifically cysteine-dependent aspartate-directed proteases, primarily studied in eukaryotic apoptosis (Kesavardhana et al., 2020). These proteins are autocatalytically cleaved by the P20 subunit, producing an active protease. Homologues, called orthocaspases, have been identified in some bacteria. During cyanobacterial bloom, certain conditions can cause the bacteria to enter programmed cell death; expression of these orthocaspases has been shown to coincide with this in *Trichodesmium erythraeum* (Bar-Zeev et

al., 2013). This has also been seen in *Xanthomonas campestris* stress induced programmed cell death (Wadhawan et al., 2010). Other homologues have been found in bacteria, but their roles are unknown. These orthocaspases contain the P20 subunit domain seen in eukaryotic examples, but they do not always have the conserved active site His-Cys dyad.

A non-bdellovibrionales pBlast of Bd3194 only returns β-proteobacterial homologues, such as those in *Leptothrix* and *Ideonella*, but alignments with Bd3195 shows homology is only for the N terminal region; full length homologues are only found in other *Bdellovibrio* species but excluding *Bdellovibrio exovorus*. This could be an indicator of another specifically intracellular predation gene. Interestingly, it is also active early in the HD cycle, **appendix 8.1.2d**, from attack phase to 45 minutes, much like *bd3199* which had no homologues outside of *Bdellovibrio* species and no *B. exovorus* homologue.

Among bacteria, orthocaspases have been most studied in cyanobacteria, as they are thought to share a common ancestor with plant mitochondria. *Microcystis aeruginosa* PCC 7806 has had six orthocaspases identified, MaOC1-6 (Klemencic et al., 2015). Of these, MaOC1 and MaOC2 have the highest similarity to Bd3194 (20.5% and 19.3% respectively). Both *M. aeruginosa* genes do not code for predicted domains following the P20 subunit, like Bd3194, and only MaOC1 has both catalytic residues, His110 and Cys170, conserved in the P20 subunit. Neither of the catalytic dyad are conserved in Bd3194, likely rendering this domain catalytically inactive. Although this is not uncommon in orthocaspases, there is currently no indication of the functions of such proteins.

As well as the intergenic promoter bd3194p1, there is a promoter immediately before this gene, bd3194p2. This has a recognition sequence for RpoS, σ^{38}. In *E. coli*, this is a master regulator of stationary phase and stress response genes. A pBlast shows that the closest, full-length homologue is Bd3314, however this is annotated as σ^{32}. Further investigation would be needed to determine if σ^{38} is encoded in the *B. bacteriovorus* genome.

5.3.3.11 Bd3193 has tandem universal stress protein A domains

Bd3193, labelled 11 in **figure 5.3.1**, is annotated as a universal stress protein (USPs) and domain predictions suggest it has tandem UspA domains. UspA is a protein that was first studied in *E. coli*, where transcription of the encoding gene was increased when cells were put under stresses; heat shock, nutrient starvation, hypoxia, agents that arrest cell growth, DNA damaging substances are just a few. Perhaps importantly, USPs have also been associated with the virulence of intracellular pathogens *Salmonella typhimurium* and *Mycobacterium tuberculosis* (O'Toole and Williams, 2003, Liu et al., 2007, Jia et al., 2016). Both the environmental changes and host response to pathogens activate the USPs, increasing the persistence of these pathogens once they have invaded their host. The parallels with *B. bacteriovorus* lifecycle suggest this is also a possibility with USPs in this invasive predator.

A pBlast of Bd3193 shows several homologues in euryarchaeotes, the highest similarity being from *Halovivax ruber* (32% identity), an extremely halophilic archaeon. Of the solved crystal structures of this family of proteins, *Archaeoglobus fulgidus*, an extremely thermophilic, sulfate reducing archaeon, has the closest predicted structure (AF_2234, PDB 3LOQ, 23.5% identity). However, the paper detailing this is yet to be published. The structure of YdaA, another USP, from *Salmonella typhimurium* has been published, and is also reported to have tandem USP domains (Bangera et al., 2015). A comparison of Bd3193, AF_2234 from *A. fulgidus* and $YdaA_{Styp}$ shows that both Bd3193 and AF_2234 have identifiable G-2X-G-9X-(S/T/N) ATP binding motifs in both domains, whereas $YdaA_{Styp}$ has this motif in only the C terminal; in Bd3193, the second glycine is replaced with an alanine in the N terminal domain and a serine in the C terminal domain, **Figure 5.3.7**. $YdaA_{Styp}$ is a homologue of *E. coli* UspE, however they both have only one functional ATP binding motif, despite having tandem USP domains. The function of Bd3193 and AF_2234 may differ from these, but as a USP homologue it may still be elevated by conditions of stress.

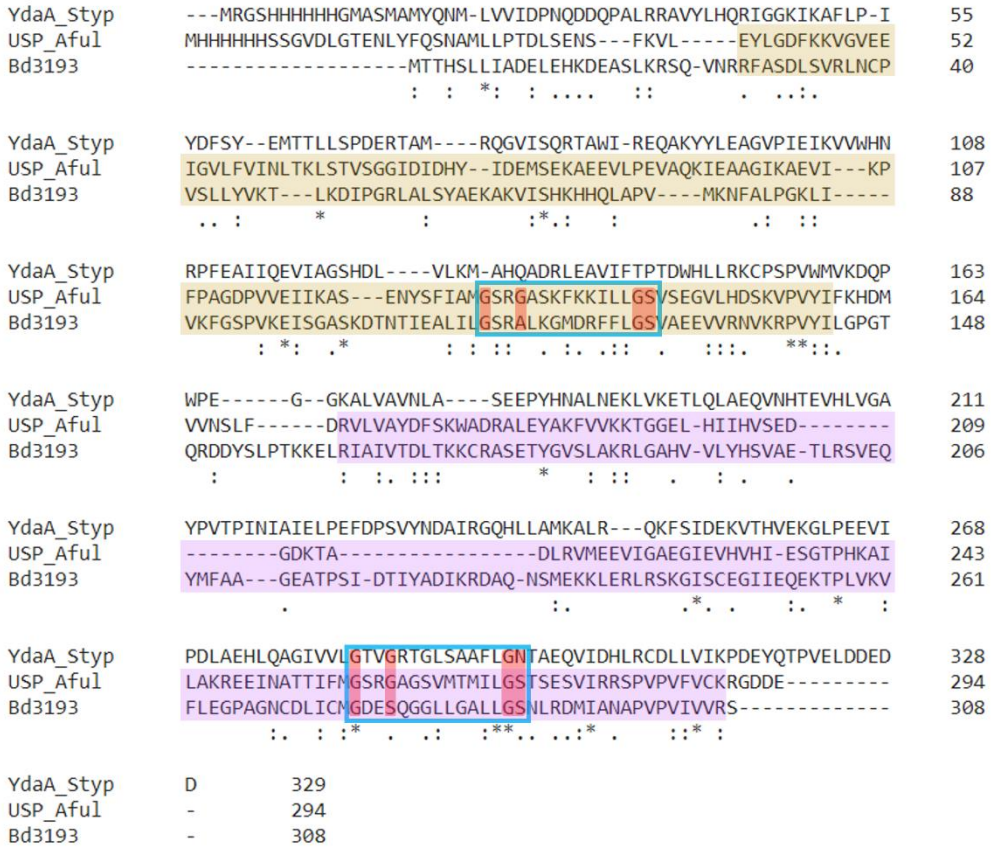

Figure 5.3.7. An alignment with YdaA from *Salmonella typhimurium* and a universal stress protein (USP) from *Archaeoglobus fulgidus* show predicted USP Bd3193 has two USP domains. The yellow and purple highlights show the twin USP domains of these proteins. The blue boxes show the ATP binding motif in each domain, with the red highlighting the key residues. Both are conserved in the *A. fulgidus* USP and Bd3193.

If Bd3193 functions as a universal stress protein, there are numerous roles it could have relating to the *dcw* cluster, or perhaps a more general protective role. Expression of *bd3193* occurs from 120 minutes to 300 minutes, **appendix 8.1.2e**, covering chromosome replication from multiple replisomes, through septation and maturation, to release of the mature progeny. The predicted promoter for *bd3193* has a recognition sequence for IHF, which has been seen for several other promoters in this section. Stresses may become more pronounced as filament growth progresses and biomass is digested; changes in salt concentrations and osmolarity, and the presence of oxidative molecules in

the periplasm from the host and from the *B. bacteriovorus* lytic enzymes could cause harm to the predator at a time when DNA is being replicated. Detecting these and responding quickly would prevent any stall in growth, and damage to the replicating genome. However, a sensory role for the transition into the prey periplasm would require expression earlier in the HD cycle, at the time points where invasion would occur. Given the range of stressors that known USP proteins react to, it is possible that Bd3193 is used to generally detect the changing, potentially harsher, environment as prey biomass is digested, which presents its challenges post-invasion. It may be expressed to protect the replicating genomes in the growing filament, working with proteins such as Bd3210, the putative RecQ identified above.

5.3.3.12 Bd3192 may interact with a CheW homologue to determine post-lysis flagellar motility

Gene *bd3192*, labelled 12 in **figure 5.3.1**, is annotated as encoding an MCP, methyl-accepting chemotaxis protein (Huang et al., 2019). The MCP receptor and several associated proteins couple sensing of ligands with flagellar rotation. Typically, when an MCP becomes bound to a ligand, CheA, which is bound to the MCP, autophosphorylates. It then passes a phosphoryl group to a response regulator, CheY, which diffuses to the flagellar motor and binds FliM, increasing the probability of flagellar rotation. Ligand binding affinity can be modulated by methylation, with a methylated MCP having a higher affinity; methylation is performed by methyltransferase CheR and demethylation by methylesterase CheB. An associated protein, CheW, can form a complex with CheA. A recent study has shown that SOS response protein RecA interacts with the CheA/W in *Salmonella enterica* and is necessary for the complex assembly to function (Frutos-Grilo et al., 2020). RecA is a highly conserved SOS response activator with multiple activities, including DNA repair, polar chemosensor array formation and flagellar rotation switching. When the SOS response is activated, RecA moves from the poles, inhibiting the function of the chemosensor arrays.

MCP proteins are composed of a signal sequence, periplasmic domain, transmembrane region, and a cytoplasmic domain. Further domain predictions of Bd3192 suggest that these are present, with a CheW interaction interface in

the cytoplasmic domain. The ligand binding periplasmic domain is predicted to be a domain of unknown function (DUF3365); the ligand this chemosensor binds is currently unknown. An interaction with a CheW could link this MCP to the SOS response and DNA repair, as well as maturation and development of flagellar motility. Expression of *bd3192* is highest at 240 and 300 minutes, **appendix 8.1.2e**, although low expression is seen from 15 to 60 minutes. At these later time points, the recently septated progeny will be maturing, developing flagellar motility, and preparing for release. This suggests that Bd3192 could act in developing flagellar motility before lysis of the bdelloplast.

A pBlast for CheW in HD100 shows three putative homologues: Bd0579, Bd2828 and Bd3471. Gene *bd0579* is predicted to be in an operon between putative *cheA* and *cheB* homologues. Expression for this operon is high at all time points except for 180 and 240 minutes. Gene *bd2828*, which is annotated as *cheW2*, is in an operon with putative *mcpA*, *cheR* and *cheD* homologues. Expression for this operon is highest at attack phase and five-hour time points, although expression is seen at a lower level throughout the cycle. Gene *bd3471* is not in an operon but is nearby another operon which contains potential *cheA*, *cheR* and *cheB* homologues (*bd3469-bd3467*). While *bd3471* is transcribed throughout the cycle, it has higher expression at attack phase and five hours, like the *bd2828* operon. The operon of *cheA bd3469*, near to putative *cheW bd3471*, has a profile like the *bd0579* operon, which is lower at three and four hours, with expression throughout the cycle.

Between these, *B. bacteriovorus* HD100 is predicted to have three CheW homologues and two each of CheA, CheB and CheR homologues. In studied systems, multiple copies of *che* genes tend to have independent signaling pathways, though some MCPs will bind multiple CheW proteins (Martin et al., 2001, Zhang et al., 2012). All the putative *cheW* genes are expressed throughout the cycle, making them all candidates for interaction with Bd3192. Interaction studies would be needed to determine which, if any, interact. Altogether, this provides the basis for Bd3192 to interact with the RecA stress response system via one or more CheW homologues. As an MCP, this could be a sensory role for determining when to develop or activate flagellar motility.

The upregulation of two CheW proteins at attack phase and 300 minutes, when the flagellar will be active, suggests that an interaction with Bd3192 would activate this motility.

The promoter for *bd3192* is predicted to have recognition sequences for RpoD, LacI and AraC. There is no LacI homologue found in *B. bacteriovorus* when searching with the *E. coli* protein sequence, but a search for AraC returns Bd2916, annotated as PobR, a member of the AraC family of transcriptional regulators. The homology between *E. coli* AraC and Bd2916 only covers 30% of the AraC protein, however; it is possible that *B. bacteriovorus* do not have a true AraC homologue.

5.3.3.13 Overview of insertion genes

The analysis of the genes inserted into the cluster suggests crosstalk between many processes that must be synchronized with the functions of the ancestral *dcw* genes, and some of these systems have several potential members amongst these gene products. Multiple genes from the *dcw* cluster could be associated with the outer membrane. Bd3209 and Bd3188 are both potential LpxH homologues, involved in the synthesis of Lipid X. Additionally, Bd3206 EstB homologue could modify outer membrane lipids, and Bd3208 may produce sugars for incorporation into the membrane. Encoding genes show upregulation from 120 minutes, for *bd3206* and *bd3188*, or 180 minutes, *bd3208* and *bd3209*. This places expression at the end of growth and replication, leading into septation, suggesting that they are targeting the septa or modifying the outer membrane prior to release. Of course, the outer membrane needs to grow, just as with the peptidoglycan wall, and new lipids will have to be inserted at the septa. There is the additional possibility that the outer membrane must be modified for lysis and release; the conditions in the bdelloplast will be different to the extracellular environment, and the outer membrane may be adapted for the transition, hence why these genes are expressed at 240 and 300 minutes.

There is also evidence for a close association of protective processes with the cluster. One such Bd3210, a putative RecQ that fixes stalled replication forks and contributes to genome stability. This is expressed throughout growth and

genome replication, and could be crucial to an accurate and fast production of several copies of the genome. Bd3193 shows homology to UspA, expressed from 120 minutes. Its expression could have a wide range of protective purposes; preventing damage to the replicating DNA, addressing a lack of certain nutrients as the host is consumed and countering an increase in reactive oxygen species or other toxic byproducts. Its expression also shows that it is active during and after lysis. As with the outer membrane proteins, this could be to ensure the progeny can survive the transition between environments, which would come with osmotic stresses.

There are also links to carbon source utilisation with Bd3195, the glyoxylate hydroxypyruvate reductase, as well as flagellar motility, Bd3192, and intracellular ATP sensing, Bd3203. The association of these encoding genes with the *dcw* cluster, as well as the fragmentation their insertion has caused, shows that the *dcw* cluster of *B. bacteriovorus* has been heavily modified to adapt to its unique lifecycle. With that in mind, the next section shows a comparison of the *dcw* clusters of several *Bdellovibrio* species with the goal of identifying genes in the *B. bacteriovorus* cluster that may be specific to intracellular predation and others that could be generally predation related.

5.3.4 Comparing *dcw* clusters of *B. bacteriovorus* HD100 and other *Bdellovibrio* strains and species.

While the above analysis has provided some explanation as to the roles the inserted genes may have in the *dcw* cluster, most, if not all, require further study to determine their true function. A comparison of the HD100 cluster and those of closely related BALOs may help provide more insight. Most of the bacteria compared will be invasive predators, such as *B. bacteriovorus* Tiberius and *B. ArHS*. The purpose of homologous inserted genes in these bacteria could specifically be in intracellular growth; as has been discussed, the challenges in the periplasm of a host are numerous, coordinating many processes of self-protection, digestion, and growth. A comparison of clusters with *B. exovorus* may, however, give a polar insight. As an extracellular predator, the challenges faced by *B. exovorus* will differ significantly from the intracellular BALOs. This could be represented in the structure of the *dcw* cluster, as well as the nature of any inserted genes; those that are conserved

between HD100 and *B. exovorus* are unlikely to be specific to intra- or extracellular predation but could be used in shared growth and division processes. Insertions that are not conserved between them could be related to their differing predatory lifecycles. I have initially compared the *dcw* clusters of *B. bacteriovorus* strains HD100 and Tiberius, *B. ArHS,* and *B. exovorus*, **Figure 5.3.1** (Sangwan et al., 2015, Koval et al., 2013, Hobley et al., 2012b).

All these bacteria have similarly adapted *dcw* clusters, with multiple gene insertions breaking up the ancestral genes into novel groups. Ancestral genes are conserved between HD100, Tiberius and *B. ArHS*. This includes the genes themselves, missing *mraZ, murB* and *ddlB,* and the smaller groups they are now broken into. As with HD100, there is a *murB* homologue in both genomes distal to the cluster, but *mraZ* and *ddlB* are missing homologues entirely. All fifteen inserted genes from HD100 are conserved in Tiberius, with one additional inserted gene: *bdt_3136*. This is located between homologues of *bd3206* and *bd3207* potentially as a part of the operon that, in HD100, is predicted to start with *bd3207*. It is likely that the common ancestor of HD100 and Tiberius contained the fifteen inserted genes seen in HD100, and Tiberius has acquired *bdt_3136* since. Interestingly, *bdt_3136* does not have a homologue in HD100, *B. ArHS* or *B. exovorus*. It could be a recent acquisition via horizontal gene transfer.

In the *B. ArHS* cluster, fewer of the inserted genes are conserved. There are a total of fourteen insertions with only six being homologous to those in HD100. In *B. exovorus* only two of its thirteen insertions are homologous to HD100 genes. The two conserved genes in *B. exovorus* are also the only genes to have homologues in all four of these bacteria; these are *bd3206* (Tiberius *bdt_3135, B. ArHS OM95_05145, B. exovorus A11Q_2022*) and *bd3188* (Tiberius *bdt_3118, B. ArHS OM95_05250, B. exovorus A11Q_2006*). As above, *bd3206* was identified as a putative acyl-protein thioesterase that could be modifying outer membrane lipids during growth and division. Its presence in the clusters of all four predatory bacteria suggests it may not be specific to intracellular predation; *B. exovorus* is extracellular. An alignment of the protein products of these homologues shows high similarity between them; compared to HD100, Tiberius has 98% identity, *B. ArHS 80%* and *B. exovorus*

49%. All have 180 residues except for *B. exovorus,* which is missing a run of eight residues that are completely conserved in the other homologues. Lesser similarity in *B. exovorus* could be due to the extracellular nature of its lifecycle and evolutionary distance. The outer membrane would need less protection from its own lytic enzymes as most of the cell has no contact with the prey being digested. Environmentally, *B. exovorus* would not have to deal with the changing osmotic conditions in the periplasm as the other, intracellular *Bdellovibrio* would.

The other gene conserved in all four *Bdellovibrio* is the predicted *lpxH bd3188*. This is also related to the outer lipid membrane as part of the biosynthesis pathway of LPS. This could show the importance in all *Bdellovibrio* of crosstalk between division and the outer membrane, as both conserved genes relate to the growth and maintenance of the outer membrane. Similarly, high identity is seen between Bd3188 homologues with an alignment showing 98% identity in the Tiberius homologue, 78% in *B. ArHS* and 47% in *B. exovorus*.

There are four genes that are conserved in the intracellular *Bdellovibrio* but not in *B. exovorus*. It is possible that these have a role specific to growing in the conditions of a host periplasm. The first of these are *bd3210* homologues. Bd3210 is a predicted RecQ, important for DNA maintenance during replication. It could be that the intracellular lifecycle increases the risk of damage to the DNA of the predator. This could be due to a buildup of oxidative agents from the digestion of the prey biomass, and an influx of these into the cell could lead to stalling of genome replication. Therefore, Bd3210 could be a response to this. There is a homologue in *B. exovorus*, *A11Q_1047*, but this is distal to the *dcw* cluster. Being extracellular, and having less contact with ROS, *B. exovorus* would sustain less damage and a response tied into the *dcw* cluster would be unnecessary.

The next is *bd3203*, coding for the putative tandem CBD domain protein, which could bind to adenosyl containing ligands. I have previously discussed its potential role of energy sensing during invasion and when digestion begins; this is another example of a role that would be unnecessary in *B. exovorus*,

which would not need to sense the change in its environment. Another consequence of not having a homologue could be the loss of the potential convergent asRNA and resulting regulation of the *murE-murF* operon. Tighter regulation of these in intracellular *Bdellovibrio* could be due to conserving resources, as discussed above, or it could be due to expansion room. The intracellular predators may need tighter regulation on peptidoglycan synthesis as too much expansion could compromise the integrity of the bdelloplast by applying too much internal pressure, threatening lysis before the filament has septated. While *B. exovorus* will still need to regulate peptidoglycan synthesis for growth, its environment at this time may not be so stringent.

The third gene conserved in only the intracellular predators is *bd3199*. The encoded protein is hypothetical; however, it does appear to be a lipoprotein. As discussed, its highest expression is at attack phase, which is unusual in this cluster. It could serve in a sensory pathway related to transitioning from attack phase to growth once prey is detected. Its lack of homologue in *B. exovorus* also suggests that it is invasion specific; if sensory, it could activate processes that include other invasion specific proteins.

The last gene conserved only in these invasive *Bdellovibrio* is *bd3192*. This was identified as an MCP with an additional domain of unknown function. Bd3192 could have a link to the SOS response and RecA, via interaction with one of the CheW homologues. RecQ homologue Bd3210, which could have a role in the SOS response, has already been identified as conserved in only the intracellular predatory *Bdellovibrio* species. This suggests that crosstalk between the SOS response and growth processes is important when predation occurs within the host periplasm. As above, this could be due to conditions within the bdelloplast and a higher likelihood of genomic damage for the invader which is not shared with extracellular predation and growth.

Altogether, these results show several candidates for further study as proteins specific to general predation and others specific to invasion. Their position in the *dcw* clusters of these BALOs suggest that many could be the keys to crosstalk between their own processes, such as the SOS response or outer

membrane maintenance, and the roles of the ancestral cluster genes in growth and division.

5.3.4.1 Novel insertions in the *dcw* clusters of *Bdellovibrio ArHS* and *Bdellovibrio exovorus*

So far, several genes from HD100 have had their homologues identified in other BALOs, giving us an insight into processes not normally associated with the cluster and how they are coordinated with division and growth. There are, however, many genes that have been inserted into the *dcw* clusters of the other *Bdellovibrio* species that are do not have immediately recognisable homologues in the HD100 cluster. Characterising these genes and, if present, identifying homologues in the HD100 genome could provide further examples of processes that relate to those of the cluster. Additionally, this could show genes that are related to the extracellular nature of *B. exovorus* predation, although further study of these genes is beyond the scope of this thesis.

5.3.4.2 The *B. exovorus dcw* cluster operon *drrABC* has homologues in *B. bacteriovorus* species distal to the *dcw* cluster

Within the *B. exovorus* cluster, most of the gene inserts do not have homologues in the other *Bdellovibrio* species *dcw* clusters; the notable exceptions have been identified above as *A11Q_2022*, the *bd3206* homologue, and *A11Q_2006*, the *bd3188* homologue, which are conserved in all four *Bdellovibrio* clusters. Of the non-conserved genes, most do not have homologues anywhere in the genomes of the other species; exceptions are genes *A11Q_2023-5* and *A11Q_2018*. One can assume that the genes with no homologues at all are related to extracellular predation, which must carry its own challenges when compared to intracellular predation. However, characterizing these genes is beyond the scope of this thesis.

The three gene inserts *A11Q_2023, A11Q_2024* and *A11Q_2025* have homologues in the other *Bdellovibrio* genomes in the same configuration but distal to the cluster. In *B. bacteriovorus* HD100 these are *bd3590, bd3591* and *bd3592*; all three are annotated as ABC-2 (ATP-Binding Cassette type 2) transporter related genes with *bd3590* and *bd3591* predicted as coding for DrrA and DrrB respectively which, with DrrC, form the doxorubicin resistance

complex DrrABC (Davidson et al., 2008, Malla et al., 2010, Brown et al., 2017, Khosravi et al., 2019). The encoding genes are found in an operon in studied systems such as *M. tuberculosis*, so it seems reasonable that Bd3592 is also a DrrC homologue, and domain predictions suggest it is a transmembrane protein. These three proteins form a complex of two ATP-binding DrrA proteins and two transmembrane proteins, one each of DrrB and DrrC. RNA-seq data does not predict these three genes to be an operon in HD100, but their expression is highest from two to four hours, as is also typical with most of the *dcw* cluster genes seen in this thesis. The *drrABC* operon may have been transferred to the *B. exovorus* cluster due to a need to closely tie growth with environmental protection. Doxorubicin is produced by *Streptomycetes*, Gram-positive bacteria that are not prey to *Bdellovibrio*. The antibiotic itself causes DNA and RNA damage, which could stall or prevent division in the growing *B. exovorus*. Being extracellular as the genome is copied could lead to a higher vulnerability and therefore this operon could be associated with this cluster to coordinate protection.

A11Q_2018 is the only other gene with homologues in the other *Bdellovibrio* species; *bd0082* in HD100. Domain predictions only indicate that it has an N terminal signal peptide; RNA-seq data shows that it is expressed throughout the cycle, but peaks at five hours.

5.3.4.3 *B. ArHS* have nine insertions not seen in the *dcw* clusters of other *Bdellovibrio* species

In the *B. ArHS* cluster, there are nine inserted genes that are not conserved in the clusters of the other *Bdellovibrio* species. The first two of these follow the *recQ* homologue, *OM95_05130*, which is conserved in all these *Bdellovibrio* species; *OM95_05135* and *OM95_05140*. The only homologues found for these were in *B. exovorus*, distal to the *dcw* cluster and to each other; *A11Q_292* homologous to *OM95_05135*, and *A11Q_2479* homologous to *OM95_05140*. Neither strain of *B. bacteriovorus* have homologues in their genomes. Initial predictions of OM95_05135 suggest it may have a nucleotidyltransferase domain, which shares homology with DNA polymerases. Other proteins with this domain include kanamycin nucleotidyltransferases, which confer resistance to certain aminoglycosides

(Osterman et al., 2020). This agrees with other genes inserted into *Bdellovibrio* clusters that could also confer antibiotic resistances. OM95_05140 has a predicted NAD-dependent epimerase/dehydratase domain, where the best studied examples function in galactose metabolism in humans (Thoden et al., 1997, Thoden et al., 2001). Again, this is a process that would be relevant during growth and division, as the prey biomass is digested. A recent study in *Pectobacterium carotovorum*, an agriculturally significant plant pathogen, has shown that an NAD-dependent epimerase/dehydratase, WcaG, is important to biofilm and exoenzyme production, and plays a role in maintaining outer membrane properties and virulence (Islam et al., 2019). However, it is beyond the scope of this study to further characterise these proteins in *B. ArHS* as they do not have homologues in HD100.

Further into the *B. ArHS* cluster is a group of six inserted genes, differing in orientation, which are not found in the clusters of the other *Bdellovibrio* species. The first is *OM95_05160*; a Blast of the coded protein suggests there are no homologues in any of the other *Bdellovibrio* species being investigated here. This could relate to the unique environment in which *B. ArHS* was found, but is beyond the scope of this thesis.

The second, *OM95_05165*, has predicted homologues in all three of the other *Bdellovibrio* species distal to the *dcw* cluster; *bd3394* in HD100, *bdt_3362* in Tiberius and *A11Q_659*. These are predicted to code for WalR-like transcriptional regulatory proteins. WalR has been shown to be part of the two-component regulatory system with WalK, regulating transcription of the *ftsAZ* operon (Takada and Yoshikawa, 2018). In *B. ArHS*, *OM95_05170*, the next inserted gene, is predicted to be a histidine kinase, making it a very likely candidate to code for the other half of the two-component signaling system. Given that this system is in the *dcw* cluster, it could be reacting to conditions in the bdelloplast and regulating some of the genes in the cluster itself to coordinate the processes as biomass in the bdelloplast is digested. Homologues for *OM95_5170* are *bd1018* in HD100, *bdt_0964* in Tiberius, and *A11Q_2113* in *B. exovorus*; none of these neighbour the homologues for *OM95_05165*.

RNA-seq predicts that *bd3394*, the HD100 homologue distal to the cluster, occurs in a two gene operon with *bd3393*, which is predicted to be a histidine kinase and is likely the other part of the two-component response regulator in this bacterium. Upregulation of this operon occurs between one and five hours, so it is possible that its function also relates to conditions in the bdelloplast and coordination of growth and division, but further study would be needed to determine this. Interestingly, these are annotated as coding for RagA (Bd3394) and RagB (Bd3393) homologues, which have been the subject of a deletion study in Bacteroidetes *Porphyromonas gingivalis*, a member of the human salivary microbiome implicated in periodontal disease (Nagano et al., 2007). Deletion strains exhibited slow growth on a medium comprised of undigested, native protein, and had reduced virulence in mouse models. The authors suggest that RagAB associate with the outer membrane and are necessary for the uptake of large, undigested proteins, with deletion strains having to wait for the excreted proteases to break down the proteins before they can be absorbed. In HD100, the uptake of undigested proteins, as well as the smaller products of the predatory proteases, could increase the rate at which the predator processes prey biomass, reducing the time needed for the HD cycle.

The homologue to the predicted histidine kinase OM95_05170, HD100 Bd1018, is predicted to be a PhoB protein coded from a three gene operon of *phoU, phoB* and *bd1019*. This operon is involved in phosphate homeostasis, with PhoR and PhoB being a two-component sensory signal system which is active in the SOS starvation response, and PhoU as a regulator (Lubin et al., 2016). Several SOS response genes have already been identified in relation to the *dcw* cluster of these *Bdellovibrio*. That the homologues for both *B. ArHS* genes do not themselves appear as an operon or in the cluster of other *Bdellovibrio* suggests that this *B. ArHS* sensory system may be unique and not replicated in the other *Bdellovibrio* species. However, the homologues in other *Bdellovibrio* may still be relevant to the functions in the cluster.

Of the following three inserted genes, *OM95_05175* and *OM95_05185* do not have homologues in the genomes of these other *Bdellovibrio* species. Interestingly, a pBlast of OM95_05180 shows that it has homologues in *B. exovorus* (A11Q_1135) and *B. bacteriovorus* Tiberius (Bdt_2776), but not in

HD100. A wider Blast shows that the closest homologues are in *Bdellovibrio*, still excluding HD100, and *Leptospira*. All are annotated as an N-acetyltransferase, with domain predictions suggesting a Yjdj-type Gcn5-related N-acetyltransferase. Currently the function of Yjdj is unknown but Bd0335, a predicted Gcn5-related N-acetyltransferase (GNAT), has been identified as potentially functioning in peptidoglycan recycling earlier in this thesis.

OM95_05190 follows these six genes and is homologous to *bd3203*, which has already been discussed as an insert in the HD100 cluster. This is the gene that potentially has a role in regulating *murE/F* with UTR convergent asRNA, however in *B. ArHS* the six inserted genes discussed above are now between *murF* and the *bd3203* homologue. This could impact the regulation of *murE/F* in *B. ArHS* but further investigation is beyond the scope of this thesis.

The final inserted gene seen only in the *B. ArHS* cluster is *OM95_05225*, seen downstream of the *murC* homologue. This is annotated as a pseudo gene encoded on the minus strand; translation of this does not provide a seemingly functional protein. However, a reverse complement of the gene shows that a full protein can be translated on the plus strand. A domain prediction suggests it is a methyl-accepting chemotaxis protein, similar to *bd3192* for which *B. ArHS* has a homologue neighbouring this gene: *OM95_05230*. This could mean that a duplication event has occurred and the *bd3192* homologue has been copied. A Blast of OM95_05225 shows that its closest homologue in HD100 is Bd3192 and Bdt_3122 in Tiberius. An alignment of Bd3192, Bdt_3122, OM95_05225 and OM95_05230 show high identity between all homologues, ranging from 56% to 94% identity. Duplicating the MCP in the *B. ArHS* cluster could allow greater sensitivity to the chemical signal being received or it may be adapted to sense a different signal. The environment, and thus the nature of the prey, in which *B. ArHS* was isolated could mean that signalling must differ to *B. bacteriovorus*.

5.3.5 Analysis of peptidoglycan synthesis genes in and outside of the *dcw* cluster

In the above sections, I have detailed the similarities and differences of the *B. bacteriovorus* compared to other systems. This includes canonical *dcw* genes,

conserved in their transcription sequence and orientation, as well as multiple novel insertions. In *B. bacteriovorus*, the *dcw* cluster pathways of septation and peptidoglycan synthesis are juxtaposed with insertions involved in outer membrane growth and modification, amino acid and nucleotide metabolism, DNA repair and protection, flagellar motility, stress response, and sensory systems. Crosstalk between these pathways clearly facilitates an efficient HD cycle, utilising the maximum amount of resources to produce the highest number of progeny in as short a period as possible.

While this analysis has detailed several of the genes that encode for peptidoglycan synthesis enzymes, this pathway has not been completely accounted for. While all the genes considered here to be ancestral to the *dcw* cluster are present in the *B. bacteriovorus* genome, there are many other genes in this pathway that are not *dcw* cluster associated. The presence of two *murD* homologues, *bd3200* in the cluster and *bd0052*, also suggests that non-traditional muropeptides are being synthesised. Peptidoglycan synthesis is a pathway closely linked to division, and further detail of this pathway, as well as other sources of peptidoglycan, could further elucidate the regulation and synchronisation of growth and division in the bdelloplast.

In this section, I will explore the traditional peptidoglycan synthesis pathway in *B. bacteriovorus*, accounting for the conservation of genes, their expression, as well as any other genes of interest cotranscribed with them. Further, I will explore how *B. bacteriovorus* recycle their cell wall, and how the absorption of exogenous, prey cell wall feeds into these pathways.

RNA-seq analysis of the *dcw* cluster revealed that the *mraY-murD* operon is transcribed throughout the HD cycle, as seen in **Appendix 8.1.1c**. While transcription for these genes peaks at 3 hours, the typical time of division related processes, they are upregulated from 15 minutes onwards. This is unexpected for two reasons. Firstly, this is the period in which the *B. bacteriovorus* cell is invading the prey and there is no growth of the predator cell. Secondly, *B. bacteriovorus* use the host biomass to fuel their growth, suggesting that there is no raw material with which to start the synthesis of peptidoglycan this early in the cycle. If these were both true, peptidoglycan

synthesis would not begin until the predator had begun to digest the prey cell and would end as soon as the biomass of the prey had been exhausted, requiring the peptidoglycan synthesis pathway to be exclusively expressed in the period of growth and division, between 60 and 180 minutes into the cycle. Before exploring alternative pathways for the recycling and uptake of muropeptides, I will detail the traditional peptidoglycan synthesis pathway in *B. bacteriovorus*.

5.3.5.1 Identifying homologues for early peptidoglycan synthesis in *B. bacteriovorus* HD100

Of the proteins listed in the introduction, all have homologues in *B. bacteriovorus* HD100 except for MurJ. Many genes can be found in the *dcw* cluster, as previously noted; *murC* (*bd3196*), *murD* (*bd3200*), *murE* (*bd3205*), *murF* (*bd3204*), *murG* (*bd3197*), *mraY* (*bd3201*) and *ftsW* (*bd3198*). These are all homologues of ancestral *dcw* cluster genes; it is common for other bacteria to have these in their *dcw* cluster. The other genes are present outside of the cluster. Interestingly, there is a second gene annotated as a *murD* in *B. bacteriovorus, bd0052*. This is the only instance of a duplicated gene in this pathway. One gene, *murB*, is an ancestral *dcw* cluster gene but is located downstream of that locus at *bd3232*. Genes *murA* (*bd0071*) and *ddlA* (*bd0585*) are distal to the cluster, as is *murI* (*bd1778*).

Shown in introductory **figure 1.3**, these constitute the complete synthesis pathway up to the incorporation of the new muropeptide into the cell wall. This shows that *B. bacteriovorus* can produce its own peptidoglycan and does not have to rely on exogenous muropeptides to grow and divide. There are some anomalies that require further investigation. An additional *murD* homologue could mean that different, or modified, muropeptides are being produced in conjunction with the traditional molecule. Additionally, there are several more operons containing peptidoglycan synthesis genes distal to the cluster that may have relevance. Further analysis of these follows.

5.3.5.2 The two *murD* homologues have different transcription profiles.

As stated, there are two genes in *B. bacteriovorus* annotated as *murD*; *bd3200* in the *dcw* cluster and *bd0052*. When comparing transcription profiles,

Appendix 8.1.3a, they are very distinct. Gene *bd0052* is transcribed, almost exclusively, at 120 to 240 minutes of the cycle, peaking at 180 minutes, and is not in an operon. The *murD* homologue transcribed from the *dcw* cluster, *bd3200*, is transcribed with *mraY* throughout the cycle, also peaking at 180 minutes. Additionally, the *mraY-murD* operon in the cluster has two promoters, one preceding each gene. These promoters are not found in *E. coli*, as most of the cluster is transcribed from promoters at the start of the operon, some five genes upstream, seen in **Figure 5.3.2**. Additional promoters in the *dcw* cluster are not unprecedented in other systems, however; *B. subtilis* contains several, preceding *spoVD*, *murE*, *spoVE* and *divIB* (Real and Henriques, 2006).

Domain predictions show both encoded proteins have the central and C-terminal domains that characterise Mur enzymes, and an alignment of both MurD proteins is shown in **Figure 5.3.8**. As seen in the *E. coli* protein, ATP binding residues Lys115, Asn271, Arg302 and Asp317 in the central domain are all conserved (Bertrand et al., 1999, Šink et al., 2013, Sink et al., 2016). Two pairs of key residues in the C-terminal domain hold D-Glu: Lys348/Thr321 and Ser415/Phe422. Thr321 is conserved in both HD100 MurD proteins, however Lys348 is only conserved in Bd0052 and is replaced by a threonine in Bd3200. Both Ser415 and Phe422 are conserved in both. Residues that bind UDP-N-acetylmuramoyl-L-alanine (UMA) are found in both the N-terminal region and central domain; Leu15, Thr36, Asn138 and His183 all interact with UMA. Neither HD100 MurD proteins have a conserved Leu15 or Thr36. Only Bd0052 retains the Asn138, but both have His183. Comparatively, Bd0052 has more of these conserved residues, lacking one D-Glu and two UMA binding residues, than Bd3200, which lacks additional UMA and D-Glu binding residues. This could indicate that the substrate(s) for Bd3200 may be altered.

Interestingly, the MurD homologue encoded in the *dcw* cluster, Bd3200, shows less conservation than the distal homologue, Bd0052, to other studied systems, with considerably fewer binding residues conserved. The fact that *bd0052* is transcribed only around the point of septation also suggests that it is the canonical homologue. Recently, a study on *Xanthomonas oryzae* identified a

Figure 5.3.8. An alignment of *E. coli* MurD with both *B. bacteriovorus* MurD homologues shows that Bd0052 is more highly conserved than Bd3200. Highlighted residues indicate that they were found to be functional for the *E. coli* homologue. Green residues bind ATP, purple residues are important to D-Glu binding, and blue for UMA binding. Bd0052 has more of these residues conserved than Bd3200. The lower conservation of Bd3200 may mean that it is not the canonical homologue and could produce an alternate muropeptide. Below is an identity matrix showing the percentage identity between the protein sequences; both *B. bacteriovorus* homologues have similar overall identity to the *E.coli*.

MurD homologue with a different substrate (Ogasawara and Dairi, 2021). The authors found a MurD-like protein that they labelled as MurD2, that attached

L-Glu, instead of D-Glu, to the starting D-Ala of the peptide chain. Another enzyme, an epimerase labelled MurL, could convert the D-Ala-L-Glu peptides on the UDP-MurNAc to D-Ala-D-Glu. These enzymes, therefore, form an alternative pathway to MurD and MurI, the glutamate racemase.

An alignment shows that the two mutated residues that the authors found to account for L-Glu recognition in MurD2, are not found in either *B. bacteriovorus* MurD homologue, and there is also no MurL homologue either. While there is no MurL homologue in *B. bacteriovorus*, and neither MurD proteins share the L-Glu recognition residues, this does show that alternative substrates can be employed by MurD-like enzymes in other bacteria.

This evidence suggests a function for *mraY* and *murD* early in the HD cycle. Both produce proteins involved in the cytoplasmic formation of Lipid I, indicating that their substrates are available at these time points. In the early stages of the HD lifecycle, however, there is no prey biomass to use for synthesis or for absorption of host muropeptide fragments. This raises the question as to whether there is an alternative source of substrates for the enzymes. One such source is cell wall maintenance and recycling whereby the regular maintenance of the wall produces muropeptide turnover products; this is explored later. For traditional peptidoglycan synthesis, the other genes would have to be active at this time as well, but the *dcw* cluster analysis showed that no other pathway genes in the cluster showed appreciable expression at these early HD cycle stages. There are several other synthesis genes outside of the cluster, however, and these are explored below, beginning with *murB*.

5.3.5.3 *murB* forms the ultimate gene in an operon distal to the *dcw* cluster

The HD100 genome contains a single homologue for *murB*; *bd3233*. Gene *murB* is often found in the *dcw* cluster of bacteria but its occurrence outside of it is not unprecedented, such as in *E. coli* MG1655. In HD100, *murB* is located close to the cluster and occurs as the final gene of a four gene operon. In order, it is preceded by a *thyA* (*bd3230*), *folA* (*bd3231*) and a hypothetical gene that encodes a PilZ domain containing protein (*bd3232*). Both *thyA* and *folA* are

involved in DNA metabolism, specifically purine for *thyA* and pyrimidine for *folA*. Their presence in an operon with *murB* has not yet been investigated in any bacteria but MurB was shown to interact with ThyA and FolA in a genome scale genetic interaction screen specifically looking at crosstalk between cell envelope biogenesis pathways in *E. coli* (Babu et al., 2011). The HD100 operon reinforces this, and further Bacterial Two Hybrid studies may confirm an interaction between proteins encoded by this operon.

Promoter predictions suggest two promoters in this operon; one at the start of the operon, preceding *thyA* (thyAp) and one 50 bps into the PilZ domain encoding gene *bd3232* (bd3232p). No strong prediction was made for a promoter immediately preceding *murB*. The first two genes, *thyA* and *folA*, are clearly upregulated during division, between 120 and 240 minutes, **Appendix 8.1.3b**. Transcription from bd3232p shows that *bd3232* and *murB* are transcribed throughout the cycle, much like *mraY-murD*, also peaking at 180 minutes.

It is possible that *bd3232* may encode a protein that signals between the DNA metabolism and cell envelope pathways. In a bdelloplast, the predator filament must dynamically control the growth and division processes to the biomass available. The exhaustion of materials in one pathway may require a signal to another process to begin; in this case, it may be that once resources for the DNA metabolism pathway are mostly consumed, Bd3232 signals to MurB that peptidoglycan synthesis can begin. Alternatively, the signal could stop another process. This could preserve resources shared by other pathways. For example, if DNA metabolism has exhausted its materials, continuing other processes, such as elongating the cell, may be pointless. Having a filament capable of producing a dozen progeny is a waste of resources if only a few copies of the genome could be created from the biomass of the prey.

As with *mraY-murD*, *bd3232* and *murB* are transcribed throughout the HD cycle. This could indicate that both pairs are active in a peptidoglycan synthesis pathway before the prey has been invaded and filament growth has begun. MurB acts with MurA to convert UDP-GlcNAc to UDP-MurNAc early in the pathway. As such, a similar transcription pattern would be expected

from *murA*, early in the cycle, if these also act in an alternative peptidoglycan pathway with MurD and MraY.

5.3.5.4 Gene *murA* is cotranscribed with genes encoding a polypeptide release factor and its associated methyltransferase

From RNA-seq data, as with *murB*, *murA* is the final gene in a predicted operon, **Appendix 8.1.3c**. Homologues of *murA* are typically not seen in the *dcw* cluster, as is the case with *B. bacteriovorus murA, bd0071*. In the operon, putative *prfA* and *hemK* genes precede *murA*. PrfA is a class 1 polypeptide chain release factor homologue; these recognise stop codons UAA and UAG during translation, binding to the ribosomal A site triggering termination of translation and disassembly of the ribosome (Heurgue-Hamard et al., 2002, Li et al., 2007, Diago-Navarro et al., 2009). HemK is a methyltransferase that methylates class 1 and 2 polypeptide chain release factors. Deletion of *hemK* in *E. coli* results in increased readthrough of stop codons during translation (Nakahigashi et al., 2002, Heurgue-Hamard et al., 2002). It seems likely that HemK (Bd0070) methylates PrfA (Bd0069) in HD100. In *E. coli*, *hemK* and *prfA* share an operon with *hemA*, which is typical in gammaproteobacterial. However, just the *hemK-prfA* genes are conserved in most other bacteria. As yet, there has been no study on an operon also containing *murA*.

There appear to be three promoters in this operon, one before each gene. Expression of *murA* is low from attack phase to one hour, increasing at one to four hours with a peak at the two-hour point. *prfA* and *hemK* have a similar pattern, although *prfA* peaks at the one-hour point. This makes sense, as most translation in the HD100 cell will occur once the prey has been invaded and the biomass is available for consumption. This also agrees with the addition of *murA* to the operon, which should be active when the cell wall is being extended. This does not, however, fit in with the hypothesis of early peptidoglycan synthesis. It is possible that this step is not needed; either through use of a different substrate by *murB*, or by recycling the cell wall of the prey, which is discussed later.

5.3.5.5 Gene *murI* is cotranscribed with a purine metabolism *guaB* homologue

Similar to *murA* and *murB*, *murI* (*bd1778*) also appears as the final gene in a three gene operon following *bd1781*, encoding a protein of unknown function, and a *guaB* homologue, *bd1779*, **Appendix 8.1.3d**. GuaB is involved in purine metabolism, specifically the *de novo* synthesis of guanine nucleotides. A motif prediction scan of Bd1781 only shows that it has a predicted N terminal signal peptide with at least three transmembrane regions. Further study would be required to discern its function, which could be related to cell wall growth and/or division. As with *folA* (*bd0051*) and *murD* (*bd0052*) above, an operon containing *murI*, for peptidoglycan synthesis, and *guaB*, purine metabolism, suggests high levels of crosstalk between these systems.

A protein prediction scan of Bd1781 only suggests that it has an N terminal signal peptide with two transmembrane regions; no homologous domains were detected. It could be part of a signalling pathway

Transcription for the operon is high from one to five hours, with minimal transcription before this. Promoter predictions place one before *bd1781* (bd1781p) and one before *bd1779* (bd1779p). Both are predicted to have RpoD recognition sequences.

5.3.5.6 Gene *ddlA* may be in an operon, and is transcribed late in the HD cycle

The *ddlA* homologue (*bd0585*) in HD100 is not positioned in or near the *dcw* cluster, and RNA-seq data suggests it is not part of an operon. Its transcription pattern shows minimal levels from attack phase to two hours, with an increase starting at three hours and continuing to five hours, **Appendix 8.1.3e**. This is later than other studied division proteins in this chapter, which typically show increased transcription from one or two hours into the cycle.

Two strong promoter predictions were found; one before the gene (ddlAp) and one 570 bps in. This gene is not predicted to be an operon by Rockhopper, however there could be some cotranscription evident in the RNA-seq data from three to five hours. If so, this would mean that *ddlA* is being cotranscribed with *bd0584*, annotated as a two component sensor histidine kinase. While this gene

is transcribed throughout the cycle, it is strongest at the same time points as *ddlA*; one to five hours. Bd0584 could be used as sensor to coordinate conditions inside the bdelloplast, such as diminished biomass or the abundance of PG synthesis subtrates, with the PG biosynthesis pathway.

5.3.6 *B. bacteriovorus* has a complete peptidoglycan synthesis pathway and could also produce alternative muropeptides.

In this chapter I have identified and explained the *de novo* synthesis pathway for peptidoglycan in *B. bacteriovorus*. This has revealed several operons with varying transcription patterns. MurD (Bd3200), which shows less conservation in key residues than Bd0052, could be active early in the HD cycle but other proteins in the pathway are not. While *mraY, murB, ftsW, murG* and *murC* all show some level of transcription from attack phase/15 mins, *murA, murE, murF, murI* and *ddlA* do not. There is the possibility that MurD (Bd3200) is acting on different substrates to the more conserved Bd0052, and that it and other members of the pathway are producing a peptidoglycan different to that produced traditionally in the pathway. This could mean that the other ligases that form the peptide chain are not required; MurE, MurF, MurI and DdlA are all involved in the formation of the traditional peptide chain and are not transcribed until later in the cycle.

This does not, however, account for the source of MurNAc for this alternative peptidoglycan pathway. While *murB* is expressed early in the cycle, MurA would also be needed to convert GlcNAc to MurNAc before the peptide chain could be attached. Early in the HD cycle, there is no source of peptidoglycan from a host. Therefore, another source would be necessary. This is explored below.

5.3.7 Investigating alternative sources of peptidoglycan substrates

Overall, this investigation shows a complete pathway for the *de novo* synthesis of peptidoglycan, with the possibility that alternative muropeptides are being produced before *B. bacteriovorus* is established in the periplasm of the host. However, this does not provide a complete picture of the process as there are other sources of peptidoglycan that the predator will be able to use, potentially bypassing stages of *de novo* synthesis.

Firstly, like non-predatory bacteria, there is the peptidoglycan recycling pathway. This system has recently been reviewed (Mayer et al., 2019). During a single cell doubling event, *E. coli* cells recycle up to 50% of their cell wall. In Gram-negative bacteria, continual cleavage of the peptidoglycan wall by lytic transglycoslyases produces anhydro-MurNAc containing fragments, the prime substrate for cell wall recycling. This maintains the cell wall during growth and stationary phases. The products of these enzymes are mostly transported into the cytoplasm for recycling, with some being excreted out of the cell. The peptidoglycan fragments and side chains in the cytoplasm can then be fed back into the synthesis pathway. This activity may occur in *B. bacteriovorus* during attack phase and earlier in the cycle, representing necessary maintenance even without a host to provide further resources.

The other source of peptidoglycan for *B. bacteriovorus* is from the invaded host cell. While digestion genes are largely upregulated from 30 minutes, peptidoglycan fragments could be generated from the time of invasion, as the predator must digest a hole through the host cell wall to reach the periplasm. From then on, digestion of the host cell wall by excreted lytic enzymes will generate peptidoglycan fragments that *B. bacteriovorus* can use to feed into the synthesis pathway, much like the recycled material. While this would appear to solely be a predatory pathway, it is possible that there is homology to non-predatory systems that use the peptidoglycan transported out of other bacteria during the recycling process.

In this section I will compare the genes and proteins present in *B. bacteriovorus* with those of studied, non-predatory bacteria for peptidoglycan recycling and other sources of peptidoglycan, and how their utilisation interacts with the synthesis pathway. Once identified, the expression patterns of these genes can also be compared with the synthesis genes and operons, which could elucidate the time points at which the different sources of peptidoglycan are being utilised.

5.3.8 Peptidoglycan recycling and salvaging

The peptidoglycan recycling system has recently been reviewed (Mayer et al., 2019). During a single cell doubling event, *E. coli* cells recycle up to 50% of

their cell wall. In Gram-negative bacteria, continual cleavage of the peptidoglycan wall by lytic transglycoslyases produces anhydro-MurNAc containing fragments, the prime substrate for cell wall recycling. In non-predatory bacteria, this is a constant process; in *B. bacteriovorus*, it is possible that this pathway is activated mainly during growth and division. This would be true if the pathway is primarily used for salvaging and recycling prey peptidoglycan. The use of lytic transglycosylases to break down the prey cell wall would produce similar, if not identical products to those that the prey cell would be using in its own recycling system. Transporting them from the prey periplasm into the *B. bacteriovorus* cytoplasm for processing would mimic that system. Additionally, the prey cytoplasm could contain a substantial amount of material currently being recycled. These could easily be transported into the *B. bacteriovorus* cell and funnelled into the recycling/synthesis pathways. However, the range of MurNAc and GlcNAc related molecules and fragments in all Gram-negative bacteria would be substantial if recycling pathways differ. HD100 would need a complement of enzymes capable of processing all of these to maximise use of prey biomass. This could be evidenced by HD100 containing enzymes homologous to multiple bacterial recycling pathways.

The following is an investigation into studied peptidoglycan recycling genes and proteins, and identifying homologues and other genes of interest in *B. bacteriovorus*. Should their expression be early in the cycle, as seen with *mraY-murD*, this could provide substrates for the peptidoglycan synthesis proteins that are produced early in the cycle.

5.3.8.1 *B. bacteriovorus* has limited conservation of the peptidoglycan recycling pathway in *E. coli*

In the recycling pathway, lytic transglycosylases act on the cell wall to produce anhydromuropeptides, fragments of peptidoglycan, which are transported into the cytoplasm. These are then processed into MurNAc and GlcNAc derivatives, and peptide chains. These can then be further broken down for use in other pathways or converted into substrates for the peptidoglycan synthesis pathway.

A key enzyme in *E. coli* is MurQ, a N-acetylmuramic acid 6-phosphate etherase, necessary for the processing of anhydromuropeptides generated by lytic transglycosylases, initially characterised as being essential to growth on pure peptidoglycan substrates. MurQ is aided by phosphotransferase protein MurP, a part of the sugar phosphotransferase system that transports MurNAc 6P into the cytoplasm. Additionally, MurNAc 6P is converted from anhMurNAc, derived from anhydromuropeptides, by AnmK. MurQ converts this to GlcNAc 6P, which is then fed into the peptidoglycan synthesis pathway by NagA, a N-acetylglucosamine-6-phosphate deacetylase, that converts it to GlcN 6P. However, many Gram-negative bacteria do not possess a MurQ homologue and must feed the recycled peptidoglycan into the peptidoglycan synthesis pathway using other enzymes. pBlasts of *E. coli* MurQ, MurP, and NagA return no results in *B. bacteriovorus* HD100. Already this suggests major differences between the two systems, though there are likely homologues to other proteins present.

There are several other proteins solely used for peptidoglycan recycling in *E. coli*. Another transporter, AmpG, transfers lytic transglycosylase products GlcNAc-anhMurNAc and GlcNAc-anhMurNAc-peptides into the cytoplasm. This has a homologue in HD100, Bd0333, annotated as a Major Facilitator Superfamily protein. A further domain prediction agrees that this protein is an AmpG homologue. RNA-seq data, **Appendix 8.1.4a**, suggests it is the ultimate gene in a three gene operon (*bd0335-bd0334-bd0333*), with transcription occurring throughout the cycle but highest at attack phase and from 180 to 300 minutes. As said above, this is the period in which activity is expected, but a lower transcription at non-growth time points also suggests transport when in attack phase or entering the bdelloplast. At these time points, peptidoglycan fragments could be recycled from the *B. bacteriovorus* cell wall, for maintenance, or potentially taken from the initial entry point when the prey cell is invaded, or from any of the prey lytic transglycosylase products already in the periplasm.

Predictions for the function of the protein product of *bd0334* suggest a metal dependent hydrolase, potentially an Adenosine/AMP deaminase. Adenosine and AMP deaminases show sequence similarity, hence the dual prediction, and

are involved in purine metabolism. This could be evidence of crosstalk between peptidoglycan recycling and DNA synthesis for growth. This was also seen between the peptidoglycan synthesis pathway and DNA synthesis, with the *folA-thyA-murB* operon.

Bd0335 is predicted to have a GNAT (Gcn5-related N-acetyltransferases) family domain. This family is host to a range of acetyltransferase proteins, spanning eukaryotes and bacteria (Ud-Din et al., 2016). Functions of some bacterial GNAT proteins include modification of cell wall components such as the FemABX aminoacyl transferases of *Escherichia* and *Staphylococcus* species. However, the range of functions among GNAT proteins in bacteria is vast, including antibiotic resistance, toxins and antitoxins, and tRNA synthetases, to name a few (Ud-Din et al., 2016, Favrot et al., 2016). A pBlast of Bd0335, excluding Bdellovibrionales, solely returns Firmicute proteins. Specifically, N-acetyltransferases homologous to *B. subtilis* YitI, an N-acetyltransferase of unknown function. A domain prediction of both proteins predicts they have a glucosamine 6-phosphate N-acetyltransferase domain, GNPNAT1. This enzyme has mostly been studied in Eukaryotic models, particulary human and mouse. There is one notable bacterial study that identified one in *Clostridium acetobutylicum*, GlmA, and a further study solving its crystal structure (Reith and Mayer, 2011, Dopkins et al., 2016). Bd0335 and $YitI_{Bsub}$ only constitute the N terminal domain of GlmA, however the authors, Dopkins *et al*, suggest that the two, structurally similar domains of GlmA arose from a gene duplication event. Both domains of GlmA can bind the substrates, but only the C terminal domain is catalytically active. This suggests that even though Bd0335 aligns with the N terminal domain, it could retain catalytic function.

This could be evidence of a pathway that replaces the *E. coli* pathway that utilises MurQ. In *E. coli*, recovered MurNAc 6P is converted to GlcNAc 6P by MurQ, which is then converted to GlcN 6P by NagA. The absence of these proteins in HD100 suggests an alternate pathway must exist for introducing GlcNAc into the peptidoglycan synthesis pathway, and the conversion of GlcN to GlcNAc by Bd0335 may be one of the steps. Aside from recycling, the only other source of GlcN 6P comes from conversion of fructose 6P by GlmS, a

glutamine--fructose-6-phosphate aminotransferase, in the initial steps of the synthesis pathway. It is then converted to UDP-GlcNAc sequentially by GlmM and GlmU. However, HD100 has homologues of all these genes, making this role redundant in Bd0335, suggesting its function is in recycled peptidoglycan materials.

In *E. coli*, NagZ, LdcA and AmpD break down the anhydromuropeptides into GlcNAC, anhMurNAc and peptide chains. NagZ, a Beta-hexosaminidase that cleaves muropeptides into anhMurNAc-peptides and GlcNAc, has two predicted homologues; Bd0146, annotated as BglX2, and Bd3895, annotated as BglX. This means that GlcNAc can be cleaved from the initial anhydromuropeptides in *B. bacteriovorus*. In *E. coli*, GlcNAc is converted to GlcNAc 6P by NagK, an acetylglutamate kinase, to be converted to GlcN 6P by NagA, as above. GlcN is the possible substrate for Bd0335 to bypass the MurQ aspect of the *E. coli* pathway; however, there is no homologue for NagK in *B. bacteriovorus*. As such, the source of recovered GlcN 6P remains unknown.

AmpD, an anhMurNAc-L-alanine amidase, does not have a homologue in *B. bacteriovorus*. AmpD and LdcA remove the peptide chains from the anhMurNAc (AmpD) and cleave them (LdcA) to produce the murein tripeptide L-Ala-iso-D-Glu-mDAP. The peptides cleaved from the anhydromuropeptides by AmpD and LdcA can be further broken down but usually the murein tripeptide L-Ala-iso-D-Glu-mDAP will be attached to UDP-MurNAc by Mpl, a muropeptide ligase similar to MurC, bypassing enzymes MurCDE. In *B. bacteriovorus*, Bd1950, annotated as microcin C7 self-immunity protein (MccF), is homologous to *E. coli* LdcA, murein tetrapeptide carboxypeptidase, and Bd1952 is an Mpl, UDP-N-acetylmuramate--L-alanyl-gamma-D-glutamyl-meso-2,6-diaminoheptandioate ligase, homologue. As *B. bacteriovorus* does not appear to have an AmpD, the enzyme that initially cleaves the pentapeptide from MurNAc, another method of cleavage or an alternative source of the pentapeptide would be needed to create the tripeptide for attachment to UDP-MurNAc. This leaves both the GlcNAc and peptide chain pathways incomplete when only considering the *E. coli* system.

The remaining anhMurNAc is phosphorylated to MurNAc 6P by AnmK, an Anhydro-N-acetylmuramic acid kinase, and MurQ, mentioned above, converts this to GlcNAc 6P. There is no homologue for AnmK in *B. bacteriovorus*, therefore the method by which anhMurNAc is introduced into the synthesis pathway in has not yet been addressed.

In the overall comparison with *E. coli*, the recycling pathway in HD100 is incomplete. However, a potential connection to DNA synthesis has been found in Bd0344, providing further evidence of crosstalk between division and peptidoglycan synthesis/recycling. To try to find other homologues in the recycling pathway, further studied bacteria were compared.

5.3.8.2 An alternate peptidoglycan recycling pathway in *Pseudomonas putida* is conserved in *B. bacteriovorus*

Even though *B. bacteriovorus* has potential homologues for several *E. coli* recycling proteins, they do not form a complete recycling pathway. Other bacteria have shown differing pathways, such as *Pseudomonas putida* (Fumeaux and Bernhardt, 2017, Mayer et al., 2019). Like *B. bacteriovorus*, this lacks MurQ, MurP and NagK; however, it still retains AmpD and AnmK. This means that it still processes the cleaved peptides in the same way as *E. coli*, and anhMurNAc can be converted into MurNAc 6P. Instead of using MurQ, MurP and NagK, *P. putida* uses three enzymes to convert MurNAc 6P to UDP-MurNAc: MupP, a murNAc 6P phosphatase, AmgK, an anomeric MurNAc/GlcNAc kinase that also phosphorylates and introduces GlcNAc into the synthesis pathway, and MurU, a MurNAcα-1-phosphate uridylyltransferase ultimately producing UDP-MurNAc.

Initial searches for these three proteins show each has a potential homologue. Bd0379, a predicted phosphoglycolate phosphatase, is homologous to MupP; Bd0154, a predicted phosphotransferase, is homologus to AmgK. Bd0153, a predicted NTP nucleotide-diphospho-sugar transferase, is homologous to MurU. Both *P. putida* AmgK and Bd0154 have the aminoglycoside phosphotransferase domain and are predicted to be in the same N-acetylmuramate/N-acetylglucosamine kinase family for the whole of their sequences. An alignment shows 27.5% identity and 43.1% similarity between

the two proteins. The presence of an AmgK homologue in *B. bacteriovorus* explains how the GlcNAc is introduced into the synthesis pathway, following the extraction of GlcNAc from the anhydromuropeptides by NagZ. However, this raises further questions as to the need for Bd0335, the putative GlcN 6P acetyltransferase. Both GlcNAc and GlcN 6P can be introduced into the synthesis pathway already, making Bd0335 redundant. It is possible that it no longer functions as an enzyme; other possible uses could be in sensing peptidoglycan precursors.

Domain predictions for Bd0153 suggest that its annotation as a nucleotide-diphospho-sugar transferase is correct. Whether it functions as a MurU specifically is harder to determine as there are many similarities between proteins that bind a sugar-1P to a nucleotide, but an alignment shows 31.6% similarity with the *P. putida* protein, with the catalytic site conserved. Interestingly, RNAseq data predicts that AmgK (Bd0154) and Bd0153 are encoded from a four gene operon, *bd0155* to *bd0152*, potentially identifying a peptidoglycan recycling/salvaging operon. This lends further credence to Bd0153 acting as a MurU, as both occur in the studied *P. putida* pathway, for which all proteins have potential homologues in *B. bacteriovorus*. RNA-seq data show that this operon has the same expression profile as the *ampG* operon above, **Appendix 8.1.4b**; transcription throughout the cycle but upregulated at attack phase and from 180 to 300 minutes.

The first protein encoded in this operon, Bd0155, is annotated as containing an RNA polymerase sigma factor 54 interaction domain. A domain prediction shows only this domain, at residues 152-263 of the 289 amino acid protein. There is no prediction for N terminal domains before this. The interaction domain is typically found in proteins involved in two component signal transduction systems, and typically have an N terminal domain that can be phosphorylated by a sensor kinase. As there is no prediction for the N terminus of Bd0155 there is no suggestion as to what the sensor might be. However, the presence of *bd0155* in an operon with peptidoglycan recycling genes indicates a likely involvement with the activation of such genes. Sigma factor 54 has been shown to require activators to initiate transcription, and regulates a wide array of cellular processes, which may include the peptidoglycan

salvaging/recycling pathways in *B. bacteriovorus* (Bush and Dixon, 2012, Zhang et al., 2016). Bd0152, the product of the ultimate gene in the operon, is introduced in the next section.

Overall, this shows that the peptidoglycan recycling pathway in *B. bacteriovorus* has a greater resemblance to the *P. putida* system than to *E. coli*. However, there are still sections of the pathway not present in *B. bacteriovorus*. AnmK, which converts the anhydrous-MurNAc fragments to MurNAc-6P, does not have a homologue even though later members of the pathway do. AmpD, which removes the peptide chains from anhydrous-MurNAc, is the same. While members of the recycling pathway have been identified, it is clearly not yet complete. One further system is compared below that helps to complete the pathway.

5.3.8.3 Peptidoglycan salvaging pathway of *Tannerella forsythia* is also partially present in *B. bacteriovorus.*

Recent studies on *Tannerella forsythia*, a Gram-negative Bacteroidete and oral pathogen that contributes to periodontitis, have shown that it lacks the enzymes involved in the early stages of peptidoglycan synthesis, including MurA and MurB (Hottmann et al., 2021). Instead, it relies on other bacteria in the oral microbiome to provide peptidoglycan in a process the authors term "peptidoglycan salvaging". This bears similarity to *B. bacteriovorus* which also relies on external sources of biomass. A salvaging pathway in *B. bacteriovorus* could tie into both recycling and *de novo* synthesis, making a dynamic system that balances these pathways based on available resources and/or the current point in the HD cycle.

The authors speculate that the exogenous peptidoglycan is transported through the outer membrane via a SusCD-like uptake complex. Several NamZ exo-lytic N-acetylmuramidase homologues were identified in *T. forsythia*, found by searching with the *B. subtilis* NamZ homologue. In *T. forsythia* these can cleave exogenous peptidoglycan, stripped of the peptide chains by unknown amidases, into MurNAc and anhydro-muropeptide molecules. NamZ2 was found to cleave off MurNAc from the end of the peptidoglycan, while NamZ1 cleaves off GlcNAc-MurNAc disaccharides. These enzymes specifically

cleave peptide-free peptidoglycan which, if the amidases can only target the exogenous peptidoglycan, could be a way of protecting their own peptidoglycan wall from being processed in this manner; a function equally important in *B. bacteriovorus*. The cleaved peptides can then be imported separately and metabolised.

In *T. forsythia*, the cleaved MurNAc is then transported across the inner membrane by MurT while the disaccharides are transported by AmpG. MurNAc is then processed by AmgK (*B. bacteriovorus* homologue Bd0154) and MurU (Bd0153), as seen in *P. putida*, and fed into the synthesis pathway. The GlcNAc can also be fed into the earlier stages of synthesis as GlcNAc-1P, also converted by AmgK.

While no MurT homologue could be identified, a single putative NamZ homologue is found in *B. bacteriovorus*, Bd0152, with 39% identity to the *B. subtilis* NamZ and very similar domain predictions. A Swissmodel search for Bd0152 also shows that the closest known protein structures come from *Bacteroides fragilis*, which is closely related to *T. forsythia*. This is encoded from the final gene of the operon that also codes for the putative AmgK and MurU homologues. If this acts similarly to the NamZ1 it will provide the same disaccharides for AmpG to transport into the cell for "salvaging". This is where the salvaging and recycling pathways converge. As with *T. forsythia*, the turnover products from the peptidoglycan wall, typically the same disaccharides as with salvaging, could also be imported via AmpG and fed back into the synthesis pathway in the same manner.

Taken together, the pathways presented here form an outline of the peptidoglycan synthesis, recycling and salvaging pathways that are employed during host dependent growth. This does not, however, answer the question of whether peptidoglycan is being synthesised and processed during the early, pre-invasion stages of the HD cycle. The expression patterns of the genes encoding for salvaging and recycling should indicate whether these pathways are active at the same time as the synthesis genes that are expressed pre-invasion. If so, it may be possible that *B. bacteriovorus* is able to take in exogenous peptidoglycan turnover products, such as the MurNAc-GlcNAc

disaccharides and larger muropeptides, produced by other bacteria, much like *T. forsythia*.

Additionally, it is still uncertain how the peptide chains removed from the muropeptides are recycled. While there are homologues for the processing of pentapeptides, LdcA and Mpl, there seems to be no homologue for the enzyme in *E. coli* and *P. putida* that cleaves the pentapeptide from the muropeptide itself: AnmK. If the peptides are cleaved off by an amidase in the periplasm, as is speculated in *T. forsythia*, then these could be transported across the inner membrane to be processed in the cytoplasm and fed into the synthesis pathway.

5.3.8.4 Pentapeptides can be cleaved in the periplasm by AmiC and transported into the cytoplasm by OppA.

For NamZ to cleave disaccharides from the salvaged peptidoglycan fragments, the peptide chains would first have to be removed; specifically, this would be by N-acetylmuramyl-L-alanine amidase that cleaves the bond between the first alanine of the peptide chain and MurNAc. Afterwards they could be transported into the cytoplasm and recyclyed by the LdcA and Mpl homologues detailed above.

E. coli has three cell separation N-acetylmuramyl-L-alanine amidases, AmiA, AmiB and AmiC. These all act on peptidoglycan at the septa to detach the two daughter cells. These can only act on macromolecular peptidoglycan molecules, cross-linked in the cell wall, and have no activity on smaller peptidoglycan fragments. Searches using *E. coli* protein sequences show that *B. bacteriovorus* have only one homologue, Bd2699, annotated as AmiC. Another system, *Neisseria gonorrhoeae*, has also recently been identified as only encoding for AmiC, along with its cognate activator NlpD, for which *B. bacteriovorus* also has a homologue, Bd0168 (Lenz et al., 2016). In *N. gonorrhoeae*, mutations in key residues showed that it still acted at the septa, separating daughter cells. However, they also found that it could remove a pentapeptide chain from a tetrasaccharide (GlcNAc-MurNAc(pentapeptide)-GlcNAc-MurNAc(pentapeptide). This could mean that, in *Bdellovibrio bacteriovorus*, AmiC can act on the peptidoglycan fragments that are being

salvaged from the prey, releasing the pentapeptide chains and making a valid substrate for NamZ. As with *N. gonorrhoeae*, the lack of AmiA and AmiB also suggests that AmiC still performs as the cell separation amidase. As the pentapeptides are generated in the periplasm, there would have to be a means of transporting them across the inner membrane for recycling.

One other potential N-acetylmuramyl-L-alanine amidase is annotated in *B. bacteriovorus*: Bd0992 is annotated as a CwlJ. These, along with related, redundant protein SleB, are cell wall hydrolases found in *Bacillus* species (Moir and Cooper, 2015). When the spore is forming, these enzymes associate to the spore wall, or spore cortex, in an inactive state. Germination of the spores requires the degradation of the cortex, which is achieved by activating these enzymes. A domain prediction of Bd0992 shows a transmembrane region, with an unknown cytoplasmic domain and a periplasmic SleB-like hydrolase domain. This is most like SleB homologues, which have a signal sequence and hydrolase domain, whereas CwlJ, a shorter protein, just has the hydrolase domain. However, neither SleB nor CwlJ have a transmembrane region, as does Bd0992. An alignment of all three also shows that Bd0992 has a higher similarity to SleB (26.38%) than CwlJ (15%). It also shows that the only homologous region between Bd0992 and SleB is the hydrolase region; the N terminal domains are not shared. A structural search confirms this, with the highest structural similarity being the hydrolase region of a *B. cereus* SleB (PDB ID 4f55).

The oligopeptide permease transport system, OppABCDF, has been documented in many model bacteria as a method for peptide uptake (Picon and van Wely, 2001, Nakamatsu et al., 2007). It is an ATP binding cassette (ABC) complex formed from five subunits. OppB and OppC form the translocation pore and OppD and OppF bind ATP to fuel the process. OppA recognises peptides for uptake into the cytoplasm. The specificity of homologues varies between OppA homologues; they agree, however, that OppA will only recognise peptide chains with five or fewer residues (Rostom et al., 2000, Picon and van Wely, 2001, Berntsson et al., 2009). There are other oligonucleotide permease systems with significant homology to this, such as DdpA, which recognises dipeptides, and AppA, which can substitute OppA for

some functions in *B. subtilis*, which recognises tetra- and pentapeptides (Olson et al., 1991, Smith et al., 1999, Picon and van Wely, 2001).

A search using the OppA homologues of *E. coli* and *B. subtilis* shows three potential homologues in *B. bacteriovorus*. It should be noted, however, that there is considerable homology between substrate recognition proteins for the different oligopeptide permease systems. Gene *bd0357* is annotated as *dppA*, *bd1972* as *oppA*, and *bd2191* as *appA*. Should these be correct, that gives *B. bacteriovorus* the transporters for the uptake of oligopeptides cleaved from the muropeptides during peptidoglycan salvaging and recycling, as well as any other small oligopeptides provided by the digestion of host biomass.

5.3.8.5 Peptidoglycan synthesis and recycling/salvaging genes show attack phase and septation expression

RNAseq data shows that many of the above genes in the recycling and salvaging pathways have a few discrete expression patterns. As above, the disaccharide transporter gene *ampG* is expressed from a three gene operon. This operon shows upregulated expression from 180 to 300 minutes, as well as at attack phase. However, lower expression is seen through the other stages of the cycle. The salvaging operon, which includes the putative σ^{54} enhancer, *amgK*, *murU*, and *namZ*, has the same pattern, **appendix 8.1.4b**, as does *nagZ1* (*bd0146*), **appendix 8.1.4c**. This suggests that disaccharide uptake is possible preinvasion, and this may be the time that this pathway is most highly expressed. This could be for processing the turnover products of their own peptidoglycan recycling, but it is also possible that exogenous muropeptides, excreted by other bacteria, can also be transported and processed at this time, much like *Tannerella forsythia*, using the same uptake system that will later be used on host muropeptides. Further work would be required to determine the proteins of the uptake system, however the recycling pathway appears to be active at attack phase, possibly providing material to the cell wall synthesis proteins seen to also be active early in the cycle.

Interestingly, the recycling genes are downregulated through the growth phases, 15 to 120 minutes specifically. While a low level of expression is seen, this does suggest that these pathways are minimally active during growth and

genome replication. This could indicate that *de novo* synthesis is preferred through these phases, as materials for growth are abundant, with the recycling and salvaging pathways becoming active at septation and during attack phase when resources are limited. Expression may be triggered when the materials for synthesis are low, and recycling/salvaging is employed to aid in the incorporation of peptidoglycan at the septa, and subsequently for maintaining the cell wall once substrates are exhausted and the progeny have been released to the extracellular matrix. The recycling/salvaging pathways feed UDP-MurNAc into the synthesis pathway, bypassing MurAB, suggesting that the presence or absence of substrates at or before this step in the pathway is detected, and could act as a signal to switch from synthesis to salvage.

The expression profile of *amiC* complements the other genes of the recycling pathway. While expressed throughout the cycle, its highest expression occurs at attack phase which fits with these pathways being active pre-invasion. This would mean it could actively strip peptide chains from recycled or salvaged muropeptides. It then sees upregulation at 180 minutes, which coincides with septation, allowing AmiC to perform its canonical function in cell separation.

Gene *ldcA*, which encodes the enzyme that produces tripeptides from pentapeptides for recycling, is upregulated at 60 minutes, and *mpl*, the ligase that attaches the tripeptide to MurNAc, is upregulated from 120 minutes; both are active to some degree through the growth phase, although their peak expression is at 120/180 minutes, **appendix 8.1.4d**. These genes are not active at attack phase, however, suggesting that recycled oligopeptides are not used for cell wall maintenance even though other enzymes in the recycling pathway are expressed. It is possible that the alternative peptidoglycan pathway, for which there is an additional MurD protein, is active instead. This would mean a switch from synthesis of the alternative peptidoglycan, produced at attack phase for maintenance, to traditional peptidoglycan for growth and septation.

Of the three oligopeptide transport binding recognition genes, *dppA* and *appA* are active from 15/30 minutes. Upregulation at attachment and invasion could suggest either preparation for wholesale digestion or possibly to transport oligonucleotides produced as the *B. bacteriovorus* cell digests a hole through

the cell wall to gain access to the periplasm. They remain active throughout the cycle, peaking during growth and replication, 120 minutes. Gene *oppA*, however, follows a similar pattern to the peptide recycling genes *ldcA* and *mpl*, with upregulation only occurring at 120 minutes and continuing to 300 minutes, with minimal expression at attack phase, **appendix 8.1.4e**. This suggests that Bd1972 OppA is used specifically for peptides produced from PG turnover and salvaging, whereas *ddpA* and *appA* are for more general, smaller oligopeptide uptake. It also suggests that the peptide chain products of recycling and salvaging are not transported into the cytoplasm until 120 minutes into the cycle, when the filament is growing and multiple replisomes are present, possibly in preparation for septation at 180 minutes.

5.4 Chapter 5 Discussion

5.4.1 Adaptations to the *dcw* cluster of *B. bacteriovorus* complement a predatory lifecycle.

As seen in this analysis, the adaptations to the *dcw* clusters of *B. bacteriovorus*, *B. ArHS* and *B. exovorus* are extensive, and this work provides a preliminary assessment that could spur future investigation. The conservation of the *B. bacteriovorus dcw* cluster seems somewhat paradoxical. The ancestral genes are largely conserved; thirteen are present in the cluster, missing only *mraZ* and *ddlB* completely, and *murB* having moved downstream. Indeed, these genes are in the conserved order and transcribed in the same direction. What seems counterintuitive are the copious additional genes seen only in *B. bacteriovorus* and their disruption of the transcription of the ancestral operon; ten of the fifteen non-ancestral genes occur mid-cluster and transcribed opposite to the ancestral operon.

Also interesting is the comparison of *B. bacteriovorus* with *B. ArHS* and *B. exovorus*. While all their *dcw* clusters have a similar quantity and placement of inserted genes, very few are conserved between the species. This would indicate that *Bdellovibrio* species are, in general, prone to these insertions, however they are likely specific to the varying lifestyles and environments of the predator.

5.4.2 Inserted genes have a variety of potential roles

Among the genes inserted into the *B. bacteriovorus dcw* cluster, several can be identified as being for some form of protection. There is a putative β-lactamase, *bd3212*, could protect peptidoglycan incorporation at the cell wall, and a *recQ* homologue, *bd3210*, for protecting and repairing the duplicated genomes. Three genes, *bd3208, bd3209* and *bd3188* could encode for proteins that modify the outer membrane, protecting the cell from its own lytic enzymes. Finally, *bd3193* encodes for a Universal Stress Protein A homologue. This clearly suggests a need to monitor and protect the growing invader against the environmental conditions of the bdelloplast as it is being digested.

Other putative roles for proteins encoded by inserted genes include signaling, such as with tandem CBS domain protein Bd3203 which could sense AMP or ATP levels in the growing cell, flagellum development, with CheW homologue Bd3192, and carbon source utilisation near the end of the cycle with Bd3195. This clearly shows a diverse number of systems that must be synchronised with the classical functions of proteins encoded from the *dcw* cluster.

5.4.3 Peptidoglycan synthesis, recycling and salvaging pathways contribute to an efficient use of host biomass.

Putative pathways for complete peptidoglycan synthesis and recycling are present in *B. bacteriovorus*. Additionally, I have identified a potential means for the processing of exogenous peptidoglycan, either from the host, during digestion, or from the environment, as *T. forsythia* does. These pathways are shown in **figure 5.4.1**.

The transcription profiles of these pathways clearly show that while the pathways are interlinked, there is the definite possibility that the synthesis and the uptake of peptidoglycan are discretely regulated during the HD cycle. The synthesis pathway has some variation between the expression of enzymes. Some are seen to be upregulated early in the cycle, such as *murB, murD* (*bd3200*) and *mraY*, while others are expressed more so when replication is ending, and the cell is preparing to septate.

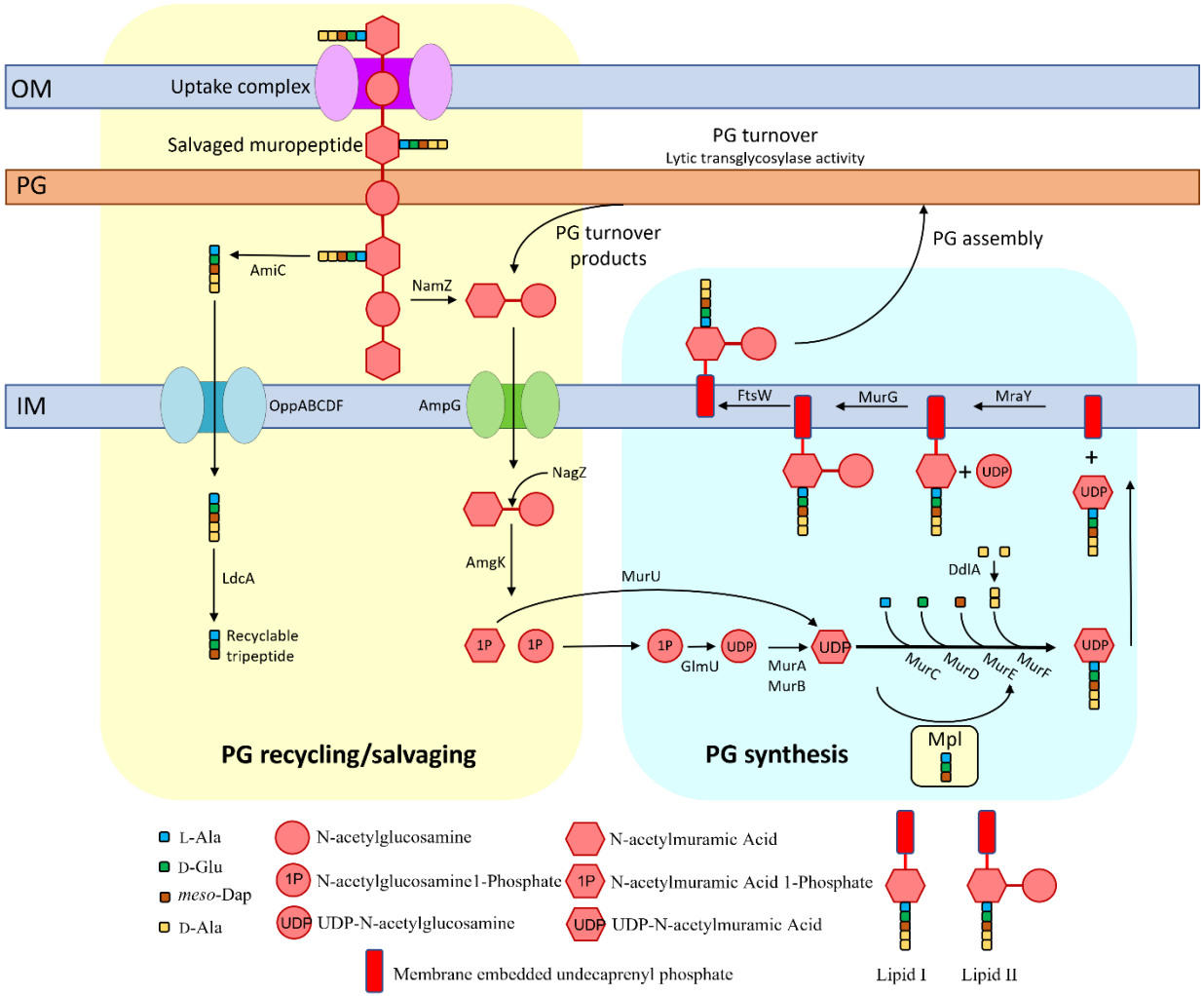

Figure 5.4.1. A cartoon of the putative peptidoglycan synthesis, recycling and salvaging pathways of *B. bacteriovorus*. These show the putative roles of the proteins from genes identified as potential homologues in these pathways. *B. bacteriovorus* may be able to take up peptidoglycan, through an unknown uptake complex, in a salvaging route like that seen in *Tannerella forsythia*. In this putative pathway, salvaged muropeptides would be stripped of peptide chains by AmiC (Bd2699). The MurNAc-GlcNAc disaccharides are cleaved from longer chains and imported to the cytoplasm by AmpG (Bd0154). NagZ (Bd0146) cleaves these into individual sugars. MurNAc can be fed into the peptidoglycan synthesis pathway by MurU (Bd0153). The cleaved pentapeptide can be imported to the cytoplasm by the OppABCDF complex (OppA Bd1972) and a recyclable tripeptide cleaved off by LdcA (Bd1950). This can also be fed into the PG synthesis pathway by Mpl (Bd1952). Peptidoglycan salvaging could be active for processing of prey PG in the bdelloplast, or for the uptake of PG excreted by other bacteria while *B. bacteriovorus* cells are in attack phase (Mayer et al., 2019, Hottmann et al., 2021).

Contrastingly, all the genes for the salvaging and recycling pathways share a similar expression pattern; upregulation at attack phase, downregulation for invasion and growth, then upregulation for septation and release. This very clearly shows that the salvaging pathway is active at attack phase and division, but is not highly expressed during growth, when one would expect the peptidoglycan wall to need substrates for growth. Should there be no uptake of peptidoglycan, another source or alternative method of cell wall elongation would be necessary.

5.4.4 *B. bacteriovorus* may import exogenous peptidoglycan excreted by other bacteria during attack phase.

Expression of the salvaging pathway at attack phase is also interesting, as it suggests that *B. bacteriovorus* can import exogenous peptidoglycan. When free swimming, the only source of this would be that excreted by other bacteria. The muropeptides imported could then be fed into the synthesis pathway, with a source of UDP-MurNAc bypassing MurA and MurB. Should a synthesis pathway be active, a combination of exogenous muropeptides and those generated through cell wall maintenance would fuel further synthesis before the predator has a host to digest.

Additionally, the expression of genes encoding these pathways at 300 minutes suggests ongoing cell wall activity once the progeny are newly released. A change in morphology is observed between the newly released *B. bacteriovorus* and those that have been in attack phase for some time, as seen in Fenton *et al*. (Fenton et al., 2010). This could be due to ongoing alterations to the cell wall to better adapt to attack phase and preparing to begin the next cycle.

5.4.5 *B. bacteriovorus* could produce an alternative muropeptide at attack phase.

As stated, the recycling and salvaging pathways are not expressed during elongation of the filament. This is further compounded by the fact that not every gene in the synthesis pathway is upregulated during growth, particularly at 60 minutes. There are several reasons why this might be. Firstly, it could be that the growing filament does not actually need much input during growth,

and that low levels of synthesis are all that is required. Modification of the cell wall may make it malleable enough for growth, with minimal synthesis providing some new substrate.

An alternative could be that the synthesis genes that are expressed at these time points are producing an alternative muropeptide. I have investigated the additional MurD homologue and concluded that one, most likely Bd3200, ligates an alternative amino acid to the peptide chain. Other elements of the synthesis pathway are expressed at the same time. The downregulated genes code for the canonical amino acid ligases, whereas genes whose products contribute the formation of the MurNAc-GlcNAc attached to undecaprenyl phosphate are expressed. Therefore, it is possible that there is an alternative synthesis pathway producing a muropeptide with an altered peptide chain. This could account for the cell wall growth with canonical synthesis occurring when septation begins. At this point, peptidoglycan is incorporated at the septa, with further peptidoglycan possibly used to reinforce the cell wall.

5.5 Further work

Given the scope of gene insertions, this bioinformatic analysis provides ample scope for future practical work. Bacterial two hybrid assays could be applied to the proteins encoded from the *dcw* cluster to confirm known interactions from other systems, such as FtsQ with FtsL in the absence of FtsB, as well as to see if the novel insertions interact with any of the known cell division proteins.

Studying the mechanisms of the MurD homologues could show whether alternative muropeptides are being produced before invasion. In other systems, deletion of the *mur* genes is not lethal, only impairing growth. Deletion of the *murD* homologues may produce distinct phenotypes; impaired growth for the canonical homologue and perhaps altered morphology of the newly released and attack phase cells when deleting the alternative MurD. Analysis of the peptidoglycan may also show what amino acids are being incorporated. This could also show which of the two homologues is the canonical homologue; despite being encoded from the *dcw* cluster, the MurD homologue Bd3200 has lower conservation of functional residues from the *E. coli* MurD homologue than Bd0052.

6 Final discussion

The initial aim of this study was to continue the investigation of *divIVA* and its operonal neighbours. An additional aim came later; to bioinformatically investigate the *dcw* cluster, as well as the peptidoglycan synthesis and utilisation pathways. This has been largely successful, with a DivIVA-ParA3 interaction network, identification of novel interactions with other systems, and a robust initial analysis of the *dcw* cluster and peptidoglycan pathways.

6.1.1 DivIVA and cell morphology

This thesis has provided further evidence of the effect of DivIVA on cell morphology. Milner's initial analysis of the cell morphology of the *ΔdivIVA* strain determined that they were shorter and wider than wild type. While my analysis agreed with this, further insights were made. I found that the morphology of the prey cells affected not only the mutant strain, but also wild type *B. bacteriovorus*. When preying upon the consistently smaller, and less variable *E. coli* strain MG1655, the attack phase cells produced were

significantly wider than when preying upon the longer, more variable strain S17-1. Additionally, there was a correlation between progeny cell length and width for wild type *B. bacteriovorus* when preying on either prey strain, but this was lost when the *ΔdivIVA* strain preyed upon S17-1. This could indicate that *B. bacteriovorus* is able to adapt the morphology of the filament, and thus progeny, to the size of the bdelloplast.

I also found that expression of the DivIVA A78T mutant strain in WT *B. bacteriovorus* led to an increase in shorter and longer cells. This mutation affects the conserved residue targeted for phosphorylation in other systems, suggesting that this is also the case in *B. bacteriovorus*. While the kinase responsible for this has not been found through the interaction studies in this thesis, further work may be able to identify it.

6.1.2 Metabolic cues for division

A theme repeatedly found in this investigation is the crosstalk between the division systems and other processes related to either the conditions in the bdelloplast or the availability of certain metabolites. This was seen in both the interaction assays of DivIVA and the bioinformatic investigation of the *dcw* cluster and peptidoglycan synthesis.

6.1.3 The DiviVA network: multiple systems progressing the lifecycle

Methodologically, the principal advancement of this thesis was the development of a BTH library, the first of its kind in *B. bacteriovorus*. This has allowed me to find novel interactions for DivIVA that would have not been tested for in a pairwise manner and has already been used for additional proteins unrelated to those initially investigated in this thesis.

Both the pairwise and library assays showed different elements of the DivIVA network. The pairwise assays revealed interactions between DivIVA and the products of its genomic neighbours. The interaction with Bd0465, a pyrroline-5-carboxylate reductase, and the interaction of Bd0465 and Bd0466, a YggS homologue, initially implicated crosstalk of amino acid metabolism, specifically proline for Bd0465 and valine, leucine and isoleucine for Bd0466, as well as pyridoxal phosphate homeostasis, with the cell morphology and division roles of DivIVA. Finding an interaction between Bd0465 and Bd3906,

the canonical ParA3, showed that this network also extends to chromosomal partitioning. The library assay then showed a potential interaction between the DivIVA-ParA3 network and the stress response towards reactive oxygen species, via a direct interaction between DivIVA and TrmJ, as well as with menaquinone synthesis (Bd0548 MenE) and utilisation (DsbA Bd2107).

The state of amino acid metabolism could be a strong indicator for the stage in the HD cycle the growing *B. bacteriovorus* filament is undergoing. An abundance of exogenous peptides being digested and transported into the predator could maintain the growth phase, with a lack of material causing a transition to division. Of course, this thesis has shown that there are multiple signals involved in this complex process, however, DivIVA is regulated post-transcriptionally in many models, and this could be one of the cues that activates or represses it in *B. bacteriovorus*.

An interesting point on Bd0465, predicted to function as the final step in proline synthesis, is that there seems to be no other enzymes present for this pathway. If this is the case, and no alternative exists, then *B. bacteriovorus* would be entirely reliant on exogenous sources of proline. Without this pathway, Bd0465 may have taken on an alternative role in sensing proline levels, and could perhaps use this as a signal to activate the division systems it interacts with.

If, as Milner hypothesised, DivIVA is a determinant of the final septum, the quantity of resources for further growth would be a key indicator as to whether another daughter cell could be completed; should resources be running out, then the final septum can be determined, and the filament can transition to division. If this signal is given via Bd0465, it could relay this to the ParAB system as well as to DivIVA.

6.1.4 The *dcw* cluster and peptidoglycan pathways

The investigation into the *dcw* cluster, and the further examination of the peptidoglycan pathways, revealed a similar story. The sheer quantity of genes involved presented many potential avenues to investigate regarding crosstalk between the canonical pathways of the cluster, namely peptidoglycan synthesis and septation, with the novel genes inserted into the cluster. These genes

include predicted roles in outer membrane lipid synthesis and modification, DNA repair, alternate carbon source utilisation and stress response, all of which can be plausibly connected to division for the same reasons as with DivIVA.

Members of these pathways distal to the cluster provided further examples of metabolic cues. Peptidoglycan synthesis gene *murB* is cotranscribed with pyrmidine and purine metabolism genes *thyA* and *folA*, and *murI* is cotranscribed with *guaB*, also involved in purine metabolism. Much like the DivIVA network, nucleotide uptake and synthesis for chromosomal replication could be an indicator of how many progeny the filament will ultimately produce, and when it must stop to determine the final septum and divide.

RNA-seq data was invaluable when assessing the different elements of these pathways. Temporally, these pathways are activated at specific times through the HD cycle, and not always when one might expect. Investigating the MurD homologues provides evidence of alternate muropeptide synthesis occurring before invasion, while utilisation of prey peptidoglycan only appears to occur before and after the growth phase of the cycle.

I also identified the putative pathway for peptidoglycan salvaging. An interesting feature of this pathway was its upregulation at 180 minutes, when the filament is preparing to septate. This suggests that prey peptidoglycan is not substantially required for growth of the predator, and its activation before septation could mean it is largely utilised at the new cell poles and possibly for the morphological changes that occur after the release of progeny. Its continued expression at attack phase also suggest that exogenous peptidoglycan can be taken in and processed for cell wall maintenance. This could indicate that during growth and chromosomal replication it is more advantageous to maintain a robust bdelloplast for protection, and only when the *B. bacteriovorus* are dividing and maturing is it safe to weaken it.

Ultimately, this all adds up to a complex division and septation system with input from all the above pathways. Sensing the available resources and the state of digestion through the cycle, and monitoring the changing conditions in

the bdelloplast, the growing predator can grow and divide into the appropriate number of progeny as quickly and efficiently as possible.

6.1.5 DslA as an example of horizontal gene transfer in ancestral *Bdellovibrio*

My work on the DslA publication also had some interesting outcomes. The phylogenetic analysis of this protein showed the clear possibility of a lateral gene transfer event in a *B. bacteriovorus* ancestor. No other Oligoflexia or closely related δ-proteobacteria appeared in the clade, which was instead populated with γ-, β- and α-proteobacteria from a range of environments. DslA was found to have been adapted to intracellular predation, specifically for lysis of the deacetylated bdelloplast wall to release the matured progeny. It has feasibly been adapted in these other bacteria to suit their lifestyles. For example, its presence in α-proteobacterial plant symbiotes, such as *Rhizobiales*, could be to reduce bacterial competition and encourage the growth of the plant root tissue.

6.1.6 Concluding remarks

In my investigation of *divIVA* and its operonal neighbours, I have found a potential interaction network that involves other division proteins, such as ParA3, and several novel systems, such as amino acid homeostasis, protection from reactive oxygen species and menaquinone biosynthesis. I have also identified a potential peptidoglycan salvaging pathway for the processing of exogenous peptidoglycan and given a preliminary analysis of the adaptations to the *B. bacteriovorus dcw* cluster.

7 References

1977. 5-Branched Figtree - Research on Khmer Buddhism - French - Bizot,F. *Man in India*, 57**,** 278-279.

ABHYANKAR, W., DE KONING, L. J., BRUL, S. & DE KOSTER, C. G. 2014. Spore proteomics: the past, present and the future. *Fems Microbiology Letters,* 358**,** 137-144.

ALARCON, F., DE VASCONCELOS, A. T. R., YIM, L. & ZAHA, A. 2007. Genes involved in cell division in mycoplasmas. *Genetics and Molecular Biology,* 30**,** 174-181.

ANASHKIN, V. A., SALMINEN, A., TUOMINEN, H. K., ORLOV, V. N., LAHTI, R. & BAYKOV, A. A. 2015. Cystathionine beta-Synthase (CBS) Domain-containing Pyrophosphatase as a Target for Diadenosine Polyphosphates in Bacteria. *Journal of Biological Chemistry,* 290**,** 27594-27603.

ANTHONY, C. 2011. How half a century of research was required to understand bacterial growth on C-1 and C-2 compounds; the story of the serine cycle and the ethylmalonyl-CoA pathway. *Science Progress,* 94**,** 109-137.

ARUMUGAM, S., PETRASEK, Z. & SCHWILLE, P. 2014. MinCDE exploits the dynamic nature of FtsZ filaments for its spatial regulation. *Proceedings of the National Academy of Sciences of the United States of America,* 111**,** E1192-E1200.

AZZOLINA, B. A., YUAN, X. L., ANDERSON, M. S. & EL-SHERBEINI, M. 2001. The cell wall and cell division gene cluster in the Mra operon of *Pseudomonas aeruginosa*: Cloning, production, and purification of active enzymes. *Protein Expression and Purification,* 21**,** 393-400.

BABINSKI, K. J., KANJILAL, S. J. & RAETZ, C. R. H. 2002. Accumulation of the lipid A precursor UDP-2,3-diacylglucosamine in an *Escherichia coli* mutant lacking the *lpxH* gene. *Journal of Biological Chemistry,* 277**,** 25947-25956.

BABU, M., DIAZ-MEJIA, J. J., VLASBLOM, J., GAGARINOVA, A., PHANSE, S., GRAHAM, C., YOUSIF, F., DING, H. M., XIONG, X. J., NAZARIANS-ARMAVIL, A., ALAMGIR, M., ALI, M., POGOUTSE, O., PE'ER, A., ARNOLD, R., MICHAUT, M., PARKINSON, J., GOLSHANI, A., WHITFIELD, C., WODAK, S. J., MORENO-HAGELSIEB, G., GREENBLATT, J. F. & EMILI, A. 2011. Genetic Interaction Maps in *Escherichia coli* Reveal Functional Crosstalk among Cell Envelope Biogenesis Pathways. *Plos Genetics,* 7(11): e1002377.

BACH, J. N., ALBRECHT, N. & BRAMKAMP, M. 2014. Imaging DivIVA dynamics using photo-convertible and activatable fluorophores in *Bacillus subtilis*. *Frontiers in Microbiology,* 5: 59.

BAILEY, E. & HULLIN, R. P. 1966. METABOLISM OF GLYOXYLATE BY CELL-FREE EXTRACTS OF *PSEUDOMONAS* SP. *Biochemical Journal,* 101**,** 755-763.

BANGERA, M., PANIGRAHI, R., SAGURTHI, S. R., SAVITHRI, H. S. & MURTHY, M. R. N. 2015. Structural and functional analysis of two universal stress proteins YdaA and YnaF from *Salmonella typhimurium*: possible roles in microbial stress tolerance. *Journal of Structural Biology,* 189**,** 238-250.

BAR-ZEEV, E., AVISHAY, I., BIDLE, K. D. & BERMAN-FRANK, I. 2013. Programmed cell death in the marine cyanobacterium *Trichodesmium* mediates carbon and nitrogen export. *Isme Journal,* 7**,** 2340-2348.

BERNTSSON, R. P. A., DOEVEN, M. K., FUSETTI, F., DUURKENS, R. H., SENGUPTA, D., MARRINK, S.-J., THUNNISSEN, A.-M. W. H., POOLMAN, B. & SLOTBOOM, D.-J. 2009. The structural basis for peptide selection by the transport receptor OppA. *Embo Journal,* 28**,** 1332-1340.

BERTRAND, J. A., AUGER, G., MARTIN, L., FANCHON, E., BLANOT, D., LA BELLER, D., VAN HEIJENOORT, J. & DIDEBERG, O. 1999. Determination of the MurD mechanism through crystallographic analysis of enzyme complexes. *Journal of Molecular Biology,* 289**,** 579-590.

BLUM, M., CHANG, H. Y., CHUGURANSKY, S., GREGO, T., KANDASAAMY, S., MITCHELL, A., NUKA, G., PAYSAN-LAFOSSE, T., QURESHI, M., RAJ, S., RICHARDSON, L., SALAZAR, G. A., WILLIAMS, L., BORK, P., BRIDGE, A., GOUGH, J., HAFT, D. H., LETUNIC, I., MARCHLER-BAUER, A., MI, H. Y., NATALE, D. A., NECCI, M., ORENGO, C. A., PANDURANGAN, A. P., RIVOIRE, C., SIGRIST, C. J. A., SILLITOE, I., THANKI, N., THOMAS, P. D., TOSATTO, S. C. E., WU, C. H., BATEMAN, A. & FINN, R. D. 2021. The InterPro protein families and domains database: 20 years on. *Nucleic Acids Research,* 49**,** D344-D354.

BONNEAU, A., ROCHE, B. & SCHALK, I. J. 2020. Iron acquisition in *Pseudomonas aeruginosa* by the siderophore pyoverdine: an intricate interacting network including periplasmic and membrane proteins. *Scientific Reports,* 10**,** 11.

BROWN, K., LI, W. & KAUR, P. 2017. Role of Aromatic and Negatively Charged Residues of DrrB in Multisubstrate Specificity Conferred by the DrrAB System of *Streptomyces peucetius*. *Biochemistry,* 56**,** 1921-1931.

BUDDELMEIJER, N. & BECKWITH, J. 2004. A complex of the *Escherichia coli* cell division proteins FtsL, FtsB and FtsQ forms independently of its localization to the septal region. *Molecular Microbiology,* 52**,** 1315-1327.

BUKOWSKA-FANIBAND, E., ANDERSSON, T. & LOOD, R. 2020. Studies on Bd0934 and Bd3507, Two Secreted Nucleases from *Bdellovibrio bacteriovorus*, Reveal Sequential Release of Nucleases during the Predatory Cycle. *Journal of Bacteriology,* 202 e00150-20.

BUSH, M. & DIXON, R. 2012. The Role of Bacterial Enhancer Binding Proteins as Specialized Activators of sigma(54)-Dependent Transcription. *Microbiology and Molecular Biology Reviews,* 76**,** 497-529.

CEASAR, S. A. & IGNACIMUTHU, S. 2012. Genetic engineering of crop plants for fungal resistance: role of antifungal genes. *Biotechnology Letters,* 34**,** 995-1002.

CHAUDHURI, R. R., LOMAN, N. J., SNYDER, L. A. S., BAILEY, C. M., STEKEL, D. J. & PALLEN, M. J. 2008. xBASE2: a comprehensive resource for comparative bacterial genomics. *Nucleic Acids Research,* 36**,** D543-D546.

CHEN, Y., LI, T. L., LIN, X. B., LI, X., LI, X. D. & GUO, Z. H. 2017. Crystal structure of the thioesterification conformation of *Bacillus subtilis* o-succinylbenzoyl-CoA synthetase reveals a distinct substrate-binding mode. *Journal of Biological Chemistry,* 292**,** 12296-12310.

CHEN, Y. Z., JIANG, Y. P. & GUO, Z. H. 2016. Mechanistic Insights from the Crystal Structure of *Bacillus subtilis* o-Succinylbenzoyl-CoA Synthetase Complexed with the Adenylate Intermediate. *Biochemistry,* 55**,** 6685-6695.

CHO, J., LEE, C.-J., ZHAO, J., YOUNG, H. E. & ZHOU, P. 2016. Structure of the essential *Haemophilus influenzae* UDP-diacylglucosamine pyrophosphohydrolase LpxH in lipid A biosynthesis. *Nature Microbiology,* 1 6456-64.

CHO, J., LEE, M., COCHRANE, C. S., WEBSTER, C. G., FENTON, B. A., ZHAO, J. S., HONG, J. Y. & ZHOU, P. 2020. Structural basis of the UDP-diacylglucosamine pyrophosphohydrolase LpxH inhibition by sulfonyl piperazine antibiotics. *Proceedings of the National Academy of Sciences of the United States of America,* 117**,** 4109-4116.

CHOUKATE, K. & CHAUDHURI, B. 2020. Structural basis of self-assembly in the lipid-binding domain of mycobacterial polar growth factor Wag31. *Iucrj,* 7**,** 767-776.

CHRISTGEN, S. L. & BECKER, D. F. 2019. Role of Proline in Pathogen and Host Interactions. *Antioxidants & Redox Signaling,* 30**,** 683-709.

CRAMER, S. D., FERREE, P. M., LIN, K., MILLINER, D. S. & HOLMES, R. P. 1999. The gene encoding hydroxypyruvate reductase (GRHPR) is mutated in patients with primary hyperoxaluria type II. *Human Molecular Genetics,* 8**,** 2063-2069.

DAI, K. & LUTKENHAUS, J. 1992. THE PROPER RATIO OF FTSZ TO FTSA IS REQUIRED FOR CELL-DIVISION TO OCCUR IN *ESCHERICHIA-COLI*. *Journal of Bacteriology,* 174**,** 6145-6151.

DAVIDSON, A. L., DASSA, E., ORELLE, C. & CHEN, J. 2008. Structure, function, and evolution of bacterial ATP-binding cassette systems. *Microbiology and Molecular Biology Reviews,* 72**,** 317-364.

DAVIS, M. C., KESTHELY, C. A., FRANKLIN, E. A. & MACLELLAN, S. R. 2017. The essential activities of the bacterial sigma factor. *Canadian Journal of Microbiology,* 63**,** 89-99.

DE LA FUENTE, A., PALACIOS, P. & VICENTE, M. 2001. Transcription of the *Escherichia coli dcw* cluster: Evidence for distal upstream transcripts being involved in the expression of the downstream *ftsZ* gene. *Biochimie,* 83**,** 109-115.

DEWAR, S. J., BEGG, K. J. & DONACHIE, W. D. 1992. INHIBITION OF CELL-DIVISION INITIATION BY AN IMBALANCE IN THE RATIO OF FTSA TO FTSZ. *Journal of Bacteriology,* 174**,** 6314-6316.

DIAGO-NAVARRO, E., MORA, L., BUCKINGHAM, R. H., DIAZ-OREJAS, R. & LEMONNIER, M. 2009. Novel *Escherichia coli* RF1 mutants with decreased translation termination activity and increased sensitivity to the cytotoxic effect of the bacterial toxins Kid and RelE. *Molecular Microbiology,* 71**,** 66-78.

DIEZ, V., TRAIKOV, S., SCHMEISSER, K., DAS ADHIKARI, A. K. & KURZCHALIA, T. V. 2021. Glycolate combats massive oxidative stress by restoring redox potential in *Caenorhabditis elegans*. *Communications Biology,* 4 151-164.

DOLAN, S. K. & WELCH, M. 2018. The Glyoxylate Shunt, 60 Years On. *In:* GOTTESMAN, S. (ed.) *Annual Review of Microbiology, Vol 72.* Palo Alto: Annual Reviews.

DONG, B. X., LAN, O. Y., QIN, L. & LI, G. 2007. A rapid and simple method for screening large numbers of recombinant DNA clones. *Journal of Rapid Methods and Automation in Microbiology,* 15**,** 244-252.

DOPKINS, B. J., TIPTON, P. A., THODEN, J. B. & HOLDEN, H. M. 2016. Structural Studies on a Glucosamine/Glucosaminide N-Acetyltransferase. *Biochemistry,* 55**,** 4495-4508.

DOU, S. X., WANG, P. Y., XU, H. Q. & XI, X. G. 2004. The DNA binding properties of the *Escherichia coli* RecQ helicase. *Journal of Biological Chemistry,* 279**,** 6354-6363.

DUNN, M. F., RAMIREZ-TRUJILLO, J. A. & HERNANDEZ-LUCAS, I. 2009. Major roles of isocitrate lyase and malate synthase in bacterial and fungal pathogenesis. *Microbiology-Sgm,* 155**,** 3166-3175.

EGAN, A. J. F., ERRINGTON, J. & VOLLMER, W. 2020. Regulation of peptidoglycan synthesis and remodelling. *Nature Reviews Microbiology,* 18**,** 446-460.

EGUCHI, Y., ISHII, E., YAMANE, M. & UTSUMI, R. 2012. The connector SafA interacts with the multi-sensing domain of PhoQ in *Escherichia coli*. *Molecular Microbiology,* 85**,** 299-313.

EL-SHANSHOURY, A. R., ABO-AMER, A. E. & ALZAHRANI, O. M. 2016. Isolation of *Bdellovibrio* sp. from Wastewater and Their Potential Application in Control of *Salmonella paratyphi* in Water. *Geomicrobiology Journal,* 33**,** 886-893.

ESCALANTE, A., CERVANTES, A. S., GOSSET, G. & BOLIVAR, F. 2012. Current knowledge of the *Escherichia coli* phosphoenolpyruvate-carbohydrate phosphotransferase system: peculiarities of regulation and impact on growth and product formation. *Applied Microbiology and Biotechnology,* 94**,** 1483-1494.

EVANS, K. J., LAMBERT, C. & SOCKETT, R. E. 2007. Predation by *Bdellovibrio bacteriovorus* HD100 requires type IV pili. *Journal of Bacteriology,* 189**,** 4850-4859.

FAVROT, L., BLANCHARD, J. S. & VERGNOLLE, O. 2016. Bacterial GCN5-Related N-Acetyltransferases: From Resistance to Regulation. *Biochemistry,* 55**,** 989-1002.

FENG, S. G., TAN, C. H., CONSTANCIAS, F., KOHLI, G. S., COHEN, Y. & RICE, S. A. 2017. Predation by *Bdellovibrio bacteriovorus* significantly reduces viability and alters the microbial community composition of activated sludge flocs and granules. *Fems Microbiology Ecology,* 93(4).

FENTON, A. K., KANNA, M., WOODS, R. D., AIZAWA, S. I. & SOCKETT, R. E. 2010. Shadowing the Actions of a Predator: Backlit Fluorescent Microscopy Reveals Synchronous Nonbinary Septation of Predatory *Bdellovibrio* inside Prey and Exit through Discrete Bdelloplast Pores. *Journal of Bacteriology,* 192**,** 6329-6335.

FICHMAN, Y., GERDES, S. Y., KOVACS, H., SZABADOS, L., ZILBERSTEIN, A. & CSONKA, L. N. 2015. Evolution of proline biosynthesis: enzymology,

bioinformatics, genetics, and transcriptional regulation. *Biological Reviews,* 90**,** 1065-1099.

FIELDS, S. & SONG, O. K. 1989. A NOVEL GENETIC SYSTEM TO DETECT PROTEIN PROTEIN INTERACTIONS. *Nature,* 340**,** 245-246.

FIGTREE, G. A., RADHOLM, K. & NEAL, B. 2019. Response by Figtree et al to Letter Regarding Article, "Canagliflozin and Heart Failure in Type 2 Diabetes Mellitus: Results From the CANVAS Program (Canagliflozin Cardiovascular Assessment Study)". *Circulation,* 139**,** 418-419.

FILIPPOVA, E. V., WESTON, L. A., KUHN, M. L., GEISSLER, B., GEHRING, A. M., ARMOUSH, N., ADKINS, C. T., MINASOV, G., DUBROVSKA, I., SHUVALOVA, L., WINSOR, J. R., LAVIS, L. D., SATCHELL, K. J. F., BECKER, D. P., ANDERSON, W. F. & JOHNSON, R. J. 2013. Large Scale Structural Rearrangement of a Serine Hydrolase from *Francisella tularensis* Facilitates Catalysis. *Journal of Biological Chemistry,* 288**,** 10522-10535.

FLARDH, K. 2003. Essential role of DivIVA in polar growth and morphogenesis in *Streptomyces coelicolor* A3(2). *Molecular Microbiology,* 49**,** 1523-1536.

FRANCIS, F., RAMIREZ-ARCOS, S., SALIMNIA, H., VICTOR, C. & DILLON, J. A. R. 2000. Organization and transcription of the *division cell wall* (*dcw*) cluster in *Neisseria gonorrhoeae*. *Gene,* 251**,** 141-151.

FRIESEN, M. L. 2012. Widespread fitness alignment in the legume-rhizobium symbiosis. *New Phytologist,* 194**,** 1096-1111.

FRUTOS-GRILO, E., MARSAL, M., IRAZOKI, O., BARBE, J. & CAMPOY, S. 2020. The Interaction of RecA With Both CheA and CheW Is Required for Chemotaxis. *Frontiers in Microbiology,* 11**,** 15.

FUMEAUX, C. & BERNHARDT, T. G. 2017. Identification of MupP as a New Peptidoglycan Recycling Factor and Antibiotic Resistance Determinant in *Pseudomonas aeruginosa*. *Mbio,* 8 e00102-17.

GARDNER, J. G. & ESCALANTE-SEMERENA, J. C. 2008. Biochemical and mutational analyses of AcuA, the acetyltransferase enzyme that controls the activity of the acetyl coenzyme A synthetase (AcsA) in *Bacillus subtilis*. *Journal of Bacteriology,* 190**,** 5132-5136.

GARDNER, J. G. & ESCALANTE-SEMERENA, J. C. 2009. In *Bacillus subtilis*, the Sirtuin Protein Deacetylase, Encoded by the srtN Gene (Formerly yhdZ), and Functions Encoded by the acuABC Genes Control the Activity of Acetyl Coenzyme A Synthetase. *Journal of Bacteriology,* 191**,** 1749-1755.

GEORG, J. & HESS, W. R. 2011. cis-Antisense RNA, Another Level of Gene Regulation in Bacteria. *Microbiology and Molecular Biology Reviews,* 75**,** 286-300.

GINDA, K., BEZULSKA, M., ZIOLKIEWICZ, M., DZIADEK, J., ZAKRZEWSKA-CZERWINSKA, J. & JAKIMOWICZ, D. 2013. ParA of *Mycobacterium smegmatis*

co-ordinates chromosome segregation with the cell cycle and interacts with the polar growth determinant DivIVA. *Molecular Microbiology,* 87**,** 998-1012.

GIRAUD, M. F., LEONARD, G. A., FIELD, R. A., BERLIND, C. & NAISMITH, J. H. 2000. RmlC, the third enzyme of dTDP-L-rhamnose pathway, is a new class of epimerase. *Nature Structural Biology,* 7**,** 398-402.

GOPHNA, U., CHARLEBOIS, R. L. & DOOLITTLE, W. F. 2006. Ancient lateral gene transfer in the evolution of *Bdellovibrio bacteriovorus*. *Trends in Microbiology,* 14**,** 64-69.

GOSSET, G., ZHANG, Z. G., NAYYAR, S. N., CUEVAS, W. A. & SAIER, M. H. 2004. Transcriptome analysis of Crp-dependent catabolite control of gene expression in *Escherichia coli*. *Journal of Bacteriology,* 186**,** 3516-3524.

GU, D. H., PARK, M. Y. & KIM, J. S. 2017. An asymmetric dimeric structure of TrmJ tRNA methyltransferase from *Zymomonas mobilis* with a flexible C-terminal dimer. *Biochemical and Biophysical Research Communications,* 488**,** 407-412.

GUAN, Y., LI, S. G., FAN, X. F. & SU, Z. H. 2016. Application of Somatic Embryogenesis in Woody Plants. *Frontiers in Plant Science,* 7:938.

GUZMAN, L. M., BARONDESS, J. J. & BECKWITH, J. 1992. FTSL, AN ESSENTIAL CYTOPLASMIC MEMBRANE-PROTEIN INVOLVED IN CELL-DIVISION IN *ESCHERICHIA-COLI*. *Journal of Bacteriology,* 174**,** 7716-7728.

HAHN, M. W., SCHMIDT, J., KOLL, U., ROHDE, M., VERBARG, S., PITT, A., NAKAI, R., NAGANUMA, T. & LANG, E. 2017. *Silvanigrella aquatica* gen. nov., sp nov., isolated from a freshwater lake, description of Silvanigrellaceae fam. nov and Silvanigrellales ord. nov., reclassification of the order Bdellovibrionales in the class Oligoflexia, reclassification of the families Bacteriovoracaceae and Halobacteriovoraceae in the new order Bacteriovoracales ord. nov., and reclassification of the family Pseudobacteriovoracaceae in the order Oligoflexales. *International Journal of Systematic and Evolutionary Microbiology,* 67**,** 2555-2568.

HAMMOND, L. R., WHITE, M. L. & ESWARA, P. J. 2019. vIVA la DivIVA! *Journal of Bacteriology,* 201:e00245-19.

HANAHAN, D. 1983. STUDIES ON TRANSFORMATION OF *ESCHERICHIA-COLI* WITH PLASMIDS. *Journal of Molecular Biology,* 166**,** 557-580.

HANDFORD, J. I., IZE, B., BUCHANAN, G., BUTLAND, G. P., GREENBLATT, J., EMILI, A. & PALMER, T. 2009. Conserved Network of Proteins Essential for Bacterial Viability. *Journal of Bacteriology,* 191**,** 4732-4749.

HANSEN, R. W. & HAYASHI, J. A. 1962. GLYCOLATE METABOLISM IN *ESCHERICHIA COLI*. *Journal of Bacteriology,* 83**,** 679-687.

HANSEN, T. & SCHONHEIT, P. 2005. *Escherichia coli* phosphoglucose isomerase can be substituted by members of the PGI family, the PGI/PMI family, and the cPGI family. *Fems Microbiology Letters,* 250**,** 49-53.

HARDING, C. J., HUWILER, S. G., SOMERS, H., LAMBERT, C., RAY, L. J., TILL, R., TAYLOR, G., MOYNIHAN, P. J., SOCKETT, R. E. & LOVERING, A. L. 2020. A lysozyme with altered substrate specificity facilitates prey cell exit by the periplasmic predator *Bdellovibrio bacteriovorus*. *Nature Communications,* 11:4817.

HARRY, E., MONAHAN, L. & THOMPSON, L. 2006. Bacterial cell division: The mechanism and its precison. *In:* JEON, K. W. (ed.) *International Review of Cytology - a Survey of Cell Biology, Vol 253.* San Diego: Elsevier Academic Press Inc.

HEMPEL, A. M., WANG, S.-B., LETEK, M., GIL, J. A. & FLARDH, K. 2008. Assemblies of DivIVA Mark Sites for Hyphal Branching and Can Establish New Zones of Cell Wall Growth in *Streptomyces coelicolor*. *Journal of Bacteriology,* 190**,** 7579-7583.

HEURGUE-HAMARD, V., CHAMP, S., ENGSTROM, A., EHRENBERG, M. & BUCKINGHAM, R. H. 2002. The hemK gene in *Escherichia coli* encodes the N(5)-glutamine methyltransferase that modifies peptide release factors. *Embo Journal,* 21**,** 769-778.

HOBLEY, L., FUNG, R. K. Y., LAMBERT, C., HARRIS, M., DABHI, J. M., KING, S. S., BASFORD, S. M., UCHIDA, K., TILL, R., AHMAD, R., AIZAWA, S., GOMELSKY, M. & SOCKETT, R. E. 2012a. Discrete Cyclic di-GMP-Dependent Control of Bacterial Predation versus Axenic Growth in *Bdellovibrio bacteriovorus*. *Plos Pathogens,* 8**,** 13.

HOBLEY, L., LERNER, T. R., WILLIAMS, L. E., LAMBERT, C., TILL, R., MILNER, D. S., BASFORD, S. M., CAPENESS, M. J., FENTON, A. K., ATTERBURY, R. J., HARRIS, M. A. T. S. & SOCKETT, R. E. 2012b. Genome analysis of a simultaneously predatory and prey-independent, novel *Bdellovibrio bacteriovorus* from the River Tiber, supports in silico predictions of both ancient and recent lateral gene transfer from diverse bacteria. *Bmc Genomics,* 13:e1002493.

HOFFMANN, T., VON BLOHN, C., STANEK, A., MOSES, S., BARZANTNY, H. & BREMER, E. 2012. Synthesis, Release, and Recapture of Compatible Solute Proline by Osmotically Stressed *Bacillus subtilis* Cells. *Applied and Environmental Microbiology,* 78**,** 5753-5762.

HOTTMANN, I., BORISOVA, M., SCHÄFFER, C. & MAYER, C. 2021. Peptidoglycan Salvage Enables the Periodontal Pathogen *Tannerella forsythia* to Survive within the Oral Microbial Community. *Microbial Physiology* 31:123-134.

HOUOT, L., FANNI, A., DE BENTZMANN, S. & BORDI, C. 2012. A bacterial two-hybrid genome fragment library for deciphering regulatory networks of the opportunistic pathogen *Pseudomonas aeruginosa*. *Microbiology-Sgm,* 158**,** 1964-1971.

HUANG, Z. W., PAN, X. Y., XU, N. & GUO, M. L. 2019. Bacterial chemotaxis coupling protein: Structure, function and diversity. *Microbiological Research,* 219**,** 40-48.

HULLIN, R. P. 1975. Glyoxylate reductase, two forms from *Pseudomonas*. *Methods in enzymology,* 41**,** 343-8.

ILAG, L. L., JAHN, D., EGGERTSSON, G. & SOLL, D. 1991. THE *ESCHERICHIA-COLI HEML* GENE ENCODES GLUTAMATE 1-SEMIALDEHYDE AMINOTRANSFERASE. *Journal of Bacteriology,* 173**,** 3408-3413.

INABA, K. 2008. Protein disulfide bond generation in *Escherichia coli* DsbB-DsbA. *Journal of Synchrotron Radiation,* 15**,** 199-201.

INABA, K. & ITO, K. 2008. Structure and mechanisms of the DsbB-DsbA disulfide bond generation machine. *Biochimica Et Biophysica Acta-Molecular Cell Research,* 1783**,** 520-529.

INABA, K., MURAKAMI, S., NAKAGAWA, A., IIDA, H., KINJO, M., ITO, K. & SUZUKI, M. 2009. Dynamic nature of disulphide bond formation catalysts revealed by crystal structures of DsbB. *Embo Journal,* 28**,** 779-791.

ISLAM, R., BROWN, S., TAHERI, A. & DUMENYO, C. K. 2019. The Gene Encoding NAD-Dependent Epimerase/Dehydratase, *wcaG*, Affects Cell Surface Properties, Virulence, and Extracellular Enzyme Production in the Soft Rot Phytopathogen, *Pectobacterium carotovorum*. *Microorganisms,* 7**,** 13.

ITO, T. & DOWNS, D. M. 2020. Pyridoxal Reductase, PdxI, Is Critical for Salvage of Pyridoxal in *Escherichia coli*. *Journal of Bacteriology,* 202(12):e00056-20.

ITO, T., IIMORI, J., TAKAYAMA, S., MORIYAMA, A., YAMAUCHI, A., HEMMI, H. & YOSHIMURA, T. 2013. Conserved Pyridoxal Protein That Regulates Ile and Val Metabolism. *Journal of Bacteriology,* 195**,** 5439-5449.

ITO, T., YAMAMOTO, K., HORI, R., YAMAUCHI, A., DOWNS, D. M., HEMMI, H. & YOSHIMURA, T. 2019. Conserved Pyridoxal 5 '-Phosphate-Binding Protein YggS Impacts Amino Acid Metabolism through Pyridoxine 5 '-Phosphate in *Escherichia coli*. *Applied and Environmental Microbiology,* 85(11):e00430-19.

ITO, T., YAMAUCHI, A., HEMMI, H. & YOSHIMURA, T. 2016. Ophthalmic acid accumulation in an *Escherichia coli* mutant lacking the conserved pyridoxal 5 '-phosphate-binding protein YggS. *Journal of Bioscience and Bioengineering,* 122**,** 689-693.

JAROENSUK, J., ATICHARTPONGKUL, S., CHIONH, Y. H., WONG, Y. H., LIEW, C. W., MCBEE, M. E., THONGDEE, N., PRESTWICH, E. G., DEMOTT, M. S., MONGKOLSUK, S., DEDON, P. C., LESCAR, J. & FUANGTHONG, M. 2016. Methylation at position 32 of tRNA catalyzed by TrmJ alters oxidative stress response in *Pseudomonas aeruginosa*. *Nucleic Acids Research,* 44**,** 10834-10848.

JENSEN, K. F. 1993. THE *ESCHERICHIA-COLI* K-12 WILD TYPES W3110 AND MG1655 HAVE AND RPH FRAMESHIFT MUTATION THAT LEADS TO PYRIMIDINE STARVATION DUE TO LOW PYRE EXPRESSION LEVELS. *Journal of Bacteriology,* 175**,** 3401-3407.

JESKE, O., SCHULER, M., SCHUMANN, P., SCHNEIDER, A., BOEDEKER, C., JOGLER, M., BOLLSCHWEILER, D., ROHDE, M., MAYER, C., ENGELHARDT, H.,

SPRING, S. & JOGLER, C. 2015. Planctomycetes do possess a peptidoglycan cell wall. *Nature Communications,* 6, 7116.

JIA, Q., HU, X. L., SHI, D. W., ZHANG, Y., SUN, M. H., WANG, J. W., MI, K. X. & ZHU, G. F. 2016. Universal stress protein Rv2624c alters abundance of arginine and enhances intracellular survival by ATP binding in mycobacteria. *Scientific Reports,* 6**,** 10.

JINDAL, L. & EMBERLY, E. 2019. DNA segregation under Par protein control. *Plos One,* 14**,** 20.

JONES, D. T., TAYLOR, W. R. & THORNTON, J. M. 1992. THE RAPID GENERATION OF MUTATION DATA MATRICES FROM PROTEIN SEQUENCES. *Computer Applications in the Biosciences,* 8**,** 275-282.

KALYNYCH, S., MORONA, R. & CYGLER, M. 2014. Progress in understanding the assembly process of bacterial O-antigen. *Fems Microbiology Reviews,* 38**,** 1048-1065.

KAMRAN, M., DUBEY, P., VERMA, V., DASGUPTA, S. & DHAR, S. K. 2018. *Helicobacter pylori* shows asymmetric and polar cell divisome assembly associated with DNA replisome. *Febs Journal,* 285**,** 2531-2547.

KANG, C. M., NYAYAPATHY, S., LEE, J. Y., SUH, J. W. & HUSSON, R. N. 2008. Wag31, a homologue of the cell division protein DivIVA, regulates growth, morphology and polar cell wall synthesis in mycobacteria. *Microbiology-Sgm,* 154**,** 725-735.

KARIMOVA, G., DAUTIN, N. & LADANT, D. 2005. Interaction network among *Escherichia coli* membrane proteins involved in cell division as revealed by bacterial two-hybrid analysis. *Journal of Bacteriology,* 187**,** 2233-2243.

KARIMOVA, G., PIDOUX, J., ULLMANN, A. & LADANT, D. 1998. A bacterial two-hybrid system based on a reconstituted signal transduction pathway. *Proceedings of the National Academy of Sciences of the United States of America,* 95**,** 5752-5756.

KARIMOVA, G., ULLMANN, A. & LADANT, D. 2000a. Bacterial two-hybrid system that exploits a cAMP signaling cascade in *Escherichia coli*. *Applications of Chimeric Genes and Hybrid Proteins, Pt C,* 328**,** 59-73.

KARIMOVA, G., ULLMANN, A. & LADANT, D. 2000b. *Bordetella pertussis* adenylate cyclase toxin as a tool to analyze molecular interactions in a bacterial two-hybrid system. *International Journal of Medical Microbiology,* 290**,** 441-445.

KARIMOVA, G., ULLMANN, A. & LADANT, D. 2001. Protein-protein interaction between *Bacillus stearothermophilus* tyrosyl-tRNA synthetase subdomains revealed by a bacterial two-hybrid system. *Journal of Molecular Microbiology and Biotechnology,* 3**,** 73-82.

KARUNKER, I., ROTEM, O., DORI-BACHASH, M., JURKEVITCH, E. & SOREK, R. 2013. A Global Transcriptional Switch between the Attack and Growth Forms of *Bdellovibrio bacteriovorus*. *Plos One,* 8(4):e61850.

KAVAL, K. G., RISMONDO, J. & HALBEDEL, S. 2014. A function of DivIVA in *Listeria monocytogenes* division site selection. *Molecular Microbiology,* 94**,** 637-654.

KE, N., LANDETA, C., WANG, X. Y., BOYD, D., ESER, M. & BECKWITH, J. 2018. Identification of the Thioredoxin Partner of Vitamin K Epoxide Reductase in Mycobacterial Disulfide Bond Formation. *Journal of Bacteriology,* 200(16):e00137-18.

KEMP, B. E. 2004. Bateman domains and adenosine derivatives form a binding contract. *Journal of Clinical Investigation,* 113**,** 182-184.

KESAVARDHANA, S., MALIREDDI, R. K. S. & KANNEGANTI, T. D. 2020. Caspases in Cell Death, Inflammation, and Pyroptosis. *In:* YOKOYAMA, W. M. (ed.) *Annual Review of Immunology, Vol 38.* Palo Alto: Annual Reviews 38: 567-595.

KHOSRAVI, A. D., SIROUS, M., ABSALAN, Z., TABANDEH, M. R. & SAVARI, M. 2019. Comparison Of drrA And drrB Efflux Pump Genes Expression In Drug-Susceptible And -Resistant *Mycobacterium tuberculosis* Strains Isolated From Tuberculosis Patients In Iran. *Infection and Drug Resistance,* 12**,** 3437-3444.

KLEMENCIC, M., NOVINEC, M. & DOLINAR, M. 2015. Orthocaspases are proteolytically active prokaryotic caspase homologues: the case of *Microcystis aeruginosa*. *Molecular Microbiology,* 98**,** 142-150.

KOIS-OSTROWSKA, A., STRZALKA, A., LIPIETTA, N., TILLEY, E., ZAKRZEWSKA-CZERWINSKA, J., HERRON, P. & JAKIMOWICZ, D. 2016. Unique Function of the Bacterial Chromosome Segregation Machinery in Apically Growing *Streptomyces* - Targeting the Chromosome to New Hyphal Tubes and its Anchorage at the Tips. *Plos Genetics,* 12(12):e1006488.

KOVAL, S. F., HYNES, S. H., FLANNAGAN, R. S., PASTERNAK, Z., DAVIDOV, Y. & JURKEVITCH, E. 2013. *Bdellovibrio exovorus* sp nov., a novel predator of *Caulobacter crescentus*. *International Journal of Systematic and Evolutionary Microbiology,* 63**,** 146-151.

KRAUSE, K., MACIAG-DORSZYNSKA, M., WOSINSKI, A., GAFFKE, L., MORCINEK-ORLOWSKA, J., RINTZ, E., BIELANSKA, P., SZALEWSKA-PALASZ, A., MUSKHELISHVILI, G. & WEGRZYN, G. 2020. The Role of Metabolites in the Link between DNA Replication and Central Carbon Metabolism in *Escherichia coli*. *Genes,* 11.

KUMAR, S., STECHER, G., LI, M., KNYAZ, C. & TAMURA, K. 2018. MEGA X: Molecular Evolutionary Genetics Analysis across Computing Platforms. *Molecular Biology and Evolution,* 35**,** 1547-1549.

KURU, E., LAMBERT, C., RITTICHIER, J., TILL, R., DUCRET, A., DEROUAUX, A., GRAY, J., BIBOY, J., VOLLMER, W., VANNIEUWENHZE, M., BRUN, Y. V. & SOCKETT, R. E. 2017. Fluorescent D-amino-acids reveal bi-cellular cell wall modifications important for *Bdellovibrio bacteriovorus* predation. *Nature Microbiology,* 2**,** 1648-1657.

LAGE, O. M., BONDOSO, J. & LOBO-DA-CUNHA, A. 2013. Insights into the ultrastructural morphology of novel *Planctomycetes*. *Antonie Van Leeuwenhoek International Journal of General and Molecular Microbiology,* 104**,** 467-476.

LAKSHMANAN, P. & TAJI, A. 2000. Somatic embryogenesis in leguminous plants. *Plant Biology,* 2**,** 136-148.

LAMBERT, C., CHANG, C. Y., CAPENESS, M. J. & SOCKETT, R. E. 2010. The First Bite-Profiling the Predatosome in the Bacterial Pathogen *Bdellovibrio*. *Plos One,* 5(2):127-32.

LAMBERT, C., LERNER, T. R., BUI, N. K., SOMERS, H., AIZAWA, S. I., LIDDELL, S., CLARK, A., VOLLMER, W., LOVERING, A. L. & SOCKETT, R. E. 2016. Interrupting peptidoglycan deacetylation during *Bdellovibrio* predator-prey interaction prevents ultimate destruction of prey wall, liberating bacterial-ghosts. *Scientific Reports,* 6.

LASSALLE, L., ENGILBERGE, S., MADERN, D., VAUCLARE, P., FRANZETTI, B. & GIRARD, E. 2016. New insights into the mechanism of substrates trafficking in Glyoxylate/Hydroxypyruvate reductases (vol 6, 20629, 2016). *Scientific Reports,* 6.

LENZ, J. D., STOHL, E. A., ROBERTSON, R. M., HACKETT, K. T., FISHER, K., XIONG, K., LEE, M., HESEK, D., MOBASHERY, S., SEIFERT, H. S., DAVIES, C. & DILLARD, J. P. 2016. Amidase Activity of AmiC Controls Cell Separation and Stem Peptide Release and Is Enhanced by NlpD in *Neisseria gonorrhoeae*. *Journal of Biological Chemistry,* 291**,** 10916-10933.

LERNER, T. R., LOVERING, A. L., BUI, N. K., UCHIDA, K., AIZAWA, S. I., VOLLMER, W. & SOCKETT, R. E. 2012. Specialized Peptidoglycan Hydrolases Sculpt the Intra-bacterial Niche of Predatory *Bdellovibrio* and Increase Population Fitness. *Plos Pathogens,* 8(2):e1002524.

LI, X., YOKOTA, T., ITO, K., NAKAMURA, Y. & AIBA, H. 2007. Reduced action of polypeptide release factors induces mRNA cleavage and tmRNA tagging at stop codons in *Escherichia coli*. *Molecular Microbiology,* 63**,** 116-126.

LIANG, X. W., ZHANG, L., NATARAJAN, S. K. & BECKER, D. F. 2013. Proline Mechanisms of Stress Survival. *Antioxidants & Redox Signaling,* 19**,** 998-1011.

LIN, L., VALERIANO, M. O., HARMS, A., SOGAARD-ANDERSEN, L. & THANBICHLER, M. 2017. Bactofilin-mediated organization of the ParABS chromosome segregation system in *Myxococcus xanthus*. *Nature Communications,* 8, 1817.

LINDER, J. U., HAMMER, A. & SCHULTZ, J. E. 2004. The effect of HAMP domains on class IIIb adenylyl cyclases from *Mycobacterium tuberculosis*. *European Journal of Biochemistry,* 271**,** 2446-2451.

LIU, B., FUREVI, A., PEREPELOV, A. V., GUO, X., CAO, H. C., WANG, Q., REEVES, P. R., KNIREL, Y. A., WANG, L. & WIDMALM, G. 2020. Structure and genetics of *Escherichia coli* O antigens. *Fems Microbiology Reviews,* 44**,** 655-683.

LIU, W.-T., KARAVOLOS, M. H., BULMER, D. M., ALLAOUI, A., HORMAECHE, R. D. C. E., LEE, J. J. & KHAN, C. M. A. 2007. Role of the universal stress protein UspA of *Salmonella* in growth arrest, stress and virulence. *Microbial Pathogenesis,* 42**,** 2-10.

LLUCH-SENAR, M., QUEROL, E. & PINOL, J. 2010. Cell division in a minimal bacterium in the absence of ftsZ. *Molecular Microbiology,* 78**,** 278-289.

LOWRY, R. C., MILNER, D. S., AL-BAYATI, A. M. S., LAMBERT, C., FRANCIS, V. I., PORTER, S. L. & SOCKETT, R. E. 2019. Evolutionary diversification of the RomR protein of the invasive deltaproteobacterium, *Bdellovibrio bacteriovorus*. *Scientific Reports,* 9**,** 15.

LUBIN, E. A., HENRY, J. T., FIEBIG, A., CROSSON, S. & LAUB, M. T. 2016. Identification of the PhoB Regulon and Role of PhoU in the Phosphate Starvation Response of *Caulobacter crescentus*. *Journal of Bacteriology,* 198**,** 187-200.

LUTKENHAUS, J. 2007. Assembly dynamics of the bacterial MinCDE system and spatial regulation of the Z ring. *Annual Review of Biochemistry,* 76**,** 539-562.

MA, Y. F., PAN, F. & MCNEIL, M. 2002. Formation of dTDP-rhamnose is essential for growth of mycobacteria. *Journal of Bacteriology,* 184**,** 3392-3395.

MAKOWSKI, L., TROJANOWSKI, D., TILL, R., LAMBERT, C., LOWRY, R., SOCKETT, R. E. & ZAKRZEWSKA-CZERWINSKA, J. 2019. Dynamics of Chromosome Replication and Its Relationship to Predatory Attack Lifestyles in *Bdellovibrio bacteriovorus*. *Applied and Environmental Microbiology,* 85 14:e00730-19.

MALIK, A. & PREETY 2019. Purification and properties of plant chitinases: A review. *Journal of Food Biochemistry,* 43 3:e12762.

MALLA, S., NIRAULA, N. P., LIOU, K. & SOHNG, J. K. 2010. Self-resistance mechanism in *Streptomyces peucetius*: Overexpression of drrA, drrB and drrC for doxorubicin enhancement. *Microbiological Research,* 165**,** 259-267.

MARKELOVA, N. Y. 2010. Predacious bacteria, *Bdellovibrio* with potential for biocontrol. *International Journal of Hygiene and Environmental Health,* 213**,** 428-431.

MARTIN, A. C., WADHAMS, G. H. & ARMITAGE, J. P. 2001. The roles of the multiple CheW and CheA homologues in chemotaxis and in chemoreceptor localization in *Rhodobacter sphaeroides*. *Molecular Microbiology,* 40**,** 1261-1272.

MARTOS, A., RASO, A., JIMENEZ, M., PETRASEK, Z., RIVAS, G. & SCHWILLE, P. 2015. FtsZ Polymers Tethered to the Membrane by ZipA Are Susceptible to Spatial Regulation by Min Waves. *Biophysical Journal,* 108**,** 2371-2383.

MARTÍNEZ-TORRÓ, C., TORRES-PUIG, S., MARCOS-SILVA, M., HUGUET-RAMÓN, M., MUÑOZ-NAVARRO, C., LLUCH-SENAR, M., SERRANO, L., QUEROL, E., PIÑOL, J. & PICH, O. Q. 2021. Functional Characterization of the Cell Division Gene Cluster of the Wall-less Bacterium *Mycoplasma genitalium*. *Frontiers in Microbiology,* 12:695572.

MAURYA, G. K., MODI, K. & MISRA, H. S. 2016. Divisome and segrosome components of *Deinococcus radiodurans* interact through cell division regulatory proteins. *Microbiology-Sgm,* 162**,** 1321-1334.

MAXON, M. E., REDFIELD, B., CAI, X. Y., SHOEMAN, R., FUJITA, K., FISHER, W., STAUFFER, G., WEISSBACH, H. & BROT, N. 1989. REGULATION OF METHIONINE SYNTHESIS IN *ESCHERICHIA-COLI* - EFFECT OF THE METR PROTEIN ON THE EXPRESSION OF THE METE AND METR GENES. *Proceedings of the National Academy of Sciences of the United States of America,* 86**,** 85-89.

MAYER, C., KLUJ, R. M., MUHLECK, M., WALTER, A., UNSLEBER, S., HOTTMANN, I. & BORISOVA, M. 2019. Bacteria's different ways to recycle their own cell wall. *International Journal of Medical Microbiology,* 309 7:151326.

MCCLURE, R., BALASUBRAMANIAN, D., SUN, Y., BOBROVSKYY, M., SUMBY, P., GENCO, C. A., VANDERPOOL, C. K. & TJADEN, B. 2013. Computational analysis of bacterial RNA-Seq data. *Nucleic Acids Research,* 41(14):e140.

MENICHE, X., OTTEN, R., SIEGRIST, M. S., BAER, C. E., MURPHY, K. C., BERTOZZI, C. R. & SASSETTI, C. M. 2014. Subpolar addition of new cell wall is directed by DivIVA in mycobacteria. *Proceedings of the National Academy of Sciences of the United States of America,* 111**,** E3243-E3251.

MILES, J. S. & GUEST, J. R. 1984. NUCLEOTIDE-SEQUENCE AND TRANSCRIPTIONAL START POINT OF THE PHOSPHOMANNOSE ISOMERASE GENE (MANA) OF *ESCHERICHIA-COLI*. *Gene,* 32**,** 41-48.

MILLER, J. 1972. *Experiments in molecular genetics,* [Cold Spring Harbor, N.Y.], Cold Spring Harbor Laboratory Press.

MILNER, D. S., RAY, L. J., SAXON, E. B., LAMBERT, C., TILL, R., FENTON, A. K. & SOCKETT, R. E. 2020. DivIVA Controls Progeny Morphology and Diverse ParA Proteins Regulate Cell Division or Gliding Motility in *Bdellovibrio bacteriovorus*. *Frontiers in Microbiology,* 11:542.

MINGORANCE, J., TAMAMES, J. & VICENTE, M. 2004. Genomic channeling in bacterial cell division. *Journal of Molecular Recognition,* 17**,** 481-487.

MIR, M. A., SRINIVASAN, R. & AJITKUMAR, P. 2019. MtFtsX a Predicted Membrane Domain of ABC Transporter Complex MtFtsEX of *Mycobacterium tuberculosis* Interacts with the Cell Division Protein MtFtsZ. *International Journal of Mycobacteriology,* 8**,** 281-286.

MOIR, A. & COOPER, G. 2015. Spore Germination. *Microbiology Spectrum,* 3.

MONAHAN, L. G., LIEW, A. T. F., BOTTOMLEY, A. L. & HARRY, E. J. 2014. Division site positioning in bacteria: one size does not fit all. *Frontiers in Microbiology,* 5**,** 7.

MUKHERJEE, P., SUREKA, K., DATTA, P., HOSSAIN, T., BARIK, S., DAS, K. P., KUNDU, M. & BASU, J. 2009. Novel role of Wag31 in protection of mycobacteria under oxidative stress. *Molecular Microbiology,* 73**,** 103-119.

MUKHERJEE, T., HANES, J., TEWS, I., EALICK, S. E. & BEGLEY, T. P. 2011. Pyridoxal phosphate: Biosynthesis and catabolism. *Biochimica Et Biophysica Acta-Proteins and Proteomics,* 1814**,** 1585-1596.

MURRAY, H. & KOH, A. 2014. Multiple Regulatory Systems Coordinate DNA Replication with Cell Growth in *Bacillus subtilis*. *Plos Genetics,* 10(10): e1004731.

NAGANO, K., MURAKAMI, Y., NISHIKAWA, K., SAKAKIBARA, J., SHIMOZATO, K. & YOSHIMURA, F. 2007. Characterization of RagA and RagB in Porphyromonas gingivalis: study using gene-deletion mutants. *Journal of Medical Microbiology,* 56**,** 1536-1548.

NAKAHIGASHI, K., KUBO, N., NARITA, S., SHIMAOKA, T., GOTO, S., OSHIMA, T., MORI, H., MAEDA, M., WADA, C. & INOKUCHI, H. 2002. HemK, a class of protein methyl transferase with similarity to DNA methyl transferases, methylates polypeptide chain release factors, and hemK knockout induces defects in translational termination. *Proceedings of the National Academy of Sciences of the United States of America,* 99**,** 1473-1478.

NAKAMATSU, E. H., FUJIHIRA, E., FERREIRA, R. C. C., BALAN, A., COSTA, S. O. P. & FERREIRA, L. C. S. 2007. Oligopeptide uptake and aminoglycoside resistance in *Escherichia coli* MG1655. *Fems Microbiology Letters,* 269**,** 229-233.

NEWMAN, J. A., SAVITSKY, P., ALLERSTON, C. K., BIZARD, A. H., OZER, O., SARLOS, K., LIU, Y., PARDON, E., STEYAERT, J., HICKSON, I. D. & GILEADI, O. 2015. Crystal structure of the Bloom's syndrome helicase indicates a role for the HRDC domain in conformational changes. *Nucleic Acids Research,* 43**,** 5221-5235.

NGUEMA-ONA, E., VICRE-GIBOUIN, M., CANNESAN, M. A. & DRIOUICH, A. 2013. Arabinogalactan proteins in root-microbe interactions. *Trends in Plant Science,* 18**,** 445-454.

NI, H., FAN, W. W., LI, C. L., WU, Q. Q., HONGFEN, H. F., HUI, D., ZHENG, F., ZHU, X. H., WANG, C. J., CAO, X. R., SHAO, Z. Q. & PAN, X. Z. 2018. *Streptococcus suis* DivIVA Protein Is a Substrate of Ser/Thr Kinase STK and Involved in Cell Division Regulation. *Frontiers in Cellular and Infection Microbiology,* 8:85.

NJAU, R. K., HERNDON, C. A. & HAWES, J. W. 2001. New developments in our understanding of the beta-hydroxyacid dehydrogenases. *Chemico-Biological Interactions,* 130**,** 785-791.

NOCEK, B., CHANG, C., LI, H., LEZONDRA, L., HOLZLE, D., COLLART, F. & JOACHIMIAK, A. 2005. Crystal structures of Delta(1)-pyrroline-5-carboxylate reductase from human pathogens *Neisseria meningitides* and *Streptococcus pyogenes*. *Journal of Molecular Biology,* 354**,** 91-106.

NOTHNAGEL, E. A. 1997. Proteoglycans and related components in plant cells. *International Review of Cytology - a Survey of Cell Biology, Vol 174,* 174**,** 195-291.

O'TOOLE, R. & WILLIAMS, H. D. 2003. Universal stress proteins and *Mycobacterium tuberculosis*. *Research in Microbiology,* 154**,** 387-392.

OGASAWARA, Y. & DAIRI, T. 2021. Discovery of an alternative pathway of peptidoglycan biosynthesis: A new target for pathway specific inhibitors. *Journal of Industrial Microbiology and Biotechnology,* 48:9-10.

OHKI, M., SUGIYAMA, K., KAWAI, F., TANAKA, H., NIHEI, Y., UNZAI, S., TAKEBE, M., MATSUNAGA, S., ADACHI, S.-I., SHIBAYAMA, N., ZHOU, Z., KOYAMA, R., IKEGAYA, Y., TAKAHASHI, T., TAME, J. R. H., ISEKI, M. & PARK, S.-Y. 2016. Structural insight into photoactivation of an adenylate cyclase from a photosynthetic cyanobacterium. *Proceedings of the National Academy of Sciences of the United States of America,* 113**,** 6659-6664.

OHSHIMA, T., NUNOURA-KOMINATO, N., KUDOME, T. & SAKURABA, H. 2001. A novel hyperthermophilic archaeal glyoxylate reductase from *Thermococcus litoralis* - Characterization, gene cloning, nucleotide sequence and expression in *Escherichia coli*. *European Journal of Biochemistry,* 268**,** 4740-4747.

OKADA, C., WAKABAYASHI, H., KOBAYASHI, M., SHINODA, A., TANAKA, I. & YAO, M. 2016. Crystal structures of the UDP-diacylglucosamine pyrophosphohydrase LpxH from *Pseudomonas aeruginosa*. *Scientific Reports,* 6, 32822.

OLIVA, M. A., HALBEDEL, S., FREUND, S. M., DUTOW, P., LEONARD, T. A., VEPRINTSEV, D. B., HAMOEN, L. W. & LOWE, J. 2010. Features critical for membrane binding revealed by DivIVA crystal structure. *Embo Journal,* 29**,** 1988-2001.

OLSON, E. R., DUNYAK, D. S., JURSS, L. M. & POORMAN, R. A. 1991. IDENTIFICATION AND CHARACTERIZATION OF *DPPA*, AN *ESCHERICHIA-COLI* GENE ENCODING A PERIPLASMIC DIPEPTIDE TRANSPORT PROTEIN. *Journal of Bacteriology,* 173**,** 234-244.

OSTERMAN, I. A., DONTSOVA, O. A. & SERGIEV, P. V. 2020. rRNA Methylation and Antibiotic Resistance. *Biochemistry-Moscow,* 85**,** 1335-1349.

OZKAN, M., YILMAZ, H., CELIK, M. A., SENGEZER, C., ERHAN, E. & KESKINLER, B. 2018. Application of *Bdellovibrio bacteriovorus* for reducing fouling of membranes used for wastewater treatment. *Turkish Journal of Biochemistry-Turk Biyokimya Dergisi,* 43**,** 296-305.

PAJARES, M. A. & PEREZ-SALA, D. 2018. Mammalian Sulfur Amino Acid Metabolism: A Nexus Between Redox Regulation, Nutrition, Epigenetics, and Detoxification. *Antioxidants & Redox Signaling,* 29**,** 408-452.

PAN, A., CHANDA, I. & CHAKRABARTI, J. 2011. Analysis of the genome and proteome composition of *Bdellovibrio bacteriovorus*: Indication for recent prey-derived horizontal gene transfer. *Genomics,* 98**,** 213-222.

PAN, X. W., SUN, C. H., TANG, M., YOU, J. J., OSIRE, T., ZHAO, Y. X., XU, M. J., ZHANG, X., SHAO, M. L., YANG, S. T., YANG, T. W. & RAO, Z. M. 2020. LysR-Type Transcriptional Regulator MetR Controls Prodigiosin Production, Methionine

Biosynthesis, Cell Motility, H2O2 Tolerance, Heat Tolerance, and Exopolysaccharide Synthesis in *Serratia marcescens*. *Applied and Environmental Microbiology,* 86**,** 18.

PANDHARE, J., DONALD, S. P., COOPER, S. K. & PHANG, J. M. 2009. Regulation and Function of Proline Oxidase Under Nutrient Stress. *Journal of Cellular Biochemistry,* 107**,** 759-768.

PASTORET, S., FRAIPONT, C., DEN BLAAUWEN, T., WOLF, B., AARSMAN, M. E. G., PIETTE, A., THOMAS, A., BRASSEUR, R. & NGUYEN-DISTECHE, M. 2004. Functional analysis of the cell division protein FtsW of *Escherichia coli*. *Journal of Bacteriology,* 186**,** 8370-8379.

PERRY, S. E. & EDWARDS, D. H. 2006. The *Bacillus subtilis* DivIVA protein has a sporulation-specific proximity to Spo0J. *Journal of Bacteriology,* 188**,** 6039-6043.

PETERKOFSKY, A. 1981. *ESCHERICHIA-COLI* ADENYLATE-CYCLASE AS A SENSOR OF SUGAR-TRANSPORT FUNCTION. *Advances in Cyclic Nucleotide Research,* 14**,** 215-228.

PICON, A. & VAN WELY, K. H. M. 2001. Peptide binding to the *Bacillus subtilis* oligopeptide-binding proteins OppA and AppA. *Molecular Biology Today,* 2**,** 21-25.

PIMKIN, M., PIMKINA, J. & MARKHAM, G. D. 2009. A Regulatory Role of the Bateman Domain of IMP Dehydrogenase in Adenylate Nucleotide Biosynthesis. *Journal of Biological Chemistry,* 284**,** 7960-7969.

PIORO, M., MALECKI, T., PORTAS, M., MAGIEROWSKA, I., TROJANOWSKI, D., SHERRATT, D., ZAKRZEWSKA-CZERWINSKA, J., GINDA, K. & JAKIMOWICZ, D. 2019. Competition between DivIVA and the nucleoid for ParA binding promotes segrosome separation and modulates mycobacterial cell elongation. *Molecular Microbiology,* 111**,** 204-220.

PITTARD, J., CAMAKARIS, H. & YANG, J. 2005. The TyrR regulon. *Molecular Microbiology,* 55**,** 16-26.

PUCCI, M. J., THANASSI, J. A., DISCOTTO, L. F., KESSLER, R. E. & DOUGHERTY, T. J. 1997. Identification and characterization of cell wall cell division gene clusters in pathogenic gram-positive cocci. *Journal of Bacteriology,* 179**,** 5632-5635.

QIN, R., SANG, Y., REN, J., ZHANG, Q. F., LI, S. X., CUI, Z. F. & YAO, Y. F. 2016. The Bacterial Two-Hybrid System Uncovers the Involvement of Acetylation in Regulating of Lrp Activity in *Salmonella typhimurium*. *Frontiers in Microbiology,* 7.

RAEMAKERS, C., JACOBSEN, E. & VISSER, R. G. F. 1995. SECONDARY SOMATIC EMBRYOGENESIS AND APPLICATIONS IN PLANT-BREEDING. *Euphytica,* 81**,** 93-107.

REAL, G. & HENRIQUES, A. O. 2006. Localization of the *Bacillus subtilis murB* gene within the *dcw* cluster is important for growth and sporulation. *Journal of Bacteriology,* 188**,** 1721-1732.

REDDY, M. C. M., PALANINATHAN, S. K., BRUNING, J. B., THURMAN, C., SMITH, D. & SACCHETTINI, J. C. 2009. Structural Insights into the Mechanism of the

Allosteric Transitions of *Mycobacterium tuberculosis* cAMP Receptor Protein. *Journal of Biological Chemistry,* 284**,** 36581-36591.

REITH, J. & MAYER, C. 2011. Characterization of a Glucosamine/Glucosaminide N-Acetyltransferase of *Clostridium acetobutylicum*. *Journal of Bacteriology,* 193**,** 5393-5399.

RENDULIC, S., JAGTAP, P., ROSINUS, A., EPPINGER, M., BAAR, C., LANZ, C., KELLER, H., LAMBERT, C., EVANS, K. J., GOESMANN, A., MEYER, F., SOCKETT, R. E. & SCHUSTER, S. C. 2004. A predator unmasked: Life cycle of *Bdellovibrio bacteriovorus* from a genomic perspective. *Science,* 303**,** 689-692.

RICHTS, B., ROSENBERG, J. & COMMICHAU, F. M. 2019. A Survey of Pyridoxal 5 '-Phosphate-Dependent Proteins in the Gram-Positive Model *Bacterium Bacillus* subtilis. *Frontiers in Molecular Biosciences,* 6:32.

RIVAS-MARIN, E., CANOSA, I. & DEVOS, D. P. 2016. Evolutionary Cell Biology of Division Mode in the Bacterial *Planctomycetes-Verrucomicrobia-Chlamydiae* Superphylum. *Frontiers in Microbiology,* 7:1964.

ROGERS, M., EKATERINAKI, N., NIMMO, E. & SHERRATT, D. 1986. ANALYSIS OF TN7 TRANSPOSITION. *Molecular & General Genetics,* 205**,** 550-556.

ROMSANG, A., DUANG-NKERN, J., KHEMSOM, K., WONGSAROJ, L., SANINJUK, K., FUANGTHONG, M., VATTANAVIBOON, P. & MONGKOLSUK, S. 2018. *Pseudomonas aeruginosa ttcA* encoding tRNA-thiolating protein requires an iron-sulfur cluster to participate in hydrogen peroxide-mediated stress protection and pathogenicity. *Scientific Reports,* 8, 11882.

ROSCHANSKI, N. & STRAUCH, E. 2011. Assessment of the Mobilizable Vector Plasmids pSUP202 and pSUP404.2 as Genetic Tools for the Predatory Bacterium *Bdellovibrio bacteriovorus*. *Current Microbiology,* 62**,** 589-596.

ROSENBERG, J., YEAK, K. C. & COMMICHAU, F. M. 2018. A two-step evolutionary process establishes a non-native vitamin B6 pathway in *Bacillus subtilis*. *Environmental Microbiology,* 20**,** 156-168.

ROSTOM, A. A., TAME, J. R. H., LADBURY, J. E. & ROBINSON, C. V. 2000. Specificity and interactions of the protein OppA: Partitioning solvent binding effects using mass spectrometry. *Journal of Molecular Biology,* 296**,** 269-279.

RUMSBY, G. & CREGEEN, D. P. 1999. Identification and expression of a cDNA for human hydroxypyruvate/glyoxylate reductase. *Biochimica Et Biophysica Acta-Gene Structure and Expression,* 1446**,** 383-388.

RUMYANTSEVA, N. I. 2005. Arabinogalactan proteins: Involvement in plant growth and morphogenesis. *Biochemistry-Moscow,* 70**,** 1073-1085.

SAMUEL, G. & REEVES, P. 2003. Biosynthesis of O-antigens: genes and pathways involved in nucleotide sugar precursor synthesis and O-antigen assembly. *Carbohydrate Research,* 338**,** 2503-2519.

SANGWAN, N., LAMBERT, C., SHARMA, A., GUPTA, V., KHURANA, P., KHURANA, J. P., SOCKETT, R. E., GILBERT, J. A. & LAL, R. 2015. Arsenic rich Himalayan hot spring metagenomics reveal genetically novel predator-prey genotypes. *Environmental Microbiology Reports,* 7**,** 812-823.

SATO, Y., YAMAMOTO, Y., KIZAKI, H. & KURAMITSU, H. K. 1993. ISOLATION AND SEQUENCE-ANALYSIS OF THE PMI GENE ENCODING PHOSPHOMANNOSE ISOMERASE OF *STREPTOCOCCUS-MUTANS*. *Fems Microbiology Letters,* 114**,** 61-66.

SATOMI, M., KIMURA, B., HAMADA, T., HARAYAMA, S. & FUJII, T. 2002. Phylogenetic study of the genus *Oceanospirillum* based on 16S rRNA and *gyrB* genes: emended description of the genus *Oceanospirillum*, description of *Pseudospirillum* gen. nov., *Oceanobacter* gen. nov and *Terasakielia* gen. nov and transfer of *Oceanospirillum jannaschii* and *Pseudomonas stanieri* to *Marinobacterium* as *Marinobacterium jannaschii* comb. nov and *Marinobacterium stanieri* comb. nov. *International Journal of Systematic and Evolutionary Microbiology,* 52**,** 739-747.

SAYERS, E. W., CAVANAUGH, M., CLARK, K., PRUITT, K. D., SCHOCH, C. L., SHERRY, S. T. & KARSCH-MIZRACHI, I. 2021. GenBank. *Nucleic Acids Research,* 49**,** D92-D96.

SCHAFER, A., TAUCH, A., JAGER, W., KALINOWSKI, J., THIERBACH, G. & PUHLER, A. 1994. SMALL MOBILIZABLE MULTIPURPOSE CLONING VECTORS DERIVED FROM THE *ESCHERICHIA-COLI* PLASMIDS PK18 AND PK19 - SELECTION OF DEFINED DELETIONS IN THE CHROMOSOME OF *CORYNEBACTERIUM-GLUTAMICUM*. *Gene,* 145**,** 69-73.

SCHINDELIN, J., ARGANDA-CARRERAS, I., FRISE, E., KAYNIG, V., LONGAIR, M., PIETZSCH, T., PREIBISCH, S., RUEDEN, C., SAALFELD, S., SCHMID, B., TINEVEZ, J. Y., WHITE, D. J., HARTENSTEIN, V., ELICEIRI, K., TOMANCAK, P. & CARDONA, A. 2012. Fiji: an open-source platform for biological-image analysis. *Nature Methods,* 9**,** 676-682.

SCHINDELIN, J., RUEDEN, C. T., HINER, M. C. & ELICEIRI, K. W. 2015. The ImageJ ecosystem: An open platform for biomedical image analysis. *Molecular Reproduction and Development,* 82**,** 518-529.

SCOTT, J. W., HAWLEY, S. A., GREEN, K. A., ANIS, M., STEWART, G., SCULLION, G. A., NORMAN, D. G. & HARDIE, D. G. 2004. CBS domains form energy-sensing modules whose binding of adenosine ligands is disrupted by disease mutations. *Journal of Clinical Investigation,* 113**,** 274-284.

SHARMA, K., SULTANA, T., DAHMS, T. E. S. & DILLON, J. A. R. 2020a. CcpN: a moonlighting protein regulating catabolite repression of gluconeogenic genes in *Bacillus subtilis* also affects cell length and interacts with DivIVA. *Canadian Journal of Microbiology,* 66**,** 723-732.

SHARMA, K., SULTANA, T., LIAO, M. M., DAHMS, T. E. S. & DILLON, J. A. R. 2020b. EF1025, a Hypothetical Protein From *Enterococcus faecalis*, Interacts With DivIVA and Affects Cell Length and Cell Shape. *Frontiers in Microbiology,* 11:83.

SHENOY, A. R. & VISWESWARIAH, S. S. 2004. Class III nucleotide cyclases in bacteria and archaebacteria: lineage-specific expansion of adenylyl cyclases and a dearth of guanylyl cyclases. *Febs Letters,* 561**,** 11-21.

SIMON, R., PRIEFER, U. & PUHLER, A. 1983. A BROAD HOST RANGE MOBILIZATION SYSTEM FOR INVIVO GENETIC-ENGINEERING - TRANSPOSON MUTAGENESIS IN GRAM-NEGATIVE BACTERIA. *Bio-Technology,* 1**,** 784-791.

SINGH, G. & ARYA, S. K. 2019. Antifungal and insecticidal potential of chitinases: A credible choice for the eco-friendly farming. *Biocatalysis and Agricultural Biotechnology,* 20: 101289.

SINK, R., KOTNIK, M., ZEGA, A., BARRETEAU, H., GOBEC, S., BLANOT, D., DESSEN, A. & CONTRERAS-MARTEL, C. 2016. Crystallographic Study of Peptidoglycan Biosynthesis Enzyme MurD: Domain Movement Revisited. *Figshare*.

SMITH, M. W., TYREMAN, D. R., PAYNE, G. M., MARSHALL, N. J. & PAYNE, J. W. 1999. Substrate specificity of the periplasmic dipeptide-binding protein from *Escherichia coli*: experimental basis for the design of peptide prodrugs. *Microbiology-Sgm,* 145**,** 2891-2901.

SOCKETT, R. E. 2009. Predatory Lifestyle of *Bdellovibrio bacteriovorus*. *Annual Review of Microbiology.* Palo Alto: Annual Reviews, 63: 523-539.

SOLOVYEV, V. A. S. A. 2011. Automatic annotation of microbial genomes and metagenomic sequences. *Metagenomics and its applications in agriculture, biomedicine and environmental studies***,** 61-78.

STOLP, H. 1968. *BDELLOVIBRIO BACTERIOVORUS* - A PREDATORY BACTERIA PARASITE. *Naturwissenschaften,* 55**,** 57-63.

SU, S. H. & HIGASHIYAMA, T. 2018. Arabinogalactan proteins and their sugar chains: functions in plant reproduction, research methods, and biosynthesis. *Plant Reproduction,* 31**,** 67-75.

SULLIVAN, J. 2005. Maximum-likelihood methods for phylogeny estimation. *Molecular Evolution: Producing the Biochemical Data, Part B,* 395**,** 757-779.

SZABADOS, L. & SAVOURE, A. 2010. Proline: a multifunctional amino acid. *Trends in Plant Science,* 15**,** 89-97.

TAKADA, H. & YOSHIKAWA, H. 2018. Essentiality and function of WalK/WalR two-component system: the past, present, and future of research. *Bioscience Biotechnology and Biochemistry,* 82**,** 741-751.

TAN, M. F., ZOU, G., WEI, Y., LIU, W. Q., LI, H. Q., HU, Q., ZHANG, L. S. & ZHOU, R. Protein-protein interaction network and potential drug target candidates of *Streptococcus suis*. *Journal of Applied Microbiology***,** 131(2):658-670.

TENG, F. Y., WANG, T. T., GUO, H. L., XIN, B. G., SUN, B., DOU, S. X., XI, X. G. & HOU, X. M. 2020. The HRDC domain oppositely modulates the unwinding activity of *E. coli* RecQ helicase on duplex DNA and G-quadruplex. *Journal of Biological Chemistry,* 295**,** 17646-17658.

TEO, A. C. K. & ROPER, D. I. 2015. Core Steps of Membrane-Bound Peptidoglycan Biosynthesis: Recent Advances, Insight and Opportunities. *Antibiotics-Basel,* 4**,** 495-520.

THODEN, J. B., HEGEMAN, A. D., WESENBERG, G., CHAPEAU, M. C., FREY, P. A. & HOLDEN, H. M. 1997. Structural analysis of UDP-sugar binding to UDP-galactose 4-epimerase from *Escherichia coli*. *Biochemistry,* 36**,** 6294-6304.

THODEN, J. B., WOHLERS, T. M., FRIDOVICH-KEIL, J. L. & HOLDEN, H. M. 2001. Human UDP-galactose 4-epimerase - Accommodation of UDP-N-acetylglucosamine within the active site. *Journal of Biological Chemistry,* 276**,** 15131-15136.

THOMASHOW, M. F. & RITTENBERG, S. C. 1978a. INTRAPERIPLASMIC GROWTH OF *BDELLOVIBRIO-BACTERIOVORUS* 109J - ATTACHMENT OF LONG-CHAIN FATTY-ACIDS TO *ESCHERICHIA-COLI* PEPTIDOGLYCAN. *Journal of Bacteriology,* 135**,** 1015-1023.

THOMASHOW, M. F. & RITTENBERG, S. C. 1978b. INTRAPERIPLASMIC GROWTH OF *BDELLOVIBRIO-BACTERIOVORUS* 109J - N-DEACETYLATION OF *ESCHERICHIA-COLI* PEPTIDOGLYCAN AMINO-SUGARS. *Journal of Bacteriology,* 135**,** 1008-1014.

THOMPSON, J. D., HIGGINS, D. G. & GIBSON, T. J. 1994. CLUSTAL-W - IMPROVING THE SENSITIVITY OF PROGRESSIVE MULTIPLE SEQUENCE ALIGNMENT THROUGH SEQUENCE WEIGHTING, POSITION-SPECIFIC GAP PENALTIES AND WEIGHT MATRIX CHOICE. *Nucleic Acids Research,* 22**,** 4673-4680.

TJADEN, B. 2015. De novo assembly of bacterial transcriptomes from RNA-seq data. *Genome Biology,* 16: 1.

TJADEN, B. 2020. A computational system for identifying operons based on RNA-seq data. *Methods,* 176**,** 62-70.

TREMINO, L., FORCADA-NADAL, A., CONTRERAS, A. & RUBIO, V. 2017. Studies on cyanobacterial protein PipY shed light on structure, potential functions, and vitamin B-6-dependent epilepsy. *Febs Letters,* 591**,** 3431-3442.

TSANG, M.-J. & BERNHARDT, T. G. 2015. Guiding divisome assembly and controlling its activity. *Current Opinion in Microbiology,* 24**,** 60-65.

TSIRIGOS, K. D., PETERS, C., SHU, N., KALL, L. & ELOFSSON, A. 2015. The TOPCONS web server for consensus prediction of membrane protein topology and signal peptides. *Nucleic Acids Research,* 43**,** W401-W407.

UD-DIN, A., TIKHOMIROVA, A. & ROUJEINIKOVA, A. 2016. Structure and Functional Diversity of GCN5-Related N-Acetyltransferases (GNAT). *International Journal of Molecular Sciences,* 17(7):1018.

VAN BAARLE, S., CELIK, I. N., KAVAL, K. G., BRAMKAMP, M., HAMOEN, L. W. & HALBEDEL, S. 2013. Protein-Protein Interaction Domains of *Bacillus subtilis* DivIVA. *Journal of Bacteriology,* 195**,** 1012-1021.

VAN DER BEEK, S. L., ZORZOLI, A., CANAK, E., CHAPMAN, R. N., LUCAS, K., MEYER, B. H., EVANGELOPOULOS, D., DE CARVALHO, L. P. S., BOONS, G. J., DORFMUELLER, H. C. & VAN SORGE, N. M. 2019. *Streptococcal* dTDP-L-rhamnose biosynthesis enzymes: functional characterization and lead compound identification. *Molecular Microbiology,* 111**,** 951-964.

VAN HENGEL, A. J., TADESSE, Z., IMMERZEEL, P., SCHOLS, H., VAN KAMMEN, A. & DE VRIES, S. C. 2001. N-acetylglucosamine and glucosamine-containing arabinogalactan proteins control somatic embryogenesis. *Plant Physiology,* 125**,** 1880-1890.

VICENTE, M., GOMEZ, M. J. & AYALA, J. A. 1998. Regulation of transcription of cell division genes in the *Escherichia coli dcw* cluster. *Cellular and Molecular Life Sciences,* 54**,** 317-324.

VICENTE, M., RICO, A. I., MARTINEZ-ARTEAGA, R. & MINGORANCE, J. 2006. Septum enlightenment: Assembly of bacterial division proteins. *Journal of Bacteriology,* 188**,** 19-27.

VOROBJEVA, N. N., KURILOVA, S. A., PETUKHOVA, A. F., NAZAROVA, T. I., KOLOMIJTSEVA, G. Y., BAYKOV, A. A. & RODINA, E. V. 2020. A novel, cupin-type phosphoglucose isomerase in *Escherichia coli*. *Biochimica Et Biophysica Acta-General Subjects,* 1864**,** 8.

WADHAWAN, S., GAUTAM, S. & SHARMA, A. 2010. Metabolic stress-induced programmed cell death in *Xanthomonas*. *Fems Microbiology Letters,* 312**,** 176-183.

WAITE, D. W., CHUVOCHINA, M., PELIKAN, C., PARKS, D. H., YILMAZ, P., WAGNER, M., LOY, A., NAGANUMA, T., NAKAI, R., WHITMAN, W. B., HAHN, M. W., KUEVER, J. & HUGENHOLTZ, P. 2020. Proposal to reclassify the proteobacterial classes Deltaproteobacteria and Oligoflexia, and the phylum Thermodesulfobacteria into four phyla reflecting major functional capabilities. *International Journal of Systematic and Evolutionary Microbiology,* 70**,** 5972-6016.

WALKER, L., LAGUNAS, B. & GIFFORD, M. L. 2020. Determinants of Host Range Specificity in Legume-Rhizobia Symbiosis. *Frontiers in Microbiology,* 11:585749.

WATERHOUSE, A., BERTONI, M., BIENERT, S., STUDER, G., TAURIELLO, G., GUMIENNY, R., HEER, F. T., DE BEER, T. A. P., REMPFER, C., BORDOLI, L., LEPORE, R. & SCHWEDE, T. 2018. SWISS-MODEL: homology modelling of protein structures and complexes. *Nucleic Acids Research,* 46**,** W296-W303.

WEISSBACH, H. & BROT, N. 1991. REGULATION OF METHIONINE SYNTHESIS IN *ESCHERICHIA-COLI*. *Molecular Microbiology,* 5**,** 1593-1597.

WHITE, M. L. & ESWARA, P. J. 2021. *ylm* Has More than a (Z Anchor) Ring to It! *Journal of Bacteriology,* 203(3):e00460-20.

WHITLEY, K. D., JUKES, C., TREGIDGO, N., KARINOU, E., ALMADA, P., CESBRON, Y., HENRIQUES, R., DEKKER, C. & HOLDEN, S. 2021. FtsZ treadmilling is essential for Z-ring condensation and septal constriction initiation in *Bacillus subtilis* cell division. *Nature Communications,* 12**,** 2448.

WIEGAND, S., JOGLER, M. & JOGLER, C. 2018. On the maverick *Planctomycetes*. *Fems Microbiology Reviews,* 42**,** 739-760.

WILHELM, S., GDYNIA, A., TIELEN, P., ROSENAU, F. & JAEGER, K. E. 2007. The autotransporter esterase EstA of *Pseudomonas aeruginosa* is required for rhamnolipid production, cell motility, and biofilm formation. *Journal of Bacteriology,* 189**,** 6695-6703.

YOSHIKAWA, S., ARAI, R., KINOSHITA, Y., UCHIKUBO-KAMO, T., WAKAMATSU, T., AKASAKA, R., MASUI, R., TERADA, T., KURAMITSU, S., SHIROUZU, M. & YOKOYAMA, S. 2007. Structure of archaeal glyoxylate reductase from *Pyrococcus horikoshii* OT3 complexed with nicotinamide adenine dinucleotide phosphate. *Acta Crystallographica Section D-Biological Crystallography,* 63**,** 357-365.

ZAPRASIS, A., BLEISTEINER, M., KERRES, A., HOFFMANN, T. & BREMER, E. 2015. Uptake of Amino Acids and Their Metabolic Conversion into the Compatible Solute Proline Confers Osmoprotection to *Bacillus subtilis*. *Applied and Environmental Microbiology,* 81**,** 250-259.

ZHANG, K., LIU, J., TU, Y. B., XU, H. B., CHARON, N. W. & LI, C. H. 2012. Two CheW coupling proteins are essential in a chemosensory pathway of *Borrelia burgdorferi*. *Molecular Microbiology,* 85**,** 782-794.

ZHANG, L., ALFANO, J. R. & BECKER, D. F. 2015. Proline Metabolism Increases katG Expression and Oxidative Stress Resistance in *Escherichia coli*. *Journal of Bacteriology,* 197**,** 431-440.

ZHANG, L., WILLEMSE, J., HOSKISSON, P. A. & VAN WEZEL, G. P. 2018. Sporulation-specific cell division defects in ylmE mutants of *Streptomyces coelicolor* are rescued by additional deletion of *ylmD*. *Scientific Reports,* 8: 7328.

ZHANG, N., DARBARI, V. C., GLYDE, R., ZHANG, X. D. & BUCK, M. 2016. The bacterial enhancer-dependent RNA polymerase. *Biochemical Journal,* 473**,** 3741-3753.

ZOU, Y. A., LI, Y. & DILLON, J. A. R. 2017. The distinctive cell division interactome of *Neisseria gonorrhoeae*. *Bmc Microbiology,* 17**,** 14.

ŠINK, R., BARRETEAU, H., PATIN, D., MENGIN-LECREULX, D., GOBEC, S. & BLANOT, D. 2013. MurD enzymes: some recent developments. *Biomol Concepts,* 4**,** 539-56.

8 Appendices

8.1.1 RNA-seq data for ancestral *dcw* genes.

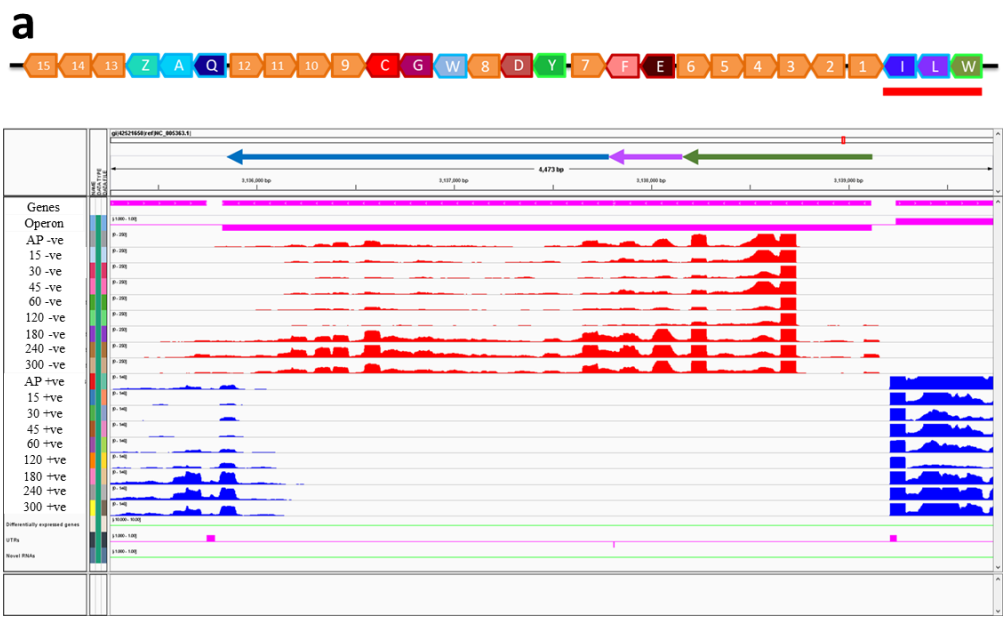

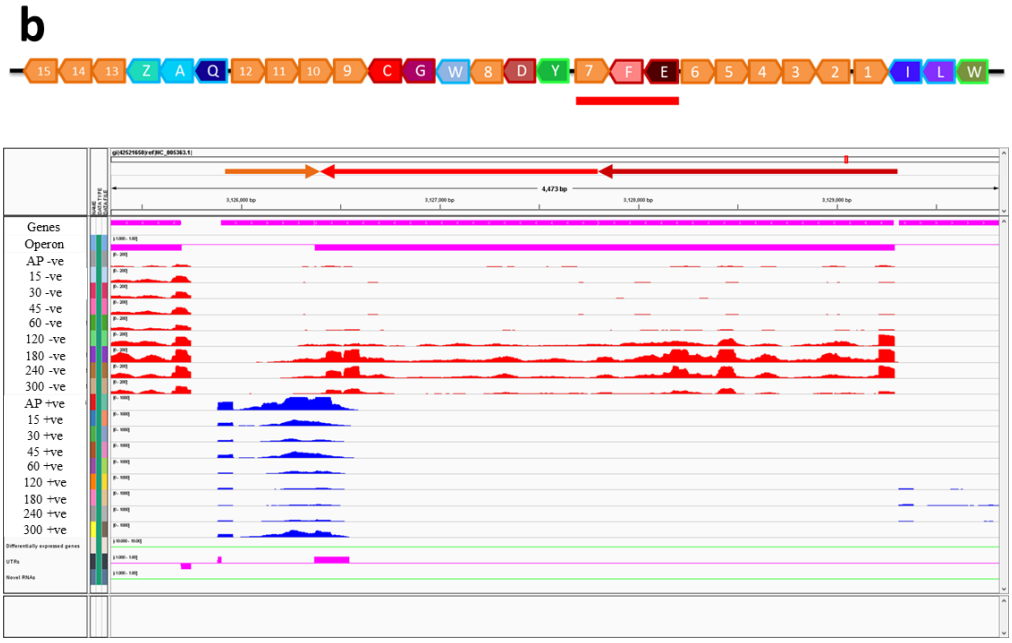

c

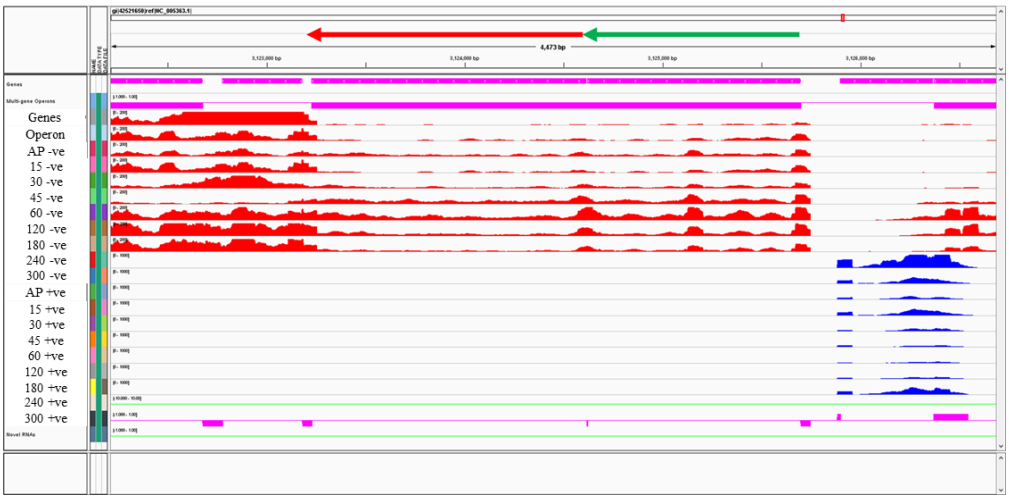
15 14 13 Z A Q 12 11 10 9 C G W 8 D Y 7 F E 6 5 4 3 2 1 I L W
4,473 bp
Genes
Operon
AP -ve
15 -ve
30 -ve
45 -ve
60 -ve
120 -ve
180 -ve
240 -ve
300 -ve
AP +ve
15 +ve
30 +ve
45 +ve
60 +ve
120 +ve
180 +ve
240 +ve
300 +ve

d

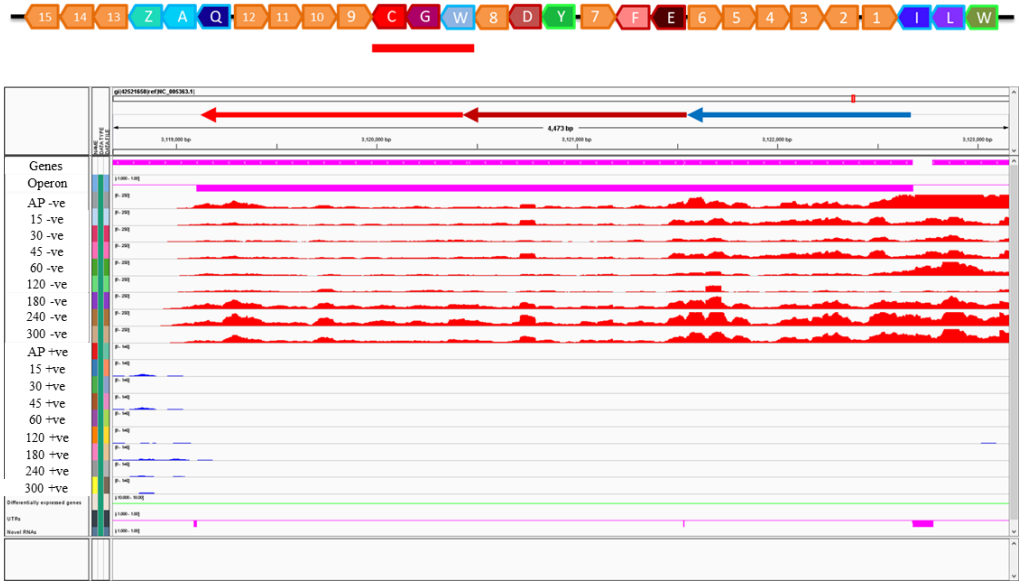
15 14 13 Z A Q 12 11 10 9 C G W 8 D Y 7 F E 6 5 4 3 2 1 I L W
4,473 bp
Genes
Operon
AP -ve
15 -ve
30 -ve
45 -ve
60 -ve
120 -ve
180 -ve
240 -ve
300 -ve
AP +ve
15 +ve
30 +ve
45 +ve
60 +ve
120 +ve
180 +ve
240 +ve
300 +ve

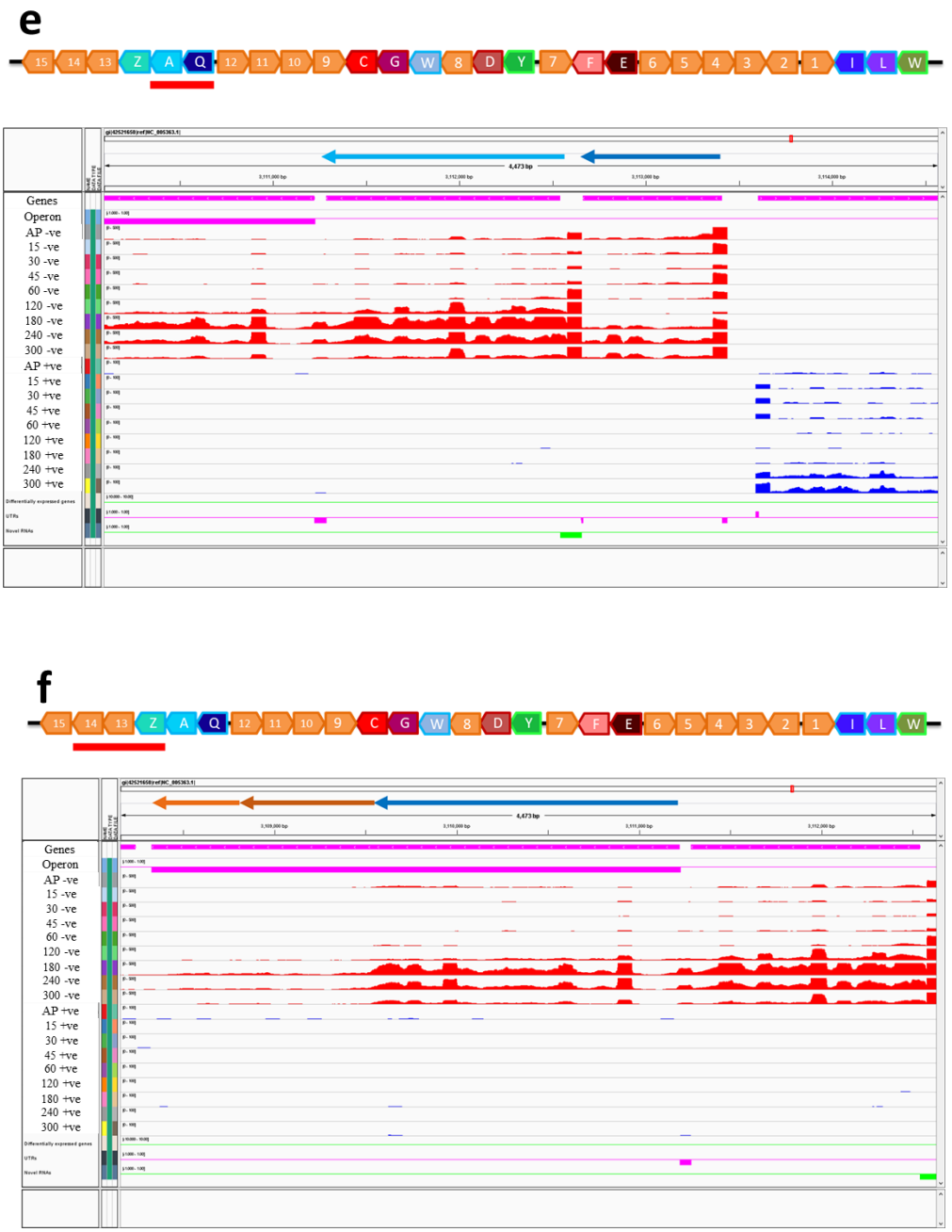

Appendix 8.1.1. RNA-seq data for ancestral genes in the *dcw* cluster. Screenshots taken from Rockhopper software using RNA-seq data of the *dcw* cluster operons: (a) *mraW-ftsL-ftsI* range 0-250 reads, (b) *murE-murF* and *bd3203*, *labelled 7*, range 0-200 reads, (c) *mraY-murD* range 0-200 reads, (d) *ftsW-murG-murC* range 0-500 reads, (e) *ftsQ-ftsA* range 0-500 reads, (f) *ftsZ-bd3188-bd3187*, labelled 13 and 14, range 0-500 reads. A cartoon representation of the *dcw* cluster is

shown above; the red bar indicates which genes are seen in the screenshot. The arrows indicate the location and transcription of the gene. Tracks are labelled on the left: gene and operon show the placement of genes and the multi-gene operon prediction in Rockhopper. The other tracks are labelled by the timepoint (AP is attack phase, 0 minutes. Other tracks show time in minutes).

8.1.2 RNA-seq data for inserted *dcw* genes

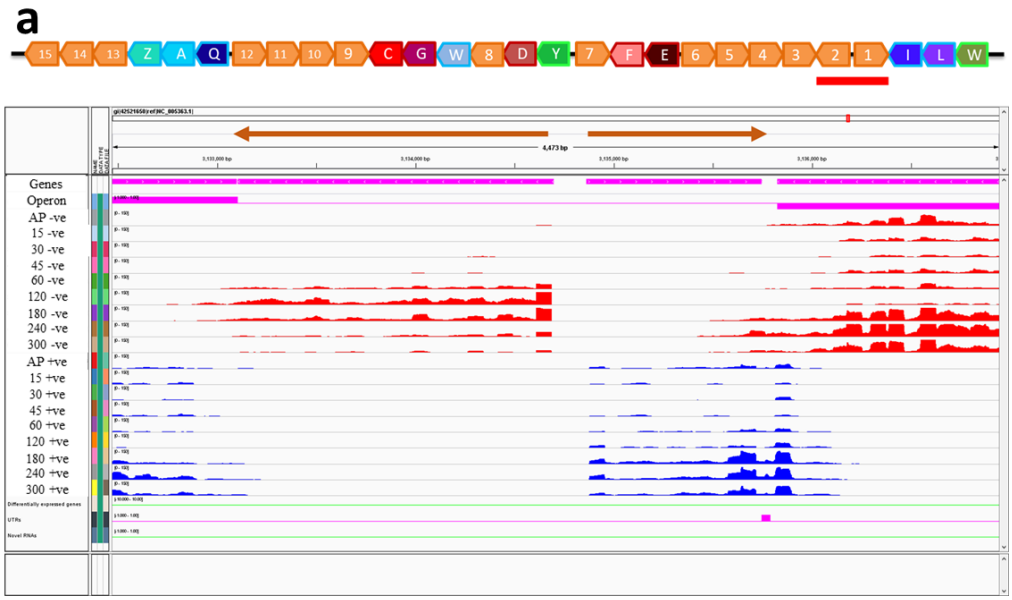

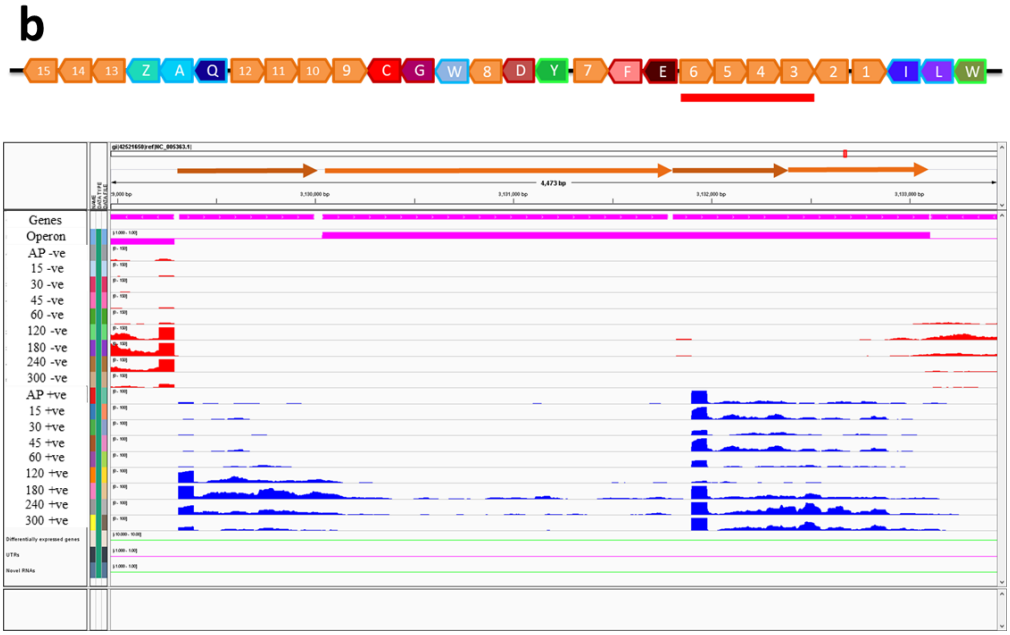

c

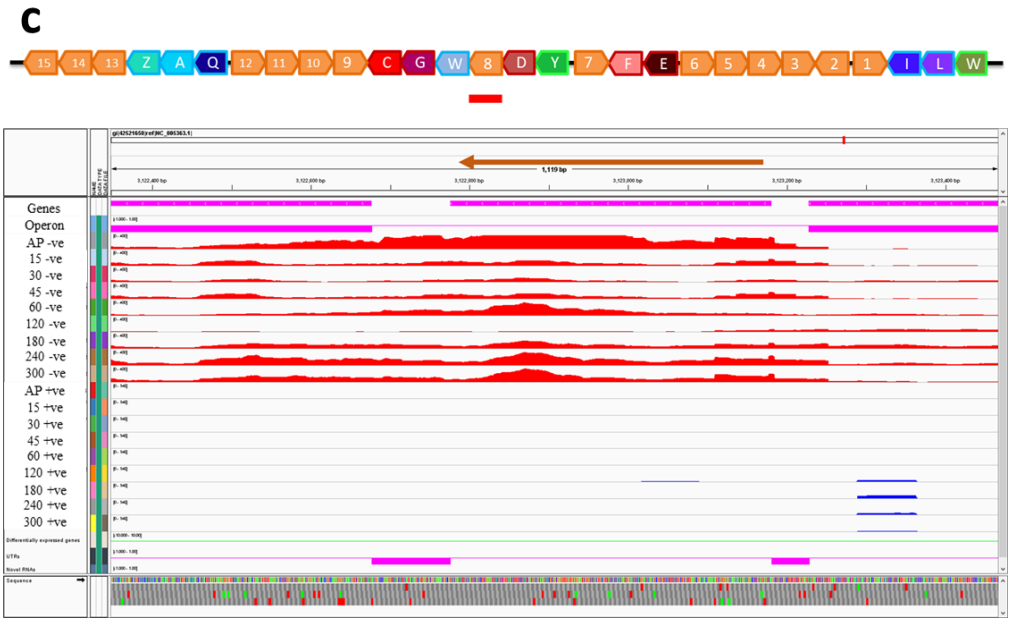
15 14 13 Z A Q 12 11 10 9 C G W 8 D Y 7 F E 6 5 4 3 2 1 I L W
1,119 bp
Genes
Operon
AP -ve
15 -ve
30 -ve
45 -ve
60 -ve
120 -ve
180 -ve
240 -ve
300 -ve
AP +ve
15 +ve
30 +ve
45 +ve
60 +ve
120 +ve
180 +ve
240 +ve
300 +ve

d

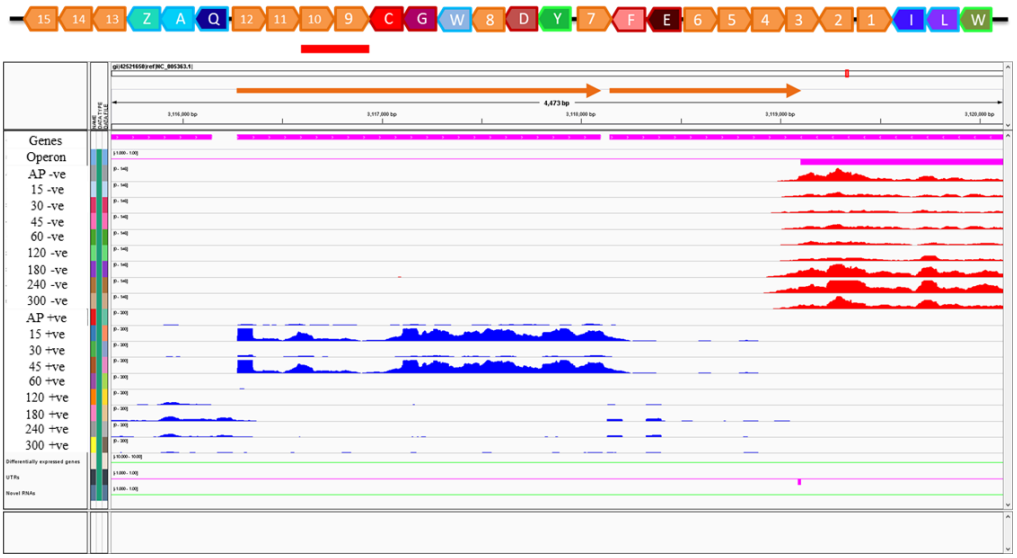
15 14 13 Z A Q 12 11 10 9 C G W 8 D Y 7 F E 6 5 4 3 2 1 I L W
4,473 bp
Genes
Operon
AP -ve
15 -ve
30 -ve
45 -ve
60 -ve
120 -ve
180 -ve
240 -ve
300 -ve
AP +ve
15 +ve
30 +ve
45 +ve
60 +ve
120 +ve
180 +ve
240 +ve
300 +ve

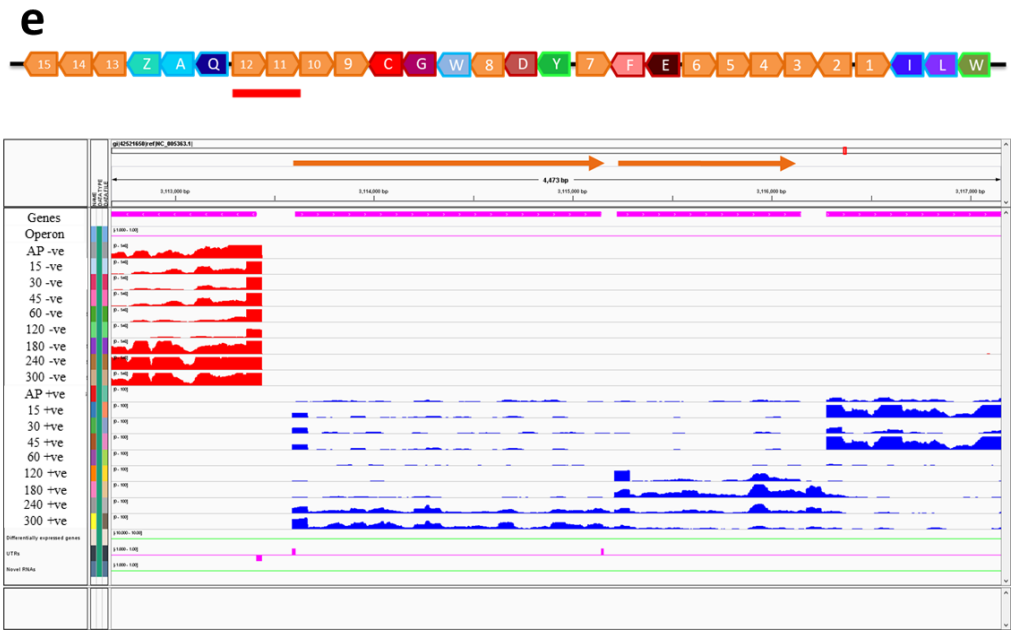

Appendix 8.1.2. RNA-seq data for inserted genes in the dcw cluster.
Screenshots taken from Rockhopper software using RNA-seq data of the genes inserted into the dcw cluster: (a) genes bd3212 [1] and bd3210 [2], range 0-150 reads, (b) bd3206 [6], bd3207 [5], bd3208 [4] and bd3209 [3], range 0-100 reads, (c) bd3199 [8], range 0-400 reads, (d) bd3194 [10] and bd3195 [9], range 0-300 reads, (e) bd3192 [12] and bd3193 [9], range 0-100 reads. The number next to the gene is the labelling system used on the cartoon of the dcw cluster above. A cartoon representation of the dcw cluster is shown above; the red bar indicates which genes are seen in the screenshot. The arrows indicate the location and transcription of the gene. Tracks are labelled on the left: gene and operon show the placement of genes and the multi-gene operon prediction in Rockhopper. The other tracks are labelled by the timepoint (AP is attack phase, 0 minutes. Other tracks show time in minutes).

8.1.3 RNA-seq data for petidoglycan synthesis genes and operons not located in the *dcw* cluster

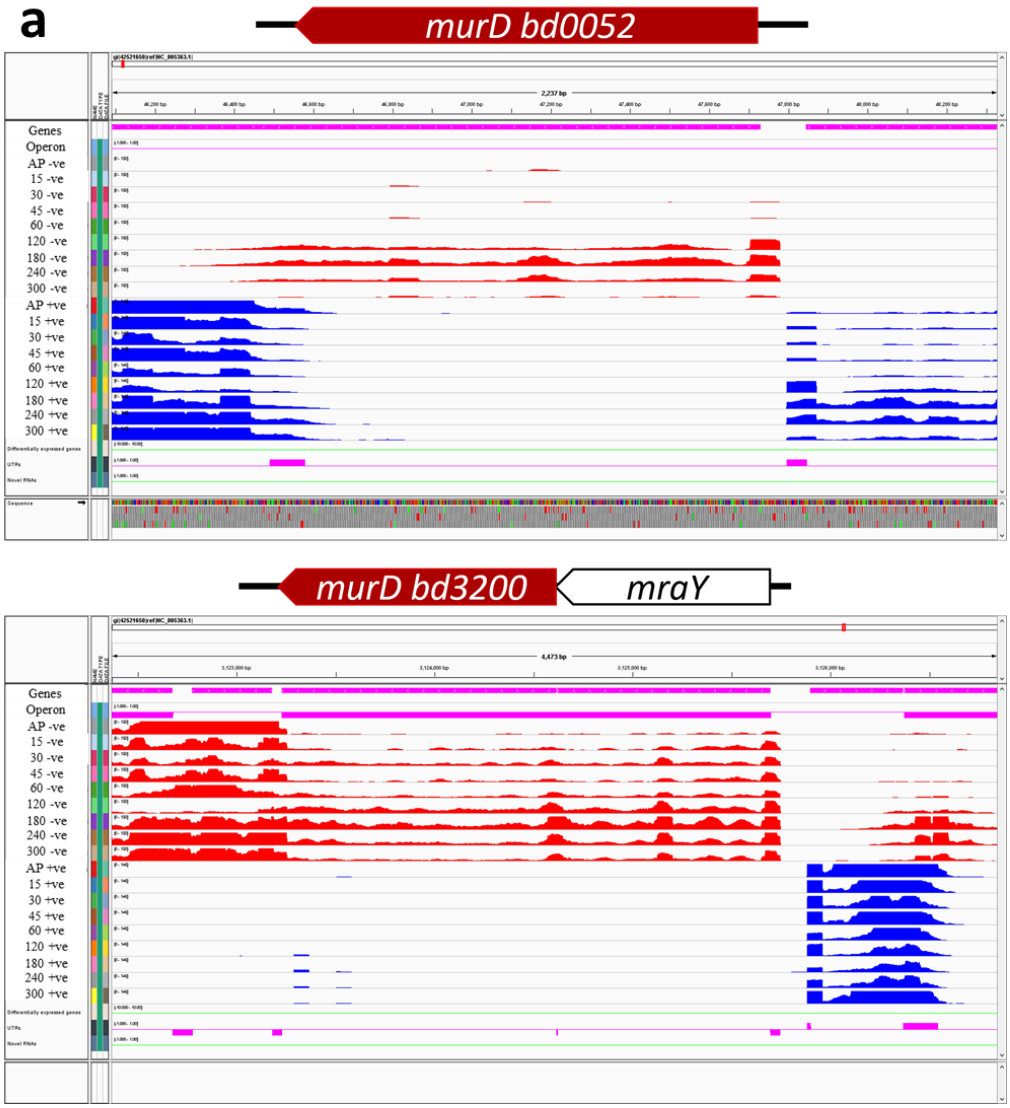

Appendix 8.1.3. RNA-seq data for petidoglycan synthesis genes and operons not located in the *dcw* cluster. Screenshots taken from Rockhopper software using RNA-seq data of the *dcw* cluster operons: (a) a comparison of *murD* homologues *bd0052* (above) and *bd3200* (below), range 0-150 reads, (b) the *murB* (*bd3233*) operon, range 0-200 reads, (c) the *murA* (*bd0071*) operon, range 0-200 reads, (d) the *murI* (*bd1799*) operon, range 0-200 reads, (e) *ddlA* (*bd0585*), range 0-200 reads. Above the screenshot, the arrows indicate the location and transcription of the gene. Tracks are labelled on the left: gene and operon show the placement of genes and the multi-gene operon prediction in Rockhopper. The other tracks are labelled by the timepoint (AP is attack phase, 0 minutes. Other tracks show time in minutes).

b

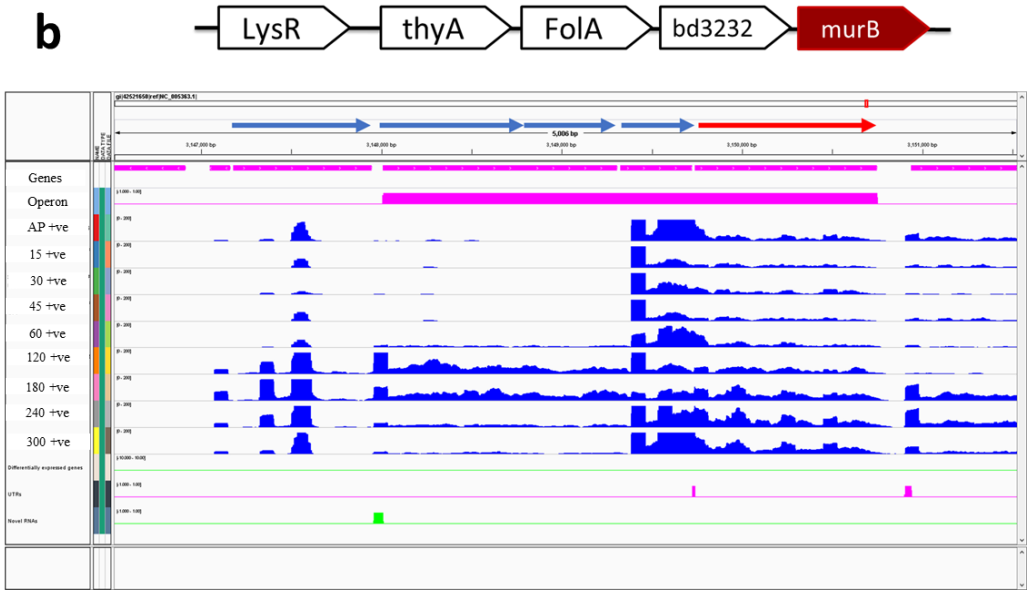
LysR
thyA
FolA
bd3232
murB
Genes
Operon
AP +ve
15 +ve
30 +ve
45 +ve
60 +ve
120 +ve
180 +ve
240 +ve
300 +ve

c

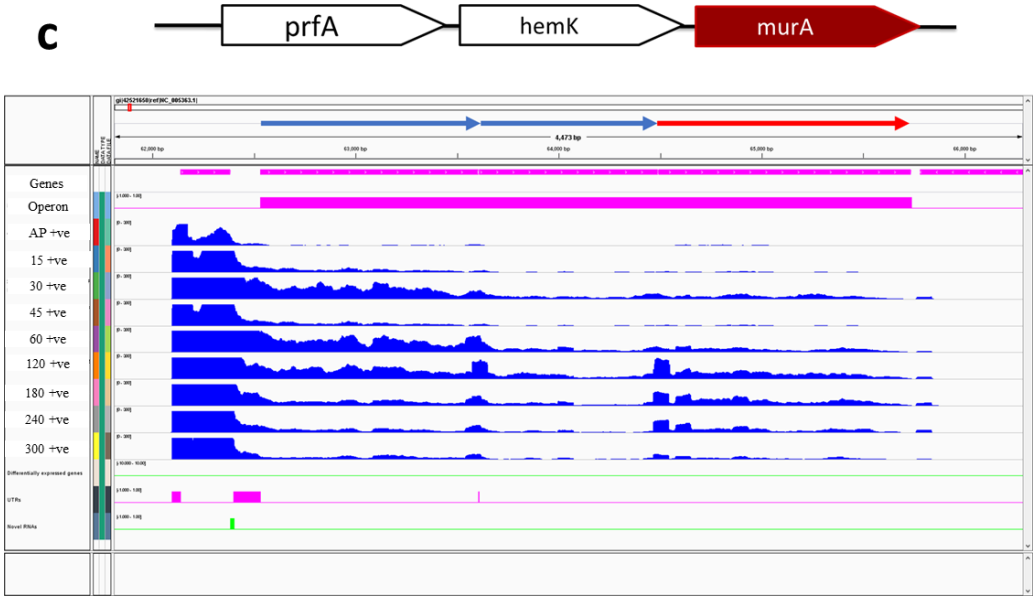
prfA
hemK
murA
Genes
Operon
AP +ve
15 +ve
30 +ve
45 +ve
60 +ve
120 +ve
180 +ve
240 +ve
300 +ve

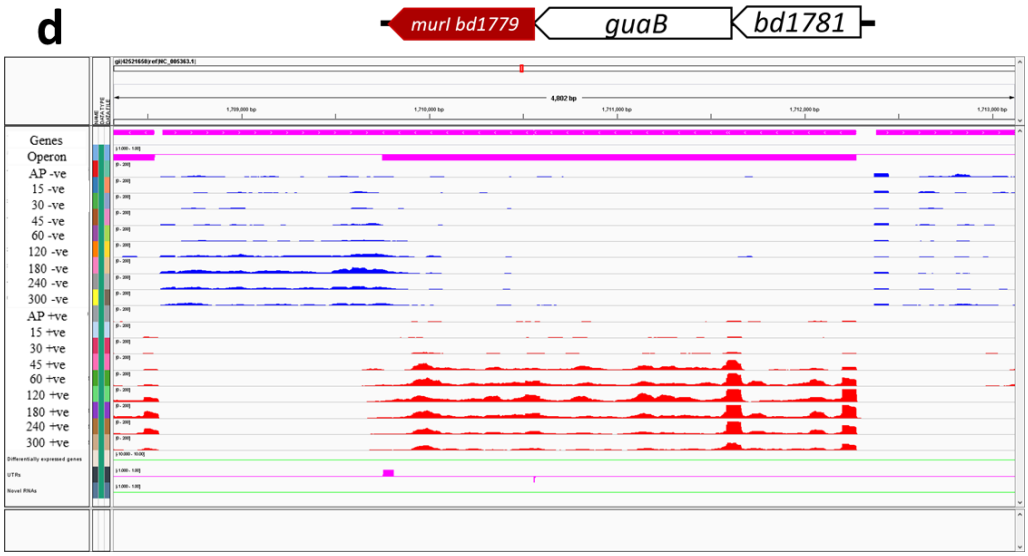
d
murI bd1779
guaB
bd1781
Genes
Operon
AP -ve
15 -ve
30 -ve
45 -ve
60 -ve
120 -ve
180 -ve
240 -ve
300 -ve
AP +ve
15 +ve
30 +ve
45 +ve
60 +ve
120 +ve
180 +ve
240 +ve
300 +ve

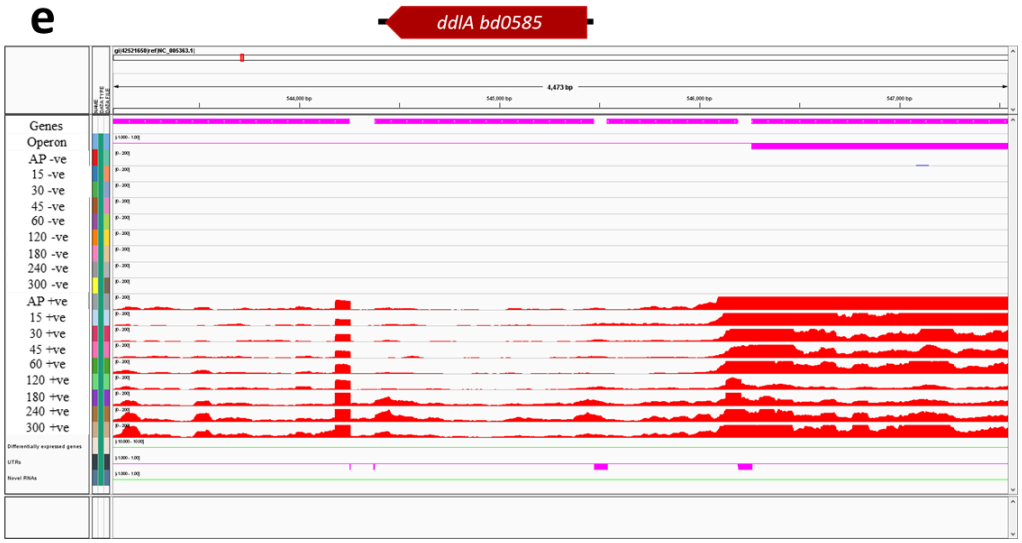
e
ddlA bd0585
Genes
Operon
AP -ve
15 -ve
30 -ve
45 -ve
60 -ve
120 -ve
180 -ve
240 -ve
300 -ve
AP +ve
15 +ve
30 +ve
45 +ve
60 +ve
120 +ve
180 +ve
240 +ve
300 +ve

8.1.4 RNA-seq data for petidoglycan recycling and salvaging genes.

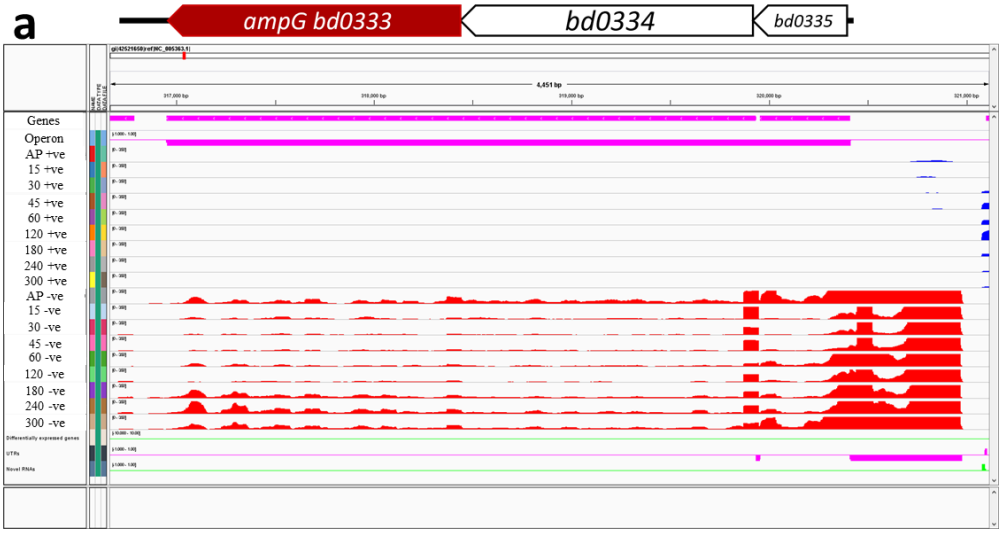

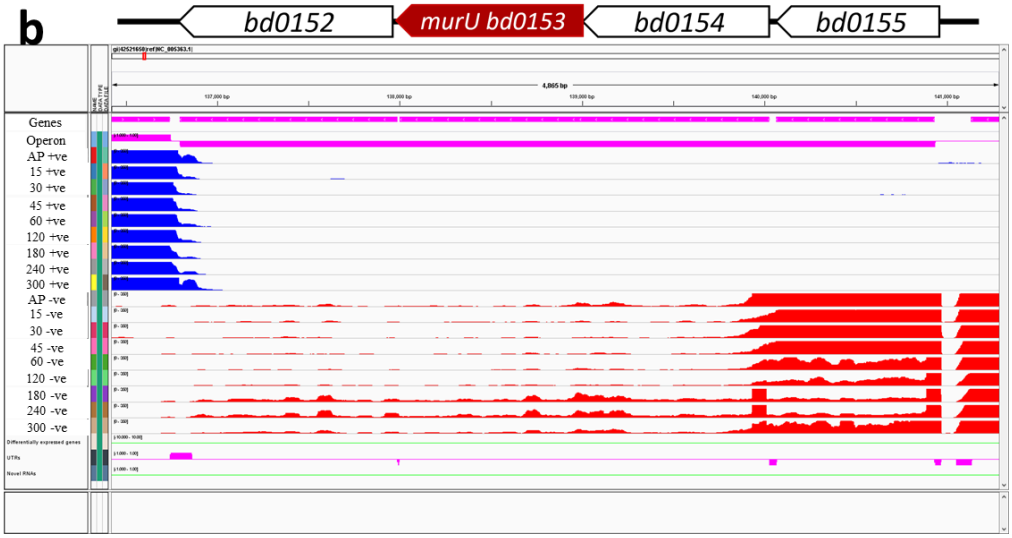

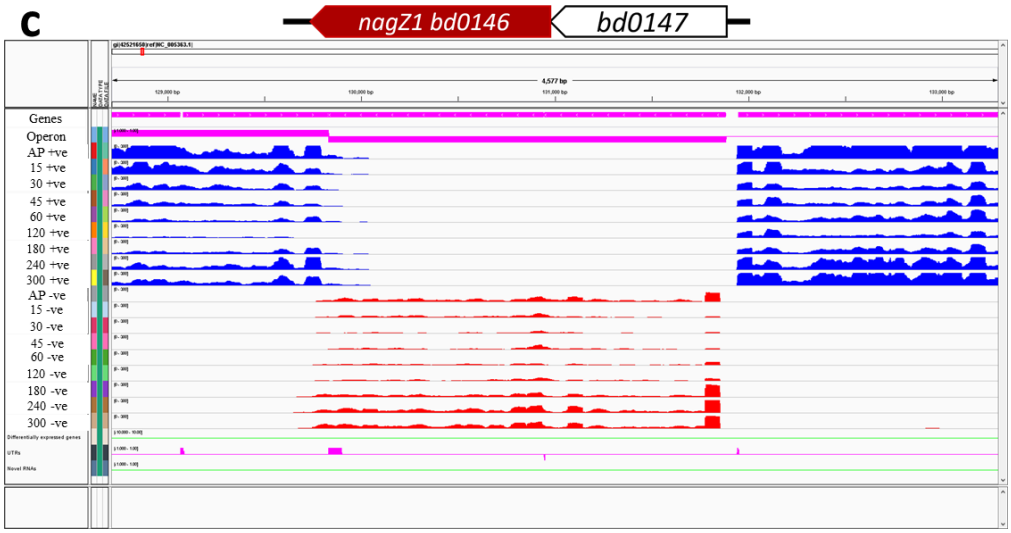
c
nagZ1 bd0146
bd0147
Genes
Operon
AP +ve
15 +ve
30 +ve
45 +ve
60 +ve
120 +ve
180 +ve
240 +ve
300 +ve
AP -ve
15 -ve
30 -ve
45 -ve
60 -ve
120 -ve
180 -ve
240 -ve
300 -ve

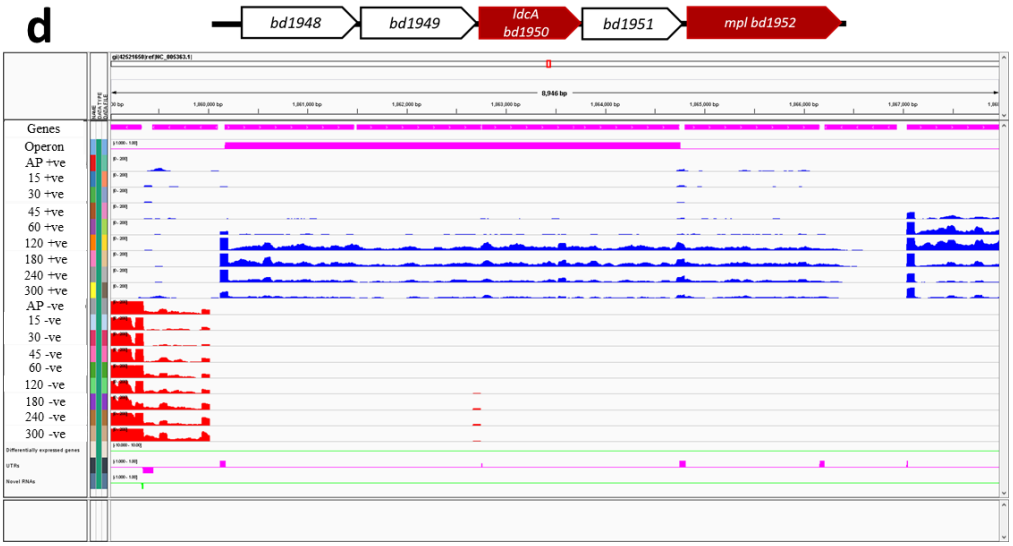
d
bd1948
bd1949
ldcA
bd1950
bd1951
mpl bd1952
Genes
Operon
AP +ve
15 +ve
30 +ve
45 +ve
60 +ve
120 +ve
180 +ve
240 +ve
300 +ve
AP -ve
15 -ve
30 -ve
45 -ve
60 -ve
120 -ve
180 -ve
240 -ve
300 -ve

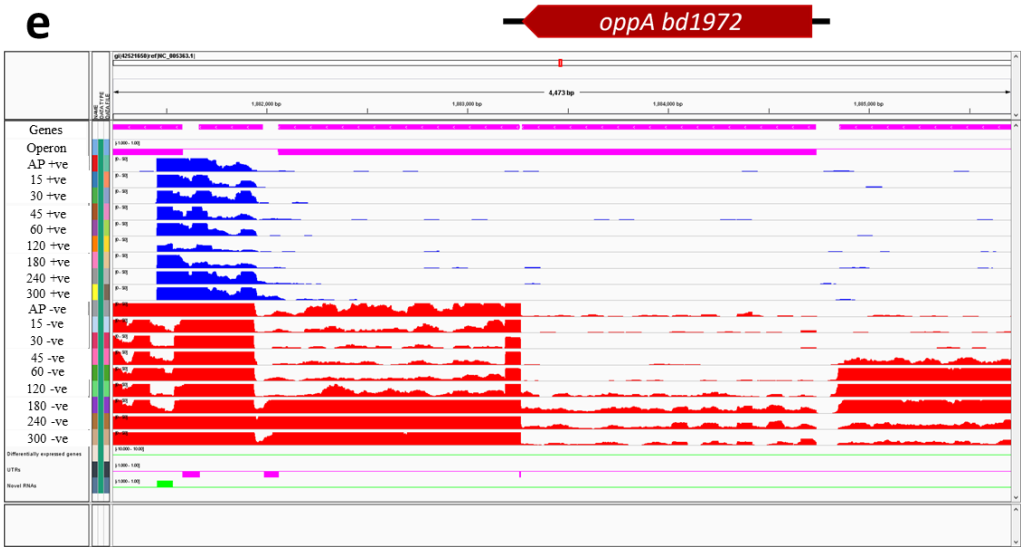

Figure 5.3.12. RNA-seq data for petidoglycan recycling and salvaging genes. Screenshots taken from Rockhopper software using RNA-seq data of the *dcw* cluster operons: (a) the *ampG* (*bd0333*) operon, range 0-350 reads, (b) the *murU* (*bd0153*) operon, range 0-350 reads, (c) the *nagZ1* (*bd0146*) operon, range 0-300 reads, (d) the *ldcA* (*bd1950*) and *mpl* (*bd1952*) operon, range 0-200 reads, (e) *oppA* (*bd1972*), range 0-50 reads. Above the screenshot, the arrows indicate the location and transcription of the gene. Tracks are labelled on the left: gene and operon show the placement of genes and the multi-gene operon prediction in Rockhopper. The other tracks are labelled by the timepoint (AP is attack phase, 0 minutes. Other tracks show time in minutes).